



UNIVERSIDAD  
**NACIONAL**  
DE COLOMBIA

# **Degradation of pharmaceuticals from municipal wastewater effluents by ozone-based advanced oxidation processes**

**María Angélica Prada Vásquez**

Universidad Nacional de Colombia  
Facultad de Minas, Departamento de Geociencias y Medio Ambiente  
Medellín, Colombia

2023



UNIVERSIDAD  
**NACIONAL**  
DE COLOMBIA

**Degradación de compuestos farmacéuticos  
presentes en efluentes de aguas residuales  
municipales mediante procesos de oxidación  
avanzada-basados en ozono**

**María Angélica Prada Vásquez**

Universidad Nacional de Colombia

Facultad de Minas, Departamento de Geociencias y Medio Ambiente

Medellín, Colombia

2023

# **Degradation of pharmaceuticals from municipal wastewater effluents by ozone-based advanced oxidation processes**

**María Angélica Prada Vásquez**

A thesis submitted in partial fulfilment of the requirements for the degree of  
Doctor in Engineering: Water Resources

**Adviser:**

Ph.D Santiago Alonso Cardona Gallo  
Universidad Nacional de Colombia

**Co-adviser**

Ph.D Ricardo Antonio Torres Palma  
Universidad de Antioquia

Line of Research:

Water treatment

Universidad Nacional de Colombia  
Facultad de Minas, Departamento de Geociencias y Medio Ambiente  
Medellín, Colombia

2023

*Life is not easy for any of us. But what or that? We must have perseverance and above all confidence in ourselves. We must believe that we are gifted for something, and this thing must be attained.*

— **Marie Curie**

To my husband, Santiago

# Table of contents

|  |              |
|--|--------------|
| <b>Acknowledgements .....</b>  | <b>v</b>     |
| <b>Abstract.....</b>   | <b>vii</b>   |
| <b>Scientific production.....</b>  | <b>xii</b>   |
| <b>List of Tables .....</b>  | <b>xiv</b>   |
| <b>List of Figures.....</b>  | <b>xv</b>    |
| <b>List of abbreviation.....</b>   | <b>xviii</b> |
| <br>   |              |
| <b>1. Chapter 1. Introduction.....</b>   | <b>10</b>    |
| 1.1 Global water situation .....   | 10           |
| 1.2 Contaminants of emerging concern: pharmaceuticals .....                    | 11           |
| 1.2.1 Pharmaceutical effects on the environment.....                           | 13           |
| 1.2.2 Regulations on micropollutants in water resources.....                   | 14           |
| 1.3 Advanced oxidation process applied to the removal of pharmaceuticals ..... | 15           |
| 1.4 Ozonation .....  | 16           |
| 1.5 Ozone-advanced oxidation processes.....                                    | 18           |
| 1.5.1 Peroxone process.....  | 18           |
| 1.5.2 Photolytic ozonation.....  | 19           |
| 1.5.3 Heterogeneous catalytic ozonation.....                                   | 20           |
| 1.5.4 Ozone/peroxymonosulfate .....  | 21           |
| 1.6 Objectives.....  | 23           |
| 1.6.1 General objective.....   | 23           |
| 1.6.2 Specific objectives.....   | 23           |
| 1.7 Novelty .....  | 23           |
| 1.8 Thesis outline .....   | 24           |

|  |           |
|--|-----------|
| <b>2. Chapter 2: Materials and methods .....</b>   | <b>25</b> |
| 2.1 Chemicals reagents.....  | 25        |
| 2.1.1 Target pharmaceuticals .....   | 25        |
| 2.1.2 Zeolites .....   | 26        |
| 2.1.3 Other chemicals and reagents employed .....  | 27        |
| 2.2 Experimental set-ups .....   | 27        |
| 2.2.1 Bubble column reactors.....  | 27        |
| 2.2.1.1 Bubble column No. 1 .....  | 27        |
| 2.2.1.2 Bubble column No. 2 .....  | 29        |
| 2.2.2 Tubular ozone membrane contactor .....   | 31        |
| 2.3 Water matrices.....  | 33        |
| 2.3.1 Distilled water spiked with a model pharmaceutical.....  | 33        |
| 2.3.2 Wastewater sample from WWTPs in Spain.....   | 33        |
| 2.3.3 Wastewater sample from WWTP in Portugal .....  | 34        |
| 2.4 Analytical methods.....  | 36        |
| 2.4.1 Determination of pharmaceuticals in wastewater samples .....   | 36        |
| 2.4.2 Determination of ibuprofen in distilled water .....  | 37        |
| 2.4.3 Identification of degradation intermediates.....   | 37        |
| 2.4.4 Dissolved ozone concentration.....   | 37        |
| 2.4.5 Total organic carbon.....  | 38        |
| 2.4.6 Wastewater characterization .....  | 39        |
| 2.4.7 Catalyst characterization .....  | 39        |
| 2.4.8 Environmental risk assessment .....  | 40        |
| <b>3. Chapter 3. Evaluation of different ozone-based AOPs in terms of elimination of a model compound in aqueous solution.....</b> | <b>42</b> |
| 3.1 Introduction .....   | 42        |
| 3.2 Experimental procedure .....   | 44        |
| 3.3 Calculation of ozone mass balance .....  | 45        |
| 3.4 Results and discussion.....  | 46        |

|   |           |
|---|-----------|
| 3.4.1 O <sub>3</sub> intensified by UVC light .....   | 46        |
| 3.4.2 O <sub>3</sub> intensified by an oxidant .....  | 49        |
| 3.4.2.1 Effect of H <sub>2</sub> O <sub>2</sub> /O <sub>3</sub> and PMS/O <sub>3</sub> molar ratios .....   | 49        |
| 3.4.2.2 Comparison of O <sub>3</sub> /H <sub>2</sub> O <sub>2</sub> and O <sub>3</sub> /PMS .....   | 51        |
| 3.4.3 O <sub>3</sub> intensified by a zeolite catalyst .....  | 54        |
| 3.4.3.1 Characterization of zeolites .....  | 54        |
| 3.4.3.2 Removal of ibuprofen by catalytic ozonation .....   | 56        |
| 3.4.4 Comparison of ozone based AOPs .....  | 60        |
| 3.4.4.1 Synergistic effect assessment .....   | 60        |
| 3.4.4.2 Analysis of energy consumption efficiency .....   | 61        |
| 3.4.4.3 Total operational costs .....   | 63        |
| 3.4.5 Identification of main degradation products of selected O <sub>3</sub> -based AOP.....  | 64        |
| 3.5 Conclusions .....   | 68        |
| <b>4. Chapter 4. Application of catalytic ozonation in the elimination of pharmaceuticals in real wastewater .....</b>  | <b>69</b> |
| 4.1 Introduction .....  | 69        |
| 4.2 Experimental procedure .....  | 70        |
| 4.3 Results and discussion.....   | 71        |
| 4.3.1 Pharmaceuticals detected in wastewater samples .....  | 71        |
| 4.3.2 Adsorption of pharmaceuticals on NaY zeolites.....  | 73        |
| 4.3.3 Ozonation treatment .....   | 76        |
| 4.3.4 Catalytic ozonation treatment.....  | 79        |
| 4.3.5 Environmental risk assessment .....   | 82        |
| 4.4 Conclusions .....   | 85        |
| <b>5. Chapter 5. Evaluation of an ozone membrane contactor to enhance gas/liquid mass transfer and its application in the removal of pharmaceuticals in real wastewater .....</b> | <b>86</b> |
| 5.1 Introduction .....  | 86        |
| 5.2 Experimental setup and procedure .....  | 88        |
| 5.3 Estimation of ozone mass transfer in the membrane contactor.....  | 89        |

|   |            |
|---|------------|
| 5.4 Results and discussion.....   | 92         |
| 5.4.1 Effect of inlet gas stream flow rate .....                                  | 92         |
| 5.4.2 Effect of the ozone concentration in the inlet gas stream.....              | 93         |
| 5.4.3 Effect of liquid flow rate .....  | 94         |
| 5.4.4 Estimation of membrane transfer coefficient and mass transfer resistances.. | 96         |
| 5.4.5 Comparison with other gas-liquid contactor systems .....                    | 99         |
| 5.4.6 Occurrence of pharmaceuticals .....   | 103        |
| 5.4.7 PhACs removal using the ozone membrane contactor.....                       | 104        |
| 5.4.8 Effect of the ozonation process on the global parameters.....               | 109        |
| 5.4.9 Mass transfer by chemical reaction in the liquid phase .....                | 111        |
| 5.5 Conclusions .....   | 113        |
| <b>6. Chapter 6. Conclusions and recommendations .....</b>                        | <b>115</b> |
| 6.1 Recommendations and future work.....  | 119        |
| <b>References .....</b>   | <b>120</b> |
| <b>Annexes.....</b>   | <b>143</b> |



## Acknowledgements

I would like to extend my heartfelt gratitude to my advisers, Prof. Santiago Cardona (Universidad Nacional de Colombia, campus Medellín) and Prof. Ricardo Torres Palma (Universidad de Antioquia) for their guidance, support and motivation throughout my PhD study. I want to express my special thanks to Prof. Javier Silva for his important contributions and excellent disposition during my PhD. I am also thankful to Javier Navarro Laboulais, who generously provided knowledge and expertise in the ozonation processes.

Thanks to the Universidad Nacional de Colombia (Medellín campus) for providing me the necessary resources, educational infrastructure and academic environment. Thanks to all my friends and officemates, Eliana, Diana, Alexander, Luna, Camila and Natalia, for your support and friendship during my PhD study.

I want to extend special thanks to GIRAB (Grupo de Investigación en Remediación Ambiental y Biocatálisis) from Universidad de Antioquia for the opportunity of joining in the research group and for providing additional resources that facilitated my research. Special thanks to my fellows: Efraim, Camilo, Elizabeth, Dayana, Martica, and Marcela, who have provided encouragement, shared valuable insights, and offered their support during the various stages of this research. Your camaraderie and discussions have enriched my academic experience.

I would also like to thank to Antonio Chica for giving me the opportunity to do a research stay in the Instituto de Tecnología Química (ITQ) at the Universitat Politècnica de València, likewise for his kind help and provided knowledge in zeolites. Many thanks to Bea, Lorena, and Raul, who participated in the field and laboratory work.

I would also like to acknowledge the support from Vitor Vilar and his team for welcoming me for six months in the Laboratory of Separation and Reaction Engineering-Laboratory of Catalysis and Materials (LSRE-LCM) at the University of Porto, Portugal. Thanks to my

colleges there: Agustina, Fabiane, Sandra, Carla, Pedro Presumido, and specially thanks to Mateus Pituco, for all support that was so valuable during my stay.

Thanks also to the Research Institute for Pesticides and Waters (IUPA) at Universitat Jaume I (Spain), specially to Felix, Ana Maria, Maria Ibañez, Elena Pitarch and Claudia Simarro for helping me with all quantification analysis of the wastewater samples and for the identification of transformation by-products.

Thanks to the entity who founded my doctoral studies with the programs: Scholarship Program No. 758-2017 - National Doctorates of the Ministry of Science, Technology and Innovation of Colombia (MINCIENCIAS).

Finally, my deepest gratitude belongs to my family, specially to my husband Santiago, who whose love, encouragement, and understanding have been a constant source of strength. I also express my thanks to my parents Luis y Arelis, to my brothers Ronny and Jonathan, to my sister-in-law Tatiana, my mother in law Isabel, and to my dear friend Yurany, for their valuable support and to kept me motivated and focused on achieving this goal.

Infinite thanks to all!!

## Abstract

Due to the ever-increasing concerns about the release of contaminants of emerging concerns (CECs) in different water compartments, the need for effective and sustainable water treatment methods has become a significant issue. These CECs, which include various pharmaceuticals active compounds (PhACs), personal care products, and other pollutants, pose challenges to conventional water treatment processes. As a result, there is a growing need to implement alternative solutions to tackle this pressing issue and ensure the protection of our water resources. In this context, the application of advanced technologies like ozonation water treatment processes has emerged as a promising approach to address the removal of recalcitrant organic compounds, specially PhACs, and safeguard the quality of our water supply.

Ozonation stands out as a versatile and powerful technology capable of directly and selectively to attack organic compounds, particularly under low pH conditions. Additionally, under alkaline pH conditions, ozone can undergo decomposition via a chain reaction mechanism and generate highly reactive and less selective hydroxyl radicals (HO<sup>•</sup>). Despite its high effectiveness as water treatment technique, conventional ozonation faces two main drawbacks: incomplete mineralization and, consequently, accumulation of unknown reaction by-products, as well as gas-liquid mass transfer limitations.

This PhD thesis work focuses to contribute to the existing knowledge regarding the different ozone-based advanced oxidation processes as strategies to enhance/intensified the chemical performance of the ozonation process towards PhACs removal. As well, to expand knowledge regarding to the evaluation of the performance of an ozone membrane contactor as a potential strategy for the intensification ozone–liquid mass transfer, and its application in the removal of PhACs in real wastewater samples.

Initially, the potential of the different O<sub>3</sub>-based AOPs including O<sub>3</sub> and combinations of O<sub>3</sub>/UVC, O<sub>3</sub>/PMS, O<sub>3</sub>/H<sub>2</sub>O<sub>2</sub> and O<sub>3</sub>/zeolite Y were investigated, and their ability to enhance the removal of ibuprofen (an ozone-resistant compound) in comparison to conventional ozonation. Process efficiency was evaluated in terms IBU mineralization level, ozone

utilization efficiency, and energy consumption. The most promising O<sub>3</sub>-based process was chosen for further investigation in the elucidation of IBU transformation products and its application in the removal of mixture of PhACs detected in real wastewater samples. The results indicated that O<sub>3</sub>-based AOPs not only enhanced the removal and mineralization of IBU but also improved the transfer and consumption O<sub>3</sub> doses during the coupled systems compared to the single ozonation. Catalytic ozonation using NaY-60 zeolites demonstrated greater benefits, proving to be the most cost-effective process in terms of operational costs for both the degradation of IBU and the reduction of mineralization. Three degradation by-products were identified for IBU in the catalytic ozonation using NaY zeolites, evidencing the attack sites of IBU by oxidative species.

The application of catalytic ozonation using NaY zeolites with two different SiO<sub>2</sub>/Al<sub>2</sub>O<sub>3</sub> molar ratios (60 and 12) was evaluated in the removal of 27 PhACs compounds present in real effluents from two municipal wastewaters treatment plants of the Mediterranean coast of Spain. Control experiments such as adsorption and single ozonation were performed in order to clarify fundamental aspects of the different systems in real wastewater samples. The results indicated that simultaneous use of ozone and NaY zeolites significantly improved the micropollutants degradation rate. The environmental risk assessment showed that the risk quotients of pharmaceuticals were diminished after ozonation in presence of NaY-60 and NaY-12 zeolites.

The characterization of a tubular porous stainless steel membrane contactor in terms of ozone-water mass transport was investigated. The volumetric mass transfer coefficient ( $K_{La}$ ) was evaluated as a function of ozone gas concentration, liquid, and gas flow rate. The results showed that  $K_{La}$  values were substantially improved with an increment in liquid flow rate, due to the enhanced turbulence on the membrane shell-side and annular zone. The influence of different specific ozone doses ( $\text{g O}_3 \text{ g DOC}^{-1}$ ) and ozone inlet gas concentration were also investigated in the removal of 23 PhACs detected in secondary-treated municipal wastewater. The elimination of PhACs was strongly correlated with kinetic reaction constants values with ozone and hydroxyl radicals ( $k_{O_3}$  and  $k_{HO\cdot}$ ), resulting in a characteristic elimination pattern for each compound group.

## Resumen

Debido a la creciente preocupación sobre la liberación de contaminantes de preocupación emergente (CECs) en diferentes compartimentos de agua, la necesidad de métodos efectivos y sostenibles de tratamiento de agua se ha convertido en un tema significativo. Estos CECs, que incluyen varios compuestos activos farmacéuticos (PhACs), productos de cuidado personal y otros contaminantes, plantean desafíos a los procesos convencionales de tratamiento de agua. Como resultado, existe una creciente necesidad de implementar soluciones alternativas para abordar este problema apremiante y garantizar la protección de nuestros recursos hídricos. En este contexto, la aplicación de tecnologías avanzadas como los procesos de tratamiento de agua mediante ozonación ha surgido como un enfoque prometedor para abordar la eliminación de compuestos orgánicos recalcitrantes, especialmente PhACs y salvaguardar la calidad de nuestras fuentes de agua.

La ozonación se destaca como una tecnología versátil y poderosa capaz de atacar directa y selectivamente compuestos orgánicos, especialmente bajo condiciones de pH ácido. Simultáneamente, bajo condiciones de pH alcalino, el ozono puede sufrir descomposición a través de un mecanismo de reacción en cadena y generar radicales hidroxilo ( $\text{HO}^\bullet$ ) altamente reactivos y menos selectivos. A pesar de su alta efectividad como técnica de tratamiento de agua, la ozonación convencional enfrenta dos desventajas principales: la mineralización incompleta y, en consecuencia, acumulación de subproductos de reacción desconocidos, así como limitaciones en la transferencia de masa gas-líquido.

Este trabajo de tesis de doctorado se enfoca en contribuir al conocimiento existente sobre los diferentes procesos avanzados de oxidación (AOPs) basados en ozono como estrategias para mejorar o intensificar el rendimiento químico del proceso de ozonación para la eliminación de PhACs. Además, tiene como objetivo ampliar el conocimiento sobre la evaluación del rendimiento de un contactor de membrana para la inyección de ozono como una estrategia potencial para intensificar la transferencia de masa ozono-líquido y su aplicación en la eliminación de PhACs en muestras de aguas residuales reales.

Inicialmente, se investigó el potencial de los diferentes AOPs basados en O<sub>3</sub>, incluidas las combinaciones de O<sub>3</sub>/UVC, O<sub>3</sub>/PMS, O<sub>3</sub>/H<sub>2</sub>O<sub>2</sub> y O<sub>3</sub>/zeolita Y, y su capacidad para mejorar la eliminación del ibuprofeno (IBU) (un contaminante resistente al ozono) en comparación con la ozonación convencional. La eficiencia del proceso se evaluó en términos de nivel de mineralización de IBU, eficiencia de utilización de ozono y consumo de energía. El proceso basado en O<sub>3</sub> más prometedor se eligió para una investigación adicional en la elucidación de los productos de transformación del IBU y su aplicación en la eliminación de una mezcla de PhACs detectados en muestras de aguas residuales reales. Los resultados indicaron que los AOPs basados en O<sub>3</sub> no solo mejoraron la eliminación y mineralización del IBU, sino que también mejoraron la transferencia y el consumo de dosis de O<sub>3</sub> durante los sistemas acoplados en comparación con la ozonación sola. Se seleccionó la ozonización catalítica utilizando zeolitas NaY como el tratamiento más adecuado, tomando en cuenta diferentes criterios como índice de sinergia, energía eléctrica por pedido (E<sub>EO</sub>) y costos totales de operación. Se identificaron tres subproductos de degradación del IBU en la ozonización catalítica utilizando zeolitas NaY, evidenciando los sitios de ataque del IBU por especies oxidativas.

Se evaluó la aplicación de la ozonización catalítica utilizando zeolitas NaY con dos relaciones molares diferentes de SiO<sub>2</sub>/Al<sub>2</sub>O<sub>3</sub> (60 y 12) en la eliminación de 27 compuestos PhACs presentes en efluentes reales de dos plantas de tratamiento de aguas residuales municipales en la costa mediterránea de España. Se realizaron experimentos de control, como adsorción y ozonación única, para aclarar aspectos fundamentales de los diferentes sistemas en muestras reales de aguas residuales. Los resultados indicaron que el uso simultáneo de ozono y zeolitas NaY mejoró significativamente la velocidad de degradación de los microcontaminantes. La evaluación del riesgo ambiental mostró que los cocientes de riesgo de los productos farmacéuticos disminuyeron después de la ozonación en presencia de zeolitas NaY-60 y NaY-12.

Se investigó la caracterización de un contactor de membrana de acero inoxidable poroso en términos del transporte de masa ozono-líquido. Para la caracterización hidrodinámica, el coeficiente volumétrico de transferencia de masa (K<sub>La</sub>) se evaluó en función de la

concentración de gas ozono, el caudal de líquido y gas. Los resultados mostraron que los valores de  $K_{La}$  mejoraron sustancialmente con un incremento en el caudal de líquido, debido a la turbulencia mejorada en el lado de la carcasa de la membrana y la zona anular. También se investigó la influencia de diferentes dosis específicas de ozono ( $\text{g O}_3 \text{ g DOC}^{-1}$ ) y la concentración de gas de entrada de ozono en la eliminación de 23 PhACs detectados en aguas residuales municipales tratadas secundariamente. La eliminación de los PhACs se correlacionó fuertemente con los valores de constantes de reacción cinética con ozono y radicales hidroxilo ( $k_{\text{O}_3}$  y  $k_{\text{HO}\cdot}$ ), lo que resultó en un patrón característico de eliminación para cada grupo de compuestos.

## Scientific production

### Published articles:

**María A. Prada-Vásquez**, Sandra E. Estrada-Flórez, Efraím A. Serna-Galvis, Ricardo A. Torres-Palma (2021). Developments in the intensification of photo-Fenton and ozonation-based processes for the removal of contaminants of emerging concern in Ibero-American countries. *Science of the Total Environment* 765 (2021) 142699 <https://doi.org/10.1016/j.scitotenv.2020.142699> (IF: 10.754; Q1).

**María A. Prada-Vásquez**, Mateus Mestriner Pituco, Mateus P. Caixeta, Santiago A. Cardona Gallo, Ana M. Botero-Coy, Félix Hernández, Ricardo A. Torres-Palma, Vitor J.P. Vilar (2024). Ozonation using a stainless-steel membrane contactor: gas-liquid mass transfer and pharmaceuticals removal from secondary-treated municipal wastewater. *Chemosphere* 349 (2024) 140888 <https://doi.org/10.1016/j.chemosphere.2023.140888> (IF: 8.943, Q1).

### Scientific article submitted for publication:

**María A. Prada-Vásquez**, Claudia Simarro-Gimeno, Santiago A. Cardona-Gallo, Elena Pitarch, Félix Hernández, Ricardo A. Torres-Palma, Antonio Chica, J. Navarro-Laboulais. Application of catalytic ozonation using Y zeolite in the elimination of pharmaceuticals in effluents from municipal wastewater treatment plants. *Science of the Total Environment* (IF: 10.754; Q1).

### Conferences: Oral and poster presentations:

**María A. Prada-Vásquez**, H. Presumido, M. M. Pituco, Ana I. Gomes, S.A. Cardona Gallo, A. M. Botero-Coy, F. Hernandez, R. A. Torres Palma, V. J. P. Vilar. Evaluation of Ozone Mass Transfer in a Tubular Porous Stainless Steel Membrane Contactor". Poster Presentation. 5th Iberoamerican Conference on Advanced Oxidation Technologies. November 7-11, 2022, Cusco, Peru. *Best Poster*



**María A. Prada-Vásquez**, P. H. Presumido, M. M. Pituco, Ana I. Gomes, S.A. Cardona Gallo, A. M. Botero-Coy, F. Hernandez, R. A. Torres Palma, V. J. P. Vilar. A Novel Ozone Membrane Contactor for the Removal of CECs from Secondary Effluent of Municipal Wastewater and Reverse Osmosis Concentrate. *Short Oral Presentation*. 5<sup>th</sup> Iberoamerican Conference on Advanced Oxidation Technologies. November 7-11, 2022, Cusco, Peru.

**María A. Prada-Vásquez**, H. Presumido, M. M. Pituco, Ana I. Gomes, S.A. Cardona Gallo, A. M. Botero-Coy, F. Hernandez, R. A. Torres Palma, V. J. P. Vilar. Evaluation of Ozone Mass Transfer in a Tubular Porous Stainless Steel Membrane Contactor”. *Poster Presentation*. 5<sup>th</sup> Iberoamerican Conference on Advanced Oxidation Technologies. November 7-11, 2022, Cusco, Peru.

Claudia Simarro-Gimeno, **María A. Prada-Vásquez**, Isabel Vidal, Santiago A. Cardona-Gallo, María Ibáñez, Elena Pitarch, Félix Hernández, Ricardo A. Torres-Palma, Antonio Chica, Javier Navarro-Laboulais. *Poster Presentation*.

### **Research stays**

- Research Center: Instituto de Tecnología Química (ITQ)  
Universitat Politècnica de València  
Valencia, Spain  
Duration: 6 months  
2021
  
- Laboratory of Separation and Reaction Engineering-Laboratory of Catalysis and Materials (LSRE-LCM)  
University of Porto  
Porto, Portugal.  
Duration: 6 months  
2022

## List of Tables

|  |     |
|--|-----|
| <b>Table 1.1</b> Redox potentials of some oxidizing agents (Parsons, 2015).....  | 15  |
| <b>Table 2.1</b> Main data of selected PhACs .....   | 25  |
| <b>Table 2.2</b> Physico-chemical characteristics of the municipal wastewater after secondary treatment- WWTP located in Portugal. ....  | 35  |
| <b>Table 3.1</b> Physicochemical properties of ibuprofen. Taken from: <a href="http://www.chemicalize.org">www.chemicalize.org</a> .   | 43  |
| <b>Table 3.2</b> Properties of NaY zeolites samples including specific surface area ( $S_{\text{BET}}$ ), external surface area ( $S_{\text{ext}}$ ), micropore area ( $S_{\text{micro}}$ ), micropore volume ( $V_{\text{micro}}$ ), mesopore volume ( $V_{\text{meso}}$ ), pore size and $\text{SiO}_2/\text{Al}_2\text{O}_3$ mol ratio.....       | 54  |
| <b>Table 3.3</b> Brønsted and Lewis acidities of zeolite samples.....  | 56  |
| <b>Table 3.4</b> Comparison of electric energy requirements in $\text{kWh m}^{-3}$ at desired removal levels for the different $\text{O}_3$ -based AOPs investigated. ....   | 62  |
| <b>Table 3.5</b> Calculated properties for the transformation products .....   | 67  |
| <b>Table 4.1</b> Initial concentration of pharmaceuticals detected in Effluent A and Effluent B.   | 72  |
| <b>Table 4.2</b> Risk Quotients calculated for effluent A and B and after different treatments applied, adsorption (1 h), ozonation and catalytic ozonation (10 min) on NaY-60 and NaY-12 zeolites (denoted as 60 and 12, respectively). Values in color green correspond to: low risk, yellow color: moderate risk, and red color 1: high risk..... | 84  |
| <b>Table 5.1</b> Experimental conditions employed in the ozone mass transfer tests and in PhACs removal experiments using secondary-treated wastewater. ....   | 89  |
| <b>Table 5.2</b> Comparison of the SOTR, VSOTR, SOTE, and SSOTE values of commonly used gas-liquid contactors devices and the membrane contactor investigated in this study. ....  | 101 |
| <b>Table 5.3</b> Initial concentration of pharmaceuticals detected in the WWTP secondary effluent .....  | 103 |
| <b>Table 5.4</b> Dimensionless Hatta number values for the target compounds .....  | 112 |

## List of Figures

|  |    |
|--|----|
| <b>Figure 1.1</b> Global water demand (as freshwater withdrawals) in 2000 and 2050 for different regions in the world. OECD (Organization for Economic Co-operation and Development); BRIICS (Brazil, Russia, India, Indonesia, China, South Africa); ROW (rest of world). Source: (OCDE, 2020). ..... | 10 |
| <b>Figure 1.2.</b> Schematic representation and classification of different treatments based on advanced oxidation processes (AOPs). .....   | 16 |
| <b>Figure 1.3</b> Resonance structures of ozone molecule (Beltran, 2003).....  | 17 |
| <b>Figure 1.4</b> The framework structure of FAU type zeolite (Nozue et al., 2012). .....  | 21 |
| <b>Figure 2.1</b> Experimental set-up scheme-bubble column No.1. ....  | 28 |
| <b>Figure 2.2</b> Photographs of bubble column No.1 .....  | 29 |
| <b>Figure 2.3</b> Schematic diagram of ozonation experiment-bubble column No.2.....  | 30 |
| <b>Figure 2.4</b> (a) Photograph of the bubble column No. 2 and (b) screenshot of the measurement of dissolved ozone through the optical probe.....  | 31 |
| <b>Figure 2.5</b> Schematic diagram of the experimental setup used in (a) ozone mass transfer experiments and (b) for PhACs removal tests.....   | 32 |
| <b>Figure 2.6</b> Photograph of the tubular ozone membrane contactor. ....   | 33 |
| <b>Figure 2.7</b> Location of WWTPs where effluent samples were collected.....   | 34 |
| <b>Figure 3.1</b> (a) Evolution of the normalized concentration of IBU (b) kinetics and (c) mineralization via UVC, O <sub>3</sub> , and O <sub>3</sub> /UVC processes. ....   | 47 |
| <b>Figure 3.2</b> Evolution of (a) gas phase ozone concentrations at the reactor inlet and outlet, (b) dissolved ozone concentration, (c) transfer O <sub>3</sub> doses and utilization O <sub>3</sub> efficiency as a function of reaction time during IBU ozonation and photolytic ozonation. ....   | 49 |
| <b>Figure 3.3</b> Effect of (a) H <sub>2</sub> O <sub>2</sub> /O <sub>3</sub> molar ratios and (c) PMS/O <sub>3</sub> molar ratios and their the pseudo-first-order rate constant (inset figure, (c) H <sub>2</sub> O <sub>2</sub> /O <sub>3</sub> , (d) PMS/O <sub>3</sub> ).....                     | 50 |
| <b>Figure 3.4</b> Mineralization level of IBU via H <sub>2</sub> O <sub>2</sub> , PMS, O <sub>3</sub> , O <sub>3</sub> /H <sub>2</sub> O <sub>2</sub> and O <sub>3</sub> /PMS processes. ....  | 52 |

|   |    |
|---|----|
| <b>Figure 3.5</b> Evolution of (a) gas phase O <sub>3</sub> concentrations at the reactor inlet and outlet, (b) dissolved ozone concentration, (c) transfer O <sub>3</sub> doses and (d) utilization O <sub>3</sub> efficiency as a function of reaction time during IBU ozonation. ....                                    | 53 |
| <b>Figure 3.6</b> X-ray diffraction pattern of NaY zeolite with SiO <sub>2</sub> /Al <sub>2</sub> O <sub>3</sub> mole ratio 12 and 60. ....   | 55 |
| <b>Figure 3.7</b> (a) Evolution of the normalized concentration of IBU via O <sub>3</sub> /NaY-60, O <sub>3</sub> /NaY-12, and their control experiments, (b) the pseudo-first-order rate constants.....  | 57 |
| <b>Figure 3.8</b> Mineralization level of IBU via O <sub>3</sub> /NaY-60, O <sub>3</sub> /NaY-12, and their control experiments. ....   | 58 |
| <b>Figure 3.9</b> Evolution of (a) gas phase ozone concentrations at the reactor inlet and outlet (b) dissolved ozone concentration, (c) transfer O <sub>3</sub> doses and (d) utilization O <sub>3</sub> efficiency as a function of reaction time during catalytic ozonation of IBU using NaY-60 and NaY-12 zeolites..... | 59 |
| <b>Figure 3.10</b> Synergy index (SI) for the O <sub>3</sub> -based AOPs investigated .....   | 61 |
| <b>Figure 3.11</b> Total operational cost (USD m <sup>-3</sup> ) to eliminate 50% of TOC for O <sub>3</sub> -based AOPs investigated.....   | 64 |
| <b>Figure 3.12</b> Tentative transformation pathway of IBU degradation by catalytic ozonation using NaY-12 and NaY-60 zeolites. ....  | 65 |
| <b>Figure 4.1</b> Adsorption of target pharmaceuticals by NaY-60 and NaY-12 zeolites at 60 min of reaction time in: (a) Effluent A and (b) Effluent B.....  | 74 |
| <b>Figure 4.2</b> Ozonation of pharmaceuticals during 10, 30 and 60 min of reaction time in: (a) Effluent A and (b) Effluent B.....   | 78 |
| <b>Figure 4.3</b> Catalytic ozonation of target pharmaceuticals during 10 min of reaction time in (a) effluent A using zeolite: NaY-60 and NaY-12 and (b) effluent B using zeolite NaY-60 and NaY-12. ....  | 80 |
| <b>Figure 5.1</b> Effect of the gas flow rate .....   | 93 |
| <b>Figure 5.2</b> Effect of the ozone gas concentration in the inlet stream. ....   | 94 |
| <b>Figure 5.3</b> Effect of the liquid flow rate on K <sub>La</sub> values. ....  | 95 |
| <b>Figure 5.4</b> Bubble size distribution in tubular porous stainless-steel membrane contactor. ....   | 96 |

|  |     |
|--|-----|
| <b>Figure 5.5</b> Graphical scheme for calculating the mass transfer coefficient in the membrane by Wilsons plot method.....   | 97  |
| <b>Figure 5.6</b> (a) Analysis of mass-transfer resistances for ozone absorption in water, (b) contribution to total mass transfer resistance (%) in the liquid phase boundary film and in the membrane as a function of liquid flow rate.....   | 98  |
| <b>Figure 5.7</b> Transfer efficiency (%) as a function of (a) liquid flow rate and (b) gas flow rate. ....  | 102 |
| <b>Figure 5.8</b> Removal efficiency for the 23 pharmaceuticals detected in a secondary-treated wastewater, using the membrane reactor coupled with a column, operated in continuous mode ( $\tau = 60$ s) as a function of specific ozone doses 0.39, 0.53, and 0.69 g O <sub>3</sub> g DOC <sup>-1</sup> (the specific O <sub>3</sub> dose was corrected for nitrite consumption)..... | 105 |
| <b>Figure 5.9</b> Removal of pharmaceuticals at 0.69 g O <sub>3</sub> g DOC <sup>-1</sup> as a function of (a) ozone kinetic rate constants (pantoprazole and O-desmethylvenlafaxine were not included due to $k_{O_3}$ values are not available).....   | 106 |
| <b>Figure 5.10</b> Removal of pharmaceuticals at 0.69 g O <sub>3</sub> g DOC <sup>-1</sup> as a function of reported HO <sup>•</sup> radical kinetic constants. Highlighted region (light blue) represents ozone-resistant compounds ( $k_{O_3} < 10^2$ M <sup>-1</sup> s <sup>-1</sup> ).....   | 107 |
| <b>Figure 5.11</b> Removal efficiency for the 23 pharmaceuticals detected in a secondary-treated wastewater, using the membrane reactor coupled with a column, operated in continuous mode ( $\tau = 60$ s) as a function of O <sub>3</sub> concentration in the inlet gas stream and same AO <sub>3</sub> D applied (12 mg O <sub>3</sub> L <sup>-1</sup> ). ....                       | 109 |
| <b>Figure 5.12</b> UV <sub>254</sub> , DOC, and turbidity removal percentages after ozonation as a function of (a) specific ozone dose applied (0.39, 0.53, and 0.69 g O <sub>3</sub> g DOC <sup>-1</sup> ) and (b) ozone concentration in the inlet gas stream (80 and 134 mg Ndm <sup>-3</sup> ). For more details on the experimental conditions of each test, see Table 5.1.....     | 110 |

## List of abbreviation

AOPs: Advanced oxidation processes

CECs: Contaminants of emerging concern

DOC: Dissolved organic carbon

dEfOM: Dissolved effluent organic matter

E<sub>EO</sub>: electrical energy per order

FAU: Faujasite

IBU: Ibuprofen

LOQ: Limit of quantification

MC: measured concentration

PNEC: Predicted no-effect concentration

PEC: Predicted environmental concentrations

PhACs: Pharmaceutically active compounds

RQ: risk quotient

SI: synergy index

SOTE: standard oxygen transfer efficiency

SOTR: standard oxygen transfer rate

TE: Transfer efficiency

TOC: Total organic carbon

TOD: Transfer ozone dose

TPs: transformations by-products

WWTPs: wastewater treatment plants

# Chapter 1. Introduction

## 1.1 Global water situation

Water is one of the natural resources indispensable for the balance of Earth and essential to living beings. The planet surface is covered by two-thirds of water, however, despite the large volume available of water, only 2.5 % of the total water on Earth is freshwater, and only 0.4% is available and suitable for human consumption (Shiklomanov, 2009).

Since the 1980s, water use has increased worldwide by about 1% per year. Currently, global water demand has been estimated to be about 4600 km<sup>3</sup> every year, and it is projected to increase by 20-30% to a range of 5500 km<sup>3</sup> annually by 2050 (Figure 1.1) (OCDE, 2020).

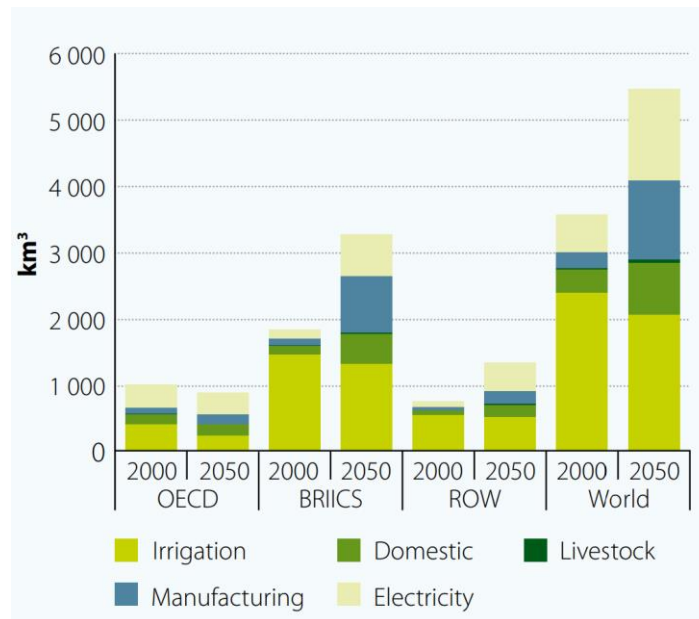


**Figure 1.1** Global water demand (as freshwater withdrawals) in 2000 and 2050 for different regions in the world. OECD (Organization for Economic Co-operation and Development); BRIICS (Brazil, Russia, India, Indonesia, China, South Africa); ROW (rest of world). Source: (OCDE, 2020).

This increase in water demand is mainly related to continuous population growth, rapid urbanization, socio-economic development, and inefficient water management practices (Sabale et al., 2022). The impact of climate change has further compromised the water quality and availability for supply. Increases in the frequency of abnormal events such as flooding, extreme temperatures, and temporary drying up of streams are affecting the availability of freshwater around the world (Gosling and Arnell, 2016).

Current consumption rates, further expansion and growth of the human population have exacerbated water stress and scarcity within regions. Water scarcity is a growing problem worldwide, affecting millions of people and leading to various social, economic, and environmental challenges (du Plessis, 2019). According to the United Nations report, 47% of the global population (equivalent to 3.6 billion) already live in areas that suffer from water scarcity at least one month every year. By 2050, this number is projected to increase to 5 billion people (World Water Assessment Programme, 2018). Another main cause to increased water stress around the globe is water pollution. The release of both natural and anthropogenic factors in the aquatic environment is affecting the quality of water bodies. Hence, the efficient and sustainable management of water resources to provide freshwater has become one of the main challenges that our society has to face nowadays.

## **1.2 Contaminants of emerging concern: pharmaceuticals**

Over the past few decades, the continuous development, the production, and disposal of an uncountable number of organic chemicals used in daily human activities have contributed to the widespread occurrence of many of these substances in the aquatic environment, including freshwater resources (Vasilachi et al., 2021). This group of chemicals, typically detected in aquatic ecosystems and wastewater at low concentrations ( $\text{ng L}^{-1}$  -  $\mu\text{g L}^{-1}$ ) is also referred to as contaminants of emerging concern (CECs) or micropollutants. These compounds have been present for a long time in environmental compartments, although their levels and harmful impact on ecosystems, are now a matter of concern among governmental institutions, the scientific community, and citizens (Rivera-Utrilla et al., 2013). According to NORMAN database (<https://www.norman-network.net>), CECs comprise a list of almost 1000 substances grouped into 21 classes: pharmaceutically active compounds, personal care products, synthetic and natural hormones, surfactants, flame



retardants, pesticides, and their degradation products, naturally occurring algal toxins, etc. (NORMAN, 2022).

Among CECs, pharmaceutically active compounds (PhACs) have received special attention due to their extensive consumption for human health and consequent discharge to the environment (Nannou et al., 2015). These compounds entailing different therapeutic groups such as: anti-inflammatories, antibiotics, hormones, anticonvulsants, anti-hypertensives, anxiolytic, antidepressants, beta-blockers, lipid regulators, contrast agents, etc. Their consumption has been increasing for decades, driven by a growing need for drugs to treat age-related and chronic diseases, and the self-medication practices (aus der Beek et al., 2016). According to the *IMS Institute for Healthcare Informatics*, by 2020, the use of pharmaceuticals reached 4500 billion doses, approximately 24% more than in 2015 (QuintilesIMS and its affiliates, 2015).

This notable worldwide increase in medicines has represented a great advance of modern society, but it has also been paralleled by the ubiquitous occurrence of these compounds in natural ecosystems (Fent et al., 2006). Once a pharmaceutical is consumed, the human body may only metabolize a fraction of the administered dose. The non-metabolized active substances are excreted mainly in the urine (55–80%) and, to a lesser extent, in the feces (4–30%), as parent compounds, conjugates, or metabolites (Jjemba, 2006). Subsequently, they enter into the water cycle, via wastewater treatment plants (WWTPs). Some of these PhACs are degraded during the sewage treatment process (e.g. biodegradation or adsorption onto sludge) (H. Jones et al., 2005). Nevertheless, the complete elimination of these contaminants in wastewater is hardly achieved, in part due these systems are designed for partial purification of wastewater (removal suspended solids and biodegradable organic matter), and therefore, many of them pass unchanged reaching water bodies (Jelic et al., 2011). Hence, wide ranges of numerous pharmaceuticals, including antibiotics, analgesics, antihypertensives, steroids, among others have been measured in low concentrations in treated urban wastewater, surface water and even in drinking water sources across various countries of the world (Bijlsma et al., 2021; Boyd et al., 2003; de Jesus Gaffney et al., 2015).

In the case of Colombia, Botero-Coy et al., (2018) detected 20 pharmaceuticals in WWTPs effluents from Bogotá and Medellín. The highest concentrations were found for the

analgesic acetaminophen ( $0.16\text{-}29.6 \mu\text{g L}^{-1}$ ), the antibiotic azithromycin ( $3.9 \mu\text{g L}^{-1}$ ), the antihypertensives losartan and valsartan and nonsteroidal anti-inflammatory drug naproxen, which were commonly above  $1 \mu\text{g L}^{-1}$ . Those levels are higher than found in urban wastewater. Similarly, Hernández et al., (2015) detected several PhACs in wastewater effluents from Bogotá and surface waters (Tunjuelo River). In this area around 2.5 million inhabitants discharge their sewage directly to this river without any treatment. The compounds most frequently found were acetaminophen, carbamazepine, clarithromycin, diclofenac, and ibuprofen.

### **1.2.1 Pharmaceutical effects on the environment**

Even though pharmaceuticals are detected at very low concentrations they are still pseudo persistent and bio-accumulate in the aquatic ecosystems due to their relatively low degradation potential, extensive use and continuous release (Kock et al., 2023).

The presence of PhACs in the environment can generate toxic biological effects including estrogenicity, mutagenicity and genotoxicity. In fact, the feminization of male fish has been reported, due to exposure to endocrine disrupting compound, which can cause reproductive abnormalities and development alterations in highly sensitive species during a chronic exposure (Valdés et al., 2016; Wang et al., 2016). They can be absorbed by organisms and adversely affect fundamental life functions. Organisms exposed to pharmaceuticals may experience lower growth rates, higher mortality rates and increased oxygen consumption (Kern et al., 2013). In addition, long-term exposure can lead to the accumulation of compounds in organisms and their further spread through the food chain. On a similar way, antibiotic-resistant organisms are generally increasing in the environment, which is not only alarming from a public health standpoint but pose risk for the microbial communities and the equilibrium of the ecosystem (Li et al., 2016). Pharmaceutical pollution has already resulted in population-level effects on aquatic organisms stressing the need to take a whole ecosystem approach encompassing multiple species over multiple trophic levels (Miller et al., 2018).

### **1.2.2 Regulations on micropollutants in water resources**

Despite CECs represent a potential threat to ecosystem integrity, the release of CECs from WWTPs into the environment are not traditionally monitored or regulated in water bodies. From a legislative perspective the first steps have been taken concerning the presence of pharmaceuticals in the water cycle in different countries (Rizzo et al., 2019).

The legislation surrounding CECs varies from country to country, and there is no universally agreed-upon framework. Most of studies on the levels of legacy and emerging pollutants in environmental matrices have been performed in US/Canada, Europe, and Asia, while there is an important scarcity of investigations reporting the spatial and temporal trends of these pollutants in Latin America (Vasilachi et al., 2021).

In the European Union, after Directive 2000/60/CE (EU, 2002), which aimed at protecting water resources and recovering water quality in European rivers, the European Parliament approved Decision 2455/2001/CE, which was the pioneer legal document regarding this subject and listed 33 priority substances. Nevertheless, the legislation shared by all European countries is still a topic of discussion, with the monitoring of CECs in WWTP effluents for agricultural reuse being a key point of debate among scientists, policy makers, and stakeholders (Rizzo et al., 2019). To date, the most progressive policies in regulation of CECs have been implemented in Switzerland (Bieber et al., 2016).

For the case of Colombia, there is no specific national legislation that imposes the removal of CEC in MWWTP to prevent surface water contamination. The existing water quality standards and monitoring programs are designed to encompass a wide range of contaminants. To regulate water quality, Colombia has established water quality standards that serve as guidelines for various water uses. Resolution 0631 of 2015, issued by the Ministry of Environment and Sustainable Development (MADS, 2015) establishes the maximum allowable concentrations of various substances and contaminants in water bodies. However, during the formulation of the standard, substances of priority interest, such as CECs, were not considered, and as a result, these substances were excluded from the establishment of permitted thresholds.

### 1.3 Advanced oxidation process applied to the removal of pharmaceuticals

Advanced Oxidation Processes (AOPs) have received growing attention due to their high efficiency in the removal of refractory organic pollutants (Cuerda-Correa et al., 2020). AOPs are considered as an additional and tertiary wastewater treatment as well as treatment applied for the drinking water purification. These processes are based on the in situ generation of powerful and relatively non-selective transient oxidizing species, such as hydroxyl radical ( $\text{HO}^\bullet$ ), sulfate radical ( $\text{SO}_4^{\bullet-}$ ), superoxide radicals ( $\text{O}_2^{\bullet-}$ ), among others. Table 1.1 contains some common oxidizing agents with their relative strengths. The hydroxyl radical is the strongest oxidant after fluorine, that have proven to be efficient in the destruction of many organic compounds due to its reactivity as a reactive electrophile. These radical species can react rapidly and non-selectively with nearly all electron-rich organic compounds (Parsons, 2015).

**Table 1.1** Redox potentials of some oxidizing agents (Parsons, 2015).

| Oxidizing agent                              | Electrochemical oxidation potential (V, 25°C) |
|--|---|
| Fluorine (F)                                 | 2.87  |
| Sulfate radical ( $\text{SO}_4^{\bullet-}$ ) | 2.5-3.1                                       |
| Hydroxyl radical ( $\text{HO}^\bullet$ )     | 2.86  |
| Oxygen atom (O)                              | 2.42  |
| Ozone molecule ( $\text{O}_3$ )              | 2.07  |
| Hydrogen peroxide ( $\text{H}_2\text{O}_2$ ) | 1.78  |
| Chlorine (Cl)                                | 1.36  |
| Chlorine dioxide ( $\text{ClO}_2$ )          | 1.27  |
| Permanganate ( $\text{MnO}_4$ )              | 1.24  |
| Oxygen molecule ( $\text{O}_2$ )             | 1.23  |

AOPs offer advantages over other conventional processes as they do not transfer contaminants to a separate phase and typically do not generate a waste stream. In addition, they require less energy consumption than other processes such as incineration. Some AOPs have

the potential to completely mineralize organic contaminants of effluents, enabling the reuse (Parsons, 2015) .

The most common technologies used to generate free radicals for water treatment are summarized in Figure 1.2. Most of the AOPs are conducted at near ambient temperature and pressure. Generally, these processes involve the integration of oxidizing agents, such as  $H_2O_2$  or  $O_3$ , catalysts, and/or radiation (e.g. ultraviolet, visible) to produce  $HO^\bullet$  radicals in sufficient concentration to effectively achieve water purification (Khan et al., 2020).

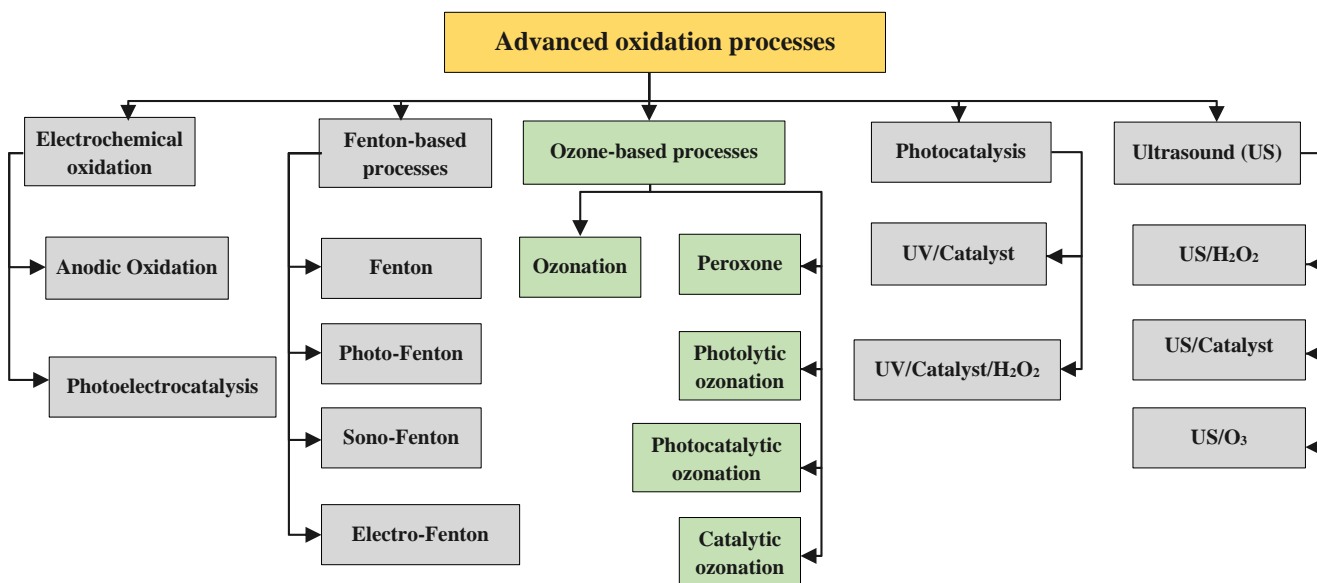


**Figure 1.2.** Schematic representation and classification of different treatments based on advanced oxidation processes (AOPs).

## 1.4 Ozonation

Ozonation is a very attractive technology that has long been employed in the treatment and purification of many types of water and wastewaters. Ozone ( $O_3$ ) is a very powerful oxidizing agent ( $E^\circ = 2.07 \text{ V vs. SHE}$  (standard hydrogen electrode)) able to oxidize a wide range of organic and inorganic contaminants (Beltran, 2003). The high reactivity of ozone can then be attributed to the electronic configuration of the molecule. Therefore, the absence of electrons in one of the terminal oxygen atoms in certain resonance structures confirms the electrophilic nature of ozone as shown in Figure 1.3. Conversely, the excess negative

charge present in some other oxygen atom imparts a nucleophilic character. These properties make ozone an extremely reactive compound (Beltran, 2003).

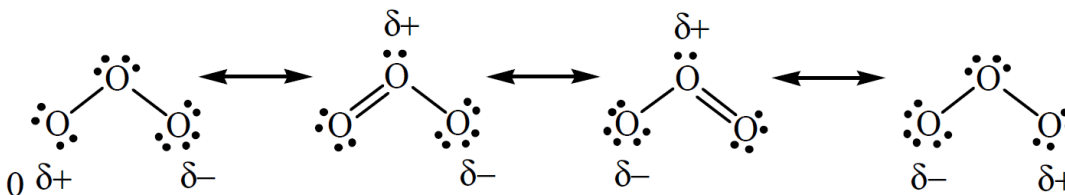
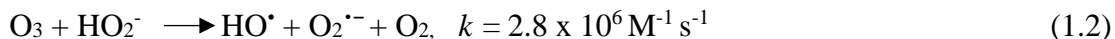


**Figure 1.3** Resonance structures of ozone molecule (Beltran, 2003)

During ozonation, the transformation of organic substances occurs through two distinct mechanisms, direct reaction with dissolved ozone or indirectly by the generation of hydroxyl free radical (von Sonntag and von Gunten, 2012). In the direct oxidation, molecular ozone reacts selectively with compounds electron-rich moieties, such as phenols, activated aromatics, non-protonated amines, and olefins with  $k_{O_3}$  values typically ranging from 1 to  $10^7 \text{ M}^{-1} \text{ s}^{-1}$ . On the other hand, indirect reactions, ozone decomposes to secondary, more reactive, and less selective oxidants, hydroxyl radicals ( $\text{HO}^\bullet$ ) in non-acid pHs (Eq. (1.1)-(1.2)) and which can react with almost all organic molecules ( $k_{\text{HO}^\bullet}$  values are in the order of  $10^9\text{--}10^{10} \text{ M s}^{-1}$  for most of micropollutants) (Staehelin and Hoigne, 1982).



The contribution of each pathway will depend mainly on factors such as the target compound, the pH of the medium, the applied ozone dose, as well as the water composition (Lee et al., 2014). The pH is one of main factors that influenced the ozone decomposition in water. For acid pH (pH <3) hydroxyl ions do not influence in the ozone decomposition, while at basic pH, the rates increases significantly (Beltran, 2003). Regarding the water matrix constitutes, the presence of substances in natural water, such as  $\text{HCO}_3^-$ ,  $\text{CO}_3^{2-}$ ,  $\text{NO}_3^-$ ,  $\text{NO}_2^-$ ,  $\text{Cl}^-$ ,  $\text{Br}^-$  and natural organic matter (NOM) may inhibit or improve the process by scavenging or generating oxidant species, respectively (Lado Ribeiro et al., 2019).

The major disadvantage that limit the ozone application is the low level of mineralization and consequent accumulation of unknown reaction by-products, with stronger refractory character towards further ozone oxidation (Gomes et al., 2017). Therefore, even if initial contaminants can be effectively removed, a low level of mineralization of organic pollutants is hardly achieved. Thus, the effective removal of these species would imply the application of larger ozone doses, which can make the process unaffordable (Cruz-Alcalde et al., 2020). To overcome this shortcoming, research efforts have centered on enhancing the action of ozone on pollutants in order to achieve higher mineralization degrees. Hence the addition of other oxidants, such as hydrogen peroxide, UV radiation or the use of a catalyst, appears to be promising alternatives to promote decomposition of aqueous ozone into HO<sup>•</sup> and consequently improve the ozone process efficiency (Fernandes et al., 2020). Details on the process intensification are presented in the following sections.

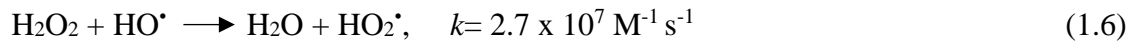
## 1.5 Ozone-advanced oxidation processes

### 1.5.1 Peroxone process

Among the strategy well-studied to improve single ozonation performance, is the O<sub>3</sub>/H<sub>2</sub>O<sub>2</sub> system (also known as peroxone). In this process, ozone decomposition is initiated by the ionic form of hydrogen peroxide (HO<sub>2</sub><sup>-</sup>), by means of electron transfer to initiate the formation of HO<sup>•</sup> precursors according to Eqs. (1.3)-(1.5) (Staehelin and Hoigne, 1985). The O<sub>3</sub>/H<sub>2</sub>O<sub>2</sub> system is considered as both efficient and low-cost process (Gomes et al., 2017).



The efficiency of O<sub>3</sub>/H<sub>2</sub>O<sub>2</sub> systems in the contaminants abatement highly depends on the ratio of ozone to hydrogen peroxide (Pipolo et al., 2017). When this reagent is in excess in the sample it could act as a radical scavenger according to Eq. (1.6), leading to hydroperoxyl radicals with lower reactivity and reducing the process efficiency.



On the other hand, the efficiency of peroxone can be increased by incorporating UV radiation to the system. The three elements that constitute the system can favor the ozone decomposition rate and enhance the  $\text{HO}^\bullet$  production. The addition of light UV to peroxone system could improve the level of organic matter mineralization. However, the high costs associated with UV lamps and reagents pose a notable disadvantage that limits the wide use of this intensification process (Cuerda-Correa et al., 2016).

### 1.5.2 Photolytic ozonation

The UV assisted ozonation ( $\text{O}_3/\text{UV}$ ) also known as photolytic ozonation or photo-ozonation has been another well-researched ozone-based AOP in the CECs removal (Cuerda-Correa et al., 2016; Souza et al., 2018). The  $\text{O}_3/\text{UV}$  may be an effective alternative to oxidize several pollutants, since there can occur three possible interactions: direct ozonation, photolysis of hydrogen peroxide, and the free radicals formed from the ozone–hydrogen peroxide (Beltran, 2003). The combination of ozone with ultraviolet radiation ( $\lambda < 300 \text{ nm}$ ) directly yields  $\text{H}_2\text{O}_2$  due to photolysis of dissolved ozone. Alternatively, the photolysis of  $\text{H}_2\text{O}_2$  formed and/or its reaction with ozone initiates the mechanism of free radical reactions to form two hydroxyl radical according to Eq. (1.7) and Eq. (1.8) (Hart et al., 1983).



The  $\text{O}_3/\text{UVC}$  combination produces large concentrations of hydroxyl radicals in a fast manner, due to ozone strongly absorbs UV light of wavelength 254 nm (when low-pressure mercury-vapor lamps are used) (von Sonntag and von Gunten, 2012), making this technique adequate to achieve higher mineralization degrees (Cuerda-Correa et al., 2016).

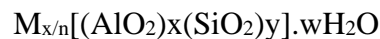


One of the main disadvantages that O<sub>3</sub>/UV processes face is the energy cost, especially when artificial UV radiation sources are applied (Solís et al., 2019). For this reason, the study of solar photo-ozonation has gained increasing interest as an environmentally friendly solution and effectively to enhance ozone decomposition, since operating costs, and energy consumption by UV lamps are avoided.

### 1.5.3 Heterogeneous catalytic ozonation

Catalytic ozonation (O<sub>3</sub>/catalyst) has received remarkable attention as an effective process to enhance ozone action over CECs oxidation and mineralization (Castro et al., 2019; Martins et al., 2015). Catalytic ozonation can be classified in homogenous catalytic ozonation which usually metal ions are used, or heterogeneous catalytic ozonation in which the presence of metal oxides or metal oxide on supports are employed on activation of ozone (Kasprzyk-Hordern et al., 2003).

Recently, zeolites have gained interest in the heterogeneous catalytic ozonation of PhACs, due to its high catalytic activity and their good availability on earth. Zeolite can act as a catalyst in the catalytic ozonation process due to the presence of various metal oxides in its composition (Ikhlaiq et al., 2012). Zeolites can be represented by the structural formula based on a crystallographic unit cell:



where n represents the valence of a cation M, w is the number of water molecules per unit cell, x and y is the number of tetrahedra per unit cell, and the y/x ratio is most often in the range of 1 to 5 (McCusker et al., 2007). The zeolite structure consists of a three-dimensional network of SiO<sub>4</sub> and AlO<sub>4</sub> - tetrahedra interconnected through the silicon or aluminum atoms in the center (T atoms) and the oxygens (O) at the vertices. These tetrahedrons (basic unit) are linked by their oxygen atoms, originating polyhedral structures that constitute the secondary structures. The charge is balanced by the presence of non-framework easily exchangeable cations (McCusker et al., 2007). Among different zeolites, the Faujasite framework is especially present for wastewater treatment due to its substantial adsorption capacity toward different molecules (Reiprich et al., 2020). The framework structure of faujasite zeolites is presented in Figure 1.4.

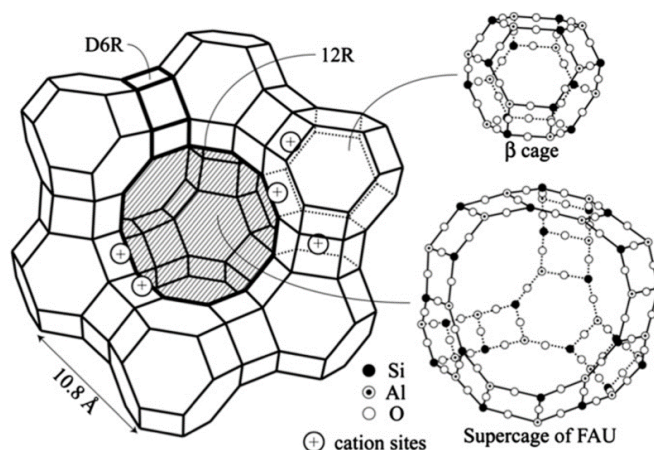


**Figure 1.4** The framework structure of FAU type zeolite (Nozue et al., 2012).

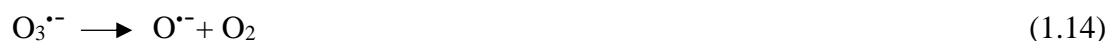
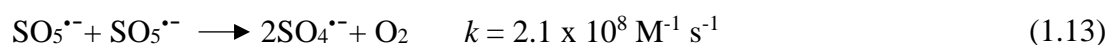
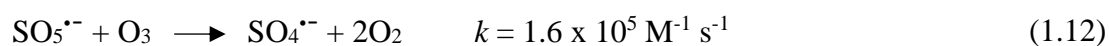
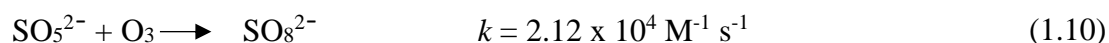
In heterogeneous catalytic ozonation using zeolites three possible reaction paths have been proposed: (i) ozone is adsorbed at the catalyst surface and decomposed to form free radicals and reacting in bulk solution; (ii) the organic compound is adsorbed on the catalyst and is oxidized directly by ozone dissolved; or (iii) adsorption of both ozone and organic compounds with consequent surface reaction (Nawrocki and Kasprzyk-Hordern, 2010). Recently, a different path was proposed by Su et al., (2022), which involves electron transfer between free hydroxide anions and Al atom in oxygen vacancies to form a new coordination bond (Al–OH). The Al–OH groups are also protonated, attacked by ozone molecules and the main reactive oxygen species  $\text{HO}^\bullet$  are generated.

### 1.5.4 Ozone/peroxymonosulfate

In last years, sulfate radical ( $\text{SO}_4^{\bullet-}$  based AOPs) have gained much attention due to some advantages compared to hydroxyl radical AOPs (Deniere et al., 2018; Yu et al., 2021).  $\text{SO}_4^{\bullet-}$  radical is a particularly strong oxidizing species that exhibits higher redox potential ( $E^\circ=2.5\text{--}3.1\text{ V}$ ) (Neta and Dorfman, 1968) and longer half-life than  $\text{HO}^\bullet$  radicals ( $\sim 10^{-9}\text{ s}$  for  $\text{HO}^\bullet$  and  $\sim 10^{-5}\text{ s}$  for  $\text{SO}_4^{\bullet-}$ ) (Yang et al., 2015). Additionally, compared to  $\text{HO}^\bullet$  radical, sulfate radical is relatively less affected by competing constituents in water, such as bicarbonate and NOM in real water, entailing that  $\text{SO}_4^{\bullet-}$  is more favorable to remove high reactive organic pollutants (Lutze et al., 2015; Yang et al., 2015).

As a common source of sulfate radicals, the chemical oxidant peroxymonosulfate (PMS;  $\text{HSO}_5^-$ ) is often used to produce  $\text{SO}_4^{\bullet-}$  radicals. Although PMS is a strong oxidant, it reacts directly with organic compounds at a very low reaction rate (Wang and Wang, 2018). Hence, an appropriate activation method is required. Different activation methods have been proposed including heat, UV irradiation, ultrasound, carbon catalyst, transition metals or metal oxides (Matzek and Carter, 2016; Ren et al., 2015; Wang and Wang, 2018). Recently, ozone has been proven to be effective in activating PMS, demonstrating that its combined role ( $\text{O}_3/\text{PMS}$ ) can significantly enhance the degradation of various organic pollutants (How et al., 2023; Yu et al., 2021). This result has been attributed to the simultaneous generation of  $\text{HO}^\bullet$  and  $\text{SO}_4^{\bullet-}$  during the process (Yang et al., 2015).

The pathway of radical formation is described below (Eqs. (1.10)-(1.15)) (Yang et al., 2015). In the mechanism of reaction, ozone reacts with PMS ( $\text{HSO}_5^-/\text{SO}_5^{2-}$ ) to generate  $\text{SO}_8^{2-}$ , which quickly decompose into precursors of  $\text{HO}^\bullet$  and  $\text{SO}_4^{\bullet-}$  ( $\text{SO}_5^{\bullet-}$  and  $\text{O}_3^{\bullet-}$ ).



## **1.6 Objectives**

### **1.6.1 General objective**

The main goal of this work is to evaluate the potential application of ozone-based advanced oxidation processes for the degradation of pharmaceutical compounds from municipal wastewater.

### **1.6.2 Specific objectives**

1. To evaluate on a bench-scale, the efficiency of different ozone-based AOPs ( $O_3/UVC$ ,  $O_3/H_2O_2$ ,  $O_3/PMS$ ,  $O_3/zeolite\ Y$ ) in terms of the degradation of a model compound in distilled water.
2. To the best ozone-based treatment, identify the main degradation products and evaluate the extent of the treatment in terms of total organic carbon removal and biocompatibility of the treated effluent.
3. To characterize a raw wastewater effluent and evaluate the performance of the selected treatment system in terms of removal of a mixture of pharmaceuticals and environmental risk.
4. To investigate the intensification of the ozone-liquid mass transfer using a tubular porous stainless-steel membrane.
5. To evaluate the performance of the tubular membrane ozonation contactor in the elimination of a mixture of pharmaceuticals in municipal wastewater matrices under continuous flow conditions.

## **1.7 Novelty**

The main contribution of this PhD thesis work is to evaluate, for the first time, the application of the catalytic ozonation using faujasite-type Y zeolite in the removal of pharmaceutical compounds present in real effluents. Additionally, it expands knowledge regarding the evaluation of the performance of an ozone membrane contactor as a potential strategy for the intensification ozone–liquid mass transfer and its application in the removal of PhCs in real wastewater samples.

## **1.8 Thesis outline**

This thesis comprises 5 chapters that have been logically structured to align with the research stages, to meet the above-mentioned objectives.

**Chapter 1** provides the background information about the research problem: the presence of contaminants of emerging concerns in water, specifically related to pharmaceuticals active compounds and their associated environmental risks. Likewise, reviews the ozonation process to degrade CECs and compiles the several ozone-based AOPs as a alternatives to overcome limitations of this technology.

**Chapter 2** presents a description of the experimental procedures and analytical methods followed throughout the research.

**Chapter 3** presents the results of the studies conducted to achieve Objective 1 and Objective 2. Different O<sub>3</sub>-based AOPs are assessed for the elimination and mineralization of an ozone-resistant compound (ibuprofen) in aqueous water. A comparison is also addressed in terms of ozone transfer utilization and energy requirements. The identification of main degradation products are presented for the selected O<sub>3</sub> intensified system.

**Chapter 4** describes the application of catalytic ozonation in the removal of 27 pharmaceuticals present in real effluents from two municipal wastewaters treatment plants of the Mediterranean coast of Spain. The environmental assessment risk associated to pharmaceuticals is also discussed in this chapter.

**Chapter 5** presents the results of the studies conducted to achieve Objective 4 and Objective 5. This chapter provides the characterization of a tubular porous stainless steel membrane contactor in terms of ozone-water mass transport and its application for the removal of 23 pharmaceuticals (PhACs) detected in the secondary-treated municipal wastewater, under continuous mode operation.

## Chapter 2: Materials and methods

This chapter describes in detail the commercial reagents, laboratory procedures, methodologies, and facilities have been used to carry out the experimental plan. They are grouped according to the purpose pursued in the present investigation.

### 2.1 Chemicals reagents

#### 2.1.1 Target pharmaceuticals

In total, 37 pharmaceuticals were selected for this study based on the following criteria: (i) occurrence at relative high concentration in the wastewater effluent, (ii) high consumption by population, and (iii) potential toxicity to health and environment. Relevant data of pharmaceuticals employed in the research are gathered in Table 2.1. All of them were analytical grade standards acquired from Sigma-Aldrich.

**Table 2.1** Main data of selected PhACs

| Compound       | Chemical formula  | (g mol <sup>-1</sup> ) | CAS Number  |
|----------------|---|------------------------|-------------|
| Alprazolam     | C <sub>17</sub> H <sub>13</sub> ClN <sub>4</sub>                  | 308.77                 | 28981-97-7  |
| Atorvastatin   | C <sub>33</sub> H <sub>35</sub> FN <sub>2</sub> O <sub>5</sub>    | 558.64                 | 134523-00-5 |
| Ciprofloxacin  | C <sub>17</sub> H <sub>18</sub> FN <sub>3</sub> O <sub>3</sub>    | 331.35                 | 85721-33-1  |
| Clarithromycin | C <sub>38</sub> H <sub>69</sub> NO <sub>13</sub>                  | 747.95                 | 81103-11-9  |
| Clindamycin    | C <sub>18</sub> H <sub>33</sub> ClN <sub>2</sub> O <sub>5</sub> S | 424.98                 | 18323-44-9  |
| Carbamazepine  | C <sub>15</sub> H <sub>12</sub> N <sub>2</sub> O                  | 236.27                 | 298-46-4    |
| Diclofenac     | C <sub>14</sub> H <sub>11</sub> Cl <sub>2</sub> NO <sub>2</sub>   | 296.15                 | 15307-86-5  |
| Enalapril      | C <sub>20</sub> H <sub>28</sub> N <sub>2</sub> O <sub>5</sub>     | 376.45                 | 75847-73-3  |
| Erythromycin   | C <sub>37</sub> H <sub>67</sub> NO <sub>13</sub>                  | 733.93                 | 114-07-8    |

**Table 2.1** (Continued) Main data of employed PhACs

|                                |  |        |             |
|--------------------------------|--|--------|-------------|
| Gabapentin                     | C <sub>9</sub> H <sub>17</sub> NO <sub>2</sub>                                 | 171.24 | 60142-96-3  |
| 4-hidroxy omeprazole sulfide   | C <sub>16</sub> H <sub>17</sub> N <sub>3</sub> O <sub>2</sub> S                | 315.39 | 103876-98-8 |
| Irbesartan                     | C <sub>25</sub> H <sub>28</sub> N <sub>6</sub> O                               | 428.53 | 138402-11-6 |
| Ibuprofen                      | C <sub>13</sub> H <sub>18</sub> O <sub>2</sub>                                 | 206.29 | 15687-27-1  |
| Iopromide                      | C <sub>18</sub> H <sub>24</sub> I <sub>3</sub> N <sub>3</sub> O                | 791.1  | 73334-07-3  |
| Losartan                       | C <sub>22</sub> H <sub>23</sub> ClN <sub>6</sub> O                             | 422.91 | 114798-26-4 |
| Levamisole                     | C <sub>11</sub> H <sub>12</sub> N <sub>2</sub> S                               | 204.29 | 16595-80-5  |
| Lorazepam                      | C <sub>15</sub> H <sub>10</sub> Cl <sub>2</sub> N <sub>2</sub> O <sub>2</sub>  | 321.2  | 846-49-1    |
| Metronidazole                  | C <sub>6</sub> H <sub>9</sub> N <sub>3</sub> O <sub>3</sub>                    | 171.16 | 443-48-1    |
| Metoprolol                     | C <sub>15</sub> H <sub>25</sub> NO <sub>3</sub>                                | 267.36 | 37350-58-6  |
| Norfloxacin                    | C <sub>16</sub> H <sub>18</sub> FN <sub>3</sub> O <sub>3</sub>                 | 319.33 | 70458-96-7  |
| <i>O</i> -desmethylvenlafaxine | C <sub>16</sub> H <sub>25</sub> NO <sub>2</sub>                                | 263.37 | 142761-12-4 |
| Primidone                      | C <sub>12</sub> H <sub>14</sub> N <sub>2</sub> O <sub>2</sub>                  | 218.25 | 125-33-7    |
| Pantoprazole                   | C <sub>16</sub> H <sub>15</sub> N <sub>3</sub> F <sub>2</sub> O <sub>4</sub> S | 383.37 | 102625-70-7 |
| Phenazone                      | C <sub>11</sub> H <sub>12</sub> N <sub>2</sub> O                               | 188.23 | 60-80-0     |
| Sulfamethoxazole               | C <sub>10</sub> H <sub>11</sub> N <sub>3</sub> O <sub>3</sub> S                | 253.28 | 723-46-6    |
| Trimethoprim                   | C <sub>14</sub> H <sub>18</sub> N <sub>4</sub> O <sub>3</sub>                  | 290.32 | 738-70-5    |
| Tetracycline                   | C <sub>22</sub> H <sub>24</sub> N <sub>2</sub> O <sub>8</sub>                  | 444.44 | 60-54-8     |
| Tramadol                       | C <sub>16</sub> H <sub>25</sub> NO <sub>2</sub>                                | 263.38 | 27203-92-5  |
| Valsartan                      | C <sub>24</sub> H <sub>29</sub> N <sub>5</sub> O <sub>3</sub>                  | 435.52 | 137862-53-4 |
| Venlafaxine                    | C <sub>17</sub> H <sub>27</sub> NO <sub>2</sub>                                | 277.40 | 93413-69-5  |

### 2.1.2 Zeolites

Two commercial Y zeolites with different SiO<sub>2</sub>:Al<sub>2</sub>O<sub>3</sub> ratios (denoted as 60 and 12), H-USY (CBV760) and NH<sub>4</sub>-USY (CBV712), were supplied by Zeolyst International in powder form. For ease of comparison, both zeolite samples were ion-exchanged to the same cation, using an aqueous sodium chloride (NaCl) solution (2.5 mol L<sup>-1</sup>) with a liquid/solid ratio of 10 under stirring for 1 h at 80 °C. After that, zeolite samples were filtered, washed with distilled water, and dried in an oven at 100 °C for 30 min. This process was repeated three times. Finally, the resulting samples were calcined at 450 °C for 3 h. The obtained samples

were named, NaY-60 and NaY-12. The particle size of all the zeolites was in the range of 0.2-0.4 mm.

### **2.1.3 Other chemicals and reagents employed**

Potassium indigotrisulfonate ( $C_{16}H_7K_3N_2O_{11}S_3$ , Sigma-Aldrich) was used to measure ozone dissolved in the aqueous phase. A phosphate-buffered solution ( $NaH_2PO_4$  and  $H_3PO_4$ , Sigma-Aldrich) were used to adjust the pH when required. Acetonitrile (HPLC grade) were provided by Merck. Formic acid (99.0%) and hydrogen peroxide (30% w/v) were provided by PanReac. The ultrapure water (resistivity  $> 18.2 M\Omega\text{ cm}^{-1}$  at 25 °C), supplied by a Milli-Q water system from Millipore (Massachusetts, USA), was used to prepare all chemical solutions. Potassium peroxymonosulfate ( $2KHSO_5KHSO_4K_2SO_4$ , PMS) were purchased from Sigma Aldrich. All chemicals used were of analytical grade and were used without further purification.

## **2.2 Experimental set-ups**

Treatment tests were carried out in three laboratory scale reactors: i) two different bubble columns reactor column diameters, and ii) tubular ozone membrane contactor. Their main characteristics are described below.

### **2.2.1 Bubble column reactors**

#### **2.2.1.1 Bubble column No. 1**

The first part of the experimental work corresponding to objective No.1 was performed in a 1 L glass-jacketed bubble column reactor in semi-batch mode. This reactor was designed and built for this purpose between November 2018 and July 2019 in collaboration with Universidad Nacional de Colombia, campus Medellín, and Universidad de Antioquia.

A detailed scheme of the experimental set up is shown in Figure 2.1, and photographs are presented in Figure 2.2. The reactor was equipped with a low-pressure mercury (40 W) lamp emitting at 254 nm located axially and protected by a quartz sleeve. A water-cooling jacket was placed around the reactor to remove the heat produced by the lamp and to maintain a



constant temperature (~20-22 °C). In order to avoid radiation losses to the outside, the reactor was covered by aluminum foil. The reactor also had three ports at the top for sampling, venting, and measuring the temperature. The ozone stream was provided by a generator (Pinuslongaeva model, China) fed by oxygen concentrator (Respironics EverFlo). The ozone-oxygen mixture was controlled by a gas flow meter and fed into the reactor through a micro-porous plate gas sparger located at the bottom of the column. Ozone concentration in the gas phase entering and leaving the reactor was monitored using O<sub>3</sub> gas analyzer (BMT 964). The residual ozone was collected in a squeeze bottle with a solution of potassium iodide 2% (KI). The volumetric mass transfer coefficient ( $K_L a$ ) of ozone in this reactor was estimated at  $2.5 \times 10^{-2} \text{ s}^{-1}$ .

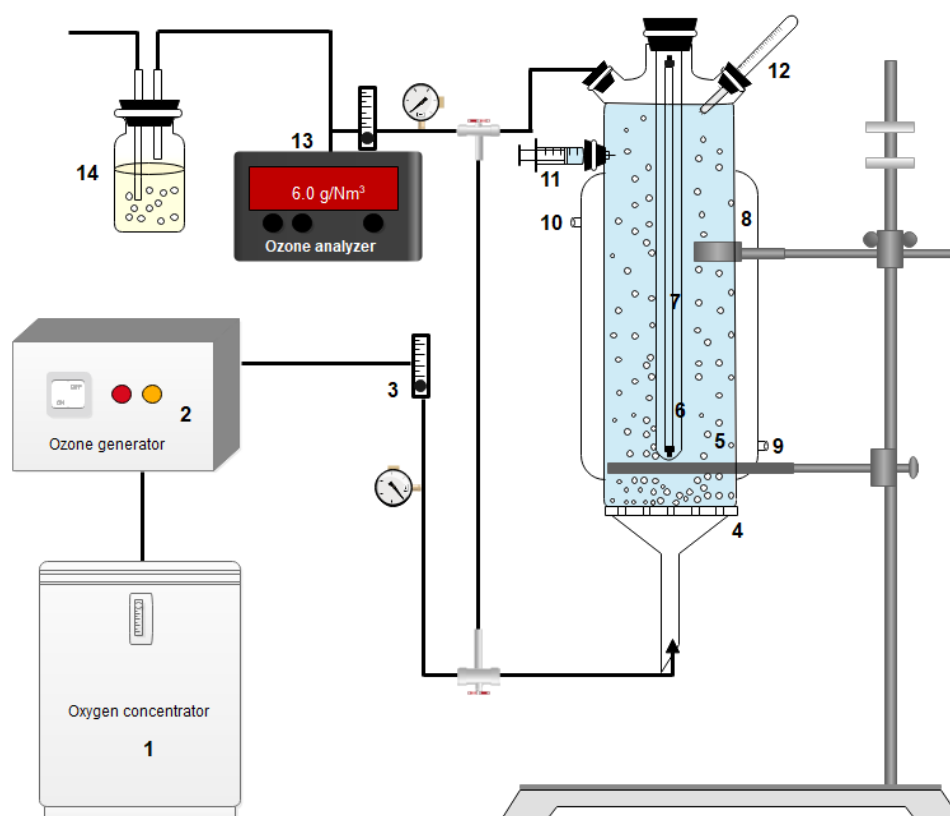


**Figure 2.1** Experimental set-up scheme-bubble column No.1.

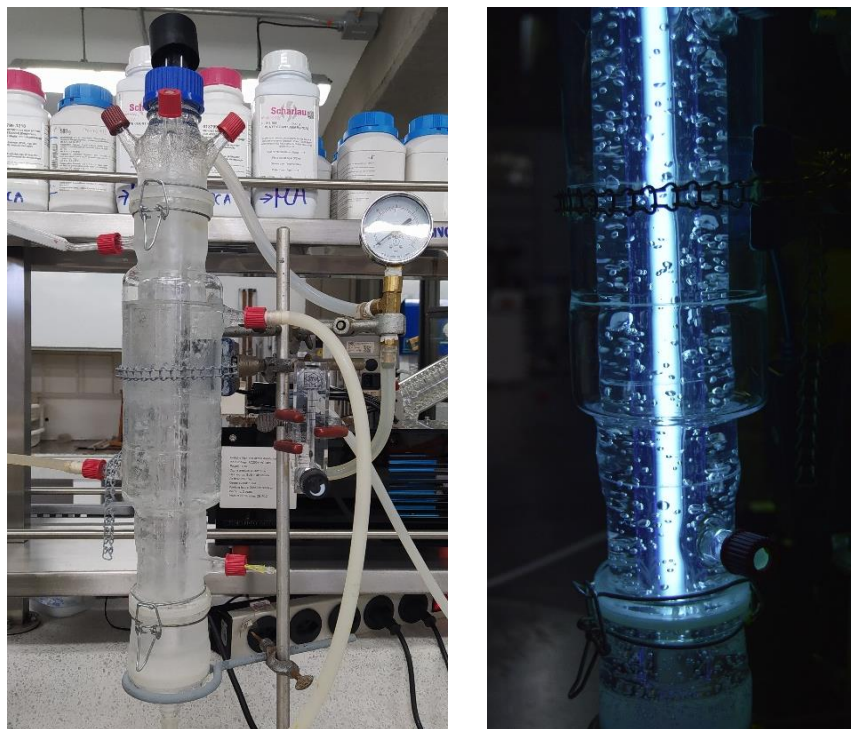


**Figure 2.2** Photographs of bubble column No.1

### 2.2.1.2 Bubble column No. 2

The second part corresponding to catalytic ozonation (objective No. 1) and objectives No. 2 and 3, were conducted in a similar reactor to bubble column No.1, in semi-continuous mode. The experiments were development in the Instituto de Tecnología Química (ITQ) facilities of the Universitat Politècnica de València in Spain. Figure 2.3 illustrates the scheme of the laboratory scale set-up used in the tests. The ozone volumetric mass transfer coefficient of this column reactor was  $2.7 \times 10^{-2} \text{ s}^{-1}$ , very similar that obtained bubble column No.1.

The reactor consists of a glass bubble column with a capacity of 1 L with a diameter of 65mm. The ozone-oxygen gas was produced by an ozone generator (Ozone Solutions, TG-20 model) fed with pure oxygen. The input gas mixture was regulated by digital mass-flow controllers (Bronkhorst) and was continuously bubbled into the aqueous phase through a porous glass plate diffuser located at the bottom of the column reactor. The ozone concentrations at the inlet and the outlet gas streams were measured using a BMT 964 ozone analyzer (BMT Messtechnik GmbH, Berlin, Germany) by switching the valves V4 and V5. Moreover, the pressures were measured at the bottom (P1) and the top (P2) of the reactor

and at the ozone-meter line (P3). The dissolved ozone was measured using an optical probe (Ocean Optics HR4000) connected to the spectrophotometer placed inside the reactor and estimated with the absolute absorbance measurements at 253.7 nm. The ozone residual gas stream was vented through the catalytic O<sub>3</sub> destruction unit before discharging to ambient air. A photograph of this reactor is shown in Figure 2.4.

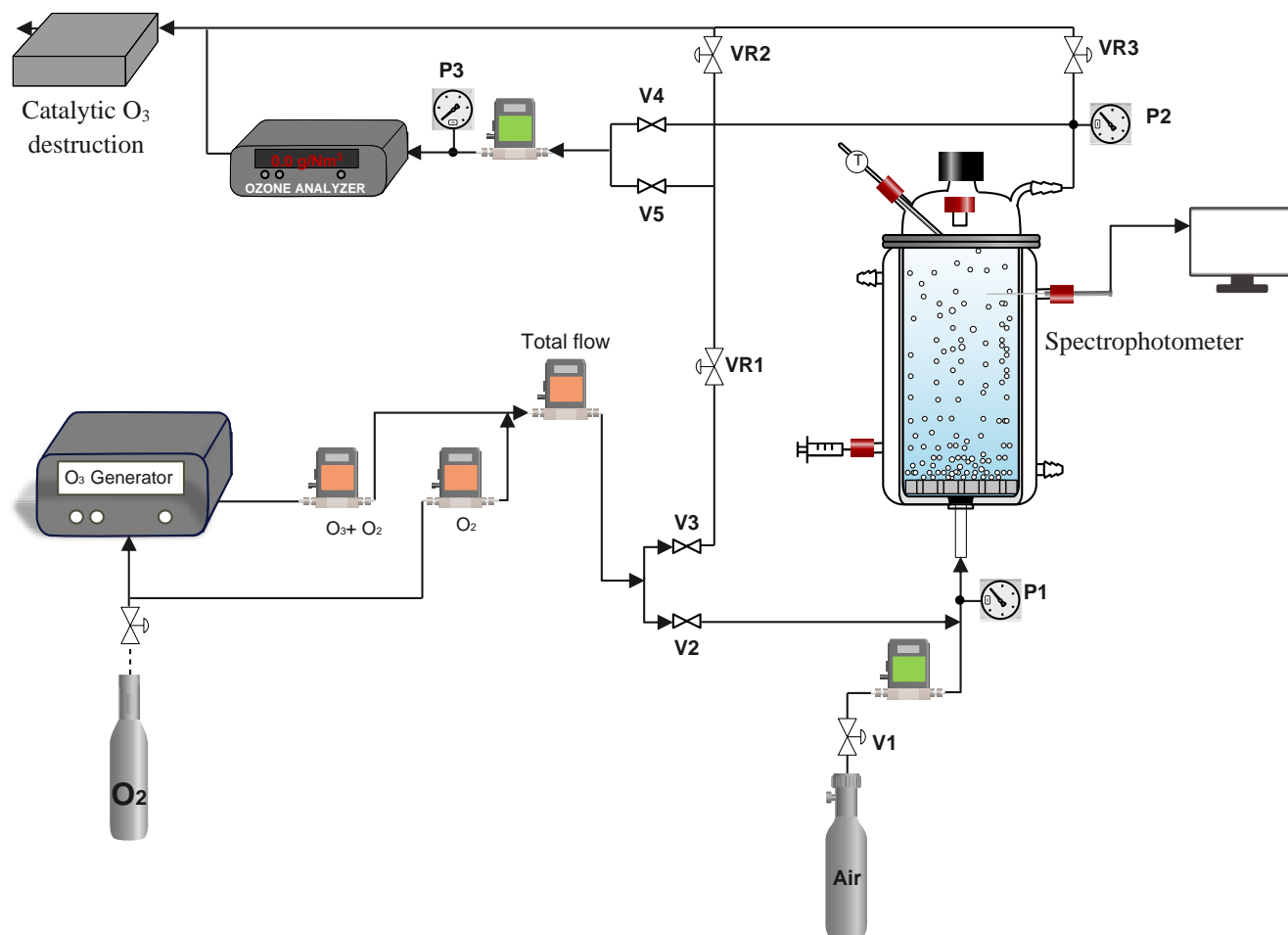


**Figure 2.3** Schematic diagram of ozonation experiment-bubble column No.2

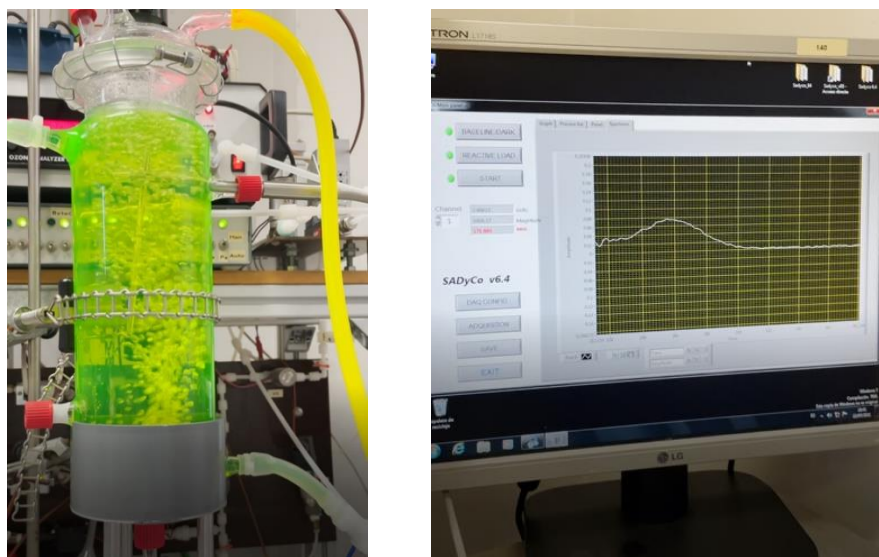


**Figure 2.4** (a) Photograph of the bubble column No. 2 and (b) screenshot of the measurement of dissolved ozone through the optical probe.

### 2.2.2 Tubular ozone membrane contactor

The experimental work corresponding to the objective No. 4 and No. 5 were performed in a tubular ozone membrane contactor in continuous mode operation, in the Laboratory of Separation and Reaction Engineering-Laboratory of Catalysis and Materials (LSRE-LCM) at University of Porto, Portugal.

The ozone contactor consists of an outer quartz tube (outside diameter = 42 mm; internal diameter = 38 mm; length = 200 mm) and a concentric inner tubular membrane made of stainless steel 316L (average pore size = 1  $\mu\text{m}$ ; porosity = 21%; outside diameter = 20 mm; internal diameter = 16 mm; wall thickness = 2.0 mm; useful length = 187 mm; provided by AmesPore®). This material is known to be an austenitic grade of stainless steel highly ozone-resistant (Sleeper & Henry, 2007). Two movable polypropylene flanges are used to seal the membrane, and the quartz tube ends. The tangential inlet and outlet points located in the flanges allow a helical motion of the water in the annular space between both tubes. Ozone-resistant Viton O-rings were used to guarantee sealing conditions within the reaction module. The membrane module was vertically fixed in a stainless-steel structure. Figure 2.5 presents a schematic representation of the experimental setup and photographs are presented in Figure 2.6.

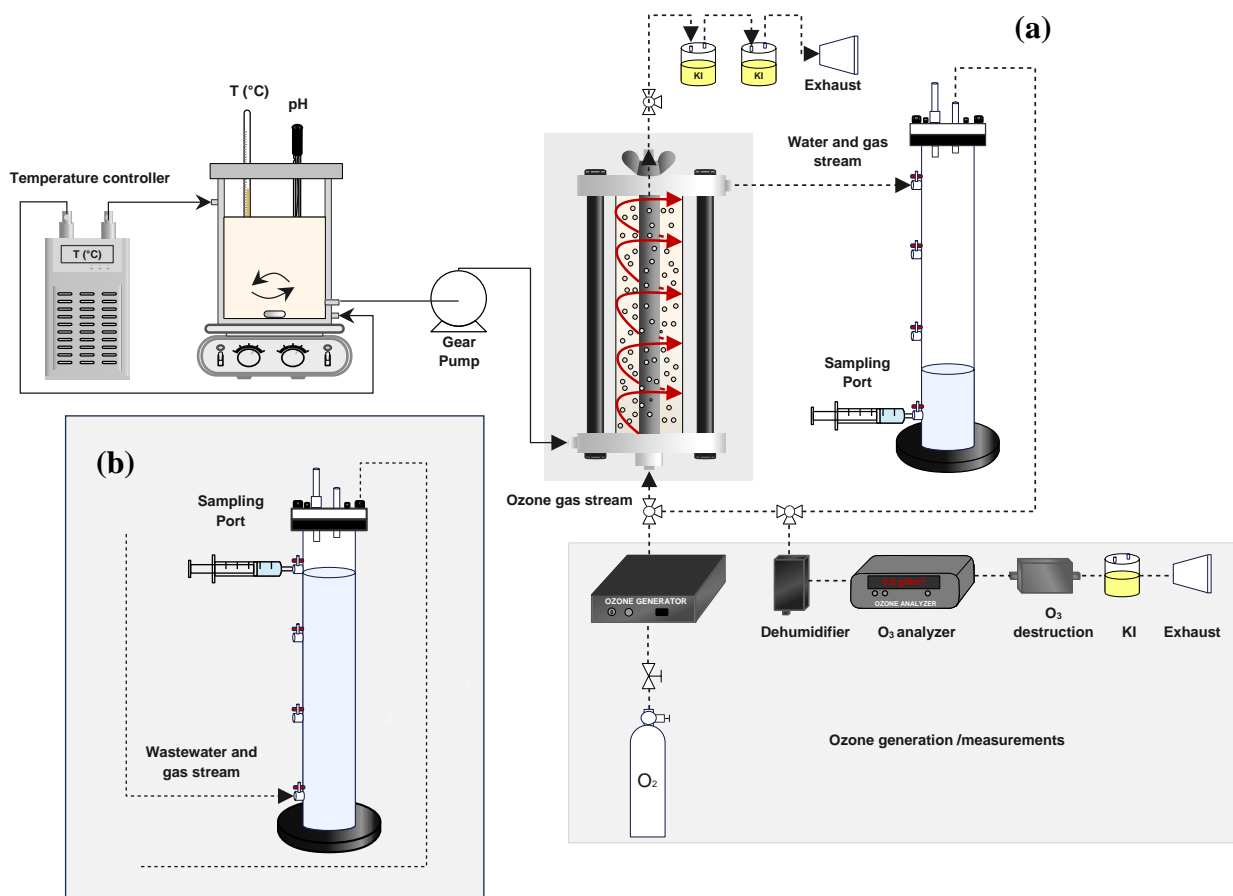


**Figure 2.5** Schematic diagram of the experimental setup used in (a) ozone mass transfer experiments and (b) for PhACs removal tests.

The ozone gas was produced by an ozone generator (BMT 802 N) fed with pure oxygen (O<sub>2</sub>, 99.995% supplied by Air Liquide). The input gas (O<sub>2</sub>) flow rate was regulated by a digital mass flow controller (Alicat Scientific), and the desired O<sub>3</sub> concentration was controlled by adjusting the power input to the ozone generator. An O<sub>3</sub> gas analyzer (BMT 964) was used to monitor the O<sub>3</sub> gas concentration in the inlet and outlet of the membrane reactor. Dissolved O<sub>3</sub> concentration was monitored using the indigo method (Bader and Hoigné, 1981). The ozone-oxygen gas mixture was fed by the lumen side of the membrane, permeating through the pores structure, and delivered to the membrane shell side. Meanwhile, the liquid phase was pumped from a 5 L-jacketed glass vessel, connected to a thermostatic bath for temperature control, to the ARZ of the membrane contactor, where O<sub>3</sub> gas-water contacting occurs. The residual gas was vented through the catalytic O<sub>3</sub>

destruction unit and sequentially to washing bottles containing a 2% KI solution before going into exhaustion.

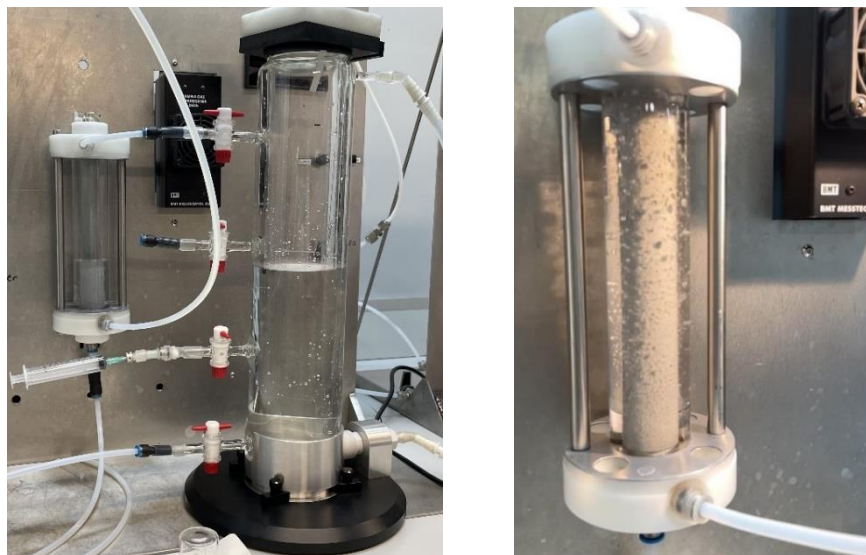


**Figure 2.6** Photograph of the tubular ozone membrane contactor.

## 2.3 Water matrices

### 2.3.1 Distilled water spiked with a model pharmaceutical

This water matrix was used to investigate the efficiency of the ozone-based processes (Objective No.1) without any other chemical interactions, i.e., organic and inorganic constituents commonly present in real water matrices. The non-steroidal anti-inflammatory drug ibuprofen (IBU) was selected as the model compound due to the large consumption and detection frequency in water environments (Chopra and Kumar, 2020). In addition, IBU is known as ozone resistant micropollutant ( $k_{\text{IBU}, \text{O}_3} = 9.6 \text{ M s}^{-1}$ ) and presents a high second-order constant for its reaction with hydroxyl radical ( $k_{\text{IBU}, \text{HO}\cdot} = 7.4 \times 10^9 \text{ M s}^{-1}$ ) (Dodd et al., 2006). The initial IBU concentration in the trials was 40  $\mu\text{M}$  (8.3 ppm).

### 2.3.2 Wastewater sample from WWTPs in Spain

These wastewater effluents were collected from two municipal WWTPs located in the Mediterranean coast from Spain (Figure 2.7), named in this study like Effluent A and Effluent B.



**Figure 2.7** Location of WWTPs where effluent samples were collected.

The plants have a treatment capacity of 36,988 and 38,311 m<sup>3</sup> day<sup>-1</sup> and served a population approximately of 124,852 and 181,806 inhabitants. For both WWTPs the water line includes a pretreatment (roughing filtration, desanding and, degreasing), a primary treatment (primary sedimentation), a conventional activated sludge biological treatment, followed by a tertiary treatment (operated with sand filtration, ultraviolet irradiation, and chlorination). Samples were collected after secondary biological treatment during one typical day of WWTP operation and used for the experimentation tests within the next 3 days. For PhACs quantification, the samples were preserved in the dark at -20 °C until analysis. The effluent samples were characterized by physical chemical analysis. Its main characteristics were: total organic carbon (TOC): 49.61, 67.3 mg L<sup>-1</sup>, dissolved organic carbon (DOC): 47.5, 65.4 mg L<sup>-1</sup>, and total inorganic carbon (TIC): 1.13, 20.3 mg L<sup>-1</sup>, for Effluent A and Effluent B, respectively. The range value of pH was 7.6-7.8.

### **2.3.3 Wastewater sample from WWTP in Portugal**

This water matrix was collected after the secondary biological treatment of a municipal WWTP located in the North of Portugal. This WWTP serves a population of approximately 120,000 equivalent inhabitants. Furthermore, industrial discharges represent around 17% of the estimated total in the low season, and the remaining 83% corresponds to domestic wastewater. The studied WWTP is mainly composed of preliminary treatment (screening, desanding, and degreasing), primary settling, activated sludge biological treatment, followed



by final disinfection using ultraviolet (UV) radiation. The sample was collected during one typical day of WWTP operation after secondary treatment and used for the experimentation tests within the next three days. For PhACs quantification, the samples were preserved in the dark at -20 °C until analysis. A summary of their main quality parameters are gathered in Table 2.2.

**Table 2.2** Physico-chemical characteristics of the municipal wastewater after secondary treatment- WWTP located in Portugal.

| Parameter (units)   | Values       |
|---|--------------|
| Color   | Light yellow |
| pH  | 7.4          |
| Conductivity (mS cm <sup>-1</sup> )   | 1095         |
| Turbidity (NTU)   | 3.7          |
| Total Suspended Solids (mg L <sup>-1</sup> )  | 13           |
| Volatile Suspended Solids (mg L <sup>-1</sup> )   | <0.1         |
| Alkalinity (mg CaCO <sub>3</sub> L <sup>-1</sup> )  | 325          |
| Absorbance at 254 nm (AU)   | 0.273        |
| Dissolved organic carbon (mg L <sup>-1</sup> )  | 15.7         |
| Dissolved inorganic carbon (mg L <sup>-1</sup> )  | 66.4         |
| Total dissolved carbon (mg L <sup>-1</sup> )  | 82.1         |
| Specific Ultraviolet Absorbance (SUVA <sub>254</sub> , L mg <sup>-1</sup> m <sup>-1</sup> ) | 1.74         |
| Chemical oxygen demand (mg O <sub>2</sub> L <sup>-1</sup> )                                 | 70.1         |
| Ammonium – NH <sub>4</sub> <sup>+</sup> (mg L <sup>-1</sup> )                               | 1.2          |
| Nitrite – NO <sub>2</sub> <sup>-</sup> (mg L <sup>-1</sup> )                                | 0.06         |
| Nitrate – NO <sub>3</sub> <sup>-</sup> (mg L <sup>-1</sup> )                                | 9.0          |
| Phosphate – PO <sub>4</sub> <sup>3-</sup> (mg L <sup>-1</sup> )                             | 18           |
| Chloride – Cl <sup>-</sup> (mg L <sup>-1</sup> )  | 141.7        |
| Sulfate – SO <sub>4</sub> <sup>2-</sup> (mg L <sup>-1</sup> )                               | 58.9         |
| Sodium – Na <sup>+</sup> (mg L <sup>-1</sup> )  | 112.9        |
| Potassium – K <sup>+</sup> (mg L <sup>-1</sup> )  | 54.8         |
| Magnesium – Mg <sup>2+</sup> (mg L <sup>-1</sup> )  | 7.7          |
| Calcium – Ca <sup>2+</sup> (mg L <sup>-1</sup> )  | 31.8         |



## 2.4 Analytical methods

### 2.4.1 Determination of pharmaceuticals in wastewater samples

The analysis of the samples was carried out in collaboration with the Research Institute for Pesticides and Waters (IUPA) at Universitat Jaume I (Spain).

The quantitative determination of PhACs in wastewater was performed by liquid chromatography coupled to tandem mass spectrometry (LC-MS/MS) with triple quadrupole (Waters Acquity H-Class UPLC, equipped with a binary pump system, interfaced to a triple quadrupole Xevo TQ-STM mass spectrometer, with ESI source (Waters Corp)). The procedure was based on those previously developed by the IUPA research group (Bijlsma et al., 2021; Botero-Coy et al., 2018), employing direct injection of the (diluted) samples, without any pre-concentration step. In this work, a dilution x2 with ultrapure water was made in order to reduce matrix complexity and to adjust the sample concentrations to the linear dynamic range of the calibration curve. Three MS/MS transitions were acquired for each compound, one for quantification and the remaining ones for confirmation of the identity of the compound. Nearly all compounds had their own analyte-ILIS available for an efficient matrix effects correction (36 ILIS out of 39 compounds).

The analytical procedure was as follows: 2 mL of wastewater sample was centrifuged at 12000 rpm for 3 min. Then, 500  $\mu\text{L}$  aliquot of sample was taken, and 450  $\mu\text{L}$  Milli-Q water and 50  $\mu\text{L}$  of ILIS mix (36 ILIS at 20  $\mu\text{g/L}$  each) were added (final ILIS concentration in the injected samples, 1  $\mu\text{g/L}$ ). Finally, 50  $\mu\text{L}$  were injected into the LC-MS/MS. More details about the analytical methodology can be found in (Botero-Coy et al., 2018).

A common default value of 0.020  $\mu\text{g L}^{-1}$  was used as limit of quantification (LOQ) for all compounds. This value, obtained from the lowest calibration level (0.010  $\mu\text{g L}^{-1}$ ) and considering the dilution factor of the samples in the analytical procedure (x2), was tested to be reached in all sample's batches analysed along this study. Quality control was performed by analyzing Quality Control (QC) samples prepared spiking selected "blank" samples with the target pharmaceuticals at two concentration levels, 0.1 and 1  $\mu\text{g L}^{-1}$ . QCs recoveries between 60 and 140% were considered acceptable, following the spirit of guidelines for residue analyses (European Commission, 2021). At least two QCs, at low and high level, were analyzed together with the samples in every sample batch.

### **2.4.2 Determination of ibuprofen in distilled water**

The concentration of ibuprofen was quantified by means of an ultra-high performance liquid chromatograph (UHPLC, Thermo Scientific Dionex UltiMate 3000 instrument) equipped with an Acclaim™ 120 RP C18 column (5 µm, 4.6 x 150 mm) and a diode array detector. The mobile phase consisted of 70:30 volumetric mixtures of acetonitrile and ultrapure water (with formic acid 10 mM and pH 3.0). The injection volume of the sample was 100 µL and a flow rate of 1.0 mL min<sup>-1</sup>. The UV detection was performed at 225 nm.

### **2.4.3 Identification of degradation intermediates**

The detection of ibuprofen transformation products was carried out in collaboration with the Research Institute for Pesticides and Waters (IUPA) at Universitat Jaume I (Spain). The transformation products were elucidated by high liquid chromatography coupled with quadrupole-time of flight mass spectrometry (UHPLC-QTOF MS) using a Waters Acquity UHPLC system (Waters, Milford, MA, USA). Equipment was coupled to hybrid quadrupole-orthogonal acceleration-time of flight mass spectrometer (XEVO G2 QTOF, Waters Micromass, Manchester, UK), with an orthogonal Z-spray electrospray interface, operated in negative ion modes.

The mobile phases used were (A) water and (B) methanol, both containing 0.01% (v/v) acid formic. The percentage of organic modifier (B) was changed linearly as follows: 0 min, 10%; 9 min, 90%; 11 min, 90%; 11.1 min, 10%; 14 min, 10%. The flow rate was 0.3 mL min<sup>-1</sup>. The MS apparatus was operated in positive and negative ionization modes under the following conditions: capillary voltages of 0.7 kV and -1.7 kV, respectively, a cone voltage of 25 V was applied, the interface temperature was set to 650 °C and the source temperature to 130 °C. The column and sample temperatures were set at 40 °C and 5 °C, respectively. More details about the analytical methodology can be found in Boix et al., (2016).

### **2.4.4 Dissolved ozone concentration**

The ozone concentration in water was determined by the colorimetric indigo method described by Bader and Hoigné (Bader and Hoigné, 1981) based on the reaction between ozone and indigo trisulfonate assuming a 1:1 stoichiometry. To determine the ozone

concentration in samples, two indigo solutions were prepared: *i*) Indigo stock solution, prepared by dissolving 770 mg of potassium indigotrisulfonate in 1 L of ultrapure acid water (0.1 % (v/v) of phosphoric acid, and storage a 4 °C. *ii*) Indigo reagent II, prepared by dissolving 10 g of monosodium phosphate (NaH<sub>2</sub>PO<sub>4</sub>) in 1 L of ultrapure acid water (0.7 % (v/v) of phosphoric acid) containing a 10 % of Indigo stock solution. The analysis was performed by preparing a vial with 3 mL of Indigo reagent II and adding 2 mL of sample. The sample was shaken and immediately the absorbance of the mixture was measured at 600 nm using a cuvette with a 1 cm path length. As a blank, a sample prepared under identical conditions was used but adding 2 mL of distilled water.

The concentration of ozone was determined as a function of the absorbance difference of the indigo after and previous the reaction with ozone followed at 600 nm, according to Eq. (2.1):

$$C_{O_3,l}(M) = \frac{(Abs_{600,blank} - Abs_{600,sample}) V_T}{\epsilon_{indigo} \cdot l V_S} \quad (2.1)$$

where  $C_{O_3,l}$  is the ozone concentration given in mol L<sup>-1</sup>;  $Abs_{600,blank}$  is the absorbance at 600 nm of the blank;  $Abs_{600,sample}$  is the absorbance of the sample at 600 nm,  $\epsilon_{600}$ , the molar absorptivity of indigo trisulfonate (20000 M<sup>-1</sup> cm<sup>-1</sup>),  $l$ , the optic path length ( $l=1$  cm);  $V_T$ , the total volume of the sample (5 mL) and  $V_S$ , the volume of the sample (2 mL).

### 2.4.5 Total organic carbon

The concentration of total organic carbon (TOC) was determined using a Shimadzu TOC-VCSN TOC analyzer, coupled with autosampler system. This equipment determines the total dissolved carbon (TDC) and the dissolved inorganic carbon (DIC) present in the sample, providing the TOC value by difference of the previous measurements. Dissolved organic carbon (DOC) was calculated as the difference between the TDC and the DIC values of the same aqueous sample. The TDC analysis is based on the catalytic combustion (Pt/Al<sub>2</sub>O<sub>3</sub>) of the sample at 680 °C, conditions in which the carbon that is part of the organic and inorganic compounds is oxidized to CO<sub>2</sub>. This is subsequently analyzed using a non-dispersive infrared (NDIR) detector, generating a peak whose area is proportional to the amount of carbon present in the sample.

Prior to the analysis of the samples, the equipment was calibrated using standard solutions (in Milli-Q ultrapure water) of potassium acid phthalate (for TDC) and anhydrous sodium carbonate (for TIC). Calibration straight lines were prepared between 0 and 20 mg L<sup>-1</sup> for both, as well as another straight line between 0 and 100 mg L<sup>-1</sup> for potassium acid phthalate. Each water sample in this research was measured in duplicate by two independent injections.

#### **2.4.6 Wastewater characterization**

Chemical oxygen demand (COD) was determined by the dichromate closed reflux method according to the SMEWW - 5220 D test, digested in a WTW CR4200 thermoreactor, followed by photometric measuring (Merck Spectroquant® Prove 300 UV/Vis spectrophotometer). The concentration of inorganic anions and cations was measured by ion chromatography (Dionex ICS-2100 LC) equipped with an IonPac® AS11-HC 250 mm × 4 mm column (T = 30 °C) and a self-regenerating anion suppressor (ASRS® 300, 4 mm) under an isocratic elution of 30 mM KOH at a flow rate of 1.5 mL min<sup>-1</sup>. Inorganic cations were also evaluated by ion chromatography in a Dionex DX-120 LC coupled with an IonPac® CS12A 250 mm × 4 mm column at ambient temperature and a CSRS® Ultra II cation self-regenerating suppressor (4 mm) under an isocratic elution of 20 mM methanesulfonic acid at a flow rate of 1.0 mL min<sup>-1</sup>. The ultraviolet (UV) absorbance was determined with a Merck Spectroquant® Prove 300 UV/Vis spectrophotometer. pH, temperature and conductivity were measured by HI 9829 Multiparameter portable meter from Hanna Instruments. Analyses for total suspended solids (TSS) and turbidity were carried out according to Standard Methods for the Examination of Water and Wastewater (APHA, 1998).

#### **2.4.7 Catalyst characterization**

Textural properties of the tested zeolites were obtained from the N<sub>2</sub> adsorption/desorption isotherms using an ASAP 2420 apparatus (Micromeritics) at 77 K. Prior to the measurements, 200 mg of each pelletized sample (0.25 -0.40 mm) were degassed at 673 K with high vacuum (~5 × 10<sup>-6</sup> bar) overnight. The specific surface area (S<sub>BET</sub>) was determined

by using the Brunauer- Emmett-Teller equation (BET), whereas micropore volume ( $V_{\text{micro}}$ ) was estimated by the t-plot method.

The crystalline phase of the powder solids was detected based on the X-ray diffraction (XRD) by a PANalytical CUBIX diffractometer using filtered  $\text{CuK}\alpha$  radiation ( $\lambda = 0.1542$  nm), with accelerating voltage 45 kV, intensity of 40 mA and scanned at  $2\theta$  from 2 to  $90^\circ$ . Acidic properties of two zeolite samples were investigated by Fourier transformed Infrared (FTIR) spectroscopy using pyridine as a probe molecule. Pyridine adsorption–desorption experiments were measured using on a Nicolet 710 FTIR spectrometer (Thermo Scientific, Waltham, Massachusetts, USA). The samples (10-15 mg) were pressed to obtain a self-supported wafer, and previously pretreated at  $400^\circ\text{C}$  under vacuum overnight. Upon activation, the samples were exposed to pyridine vapor (650 Pa) in the cell at room temperature. The excess of pyridine was removed in vacuum and desorption process were conducted increasing the temperature to 150, 250 and  $400^\circ\text{C}$ . The IR spectrum of the samples after activation and desorption were recorded at room temperature. Concentration of acid sites were quantified according to (Emeis, 1993) by the integration of the band intensities at 1545 and  $1450\text{ cm}^{-1}$  for Brønsted and Lewis sites, respectively. The pH of point zero charge ( $\text{pH}_{\text{pzc}}$ ) of zeolites was determined using the pH drift method (Eberle et al., 2022). The study was performed in 50 mL tubes containing suspensions of the zeolite (0.1 g) and 25 mL of a  $0.1\text{ mol L}^{-1}$  NaCl solution. The pH levels of the solutions in the tubes were adjusted to values ranging from 3 to 11, using 0.1 M HCl or 0.1 M NaOH solutions. These initial pH values were denoted as ( $\text{pH}_i$ ). The tubes were agitated for 24h at room temperature. Then, the final pH ( $\text{pH}_f$ ) values of solutions were then measured, and  $\text{pH}_{\text{pzc}}$  was then determined by plotting  $\Delta\text{pH}$  ( $\Delta\text{pH} = \text{pH}_f - \text{pH}_i$ ) vs.  $\text{pH}_i$ .

#### **2.4.8 Environmental risk assessment**

The toxicological risk level associated of the target pharmaceuticals released by WWTP effluents was assessed through the determination of risk quotient (RQ). The RQ values were calculated according to the European Community Guidelines (Commission, 2003), as the ratio between predicted environmental concentrations (PEC) and predicted no-effect concentration (PNEC) values, using Eq. (2.2).

$$RQ = \frac{PEC}{PNEC} \quad (2.2)$$

PNEC represents the concentration of a substance below which adverse effects will most likely not occur during long or short-term exposure. PEC values were estimated from measured concentration (MC) for each pharmaceutical compound in both wastewater samples and calculated (according to Eq. (2.3)) by taking into account that the final effluents of the WWTPs are discharged and diluted into freshwater ecosystems. In this sense, a dilution factor (DF) is considered. In the case of Spain, the DF value correspond to 25.92 according to (Keller et al., 2014). The PNEC values used in this study were collected from literature sources. The RQ of the mixture (total risk) was also calculated by summing the individual RQ of each component.

$$PEC = \frac{MC}{DF} \quad (2.3)$$

In general, the RQ value are classified into three risk levels: (i)  $RQ \leq 0.1$  indicate a low environmental risk; (ii)  $0.1 < RQ \leq 1$  indicate a moderate environmental risk; and (iii)  $RQ > 1$  reveal a high environmental risk.

## **Chapter 3. Evaluation of different ozone-based AOPs in terms of elimination of a model compound in aqueous solution**

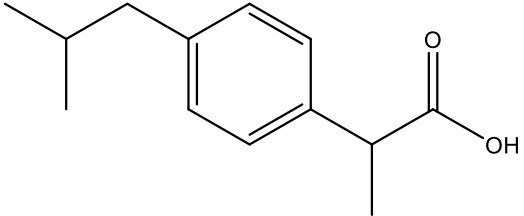
### **3.1 Introduction**

Pharmaceuticals have become an issue of great concern due to the increasing consumption worldwide and their continuous discharge into the aqueous systems (Herrmann et al., 2015). Ibuprofen (IBU), a nonsteroidal anti-inflammatory drug (NSAID), is widely used for the treatment of inflammatory and painful diseases, listed among the essential medicines by the World Health Organization (WHO, 2021). Their main physicochemical properties are summarized in Table 3.1. Globally, IBU has become the third most popular highly prescribed medicine and the second most manufactured with a production rate of 15,000 tons per year (Chopra and Kumar, 2020). Due to this increasing demand, IBU is one of the most commonly detected drugs in WWTP effluents, surface water, groundwater, and drinking water (aus der Beek et al., 2016). It has been identified up to concentrations of 25 mg L<sup>-1</sup> in WWTP effluents (Naima et al., 2022). IBU residues have been shown to act as a carcinogenic and endocrine-disrupting compound that can reduce the viability of algae and have adverse effects on the reproduction, kidney, and liver of fish (Brillas, 2022).

The pervasive existence of micropollutants in water and their potential toxicity underscore the need to develop effective technologies for the removal of PhACs from wastewater.

Advanced oxidation processes (AOPs) represent an effective option to degrade a wide variety of organic compounds, mainly characterized by the formation of powerful and non-selective species, such as hydroxyl radicals (HO<sup>•</sup>) (Miklos et al., 2018; Rizzo et al., 2019).

**Table 3.1** Physicochemical properties of ibuprofen. Taken from: [www.chemicalize.org](http://www.chemicalize.org)

|                   |  |  |
|-------------------|--|--|
| Molecular formula | C <sub>13</sub> H <sub>18</sub> O <sub>2</sub> | Chemical structure:  |
| Molar mass        | 206.285 g mol <sup>-1</sup>                    |  |
| pKa               | 4.85   |  |
| Water solubility  | 21 mg L <sup>-1</sup> at 25°C                  |  |
| Log Kow           | 3.97   |  |

For decades, ozonation has been a widely used technology for treating refractory organic pollutants in water/wastewater due to the high oxidative potential of ozone (Beltrán, 2004). The O<sub>3</sub> molecule can oxidize pollutants either by direct and selective reaction or by an indirect mechanism through the generation of HO• radicals, especially under alkaline pH conditions (Staelin and Hoigne, 1982; von Sonntag and von Gunten, 2012). Nevertheless, due to its selective oxidation property, ozonation alone often results in incomplete degradation of the organic compounds and the consequent accumulation of unknown reaction by-products (Gomes et al., 2017). These ozone-refractory compounds can only be removed by HO• radical due of their extremely low reaction rate constants with O<sub>3</sub> (von Sonntag and von Gunten, 2012). In this sense, researchers have focused their efforts on exploring ways to intensify or improve the efficiency of ozonation processes.

There are several strategies to enhance the generation of HO• radicals in ozonation, including the addition of other oxidants (such as H<sub>2</sub>O<sub>2</sub> or PMS), UV radiation, or a catalyst (Prada-Vásquez et al., 2021). These combined processes, known as ozone-based AOPs, can reduce operating costs, reaction time to achieve the same degradation efficiency with an increased degradation rate and higher mineralization levels (Almeida et al., 2022).

Recently, various studies on the degradation of IBU by different ozone-based AOPs have been reported. Jing et al., (2023) found that adding UV irradiation into 0.6 mg L<sup>-1</sup> of O<sub>3</sub> increased the IBU degradation rate by 10 times, subsequently achieving a superior mineralization result. Additionally, the authors found that the cost of O<sub>3</sub>/UV process was most acceptable compared to the individual processes, under the same IBU degradation target. Yuan et al., (2017) investigated the capacity oxidation of O<sub>3</sub>/PMS and found that the combined process demonstrated a compelling degradation ability towards IBU compared with single ozonation. This was attributed to the simultaneous generation of HO• and SO<sub>4</sub><sup>•-</sup>



radicals during the process. Saeid et al., (2018) studied the degradation of IBU by non-catalytic and catalytic ozonation using Beta zeolites. Authors found that the presence of zeolite catalysts improved the IBU decomposition rate significantly in the aqueous environment, probably due to the amount of Brønsted and Lewis acid sites in the zeolite.

According to the literature, the intensification of ozone through the presence of an oxidant, a catalyst, or UV light, has already been proven to significantly enhance the removal rate of the micropollutant and the mineralization degree. However, comparative studies between different ozone intensification processes in terms of chemical performance are still scarce. Hence, this study intends to provide new insights into these systems and evaluates how combinations of various O<sub>3</sub>-based AOPs, enhance ozone mass transfer efficiency in the degradation of an ozone-recalcitrant compound.

In this chapter, different O<sub>3</sub> processes intensified homogeneously (O<sub>3</sub>/UVC, O<sub>3</sub>/H<sub>2</sub>O<sub>2</sub>, O<sub>3</sub>/PMS) or heterogeneously intensified system (O<sub>3</sub>/zeolite) were assessed for IBU degradation, analyzing several parameters such as IBU concentration, mineralization level, ozone utilization efficiency, and energy consumption. Furthermore, the most promising one was chosen for further investigation in the elucidation of IBU transformation products.

## **3.2 Experimental procedure**

The experiments were conducted in a 1 L glass column reactor (Figure 2.1) in semi-batch mode, containing 900 mL of aqueous solution of IBU (40 μM). The ozone-oxygen mixture was manually controlled by a flowmeter and fed into the reactor through a micro-porous plate gas sparger located at the bottom of the column, with a gas flow rate of 0.7 L min<sup>-1</sup> and containing 6.0 mg O<sub>3</sub> L<sup>-1</sup>. For the O<sub>3</sub>/H<sub>2</sub>O<sub>2</sub> and O<sub>3</sub>/PMS combination, experiments were performed the same way as the ozone trials with the addition of H<sub>2</sub>O<sub>2</sub> or PMS to the reaction before the addition of ozone. Different H<sub>2</sub>O<sub>2</sub>/O<sub>3</sub> and PMS/O<sub>3</sub> molar ratios (0.25, 0.5 and 1.0) were tested. For the O<sub>3</sub>/UV experiments were performed in same reactor, equipped with a low-pressure mercury (40 W) lamp emitting at 254 nm located axially and protected by a quartz sleeve. The UV lamp was warm for 20 min before testing to water. More details are described in Section 2.1.1.

For the heterogenous ozone intensification (O<sub>3</sub>/zeolite), 0.2 g L<sup>-1</sup> of zeolite was added to the reaction prior to the addition of ozone. Adsorption experiments were performed with the

same experimental system mentioned above, but ozone and catalyst were not used. Liquid samples were withdrawn through a sampling port at different times, (ensuring that the sampled volume never exceeded 10% of initial reactor volume) and quenched with the addition of sodium thiosulfate ( 0.1 M, 1 mL) to remove residual dissolved ozone. All the experiments were performed in duplicate to ensure reproducibility. All samples were filtered by a 0.45 µm filter membrane for further analysis. For O<sub>3</sub>, O<sub>3</sub>/UVC and catalytic ozonation, the experiments were performed without adjustment at an initial pH value of the solution 6.0 and room temperature. In the case of O<sub>3</sub>/H<sub>2</sub>O<sub>2</sub> and O<sub>3</sub>/PMS experiments, pH was adjusted to pH 6.0 using NaOH and HCl.

### 3.3 Calculation of ozone mass balance

In order to compare the efficiency of the ozone intensification treatments, the IBU removal was evaluated as a function of ozone consumption considering Eqs. (3.1)-(3.4) presented by (Gottschalk et al., 2010) for semi-batch systems as follows:

Applied ozone dose, AO<sub>3</sub>D (mg O<sub>3</sub> L)

$$AO_3D = \int_0^t \frac{Q_G C_{O_3,g,in} dt}{V_L} \quad (3.1)$$

Transferred ozone dose, TO<sub>3</sub>D (mg O<sub>3</sub> L)

$$TO_3D = \int_0^t \frac{Q_G}{V_L} (C_{O_3,g,in} - C_{O_3,g,out}) dt \quad (3.2)$$

Consumed ozone dose, CO<sub>3</sub>D (mg O<sub>3</sub> L)

$$CO_3D = TO_3D - C_{O_3,l,out} \quad (3.3)$$

Utilization ozone efficiency, UO<sub>3</sub>E , (%)

$$UO_3E = \frac{CO_3D}{AO_3D} \times 100 \quad (3.4)$$

where  $Q_G$  is the gas flow rate ( $L \text{ min}^{-1}$ ),  $V_L$  is the volume of the reaction mixture (L),  $C_{O_3,g,in}$  and  $C_{O_3,g,out}$  are ozone concentrations at the inlet and outlet of the reactor, ( $mg \text{ L}^{-1}$ ) respectively.

## 3.4 Results and discussion

### 3.4.1 $O_3$ intensified by UVC light

In order to understand the combined effect of ozone and UVC light on the performance of IBU degradation, UVC photolysis,  $O_3$  and  $O_3$ /UVC experiments were performed (Figure 3.1). As can be observed, direct photolysis operating under UVC irradiation promoted the removal of IBU with high efficiencies, reaching 89% of elimination after 30 min of exposure ( $k = 0.07 \text{ min}^{-1}$ ; Figure 3.1b inset). The high efficiency of the photolytic system can be attributed to the overlapping of the emission spectrum of the UVC lamp (100–280 nm with a maximum emission at 254 nm) with the absorption spectrum of IBU (absorption up to 240 nm with a  $\lambda_{max}$  at 224 nm) (da Silva et al., 2014). This result is in agreement with those reported by Adityosulindro et al., (2022). Furthermore, this behavior can also be attributed to the formation of  $HO^\bullet$  radicals directly from the homolysis of water molecules by the 185 nm irradiation that then can react with IBU molecule (Szabó et al., 2011).

Compared with UVC photolysis, the efficiency of single ozonation was much lower, and only 67 % of IBU was removed after 30 min ( $k = 0.036 \text{ min}^{-1}$ ). This can be explained by the absence of reactive groups towards ozone in the IBU chemical structure and an aromatic ring that is only slightly activated (Huber et al., 2003). This result was also consistent with the low reaction rate constant of IBU with ozone ( $k_{IBU, O_3} = 9.6 \text{ M s}^{-1}$ ) (Dodd et al., 2006). Since the ozonation experiments were performed at an initial pH of 5.6, the direct molecular ozone attack may have partially contributed to the oxidation of IBU.

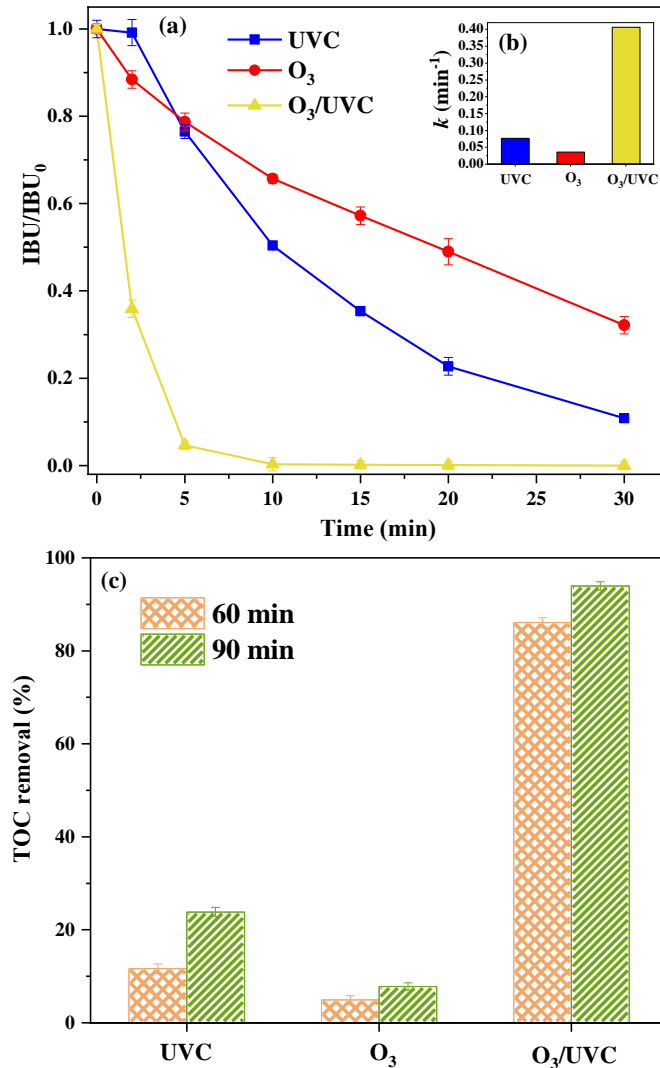


**Figure 3.1** (a) Evolution of the normalized concentration of IBU (b) kinetics and (c) mineralization via UVC, O<sub>3</sub>, and O<sub>3</sub>/UVC processes.

When UVC light was introduced into ozonation system, reaction rates was faster than during ozonation and UVC alone, especially in the first 5 min. In fact, 95% removal of IBU was reached within 5 min of reaction and above 99% after 10 min. The fast abatement of IBU is mainly ascribed to the fact that UV irradiation ( $\lambda < 300$  nm), provides an additional reaction (formation of H<sub>2</sub>O<sub>2</sub> due to photolysis of dissolved O<sub>3</sub>) that accelerates ozone rate decomposition. This, in turn, leads to the generation of more HO<sup>•</sup> radicals via Eqs. (1.7)-(1.9) (Hart et al., 1983).

The mineralization of IBU was also monitored through TOC analysis and the results are shown in Figure 3.1c. Single UV and O<sub>3</sub> processes could not effectively mineralize the IBU

compound, leading to approximately 23.8% and 7.8% TOC removal after 90 min of reaction, respectively. The low mineralization of  $O_3$  is due to the presence of compounds resistant to  $O_3$  attack, such as carboxylic acids, in which molecular ozone cannot completely oxidize these short-chain saturated compounds, and as a result, they remain in solution. Direct reactions with ozone will play a minor role during ozonation processes, and the oxidation of these compounds are mainly due to  $HO^\bullet$  radicals that originate from ozone decomposition (Huber et al., 2003). The combination of  $O_3$  with UVC significantly improved TOC removal, reaching 93% TOC elimination after 90 min reaction. This further confirms the extent of  $HO^\bullet$  radical contribution in the total organic matter removal in the  $O_3$ /UVC combination.

On the other hand, in the  $O_3$ /UV system, the rate of  $O_3$  mass transfer/consumption is generally enhanced by the UVC light (Garoma and Gurol, 2004). Figure 3.2a displays the measured inlet and outlet ozone gas concentrations as a function of time during IBU oxidation in both  $O_3$  systems. It can be observed, that  $O_3$  concentrations in the off-gas differed significantly during single ozonation and photolytic ozonation. At the end of the IBU reaction (30 min), the outlet gas concentrations of the single ozonation, and photolytic ozonation reached 5.87 and 1.5  $mg\ L^{-1}$ , respectively. In the same way, lower dissolved  $O_3$  concentrations were observed during  $O_3$ /UVC than single ozonation (see Figure 3.2b inset). The lower concentration of ozone in the gas and liquid phase at the  $O_3$ /UVC combination confirms that the UVC light considerably accelerated the decomposition of ozone depletion, resulting in more ozone being absorbed in the solution and consequently the generation of more  $HO^\bullet$  radicals.

Based on the difference between  $O_3$  concentrations in the inlet and off-gas during the experiments, the transferred  $O_3$  doses (Figure 3.2c) was 5.6 times higher during the  $O_3$ /UVC system (102  $mg\ L^{-1}$ ) than during individual ozonation process (18  $mg\ L^{-1}$ ). Consequently,  $O_3$  utilization efficiencies were significantly increased from 12.4 % for conventional ozonation to 71.3% for photolytic ozonation. These findings indicate that the  $O_3$ /UVC system not only enhances the  $HO^\bullet$  yield from  $O_3$  decomposition but also improves the ozone transfer and consumption during photolytic ozonation. This improvement allowed for higher IBU abatement compared to single ozonation.

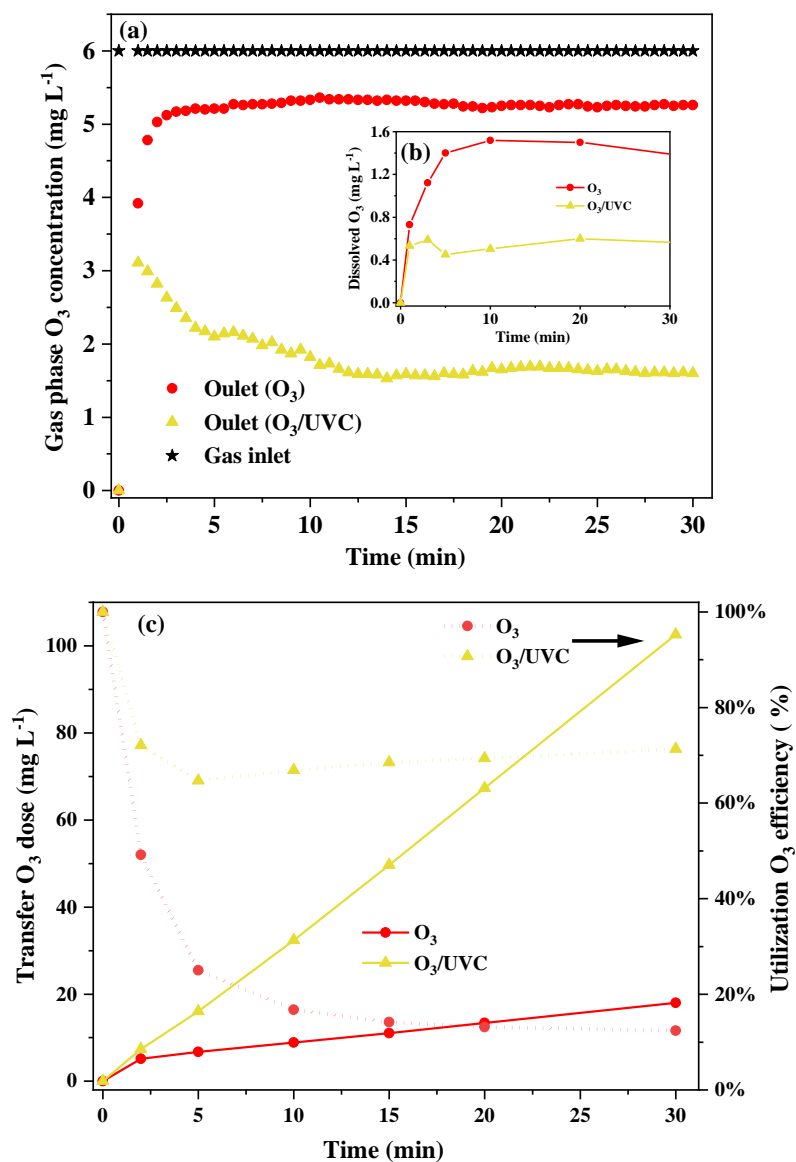


**Figure 3.2** Evolution of (a) gas phase ozone concentrations at the reactor inlet and outlet, (b) dissolved ozone concentration, (c) transfer  $O_3$  doses and utilization  $O_3$  efficiency as a function of reaction time during IBU ozonation and photolytic ozonation.

### 3.4.2 $O_3$ intensified by an oxidant

#### 3.4.2.1 Effect of $H_2O_2/O_3$ and PMS/ $O_3$ molar ratios

The  $O_3$  intensified process by oxidants were conducted through the comparison of two systems,  $O_3/H_2O_2$  and  $O_3/PMS$  in the performance of IBU elimination. The initial set of

experiments investigated the effect of different molar ratios  $\text{H}_2\text{O}_2/\text{O}_3$  (Figure 3.3a) and  $\text{PMS}/\text{O}_3$  (Figure 3.3c) on the degradation of the model compound.

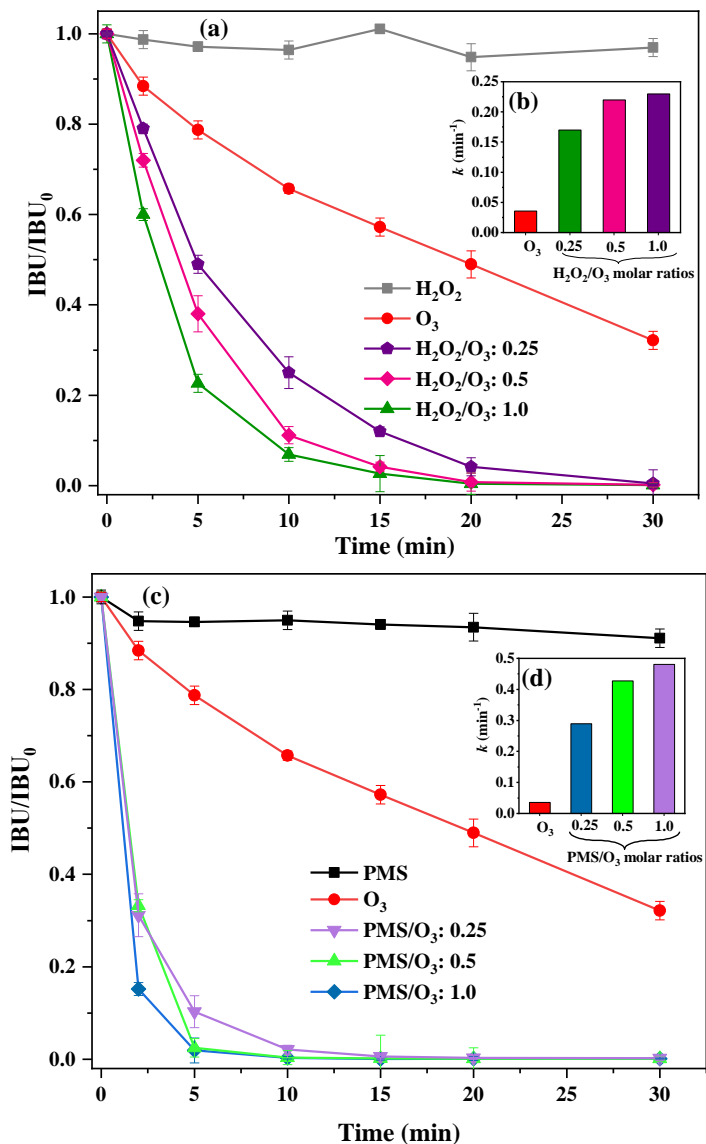


**Figure 3.3** Effect of (a)  $\text{H}_2\text{O}_2/\text{O}_3$  molar ratios and (c)  $\text{PMS}/\text{O}_3$  molar ratios and their the pseudo-first-order rate constant (inset figure, (c)  $\text{H}_2\text{O}_2/\text{O}_3$ , (d)  $\text{PMS}/\text{O}_3$ ).

The results indicated that higher dosages of  $\text{H}_2\text{O}_2$  and PMS led to an increased in IBU degradation. For the case of  $\text{O}_3/\text{H}_2\text{O}_2$ , after 5 min, IBU removal increased from 51% employed the lowest  $\text{H}_2\text{O}_2:\text{O}_3$  molar ratio of 0.25 (0.09 mM  $\text{H}_2\text{O}_2$ ) to 77% using  $\text{H}_2\text{O}_2:\text{O}_3$  molar ratio of 1.0 (0.88 mM  $\text{H}_2\text{O}_2$ ). This result is consistent with previous studies that who reported higher removal efficiency at an  $\text{H}_2\text{O}_2:\text{O}_3$  ratio molar of 1.0 and 0.5 (Cruz-Alcalde

et al., 2020). For the O<sub>3</sub>/PMS system increasing PMS dosage results in higher degradation efficiency towards IBU. As depicted in Figure 3.3, the pseudo-first-order rate constant improved from 0.29 to 0.48 min<sup>-1</sup> with increasing PMS/O<sub>3</sub> molar ratio from 0.25 to 1.0. Yuan et al., (2017) observed similar results and found that increasing PMS dosage caused the enhancement of IBU efficiencies. Authors also reported that concentrations of PMS in excess would cause self-quenching of radical species and reducing the degradation levels. It is important to mention that a 4-fold increase in the H<sub>2</sub>O<sub>2</sub> and PMS concentration did not improve, the same increasing factor in the removal of IBU. Hence, the following results presented were adopted to the H<sub>2</sub>O<sub>2</sub>:O<sub>3</sub> and PMS:O<sub>3</sub> molar ratio of 0.5.

### 3.4.2.2 Comparison of O<sub>3</sub>/H<sub>2</sub>O<sub>2</sub> and O<sub>3</sub>/PMS

With the addition of oxidants such as H<sub>2</sub>O<sub>2</sub> and PMS in the ozonation process, the IBU removal was significantly increased by 6.4 and 13.3 times, respectively, compared to single ozonation. In terms of the effectiveness of the two oxidants, the degradation rate of IBU was significantly faster in O<sub>3</sub>/PMS ( $k = 0.48 \text{ min}^{-1}$ ) than O<sub>3</sub>/H<sub>2</sub>O<sub>2</sub> combination ( $k = 0.23 \text{ min}^{-1}$ ), reaching removal rates of 98% and 77 % after 5 min, respectively. Meanwhile, a low removal of IBU was achieved under H<sub>2</sub>O<sub>2</sub> alone (less than 3 % removal) and PMS alone (less than 9 % removal) after 30 min.

As depicted in Figure 3.4 the O<sub>3</sub>/PMS was found to be more efficient in enhancing the IBU mineralization level (78%) when compared to the O<sub>3</sub>/H<sub>2</sub>O<sub>2</sub> process (31%) after 90 min. This results reveal that PMS in presence of O<sub>3</sub> have obvious synergistic effects on the degradation of total organic matter. This positive effect can be attributed to the fact that by adding PMS during ozonation, ozone can react directly with PMS, producing both HO<sup>•</sup> and SO<sub>4</sub><sup>•-</sup> radicals, as shown in Eqs. (1.10)-(1.15) (Yang et al., 2015). Furthermore, when HO<sup>•</sup> reacts with organic compounds, it involves OH-addition and H-abstraction mechanism. At the same time, SO<sub>4</sub><sup>•-</sup> follows a one-electron transfer mechanism, which facilitates the decarboxylation reactions and thus results in more efficient mineralization performance (Liu et al., 2013).

Regarding the O<sub>3</sub>/H<sub>2</sub>O<sub>2</sub> coupled system, the hydroxyl radicals generated were the active species responsible during IBU oxidation (Eqs. (1.3)-(1.5)). Thus, 33% more IBU was eliminated by O<sub>3</sub>/H<sub>2</sub>O<sub>2</sub> compared to the O<sub>3</sub> alone system due to the generation of HO<sup>•</sup> radicals. Previous studies reported that during oxidation of IBU by O<sub>3</sub>/PMS and O<sub>3</sub>/H<sub>2</sub>O<sub>2</sub>



systems both  $\text{HO}^\bullet$  and  $\text{SO}_4^{\bullet-}$  radicals were detected in  $\text{O}_3/\text{PMS}$ , and only  $\text{HO}^\bullet$  radicals were found in  $\text{O}_3/\text{H}_2\text{O}_2$  (Yuan et al., 2017).

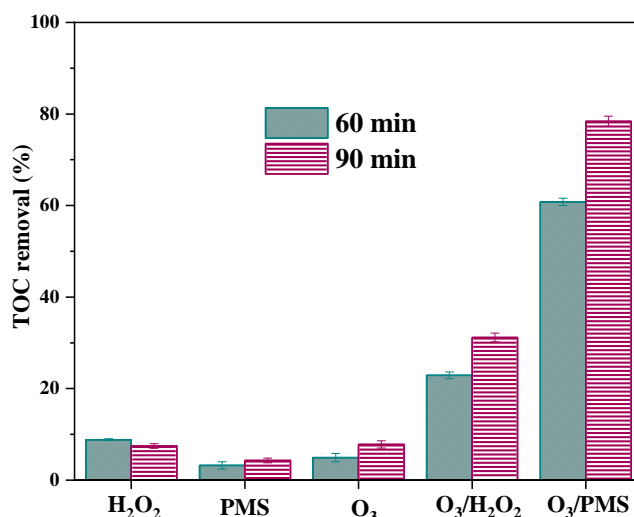


**Figure 3.4** Mineralization level of IBU via  $\text{H}_2\text{O}_2$ , PMS,  $\text{O}_3$ ,  $\text{O}_3/\text{H}_2\text{O}_2$  and  $\text{O}_3/\text{PMS}$  processes.

On the other hand, to explore the role of oxidants in the ozone mass transfer efficiency/consumption, the change of gas-off and liquid ozone concentrations with time were also recorded, and results are presented in Figure 3.5. It can be observed that the introduction of PMS and  $\text{H}_2\text{O}_2$  oxidants to the ozonation system decreased the off-gas  $\text{O}_3$  concentration during the first 15 min, reaching values of  $4.63 \text{ mg L}^{-1}$  and  $5.13 \text{ mg L}^{-1}$ , respectively. Interestingly, after 15 min of reaction, the outlet gas concentration for  $\text{O}_3/\text{H}_2\text{O}_2$  continued to rise, while it remained similar and almost constant for three ozone coupled systems ( $5.4 \text{ mg L}^{-1}$ ). This demonstrates that the ozone utilization efficiency gradually decreased in both systems.

The evolution of dissolved ozone concentration had a similar tendency, in which for  $\text{O}_3/\text{H}_2\text{O}_2$  and  $\text{O}_3/\text{PMS}$ , a lower  $\text{O}_3$  aqueous concentration was observed peaking at  $1.28 \text{ mg L}^{-1}$  and  $0.98 \text{ mg L}^{-1}$ , respectively. Therefore, as less ozone escapes into the air and ozone concentrations in aqueous solutions are reduced, it demonstrates that oxidants play an essential role in the decomposition of ozone into active radicals, particularly for the  $\text{O}_3/\text{PMS}$  system.

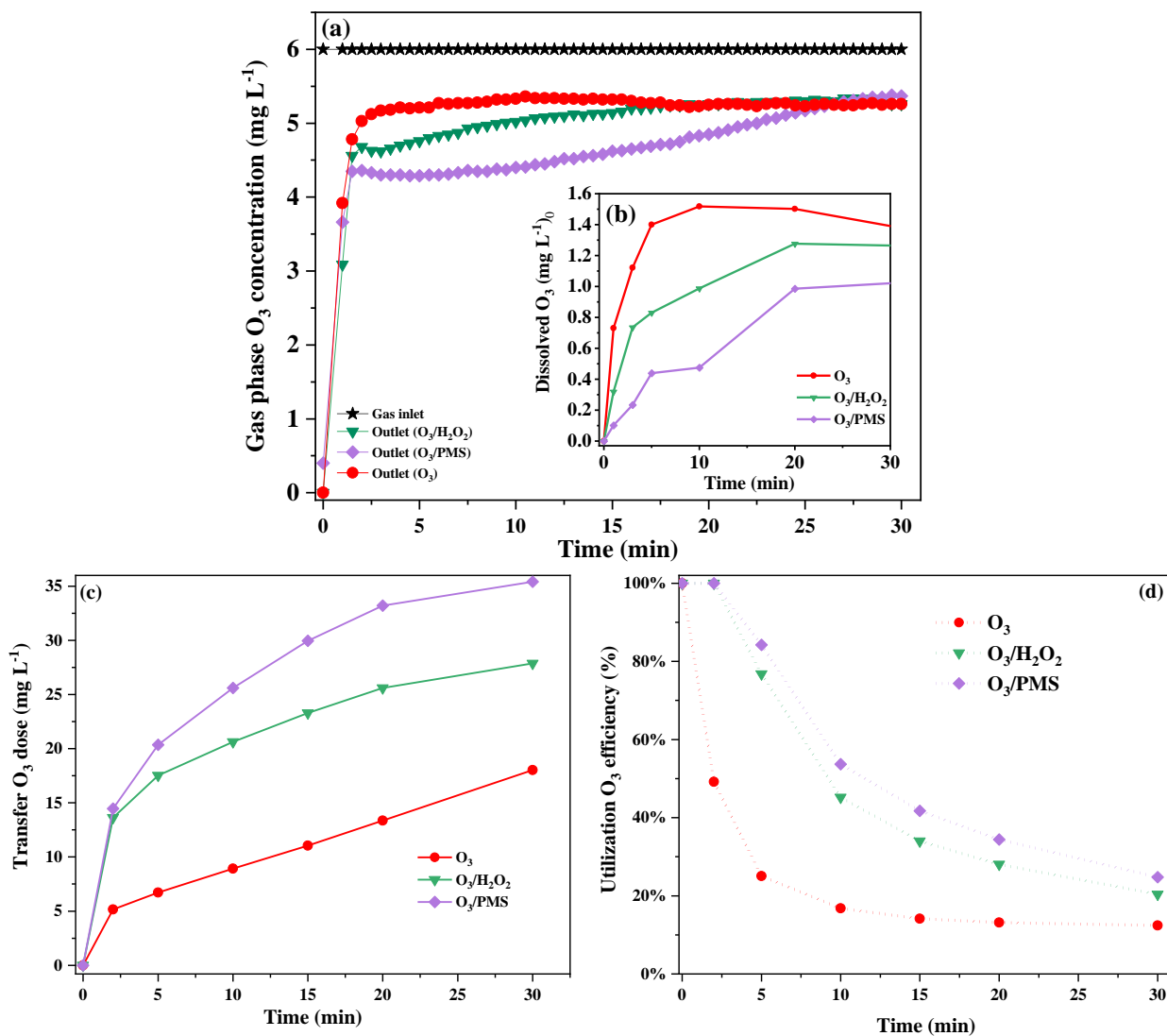


**Figure 3.5** Evolution of (a) gas phase  $O_3$  concentrations at the reactor inlet and outlet, (b) dissolved ozone concentration, (c) transfer  $O_3$  doses and (d) utilization  $O_3$  efficiency as a function of reaction time during IBU ozonation.

Likewise, Figure 3.5c indicates that for the same treatment time, higher  $O_3$  doses were transferred, from 18  $mg O_3 L^{-1}$  during single ozonation to 35  $mg O_3 L^{-1}$  and 28  $mg O_3 L^{-1}$  during  $O_3/PMS$  and  $O_3/H_2O_2$ , respectively. On comparing the ozone systems in terms of ozone utilization efficiency (Figure 3.5d), it was observed that adding chemical oxidants to ozonation could also improve the ozone utilization efficiency by a factor of ~4.5-5 times compared to ozonation alone, specifically at the beginning of the reaction (10 min). However, at the end of reaction,  $UO_3E$  decreased to reach a value of 12.4 %, 20.4% and

24.7% for O<sub>3</sub>, O<sub>3</sub>/H<sub>2</sub>O<sub>2</sub> and O<sub>3</sub>/PMS, respectively. Both oxidants in the presence of ozonation presented similar percentages of UO<sub>3</sub>E, indicating that the enhanced IBU abatement during O<sub>3</sub>/PMS may be mainly driven by the higher HO<sup>•</sup> and SO<sub>4</sub><sup>•-</sup> yields in the solution than by the enhancement of O<sub>3</sub> transfer efficiencies.

### 3.4.3 O<sub>3</sub> intensified by a zeolite catalyst

In this section, the ozonation of ibuprofen was investigated in the presence of two Y zeolites (belonging to the Faujasite family) with similar structures and different SiO<sub>2</sub>/Al<sub>2</sub>O<sub>3</sub> ratios. Firstly, the material characterization was assessed to understand its physicochemical properties and gain better insights into its behavior during catalytic ozonation reactions.

#### 3.4.3.1 Characterization of zeolites

The surface area, pore structure, and pore volume of the Y zeolites were investigated using the nitrogen adsorption–desorption test, and the obtained results were analyzed using BET isotherm (Table 3.2).

**Table 3.2** Properties of NaY zeolites samples including specific surface area ( $S_{\text{BET}}$ ), external surface area ( $S_{\text{ext}}$ ), micropore area ( $S_{\text{micro}}$ ), micropore volume ( $V_{\text{micro}}$ ), mesopore volume ( $V_{\text{meso}}$ ), pore size and SiO<sub>2</sub>/Al<sub>2</sub>O<sub>3</sub> mol ratio.

| Sample  | $S_{\text{BET}}$<br>(m <sup>2</sup> g <sup>-1</sup> ) | $S_{\text{external}}$<br>(m <sup>2</sup> g <sup>-1</sup> ) | $S_{\text{micro}}$<br>(m <sup>2</sup> g <sup>-1</sup> ) | $V_{\text{micro}}$<br>(cm <sup>3</sup> g <sup>-1</sup> ) | $V_{\text{meso}}$<br>(cm <sup>3</sup> g <sup>-1</sup> ) | Pore size<br>(nm) | pH <sub>pzc</sub> | SiO <sub>2</sub> /Al <sub>2</sub> O <sub>3</sub><br>mol ratio |
|---------|---|--|---|--|---|-------------------|-------------------|---|
| NaY- 60 | 762   | 92.13  | 670.18  | 0.33   | 0.16  | 2.8               | 7.1               | 60  |
| NaY-12  | 587   | 94.13  | 492.99  | 0.24   | 0.13  | 3.0               | 6.5               | 12  |

The specific surface area and micropore volume of NaY-60 and NaY-12 zeolites samples were 762 and 587 m<sup>2</sup> g<sup>-1</sup>, 0.33 and 0.24 cm<sup>3</sup> g<sup>-1</sup>, respectively. As can be seen from the results, the surface area and micropore volume of the zeolite samples decreased in the order of increasing aluminum content.

The zeolites were also characterized by XRD to determine the crystal properties and lattice parameters of the catalyst. Figure 3.6 shows the XRD patterns of the samples prepared with different  $\text{SiO}_2/\text{Al}_2\text{O}_3$  molar ratios (60 and 12). All samples gave similar XRD patterns and matched well with the Faujasite-type zeolite structure (JCPDS card No. 00-045-0437). The XRD data revealed that there is not contribution of amorphous material, indicating Y zeolite constituent phase crystal structure as the major product obtained. The distinct diffraction peaks observed at  $2\theta$  values of  $12.0^\circ$ ,  $20.6^\circ$ ,  $23.9^\circ$ ,  $27.4^\circ$ ,  $31.8^\circ$ ,  $54.8^\circ$  correspond to (311), (440), (533), (642), (751) and (997) of the crystal planes, respectively.

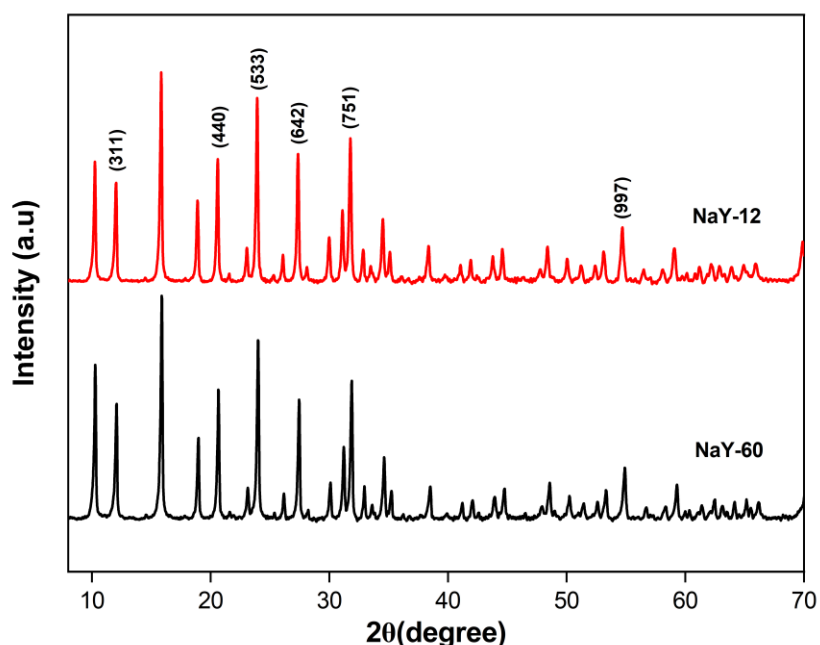


**Figure 3.6** X-ray diffraction pattern of NaY zeolite with  $\text{SiO}_2/\text{Al}_2\text{O}_3$  mole ratio 12 and 60.

The amount of Brønsted (B) and Lewis (L) acid sites of zeolites samples have been analyzed by FTIR, and they are summarized in Table 3.3. It was observed that both zeolite samples had Lewis (L) and Brønsted acidity sites (B). However, the NaY-12 zeolite sample showed the strongest surface acidity. As expected, the total amount of acid sites increases by increasing the alumina content (Saeid et al., 2018). Moreover, for both zeolite samples, the ratio of B/L was more than 1, indicating the total Brønsted acid sites were the main acid sites.

**Table 3.3** Brønsted and Lewis acidities of zeolite samples.

| Catalyst | Brønsted acidity<br>( $\mu\text{mol g}^{-1}$ ) |        |        | Lewis acidity<br>( $\mu\text{mol g}^{-1}$ ) |        |        |
|----------|--|--------|--------|---|--------|--------|
|          | 150 °C   | 250 °C | 350 °C | 150 °C                                      | 250 °C | 350 °C |
| NaY-60   | 64   | 14     | 8      | 35  | 10     | 7      |
| NaY-12   | 121  | 61     | 21     | 71  | 47     | 39     |

### 3.4.3.2 Removal of ibuprofen by catalytic ozonation

The removal efficiencies of IBU by adsorption, catalytic ozonation using NaY-60 and NaY-12 zeolites are presented in Figure 3.7. It can be observed that IBU removal by adsorption into NaY-60 zeolite reached the maximum of removal of 47.8% after 5 min, while NaY-12 zeolite just reached 4.1% within 30 min. One of the main reasons for the difference in adsorption capacities of the two zeolites can be attributed to the silica (Si) and aluminum (Al) ratios. Zeolites with a high Si/Al ratio (lower Al content) provide a greater hydrophobic surface and exhibit a higher adsorption capacity than the zeolites of the same framework with a low Si/Al ratio (Chen, 1976). Hence, the increased adsorption efficiency of IBU by NaY-60 could thus be related to the hydrophobicity of this high-silica zeolite. Moreover, the adsorption capacity of zeolites can also be well-correlated to their microporous volume (Koubaissy et al., 2011). Indeed, NaY-60 was found to have 1.4 times larger micropore volume than NaY-12 zeolite.

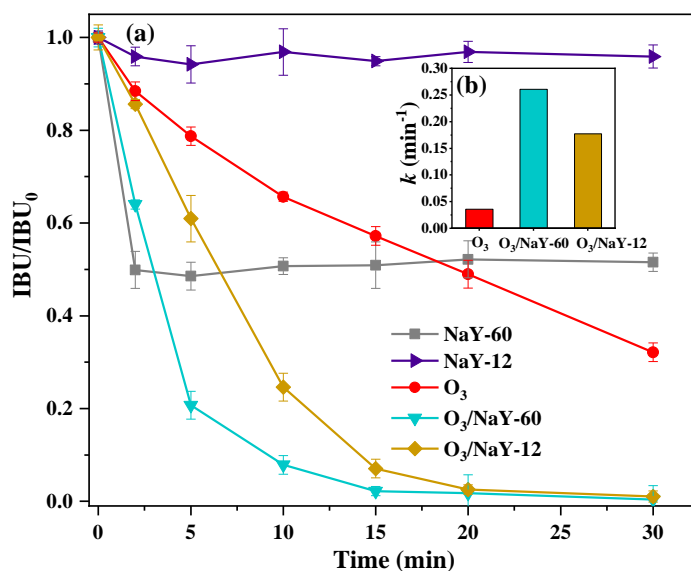


**Figure 3.7** (a) Evolution of the normalized concentration of IBU via O<sub>3</sub>/NaY-60, O<sub>3</sub>/NaY-12, and their control experiments, (b) the pseudo-first-order rate constants.

The addition of zeolite catalysts to ozonation system indicated that the use of NaY zeolites promoted the reaction between ozone and led to a faster IBU depletion, achieving 97.7% ( $k = 0.26 \text{ min}^{-1}$ ) and 92.3% ( $k = 0.18 \text{ min}^{-1}$ ) of IBU removal within 15 min for O<sub>3</sub>/NaY-60 and O<sub>3</sub>/NaY-12, respectively. This improvement in the IBU rate oxidation in catalytic ozonation (a 5-fold increase compared to single ozonation) confirms that NaY zeolites can act as initiators/promoters of the ozone decomposition process, enhancing the formation of HO<sup>•</sup> radicals in the solution.

By comparing the performance of two NaY zeolites in presence of ozonation, it can be observed that O<sub>3</sub>/NaY-12 system exhibited a lower degradation rate compared to the O<sub>3</sub>/NaY-60 combination. However, the negligible adsorption observed with the NaY-12 control demonstrated that NaY-12 showed a higher synergistic effect in terms of IBU removal and mineralization level. This result can be related to the Lewis and Brønsted acid sites of zeolites, which have been demonstrated to promote ozone decomposition and lead to the formation of free hydroxyl radicals (Alejandro et al., 2011; Valdés et al., 2009). For the particular ozone resonance structure, this molecule can react as a dipole, showing an electrophilic (Lewis acid) or nucleophilic (Lewis base) character that determines its adsorptive behavior and reaction mechanism (Kasprzyk-Hordern et al., 2003). Therefore, in the presence of NaY zeolites, dissolved ozone could act as a Lewis base and get adsorbed

onto "true" Lewis acid sites, such as extra-framework aluminum species, on the zeolite surface. Likewise, ozone might exhibit Lewis acid behavior, allowing it to be adsorbed on deprotonated surface hydroxyl groups (Valdés et al., 2012).

As it can be seen from Table 3.3, Pyridine-FTIR analysis the NaY-12 zeolite showed the strongest surface acidity as compared to NaY-60 zeolite. Hence, NaY-12 zeolite with a greater Brønsted acid sites (in the form of proton-donating OH groups) showed a higher catalytic activity in presence of ozonation and possible favored the enhancement of the redox process involved in ozone adsorption/decomposition. A similar feature has been observed by Saeid et al., (2018) who tested two Beta zeolites in the catalytic ozonation of ibuprofen in water and found that the catalyst with the higher acidity exhibited a higher degradation of the ibuprofen removal that the zeolite with the smaller amount of acid sites.

As shown in Figure 3.8, the mineralization extent of IBU during catalytic ozonation was enhanced, reaching 50.2% of TOC removal for O<sub>3</sub>/NaY-60 system, while 53.6% for O<sub>3</sub>/NaY-12 during 90 min of reaction. Although the mineralization performance was better compared to O<sub>3</sub> alone, the results might indicate that their oxidation-produced intermediates remained as refractory products, hard to oxidize by catalytic ozonation using NaY zeolites.

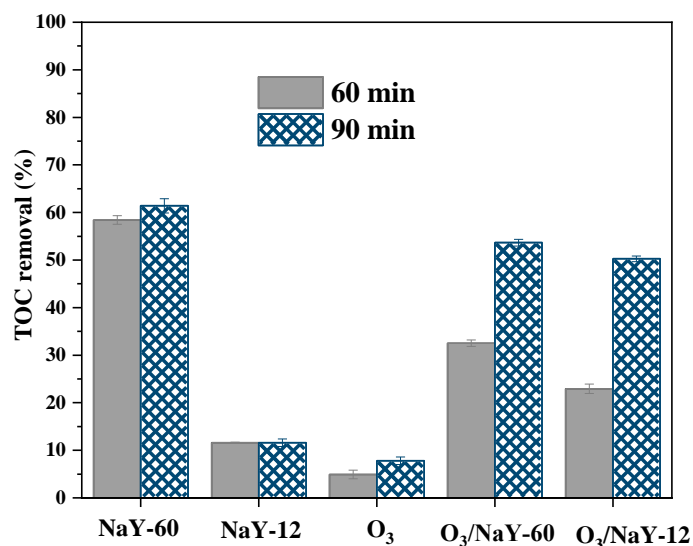


**Figure 3.8** Mineralization level of IBU via O<sub>3</sub>/NaY-60, O<sub>3</sub>/NaY-12, and their control experiments.

On the other hand, the concentrations of O<sub>3</sub> in the influent and effluent gas were monitored during the reaction, as presented in Figure 3.9a. It can be noticed that the presence of NaY

zeolites in the ozonation, resulted in lower  $O_3$  off-gas concentration compared to single ozonation. The lower ozone in the off-gas is very desirable to reduce the treatment costs and diminish off-gas treatment requirements.

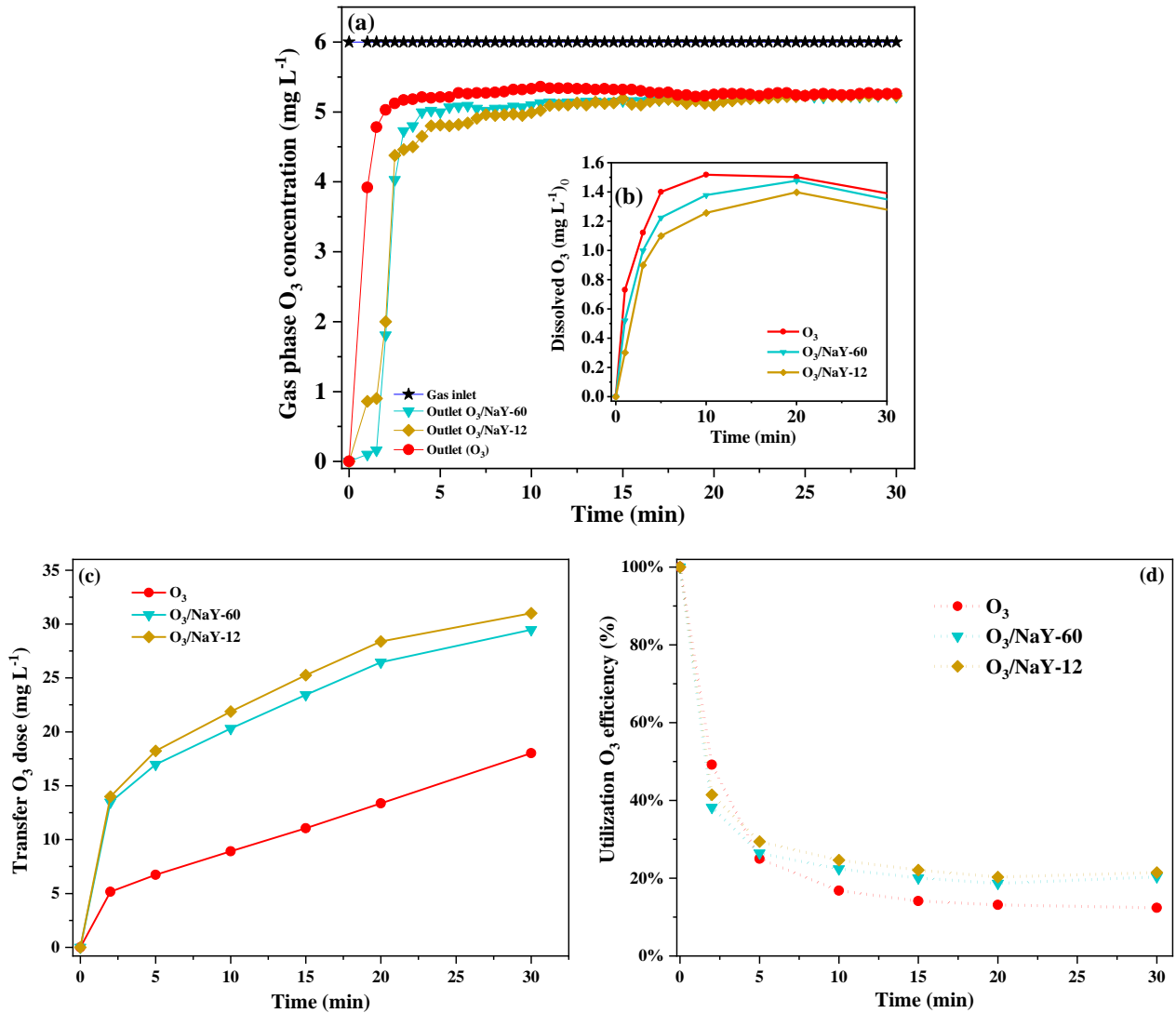


**Figure 3.9** Evolution of (a) gas phase ozone concentrations at the reactor inlet and outlet (b) dissolved ozone concentration, (c) transfer  $O_3$  doses and (d) utilization  $O_3$  efficiency as a function of reaction time during catalytic ozonation of IBU using NaY-60 and NaY-12 zeolites.

Moreover, dissolved  $O_3$  concentrations (Figure 3.9b) increased rapidly in the initial period and then reached maximum values of 1.35 and 1.47  $mg L^{-1}$ , for  $O_3/NaY-12$  and  $O_3/NaY-60$ , respectively. The lower values of  $O_3$  dissolved using NaY-12 zeolite seem to indicate that



the presence of the catalyst could have a positive effect on promoting the decomposition of aqueous ozone into more radical species.

Similarly, Figure 3.9c indicates that the introduction of NaY zeolites improved the transfer  $O_3$  doses from gas to the liquid phase, reaching values of  $29.4 \text{ mg L}^{-1}$  and  $31 \text{ mg L}^{-1}$ , for  $O_3/\text{NaY-60}$  and  $O_3/\text{NaY-12}$ , respectively. Consequently,  $O_3$  utilization efficiency in catalytic ozonation increased in an 8% the ozone mass transfer efficiency compared to single ozonation.

### 3.4.4 Comparison of ozone based AOPs

#### 3.4.4.1 Synergistic effect assessment

The synergy index (SI) was used to assesses the degree to which the  $O_3$  combined treatment produced a greater effect in terms of the IBU removal or mineralization compared to their individual process. This factor was calculated according to Eq. (3.5).

$$SI = \frac{P_{\text{combined AOPs}}}{P_1 + P_2} \quad (3.5)$$

where  $P_{\text{combined AOPs}}$  represent the removal percentage of IBU or mineralization of the simultaneous application of  $O_3$ -based AOP,  $P_1$  and  $P_2$ , the removal percentage of the individual process. A synergy index around 1 indicates a weak synergism so that the combined system performance is additive. A SI higher that 1 indicates that the combined process has positive synergic effect, while a SI lower than 1 means a negative effect.

As observed in Figure 3.10, the effect synergic was specially observed in terms of mineralization for the majority  $O_3$  intensified systems, indicating that the performance on the combined process is greater than the sum of the performance of the individual processes, particularly in terms of the organic matter removal.

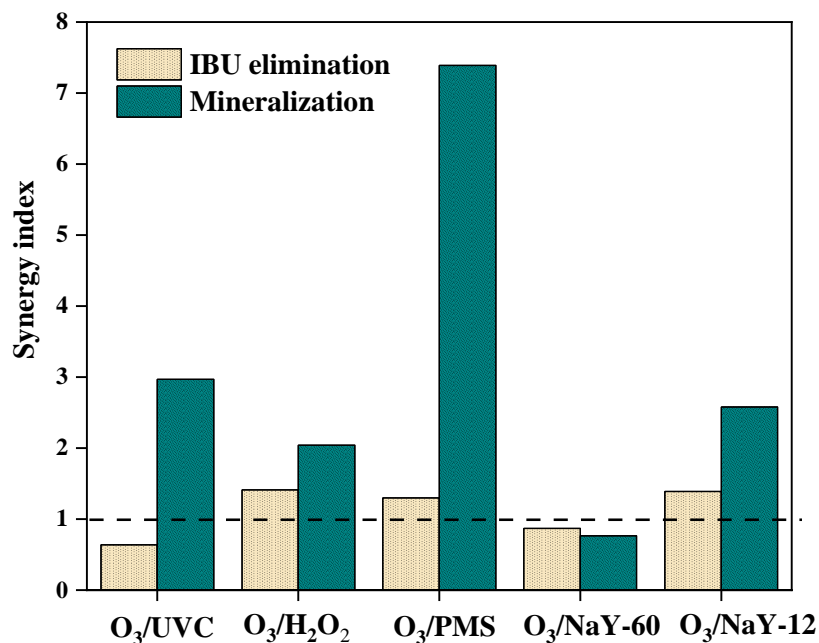


**Figure 3.10** Synergy index (SI) for the O<sub>3</sub>-based AOPs investigated

A remarkable synergy occurred in O<sub>3</sub>/PMS combination (SI=7.8) in comparison with the accumulative effect of individual processes, likely due to the different radical species formed in the process. It can be noticed that no synergy was observed in the O<sub>3</sub>/NaY-60 combination, suggesting that such combination does not offer advantages over the performance of the individual systems. This may be related to the fact that NaY-60 zeolite presented a high adsorption capacity in the removal of IBU. Regarding SI for IBU removal, photolytic ozonation and catalytic ozonation by NaY-12 zeolite enhanced the compound degradation rate considerably.

#### 3.4.4.2 Analysis of energy consumption efficiency

The energy requirement is another crucial factor to evaluate in the application of O<sub>3</sub>-based AOPs, as the degradation of organic contaminants by these technologies has been considered to be energy-intensive processes. For this purpose, a simple approach based on the electrical energy per order (E<sub>EO</sub>) was employed for comparing the energy efficiency of different treatment systems. This parameter correspond to the electrical energy in kWh required for reducing a pollutant by one order of magnitude in 1 m<sup>3</sup> in contaminated water or wastewater (Bolton et al., 2001). To calculate the energy requirements when applying single O<sub>3</sub> or O<sub>3</sub>-

based AOPs, it is assumed an average energy consumption of 15 kWh kg<sup>-1</sup> for O<sub>3</sub> and 10 kWh kg<sup>-1</sup> for H<sub>2</sub>O<sub>2</sub> production (Rosenfeldt et al., 2006). In addition, the electrical energy required for the UV lamp power (0.040 kW) and PMS (3.28 × 10<sup>-3</sup> kWh mmol<sup>-1</sup>) (Yu et al., 2021) were also taken into account. The E<sub>EO</sub> values (kWh m<sup>-3</sup> order<sup>-1</sup>) for pseudo-first-order kinetics were calculated for batch operations using Eq. (3.6).

$$E_{EO} \left( \frac{kW}{h} \right) = \frac{P \times t \times 1000}{V \times \log \left( \frac{C_i}{C_f} \right)} \quad (3.6)$$

where, P is the rated power (kW), t is the reaction time (h), V is volume (L) of reaction, C<sub>i</sub> and C<sub>f</sub> the initial and final concentration. The energy calculations were based on a 90% IBU removal. In addition, since one of the main objectives of O<sub>3</sub>-based processes is to improve TOC removal, Eq. (3.6) was also adapted to calculate the energy requirements to achieve 50% of mineralization. For this case, TOC initial and TOC final were considered for the calculation.

Table 3.4 lists the E<sub>EO</sub> values calculated for single ozonation and O<sub>3</sub>-based AOPs required to degrade 60% and 90% of IBU and 50% of mineralization. Taking into account that IBU abatement for ozonation alone was below 90%, the E<sub>EO</sub> value presented was based on a 60% removal. Likewise, since O<sub>3</sub> and O<sub>3</sub>/H<sub>2</sub>O<sub>2</sub> did not exceed at least 40 % of TOC removal during the entire experiment, the E<sub>EO</sub> values were not considered when calculating energy for those systems.

**Table 3.4** Comparison of electric energy requirements in kWh m<sup>-3</sup> at desired removal levels for the different O<sub>3</sub>-based AOPs investigated.

| Process                                       | E <sub>EO</sub> (kWh m <sup>-3</sup> ) |           |          |
|---|--|-----------|----------|
|   | IBU= 60%                               | IBU = 90% | TOC= 50% |
| O <sub>3</sub>                                | 4.27                                   | -         | -        |
| O <sub>3</sub> /H <sub>2</sub> O <sub>2</sub> | 0.80                                   | 0.89      | -        |
| O <sub>3</sub> /PMS                           | 0.34                                   | 0.43      | 17.2     |
| O <sub>3</sub> /UVC                           | 2.19                                   | 3.04      | 62.7     |
| O <sub>3</sub> /NaY-60                        | 0.50                                   | 0.62      | 18.9     |
| O <sub>3</sub> /NaY-12                        | 0.76                                   | 0.89      | 20.8     |

The results apparently indicated that the energy requirement to achieve 60% of IBU removal at the experimental conditions tested (pH 6.0 and  $O_3$  dose applied =  $4.6 \text{ mg } O_3 \text{ L}^{-1} \text{ min}^{-1}$ ) was much higher for single ozonation than for the  $O_3$ -based AOPs. This fact can be attributed to the low reactivity of IBU towards ozone under the experimental pH conditions tested.

The  $O_3$ /PMS treatment exhibited the best cost-effectiveness treatment on both IBU removal and mineralization level desired. This is attributed to the capacity of  $O_3$ /PMS system to generate both radical species,  $HO^\bullet$  and  $SO_4^{\bullet-}$ , which cause a faster IBU degradation and, consequently, make a more profitable process.

Catalytic ozonation using NaY zeolites and  $O_3/H_2O_2$  processes also had a marked benefit efficiency, which reduced the energy consumption by approximately 5.8-8.5 times compared to ozonation alone for the 60% IBU removal. Similarly, the  $O_3$ /UVC system represented energy-savings around 48% of energy compared to the single ozonation.

However, if the  $E_{EO}$  for the different  $O_3$ -based AOPs are compared in terms of a 90% IBU removal and 50% TOC removal (excluding other cost factors chemicals, capital and construction costs, etc.), the  $O_3$ /UVC system resulted in the most energy intensive process. This result is consistent with the general conclusions of many previous studies, which suggest that UV-based technologies usually are less energy-efficient than ozone-based processes in terms of micropollutant abatements. This attributed to the high energy demand for UV irradiation (Yao et al., 2018).

#### 3.4.4.3 Total operational costs

The ozone-based AOPs evaluated were also compared from an economical point of view to eliminate 50% of TOC. Target economic parameters, such as reagent consumption, labor, and electricity, were used to roughly estimate the cost of treated water in USD per  $m^3$  of wastewater. The following operating costs based on the active substances (industrial grade prizes): PMS 14 USD  $g^{-1}$ , NaY zeolites 0.15 USD  $kg^{-1}$ , labor 7.81 USD  $h^{-1}$  and electricity 0.17 USD  $kWh^{-1}$ .

Figure 3.11 presents the main ozonation operating and investment costs per  $m^3$  of treated water (WWTP effluent) necessary to remove 50% of mineralization. Notice the  $O_3$ /PMS reached the highest operational costs due to the high cost of the PMS reagent. Followed by the  $O_3$ /UVC system, while the catalytic ozonation using NaY zeolites was the most

profitable processes in terms of operational costs. According to this results, the catalytic ozonation were selected for the next analysis of objectives 2 and 3. Additionally, catalytic ozonation can offer additional energy savings, since these zeolites could be regenerate on-site by ozonation (Fu et al., 2021). Moreover, reusing zeolites can avoid high operational costs associated with the single-use of the catalyst.

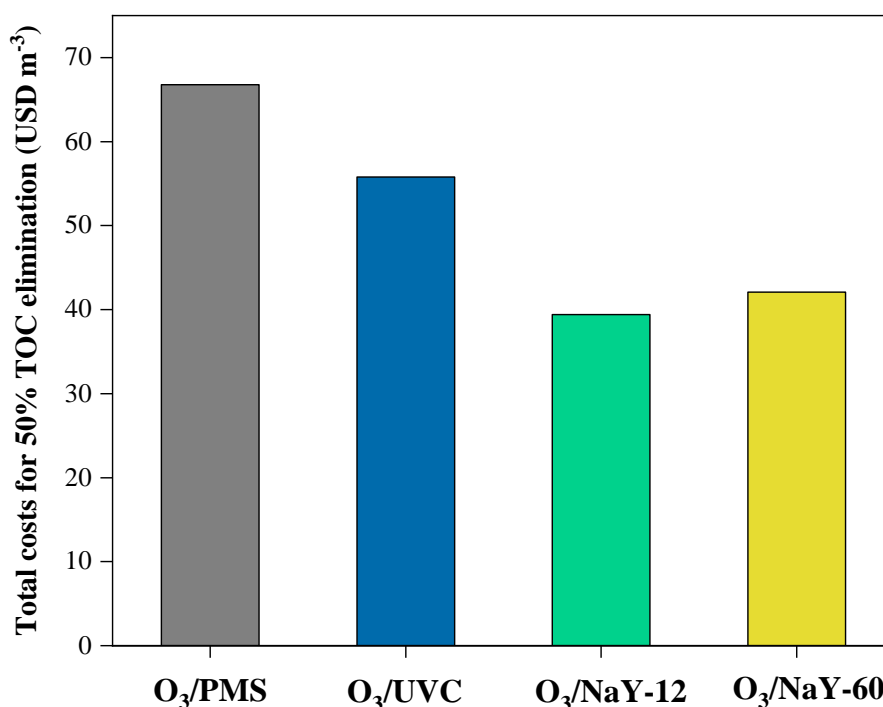


**Figure 3.11** Total operational cost (USD m<sup>-3</sup>) to eliminate 50% of TOC for O<sub>3</sub>-based AOPs investigated.

### 3.4.5 Identification of main degradation products of selected O<sub>3</sub>-based AOP

Based on several criteria determined for the different processes such as, synergy index and E<sub>EO</sub> values and total operational costs, catalytic ozonation was selected as the O<sub>3</sub>-based AOP for the study of following goals: identification of by-products and application of the process in the elimination of various pharmaceuticals in real wastewater.

The transformations by-products (TPs) of IBU generated during the O<sub>3</sub>/NaY-60 and O<sub>3</sub>/NaY-12 treatments ([IBU]=2.4 μM, catalyst = 0.2 g L<sup>-1</sup>, [O<sub>3</sub>] = 6.0 mg L<sup>-1</sup>) were

identified after 90 min of reaction by LC-QTOF-MS. The chromatograms and MS/MS for the parent compound and the identified by-products are presented in annexes in Figure A.4- Figure A.6.

The results indicated that both zeolites tested in presence of ozonation led to the formation of the same by-products. Three major IBU degradation products were identified, TP1a,b, TP2a-c, and TP3a-c, as shown in Figure 3.12.

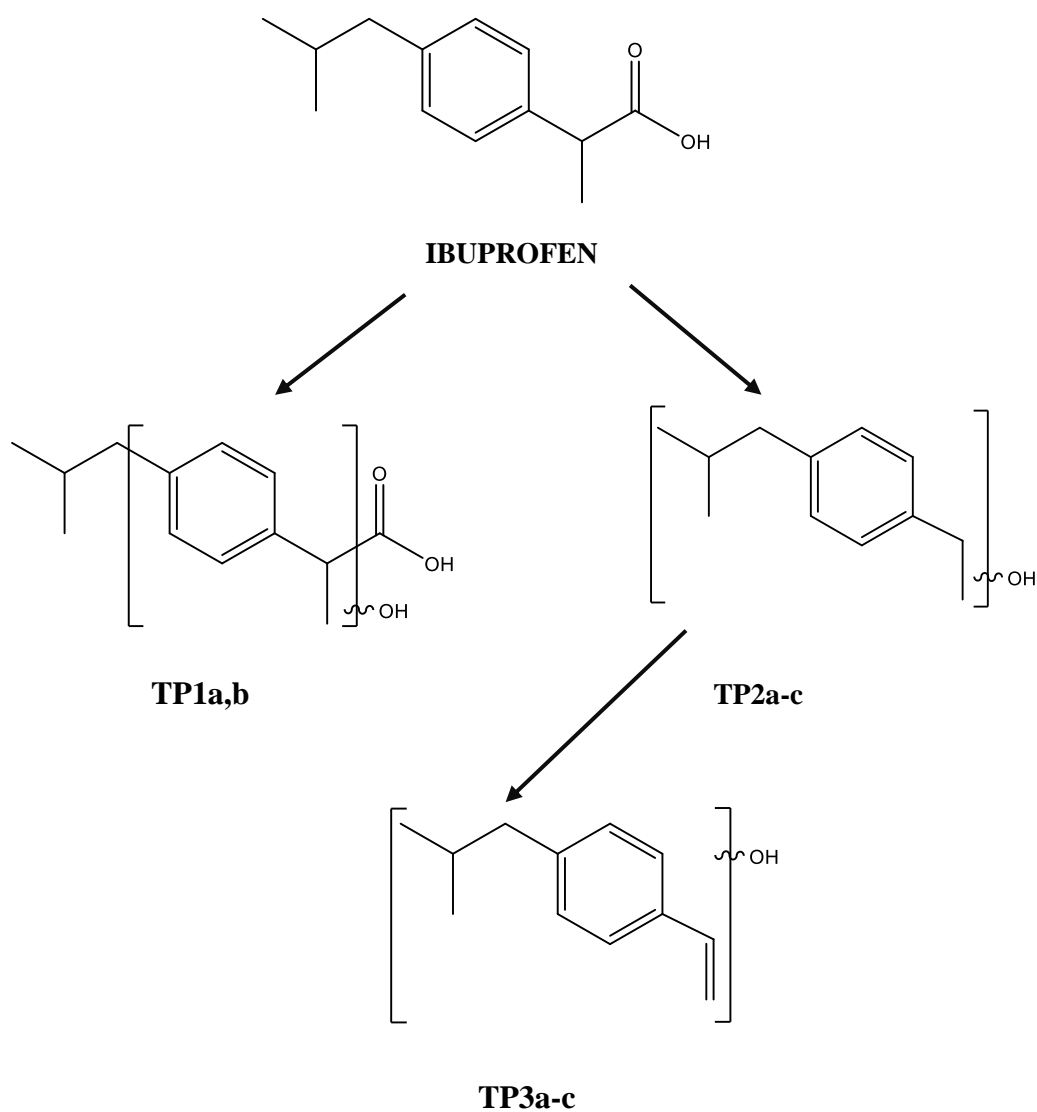


**Figure 3.12** Tentative transformation pathway of IBU degradation by catalytic ozonation using NaY-12 and NaY-60 zeolites.

The formation of TP1 with a molecular ion at  $m/z$  221.1183 and elemental composition of  $[C_{13}H_{17}O_2^-]$  was assumed to be the result of hydroxylation of the IBU molecule by  $HO^\bullet$  radical. Hydroxylation may occur at the site of the molecule most susceptible to the attack of the radical. This includes, one of the two benzyl positions, at the tertiary carbon atom position or at the aromatic ring. Different isomers could be expected, taking into account the free sites in the IBU molecule. However, the spectra fragmentation showed decarboxylation at  $m/z$  177.1277. In addition, the fragment at  $m/z$  162.104, indicated the loss of isobutane moiety. Thus, there are two possible variations for this structural TP1 by-product: either hydroxylation on the aromatic ring or hydroxylation on the phenylcarboxylic moiety (Figure A.5). Unfortunately, the exact structure of these TPs could not be confirmed by fragmentation ions. Several mono-hydroxylated products of IBU have already been reported during single ozonation (Gulde et al., 2021a), photo-Fenton (Méndez-Arriaga et al., 2010) and sonophotocatalysis processes (Michael et al., 2014).

The TP2 by-product at  $m/z$  177.1281, eluting at 8.66 min, may correspond to decarboxylation and subsequent hydroxylation of the IBU molecule, or probably could also result from decarboxylation of TP1. The MS spectrum showed a signal at  $m/z$  159.1176, indicating the loss of water and that hydroxylation did not occur in the aromatic ring. In this sense, three possible isomers of hydroxylation of TP2a-c might be formed (Figure A.6). The last by-product identified, TP3, provided a molecular ion at  $m/z$  175.1121 and an elemental composition of  $[C_{12}H_{15}O^-]$  could be formed after result from decarboxylation of TP1. Unfortunately, no fragment ions were observed in the tandem mass spectrum, maybe because it is a relative stable molecule or due to their low relative concentration. The TP2 and TP3 intermediates observed in the present study were matched with those reported in literature (Méndez-Arriaga et al., 2010; Michael et al., 2014).

Another important factor to be considered during the treatment of water contaminants is the toxicity changes. Recently, it has been demonstrated that the variation of the octanol-water partition coefficient ( $\Delta\text{Log P}$ ) could be assumed as an indirect indicator of aquatic toxicity (Melnikov et al., 2016; Serna-Galvis et al., 2019; Wang et al., 2016). Hence, in order to obtain an initial approach during catalytic ozonation the  $\Delta\text{Log P}$  for the identified primary transformations products of the IBU were calculated with respect to the parent compound

(Table 3.5). A negative  $\Delta\text{Log P}$  value (i.e., lower lipophilicity) indicates that the substance has an inferior affinity for the lipid bilayer of cells (Sandermann, 2003).

The results depicted that all transformation products of IBU showed negative  $\Delta\text{Log P}$  values, which suggest a reduction in the toxicity of the parent compound after undergoing catalytic ozonation using NaY zeolites.

**Table 3.5** Calculated properties for the transformation products

| Transformation product | $\Delta\text{Log P}^*$ | $\Delta\text{ThOD}^{**}$ ( $\text{mgO}_2 \text{ L}^{-1}$ ) |
|------------------------|------------------------|--|
| TP1                    | -0.83                  | -16  |
| TP2                    | -0.57                  | -16  |
| TP3                    | -0.45                  | -32  |

\*Calculated using ChemDraw software. Values were established for one isomer TP1a, TP2b and TP; considering the similar structure of isomers, the  $\Delta\text{Log P}$  values are expected to be close among them.

\*\* Determined as described in annexes

In addition to  $\Delta\text{Log P}$ , another interesting approach to consider is the estimation of the change in the theoretical oxygen demand ( $\Delta\text{ThOD}$ ), a parameter that indicates the degree of oxidation of the organic compounds. From Table 3.5, it can be observed that  $\Delta\text{ThOD}$  values for TPs were negative, indicating that these intermediates generated are molecules more oxidized than the initial compound. Thus, the higher oxidation of the products (i.e., negative  $\Delta\text{ThOD}$  values) can be associated with changes in the functional groups of IBU, due to the elimination of alkyl or carboxylic acid moieties (TP2, TP3), or due to the increase in the number of oxygen-carbon bonds (TP1) (Jurowski et al., 2015; Serna-Galvis et al., 2019)

In order to complement the results obtained from  $\Delta\text{ThOD}$ , an analysis of the predicted primary aerobic microbial biotransformation pathways was conducted for the identified products of IBU using the EAWAG-BBD program (See Figure A.8-Figure A.10 in annexes). The results showed that most of the predictive biotransformation pathways were referred to as “neutral” (50% probable), suggesting that TPs generated cannot be easily transformed via aerobic biodegradation under experimental conditions tested. This result may be suggested that the reaction time was insufficient to break down these intermediate molecules. Probably, prolonging the reaction time would enable  $\text{HO}^{\bullet}$  radicals to attack these molecules and lead to a greater ring-opening, resulting in the formation of short-chain aliphatic acids.



Finally, it is noteworthy to highlight that, although the above results obtained are based on rational predictions, the corresponding experimental measurements are necessary to validate these predictions.

### **3.5 Conclusions**

The results of this chapter indicated that O<sub>3</sub>-based AOPs not only enhanced the removal and mineralization of IBU but also improved the transfer and consumption O<sub>3</sub> doses during the coupled systems compared to the single ozonation. The O<sub>3</sub>/UVC system reached the highest O<sub>3</sub> utilization efficiency, compared to the other O<sub>3</sub> intensified systems. This attributed that UVC irradiation, provides an additional energy that accelerates ozone rate decomposition. The highest mineralization was observed in the O<sub>3</sub>/UVC process (98%), while the lowest was for single ozonation (8%). This demonstrated that combined rather than single processes are required to achieve larger mineralization abatements.

The O<sub>3</sub>/PMS system increased by 2.0 times the IBU degradation rate compared to O<sub>3</sub>/H<sub>2</sub>O<sub>2</sub> system, for PMS:O<sub>3</sub> molar ratio of 1.0. This high oxidation capacity of O<sub>3</sub>/PMS could be related to the simultaneous generation of HO<sup>•</sup> and SO<sub>4</sub><sup>•-</sup> radicals during the process.

The addition of zeolite catalysts to ozonation indicated that the use of NaY zeolites promoted the reaction between ozone and led to a faster IBU depletion, achieving a 5-fold increase compared to single ozonation. By comparing the performance of two NaY zeolites, the O<sub>3</sub>/NaY-60 combination exhibited better effect synergic in the IBU and mineralization removal compared to O<sub>3</sub>/NaY-12 system. This result can be related to the NaY-12 zeolite showed a stronger surface acidity compared to NaY-60 zeolite, and possible Lewis and Brønsted acid sites of zeolites favored the decomposition of ozone adsorption.

In terms of energy requirements, O<sub>3</sub>-based AOPs reduced the energy required to abate the ozone resistant micropollutant in compared to conventional ozonation. The catalytic ozonation showed larger benefits with better cost-effective results for both IBU and mineralization reduction. Predicted toxicity results indicated that catalytic ozonation was able to reduce the IBU toxicity.

## **Chapter 4. Application of catalytic ozonation in the elimination of pharmaceuticals in real wastewater**

### **4.1 Introduction**

Over the past few years, catalytic ozonation has received wide attention since the addition of a catalyst can facilitate ozone decomposition to generate more active free radicals, such as hydroxyl radicals (Wang and Chen, 2020). In most cases, this process can significantly increase the degradation rate and mineralization efficiency of various organic compounds than ozone alone system (Kasprzyk-Hordern et al., 2003; Liu et al., 2021). Among heterogeneous catalysts, zeolites have shown good application potential in catalytic ozonation for organic micropollutants removal from water (e.g., pharmaceuticals) (Ikhlaq et al., 2018; Ma et al., 2020; Valdés et al., 2012). Zeolites are crystalline and microporous aluminosilicates that offer great advantages as a catalyst due to their large specific surface area, high reusability, and chemical stability (McCusker et al., 2007). In particular, Y zeolites, which belong to the Faujasite (FAU) family, are among the most important zeolites in terms of industrial use and commercial availability (Reiprich et al., 2020). This zeolite has a typical microporous structure characterized by a three-dimensional (3D) framework, large pore diameter, and super cavities, making this material of particular interest (McCusker et al., 2007). For instance, Dong et al., (2008) reported that the presence of dealuminated Y zeolite in the ozonation of phenol exhibited an increase in the compound degradation and in the removal rate of chemical oxygen demand, mainly attributed to HO<sup>•</sup>.

The catalytic properties of zeolites are mainly related to their acidic strength sites, which can be controlled by the proportion of silica and aluminum (Si/Al) ratio (Soares et al., 2016). Some researchers have found, Brønsted and Lewis acid sites are claimed to play an important role in the catalytic ozonation, suggesting these active sites promote the decomposition of aqueous ozone to form hydroxyl radicals HO<sup>•</sup> (Alejandro-Martín et al., 2018; Su et al., 2022; Valdés et al., 2009).

Recently, in heterogeneous catalytic ozonation using zeolites, efforts have been focused on evaluating the efficiency of several types of natural and synthetic zeolites in the ozonation of individual pharmaceuticals in water. Additionally, there has been a strong interest in understanding the reaction mechanism involved and how some operational conditions affect the process performance. However, to date, no previous works have dealt with the application of catalytic ozonation using zeolites to eliminate PhACs in real effluents. Thus, considering the absence of relevant studies on this issue, this work aims at taking a step forward towards in the existing research gap.

The following chapter has focused on evaluating the application of heterogeneous catalytic ozonation using two Y-zeolites with similar structures and different SiO<sub>2</sub>/Al<sub>2</sub>O<sub>3</sub> ratios for the elimination of a wide group of pharmaceuticals in real wastewater samples. Furthermore, two main aspects were also investigated: the occurrence of relevant PhACs, including an assessment of the environmental risk associated with PhACs, and the performance of the adsorption process and single ozonation (control experiments).

## **4.2 Experimental procedure**

The experiments in this section were conducted in the bubble column reactor No. 2 in semi-continuous mode (Figure 2.3). Concerning procedure in each test, the reactor was filled with 800 mL of wastewater sample collected from two WWTPs located in Spain (effluent A and effluent B), and for catalytic ozonation experiments, 0.2 g L<sup>-1</sup> of zeolite was added. All tests were performed at a room temperature of 24 °C, at the natural pH of the wastewater. The ozone residual gas stream was vented through the catalytic O<sub>3</sub> destruction unit before discharging to ambient air. The samples were withdrawn from the reactor through a sampling port at different times interval (10, 30, and 60 min) and quenched immediately by bubbling with high-purity nitrogen gas for 1 min to remove the residual dissolved ozone. All samples

were filtered by a 0.45  $\mu\text{m}$  filter membrane for further analysis. Adsorption experiments were performed with the same experimental system mentioned above, but ozone and catalyst were not used. In order to compare the efficiency of the ozone-driven treatments, the removal of the mixture of pharmaceuticals detected was evaluated as a function of ozone consumption for each treatment considering the transferred ozone dose (Eq. (3.2)). The corresponding specific ozone dose ( $\text{g O}_3 \text{ g DOC}^{-1}$ ) based on the normalization of ozone dose to the dissolved organic carbon (DOC) content in the wastewater could be evaluated from TODs and the initial DOC value of each sample at each treatment.

## **4.3 Results and discussion**

### **4.3.1 Pharmaceuticals detected in wastewater samples**

Both samples (Effluent A and B) were firstly analyzed in order to know the initial concentrations of pharmaceuticals before undergoing the different degradation treatments. The main detected pharmaceuticals and their concentrations are presented in Table 4.1.

It can be seen that 21 and 25 compounds were above the LOQ for effluent A and effluent B, respectively. The identified pharmaceuticals belong to ten different therapeutic groups: 3 analgesics, 9 antibiotics, 3 anticonvulsants, 4 anti-hypertensive, 1 anthelmintic, 1 iodized contrast media, 1 lipid regulator, 1  $\beta$ -blocker, 1 anxiolytic and 2 antidepressants.

In effluent A, the highest concentration corresponded to the analgesic phenazone ( $2.12 \mu\text{g L}^{-1}$ ), the anti-hypertensive valsartan ( $1.49 \mu\text{g L}^{-1}$ ), the contrast media iopromide ( $1.04 \mu\text{g L}^{-1}$ ) and the metabolite O-desmethylvenlafaxine ( $1.19 \mu\text{g L}^{-1}$ ), all at concentrations above  $1 \mu\text{g L}^{-1}$ . As regards to effluent B, several compounds were also present at  $> 1 \mu\text{g L}^{-1}$ : anti-hypertensive valsartan ( $9.01 \mu\text{g L}^{-1}$ ), the anticonvulsant gabapentin ( $4.54 \mu\text{g L}^{-1}$ ), the analgesic tramadol ( $2.89 \mu\text{g L}^{-1}$ ), the antidepressant venlafaxine ( $1.27 \mu\text{g L}^{-1}$ ) and its metabolite O-desmethylvenlafaxine ( $2.25 \mu\text{g L}^{-1}$ ), and diclofenac ( $1.10 \mu\text{g L}^{-1}$ ).

The presence of valsartan at high concentrations in both effluent samples is in agreements with the high consumption of this pharmaceutical in Spain, as it is the most often prescribed anti-hypertensive drug with 13.7 daily doses per 1000 inhabitants (data from *Spanish Agency of Medicines and Medical Devices* (AEMPS, 2018)). Previous studies in different Spanish

WWTPs also revealed high concentrations of valsartan in effluent wastewaters (Bijlsma et al., 2021; Lopez et al., 2022).

**Table 4.1** Initial concentration of pharmaceuticals detected in Effluent A and Effluent B.

| Therapeutic group                   | Compound                       | Concentration ( $\mu\text{g L}^{-1}$ ) |            |
|-------------------------------------|--------------------------------|--|------------|
|                                     |                                | Effluent A                             | Effluent B |
| Analgesics                          | Diclofenac                     | 0.42                                   | 1.10       |
|                                     | Phenazone                      | 2.12                                   | 0.50       |
|                                     | Tramadol                       | 0.80                                   | 2.89       |
| Antibiotics                         | Ciprofloxacin                  | 0.89                                   | 0.61       |
|                                     | Clarithromycin                 | 0.22                                   | 0.36       |
|                                     | Erythromycin                   | 0.06                                   | 0.53       |
|                                     | Trimethoprim                   | 0.15                                   | 0.23       |
|                                     | Sulfamethoxazole               | 0.04                                   | 0.11       |
|                                     | Clindamycin                    | <LOQ                                   | 0.07       |
|                                     | Norfloxacin                    | -                                      | 0.16       |
|                                     | Metronidazole                  | 0.09                                   | 0.25       |
|                                     | Tetracycline                   | <LOQ                                   | 0.02       |
|                                     | Anticonvulsants                | Carbamazepine                          | 0.05       |
| Gabapentin                          |                                | 0.21                                   | 4.54       |
| Primidone                           |                                | 0.08                                   | 0.12       |
| Anti-hypertensive                   | Irbesartan                     | 0.51                                   | 0.87       |
|                                     | Losartan                       | 0.14                                   | 0.46       |
|                                     | Enalapril                      | <LOD                                   | 0.03       |
|                                     | Valsartan                      | 1.49                                   | 9.01       |
| Anthelmintic                        | Levamisole                     | 0.05                                   | 0.09       |
| Iodized contrast media              | Iopromide                      | 1.04                                   | <LOQ       |
| Lipid regulator                     | Atorvastatin                   | <LOQ                                   | 0.22       |
| Beta-blocker                        | Metoprolol                     | 0.03                                   | 0.17       |
| Anxiolytic                          | Lorazepam                      | 0.08                                   | 0.15       |
| Antidepressants                     | Venlafaxine                    | 0.37                                   | 1.27       |
|                                     | <i>O</i> -desmethylvenlafaxine | 1.19                                   | 2.25       |
| Total load ( $\mu\text{g L}^{-1}$ ) |                                | 10.04                                  | 26.08      |

The total concentration of target pharmaceuticals in effluent B almost triplicated that of effluent A ( $26.08 \mu\text{g L}^{-1}$  and  $10.04 \mu\text{g L}^{-1}$ , respectively). This difference between could be due to factors such as population served, and the activities involved in the area. While

effluent B collects water from an urban area and a nearby hospital, effluent A is situated in a rural area, so lower pharmaceuticals concentrations may be expected. The total pharmaceutical concentration found in this study agrees within the ranges reported for these therapeutic groups in other Spanish municipal WWTPs (Costa et al., 2021; Lopez et al., 2022). As an example, gabapentin was found in effluent wastewater (EWW) samples from a WWTP in Madrid (Spain) at average concentrations of  $3.61 \mu\text{g L}^{-1}$  and  $2.66 \mu\text{g L}^{-1}$  in two different campaigns (Lopez et al., 2022). The antibiotics ciprofloxacin and norfloxacin, the anticonvulsant gabapentin and the analgesic tramadol (Bijlsma et al., 2021), were found at concentrations similar to effluent B in the current study.

### **4.3.2 Adsorption of pharmaceuticals on NaY zeolites**

In order to gain insights into the catalytic ozonation process using Y zeolites in real effluents, the adsorption control was firstly tested on the removal of target pharmaceuticals onto the NaY zeolites using real wastewater. Figure 4.1 displays the percent removal of 21 and 25 compounds detected under adsorption process for effluent A and B, respectively. The results in Figure 4.1a. shows that in effluent A, after 60 min of contact time only 7 out of 21 compounds (venlafaxine, O-desmethylvenlafaxine, tramadol, carbamazepine, levamisole, metoprolol, and trimethoprim) were removed higher than 90% with NaY-12, whereas 9 PhACs (additional compounds removed, lorazepam and ciprofloxacin) by the NaY-60 zeolite.

In the case of effluent B, although the total load of the compounds ( $26.08 \mu\text{g L}^{-1}$ ) was higher than the effluent A ( $10.04 \mu\text{g L}^{-1}$ ), the adsorption efficiencies presented a similar pattern in the PhACs adsorption compared to the effluent A. As shown in Figure 4.1b, in the case of effluent B, 9 out of 25 compounds (venlafaxine, O-desmethylvenlafaxine, enalapril, tetracycline, tramadol, metoprolol, trimethoprim, carbamazepine, and clindamycin) were adsorbed higher than 80% on NaY-12 zeolite and 11 compounds (additional PhACs adsorbed were lorazepam and ciprofloxacin) on NaY-60 zeolite. The high adsorption of these groups of PhACs in both sample wastewater could be attributed to zeolite microporous structure, surface charge and the ionization form of the target compounds.

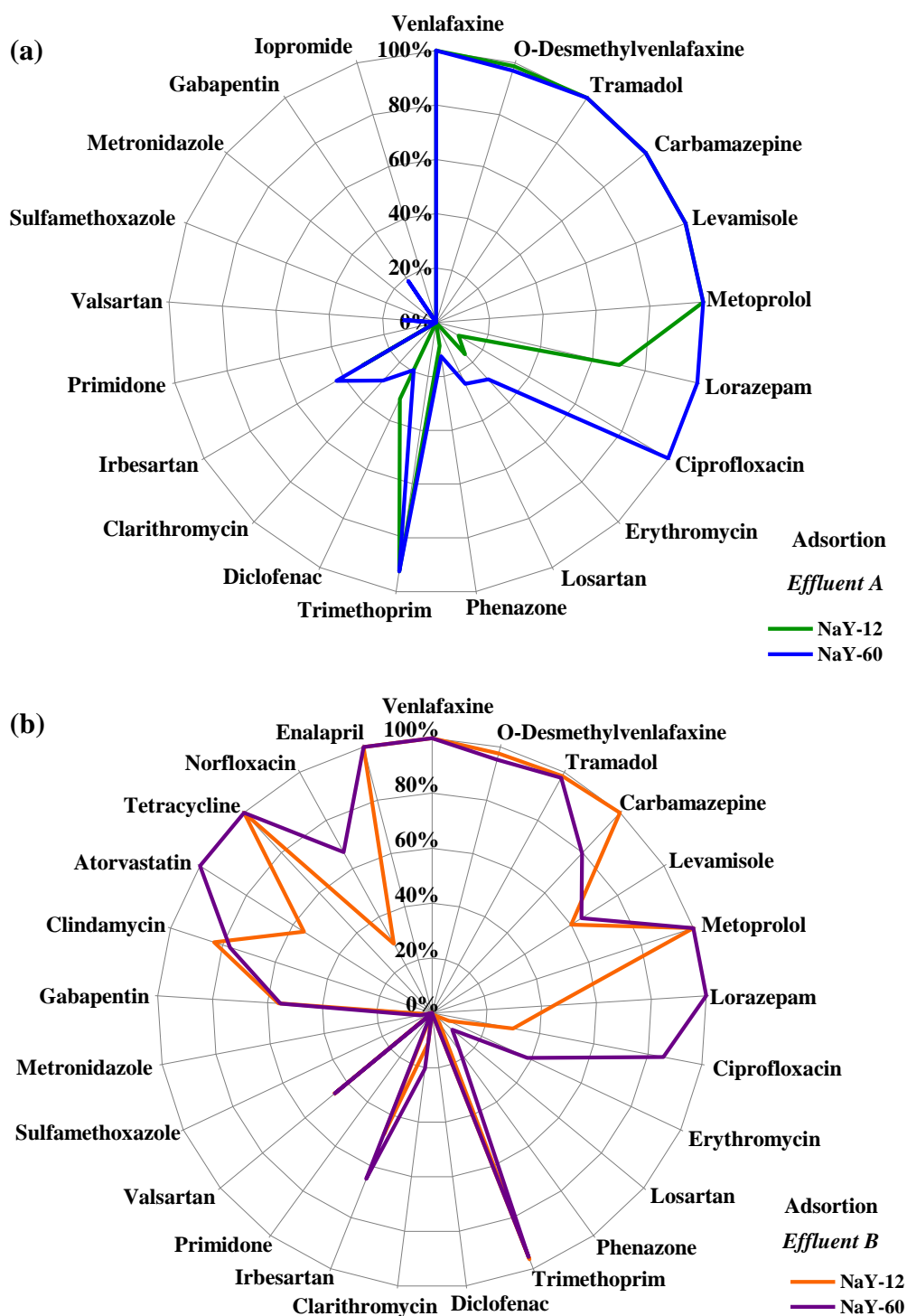


**Figure 4.1** Adsorption of target pharmaceuticals by NaY-60 and NaY-12 zeolites at 60 min of reaction time in: (a) Effluent A and (b) Effluent B.

The  $pH_{pzc}$  (point of zero charges) plays an important role in elucidating the mechanism of PhACs adsorption on zeolites (Valdés et al., 2009). The  $pH_{pzc}$  is defined as the pH at which

the net surface charge of the material becomes electrically neutral (Sposito, 1998). It is stated that the catalyst surface could be positively charged if  $\text{pH} < \text{pH}_{\text{pzc}}$  and negatively charged if  $\text{pH} > \text{pH}_{\text{pzc}}$ . The  $\text{pH}_{\text{pzc}}$  values of NaY-60 and NaY-12 zeolites were determined to be 7.1 and 6.5, respectively. This means that the zeolite surface for both samples are negatively charged.

Consequently, at the natural pH of wastewater samples,  $\text{pH} = 7.6$ , compounds such as venlafaxine, O-desmethylvenlafaxine, levamisole, tramadol, and metoprolol exist as cationic forms (see Table A1, in annexes), and exhibited a high adsorption capacity into both NaY zeolites (above 90% in both effluents, except for clarithromycin and erythromycin). The high removal capacity is attributed to the larger electrostatic attraction between the negatively charged surface of the zeolite and positively charged PhACs. Oppositely, anionic compounds such as diclofenac, irbesartan, losartan, phenazone, sulfamethoxazole, valsartan, as well as zwitterionic compounds (ciprofloxacin, gabapentin, and metronidazole), had a lower adsorption capacity onto NaY zeolites compared to cationic PhACs due to the electrostatic repulsion between the negatively charged adsorbent zeolite and these anionic PhACs. De Sousa et al., (2018) also observed influence of charge on the adsorption of pharmaceuticals by zeolites. They found that for FAU zeolite, sulfamethoxazole presented a pH-dependency, with considerably lower adsorption when the molecule was in its negative charged form compared to positively charged species.

In the case of neutral compounds (carbamazepine, trimethoprim, and lorazepam, except iopromide and primidone), had a good adsorption capacity into both NaY zeolites. In the adsorption of neutral compounds, mechanisms such as hydrophobic interactions and hydrogen bonding could be taking place in the adsorption process, instead of electrostatic interactions.

On the other side, the differences in adsorption properties can be also related to the micropore size of the zeolite, which determines the diffusivity and accessibility of micropollutants (Jiang et al., 2018). According to the data shown in Table A1, the molecular dimension of valsartan, iopromide, primidone, clarithromycin and erythromycin (although those last two molecules are positively charged), are larger than the free aperture of the 12-ring windows in Y zeolite (open diameter  $7.4 \times 7.4 \text{ \AA}$ ) (Reiprich et al., 2020), in which compounds cannot easily diffuse inside the micropores of NaY zeolyst.



Comparing the efficiency between zeolite samples, it can be noted that NaY-60 zeolite had a slightly higher adsorption capacity for pharmaceuticals compared with NaY-12. This result could be probably attributed to the hydrophobicity of the zeolite samples, which provides beneficial characteristics for organic micropollutants adsorption in aqueous solutions (Jiang et al., 2018). As mentioned above in Section 3.6, zeolites with the same framework type, the hydrophobicity increases with decreasing aluminum content. Thus, zeolites with higher Si/Al ratios are more hydrophobic (Chen, 1976). Therefore, NaY-60 is expected to be the most hydrophobic zeolite and NaY-12 the least hydrophobic.

### 4.3.3 Ozonation treatment

The removal efficiencies of detected PhACs in effluent A and effluent B by ozonation at different reaction times (10, 30, and 60 min) are presented in Figure 4.2. The results of the removal of the mixture of PhACs are also reported as function of the ozone consumption considering the transferred ozone dose ( See Fig. A1, in annexes).

In general, the application of ozonation involves two reaction pathways: a direct oxidation in which molecular  $O_3$  can react selectively with compounds containing electron-rich groups such as deprotonated amines, unsaturated double bonds, and activated aromatic; or by an indirect reaction through the formation of secondary oxidants, hydroxyl radicals, initialized by  $OH^-$  in aqueous phase, via Eqs. (1.1) and (1.2) (Staelin and Hoigne, 1982). Unlike ozone,  $HO^\bullet$  is a non-specific oxidant capable of degrading a wide range of organic and inorganic compounds via radical mechanism ( $k_{HO^\bullet}$  values are in the order of  $10^9$ – $10^{10} M^{-1} s^{-1}$  for most of micropollutants).

In order to understand the removal patterns of different compounds in both samples, the categorization based on the ozone reactivity proposed by Rizzo et al., (2019) was applied for this study. For grouping the compounds, the criteria based on the apparent second order rate constant values ( $k_{O_3}$ ) was taking into account. Group A contains compounds with electron-rich moieties and classified by a high reactivity with ozone ( $k_{O_3} > 10^3 M^{-1} s^{-1}$ ), Group B compounds with have intermediate reactivities with ozone ( $k_{O_3} = 10^2 - 10^3 M^{-1} s^{-1}$ ) and group C compounds with a low or not reactivity with ozone and which secondary oxidants ( $HO^\bullet$ ) influences in the degradation of compounds  $k_{O_3} < 10^2 M^{-1} s^{-1}$ . The literature data on of

the rate constants of the reactions of the target compounds with ozone ( $k_{O_3}$ ) and hydroxyl radicals ( $k_{HO\cdot}$ ) are presented in Table A2 in annexes.

As may be seen in Figure 4.2a, after a treatment time of 10 min, the ozonation showed partial degradation, in which 14 out of 21 compounds were removed higher than 90% in effluent A (28 mg  $O_3 L^{-1}$  consumed). Regarding effluent B, a decreased in the removal of PhACs was observed. A group of 17 of out 25 PhACs were removed above 90% during the first 10 min (25 mg  $O_3 L^{-1}$  consumed).

The abatement of 95% of the mixture of the PhACs was reached after 25 min of reaction, and the ozone consumption was 41.2 mg  $O_3 L^{-1}$  and 46 mg  $O_3 L^{-1}$  for effluent A and effluent B, respectively. These results are consistent with DOC content of effluent A (47.5 mg  $L^{-1}$ ) and effluent B (65.4 mg  $L^{-1}$ ) as 0.9 and 0.7 g  $O_3 g DOC^{-1}$  were needed for effluent A and B, respectively, to reach above 90% abatement of PhACs and in agreement with a previous study of Lee et al., (2013).

According to the data presented in Table A2 (annexes), all these PhACs that showed the highest removals, like diclofenac, phenazone ciprofloxacin, carbamazepine, clarithromycin, losartan, trimethoprim, venlafaxine and its metabolite, among others, belongs to group A, (approximately 70% of the target compounds belongs to this group). These PhACs react fast with ozone due to electron rich moieties that contain such as, non-protonated amines, olefins, and phenols. Therefore, it is expected that ozone reactions mainly contributed to the abatement of these compounds. By the contrast, at 10 min of ozonation, the most refractory compounds were iopromide, and gabapentin for the effluent A, and metronidazole, lorazepam, primidone, gabapentin, and valsartan for the effluent B, in which reached removal percentages lower than 50%. The previous PhACs have low reactivity towards ozone, and belongs to group C. The low removal efficiency is consistent with their lower  $K_{O_3}$  values. Some of the compounds contain halogen substituents (e.g. iopromide), carbonyl groups, or amide moieties than typically decrease the ozone reactivity by an electron-withdrawing effect (Lee et al., 2014). Considering that the experiments were conducted at natural pH of the wastewater effluents, their oxidation was possibly driven by hydroxyl radicals generated from the decomposition of  $O_3$ , rather than the direct reaction with molecular  $O_3$ .

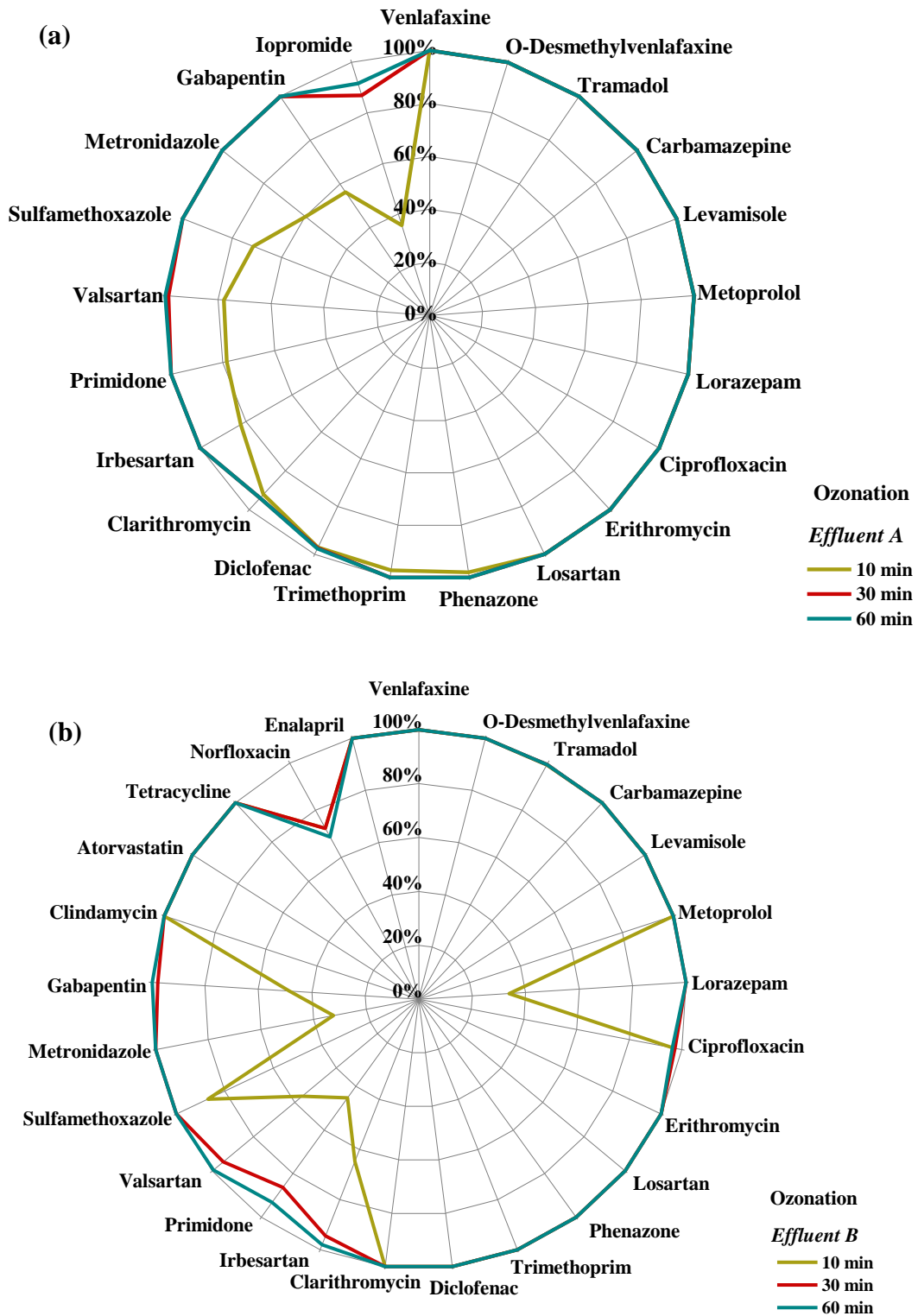


Figure 4.2 Ozonation of pharmaceuticals during 10, 30 and 60 min of reaction time in: (a) Effluent A and (b) Effluent B.

### 4.3.4 Catalytic ozonation treatment

Figure 4.3 shows results of the degradation of the micropollutants detected in both effluent samples by combining ozonation and the NaY-60 and NaY-12 zeolites at 10 min of reaction. It can be observed from Figure 4.3a., for the case of effluent A, the presence of NaY zeolites exerted a positive effect on the micropollutants elimination. 18 out of 21 compounds reached above 90% removal for NaY-60 and 20 out of 21 compounds by NaY-12 zeolite, within the early 10 min of reaction.

The elimination percentage attained for the removal of the mixture of PhACs in effluent A were 94% and 97% for the combination of O<sub>3</sub>/NaY-60 and O<sub>3</sub>/NaY-12, respectively, after 10 min. Relating to effluent B, a slight decrease in the percentage of removal was observed as compared with effluent A. For the aim above 90% removal, 18 out of 25 compounds were removed by NaY-12 zeolite, while 19 out of 25 PhACs were eliminated by the NaY-60 sample after 10 min. The degradation of the mixture of PhACs reached a removal of 77 % for O<sub>3</sub>/NaY-60 and 88% for O<sub>3</sub>/NaY-12 combination within 10 min. After 30 min, for both samples showed nearly complete degradation of all most compounds, unlike for primidone compound which reached 87% in effluent B.

It can be noted that the addition of NaY-12 zeolite sample in the ozonation could enhance the degradation rate of ozone resistant compounds ( $k_{O_3} < 10^2 \text{ M}^{-1} \text{ s}^{-1}$ ) like iopromide, gabapentin, primidone, metronidazole, and valsartan, which reached removals over 90 % in effluent A in less than 10 min. Taking into consideration previous results in control experiments, physical adsorption did not contribute to the removal of these compounds, while single ozonation showed a low PhACs abatement. It can be hypothesized that NaY-12 zeolite catalytic ozonation showed a high catalytic activity for decomposing aqueous ozone into radical species, mainly HO<sup>•</sup>. The main differences in the catalytic properties of zeolites are related to their acidic properties, and their acid strength can be controlled by the Si/Al ratio (Yu et al., 2020).

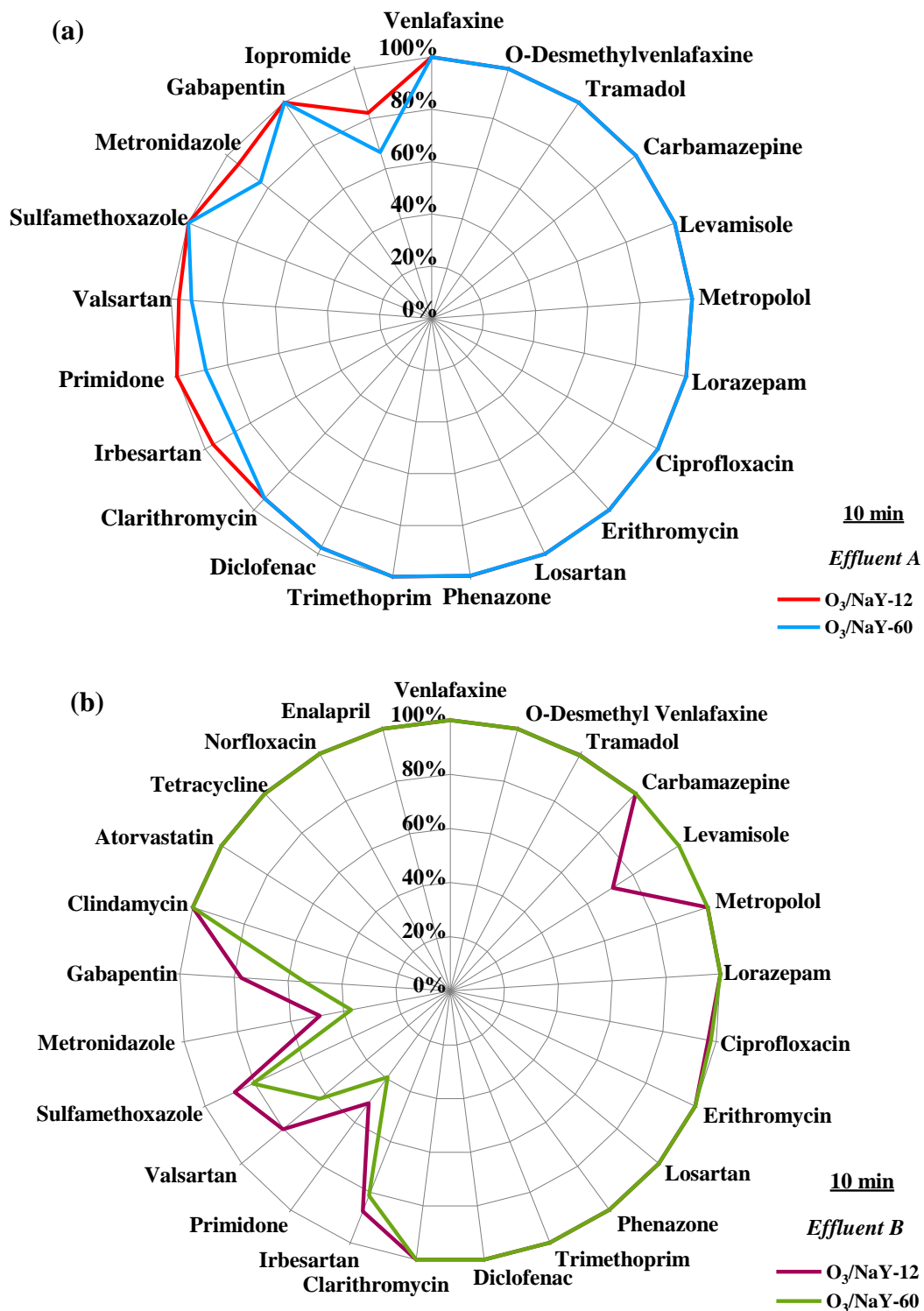


**Figure 4.3** Catalytic ozonation of target pharmaceuticals during 10 min of reaction time in (a) effluent A using zeolite: NaY-60 and NaY-12 and (b) effluent B using zeolite NaY-60 and NaY-12.

Previous studies using zeolites as ozonation catalyst have found that Lewis and Bronsted acid groups on zeolites might promote ozone decomposition and free hydroxyl radicals formation. For instance, H. Valdés et al., (2012) reported that due to the resonance structure of ozone, this oxidant can act as Lewis base and can be adsorbed in Lewis acid sites and decompose to generate HO<sup>•</sup>. According to previous results, Pyridine-FTIR analysis conducted in this study allowed identifying such acidic sites. As can be seen in Table 3.3, the NaY-12 zeolite offered a larger amount of Lewis and Brønsted acid sites to enhance the redox process involved in ozone adsorption/decomposition. Hence, more Lewis active acid sites imply more aqueous ozone attracted to oxidation of PhACs. Therefore, the high PhACs removal rates observed in the coupled treatment (O<sub>3</sub>/NaY-12) could be related to ozone interaction with acidic sites of this zeolite sample.

When comparing the efficiency of catalytic ozonation in both effluent samples at 10 min of treatment, effluent B had a lower removal of pharmaceuticals compared to effluent A. This could be attributed to the presence organic and inorganic matter in this effluent which components can react very fast with hydroxyl radicals ( $10^8$ - $10^9$  M<sup>-1</sup> S<sup>-1</sup>), decreasing the radical concentration and the direct attack of HO<sup>•</sup> to the target compounds (Rizzo et al., 2019). Additionally, pharmaceuticals are between 2 and 3 magnitude orders more concentrated in effluent B than the effluent A; thus, more amounts of degrading species and treatment time are needed to degrade the micropollutants. The activity catalytic of both zeolites in the effluent B had a slight difference in the compounds oxidation compared to the effluent A. The addition of NaY-60 zeolite in ozonation showed a higher degradation of micropollutants (>90% for 19 out of the 25 PhACs). However, for aim of removal >50%, NaY-12 zeolite exhibited a great number of compounds removed compared to NaY- 60 zeolite at 10 min.

It should be noted that in terms of ozone consumption, catalytic ozonation resulted in lower TOD compared to single ozonation in both effluents. To achieve a 95% removal of the mixture of PhACs in effluent A, 24.4 and 31 mg O<sub>3</sub> L<sup>-1</sup> was required for NaY-12 and NaY-60 zeolites, respectively (See Figure A.1). This O<sub>3</sub> requirements represents a saving of around 33% (using NaY-60) and 47% (using NaY-12) of the overall ozone needs to eliminate same level of PhACs when comparing with single ozonation. Additionally, the specific O<sub>3</sub> dose of these coupled system were slightly lowered working at 0.5 and 0.65 g O<sub>3</sub>

g DOC<sup>-1</sup> for O<sub>3</sub>/NaY-12 and O<sub>3</sub>/NaY-60 combination, respectively. This provides an economic benefit to the coupled process, considering the significant cost of ozone production, thereby making its large-scale application more practical. In the case of effluent B, 46 and 50.2 mg O<sub>3</sub>L<sup>-1</sup> were consumed to achieve a 95% removal of the mixture of PhACs using NaY-12 and NaY-60, respectively, while ozonation required 66 mg O<sub>3</sub> L<sup>-1</sup>. For the effluent B, the O<sub>3</sub> requirements when comparing with direct ozonation, represents a saving of 23% and 30% of the overall ozone needs for the same micropollutant degree of depletion employing the NaY-60 and NaY-12 zeolite sample, respectively.

From a practical standpoint, the results were very promising for the removal of PhACs in real wastewater. For a reaction time of 10 min, the catalytic ozonation system (O<sub>3</sub>/NaY-12) exhibited synergistic effects, particularly for the elimination of ozone-recalcitrant compounds. Furthermore, the low ozone dose used (15 mg L<sup>-1</sup> min<sup>-1</sup>) and the catalyst dosage employed here make this system highly attractive for real applications.

### **4.3.5 Environmental risk assessment**

The environmental risk assessment caused by the detected pharmaceuticals in the initial effluents A and B, and the applied treatment in this study, like adsorption, ozonation and catalytic ozonation using NaY zeolites was assessed using the risk quotient criteria. Furthermore, taking into consideration that each sample presented a mixture of several PhACs, the risk for the entire mixture of micropollutants (RQ<sub>mixture</sub>) in the initial wastewater and after treatment was also evaluated. Table 4.2 displays the RQ values calculated using Eqs. (2.2) and (2.3), as early indicated in Section 2.4.5. It can be observed, the RQ determined for 17 of the 21 compounds present in effluent A, resulted in low environmental risk. The four exceptions were for diclofenac, phenazone, ciprofloxacin and venlafaxine, whose exceeded the threshold of 0.1 (0.33, 0.30, 0.39 and 0.98, respectively). According to the results of this study, these 4 pharmaceuticals should be considered as posing a moderate environmental risk in water bodies.

Concerning to effluent B, of the 25 compounds detected, 4 PhACs present moderate risk such as diclofenac, ciprofloxacin, clarithromycin and gabapentin (RQ values from 0.12 to 0.85), while the anti-depressant venlafaxine was the only substance in this group that poses a high risk to the environment. The elevated risk associated with venlafaxine could be related

to its relatively high concentration in effluent B ( $1.27 \mu\text{g L}^{-1}$ ) and its lower PNEC value (0.038). Similarly, despite the relatively low concentration of ciprofloxacin ( $0.89 \mu\text{g L}^{-1}$  in effluent A and  $0.61 \mu\text{g L}^{-1}$  in effluent B) in the wastewater samples, the moderate environmental risk related to this antibiotic can also be attributed to its lower PNEC value (0.00056). The previous findings of the fluoroquinolone ciprofloxacin also highlight the potential risk associated with the proliferation of multiple antibiotic-resistance genes or strains of bacteria (Junaid et al., 2022). This compound has been included in the most recent version of the surface water Watch List under the Water Framework Directive (European Parliament, 2018).

As can also be seen in Table 4.2, for effluent A, the RQ values for all pharmaceuticals after the application of the coupled system ozonation and NaY zeolites (only 10 min of reaction) were significantly diminished compared with the initial wastewater, considerably reducing the risk in the receiving environment. Even, the single ozonation system could eliminate the risk associated with PhACs in effluent A, thus  $RQ_{\text{mixture}}$  values were also reduced.

Samples from effluent B, also RQ values were reduced when catalytic ozonation using NaY-12 zeolite was applied. However, for the combination of ozone and NaY-60 sample, the  $RQ_{\text{mixture}}$  was higher than the threshold of 0.1, indicating that the complex mixture of pharmaceuticals in the samples had a moderate risk for the environment at 10 min of reaction. This could suggest for this specific treatment ( $\text{O}_3/\text{NaY-60}$ ) that is needed more reaction time to reduce the environmental risk related to this mixture of pharmaceuticals.

In the case of adsorption, after 1 hour of contact time, 5 and 7 compounds present moderate environmental risk for effluent A and effluent B, respectively.

The data reveals the importance of implementing adequate regulations and develop tertiary treatment for municipal WWTPs in order to improve water quality and avoid the environmental risk associated with pharmaceutical drugs. In this regards, catalytic ozonation using NaY-12 zeolites emerges as a promising alternative to address the global concern related to CECs.



**Table 4.2** Risk Quotients calculated for effluent A and B and after different treatments applied, adsorption (1 h), ozonation and catalytic ozonation (10 min) on NaY-60 and NaY-12 zeolites (denoted as 60 and 12, respectively). Values in color green correspond to: low risk, yellow color: moderate risk, and red color 1: high risk.

| Compound                                 | Initial effluent |      | Adsorption |      |      |      | Ozonation |      | Catalytic ozonation |      |      |      | PNEC ( $\mu\text{g L}^{-1}$ ) | References                |
|--|------------------|------|------------|------|------|------|-----------|------|---------------------|------|------|------|-------------------------------|---------------------------|
|  | A                | B    | A          |      | B    |      | A         | B    | A                   |      | B    |      |                               |                           |
|  |                  |      | 60         | 12   | 60   | 12   |           |      | 60                  | 12   | 60   | 12   |                               |                           |
| Diclofenac                               | 0.33             | 0.85 | 0.26       | 0.22 | 0.91 | 0.90 | 0.01      | 0.00 | 0.01                | 0.01 | 0.00 | 0.00 | 0.05                          | (Loos et al., 2018)       |
| Phenazone                                | 0.30             | 0.07 | 0.26       | 0.27 | 0.06 | 0.07 | 0.01      | 0.00 | 0.00                | 0.00 | 0.00 | 0.00 | 0.276                         | (Tell et al., 2019)       |
| Ciprofloxacin                            | 0.39             | 0.27 | 0.00       | 0.35 | 0.04 | 0.19 | 0.00      | 0.01 | 0.00                | 0.01 | 0.01 | 0.01 | 0.089                         | (Loos et al., 2018)       |
| Clarithromycin                           | 0.10             | 0.17 | 0.07       | 0.10 | 0.14 | 0.16 | 0.01      | 0.00 | 0.01                | 0.00 | 0.00 | 0.00 | 0.08                          | (Tell et al., 2019)       |
| Erythromycin                             | 0.01             | 0.10 | 0.01       | 0.01 | 0.06 | 0.10 | 0.00      | 0.00 | 0.00                | 0.00 | 0.00 | 0.00 | 0.2                           | (Carvalho et al., 2015)   |
| Trimethoprim                             | 0.04             | 0.05 | 0.00       | 0.00 | 0.00 | 0.00 | 0.00      | 0.00 | 0.00                | 0.00 | 0.00 | 0.00 | 0.16                          | (Mendoza et al., 2015)    |
| Sulfamethoxazole                         | 0.00             | 0.01 | 0.00       | 0.00 | 0.02 | 0.03 | 0.00      | 0.00 | 0.00                | 0.00 | 0.00 | 0.00 | 0.6                           | (Tell et al., 2019)       |
| Clindamycin                              | d.               | 0.03 | d.         | d.   | 0.01 | 0.00 | d.        | 0.00 | 0.00                | d.   | 0.00 | 0.00 | 0.1                           | (Tell et al., 2019)       |
| Norfloxacin                              | n.d              | 0.04 | n.d        | n.d  | 0.01 | 0.03 | n.d       | 0.01 | n.d                 | n.d  | 0.00 | 0.00 | 0.16                          | (Zhou et al., 2019)       |
| Metronidazole                            | 0.03             | 0.07 | 0.03       | 0.03 | 0.07 | 0.07 | 0.01      | 0.05 | 0.00                | 0.00 | 0.04 | 0.05 | 0.13                          | (Tell et al., 2019)       |
| Tetracycline                             | d.               | 0.00 | d.         | d.   | 0.00 | 0.00 | d.        | 0.00 | d.                  | d.   | 0.00 | 0.00 | 1.0                           | (Tell et al., 2019)       |
| Carbamazepine                            | 0.00             | 0.00 | 0.00       | 0.00 | 0.00 | 0.00 | 0.00      | 0.00 | 0.00                | 0.00 | 0.00 | 0.00 | 2.5                           | (Mendoza et al., 2015)    |
| Gabapentin                               | 0.04             | 0.89 | 0.03       | 0.04 | 0.40 | 0.39 | 0.02      | 0.46 | 0.00                | 0.00 | 0.20 | 0.41 | 0.196                         | (Tell et al., 2019)       |
| Primidone                                | 0.04             | 0.07 | 0.05       | 0.05 | 0.06 | 0.07 | 0.01      | 0.04 | 0.01                | 0.00 | 0.03 | 0.04 | 0.069                         | (Tell et al., 2019)       |
| Irbesartan                               | 0.00             | 0.00 | 0.00       | 0.00 | 0.00 | 0.00 | 0.00      | 0.00 | 0.00                | 0.00 | 0.00 | 0.00 | 700                           | (Aa van der et al., 2001) |
| Losartan                                 | 0.00             | 0.00 | 0.00       | 0.00 | 0.00 | 0.00 | 0.00      | 0.00 | 0.00                | 0.00 | 0.00 | 0.00 | 63.7                          | (Godoy et al., 2015)      |
| Valsartan                                | 0.01             | 0.00 | 0.01       | 0.02 | 0.05 | 0.05 | 0.00      | 0.04 | 0.00                | 0.00 | 0.02 | 0.03 | 3.865                         | (Zhou et al., 2019)       |
| Enalapril                                | d.               | 0.09 | d.         | d.   | 0.00 | 0.00 | d.        | 0.00 | d.                  | d.   | 0.00 | 0.00 | 21                            | (Tell et al., 2019)       |
| Levamisole                               | 0.00             | 0.00 | 0.00       | 0.00 | 0.00 | 0.00 | 0.00      | 0.00 | 0.00                | 0.00 | 0.00 | 0.00 | 1                             | (Chen et al., 2015)       |
| Atorvastatin                             | d.               | 0.04 | d.         | d.   | 0.00 | 0.02 | d.        | 0.00 | d.                  | d.   | 0.00 | 0.00 | 0.19                          | (Tell et al., 2019)       |
| Iopromide                                | 0.00             | d.   | 0.00       | 0.00 | d.   | d.   | 0.00      | d.   | 0.00                | 0.00 | d.   | d.   | 256                           | (Tell et al., 2019)       |
| Metoprolol                               | 0.00             | 0.00 | 0.00       | 0.00 | 0.00 | 0.00 | 0.00      | 0.00 | 0.00                | 0.00 | 0.00 | 0.00 | 61                            | (Mendoza et al., 2015)    |
| Tramadol                                 | 0.03             | 0.12 | 0.00       | 0.00 | 0.00 | 0.00 | 0.00      | 0.00 | 0.00                | 0.00 | 0.00 | 0.00 | 0.959                         | (Zhou et al., 2019)       |
| Lorazepam                                | 0.00             | 0.00 | 0.00       | 0.00 | 0.00 | 0.00 | 0.00      | 0.00 | 0.00                | 0.00 | 0.00 | 0.00 | 1.683                         | (Mendoza et al., 2015)    |
| Venlafaxine                              | 0.38             | 1.29 | 0.00       | 0.00 | 0.00 | 0.00 | 0.00      | 0.00 | 0.00                | 0.00 | 0.00 | 0.00 | 0.038                         | (Loos et al., 2018)       |
| <i>O</i> -desmethylvenlafaxine           | 0.02             | 0.04 | 0.00       | 0.00 | 0.00 | 0.00 | 0.00      | 0.00 | 0.00                | 0.00 | 0.00 | 0.00 | 2.3                           | (Figuère et al., 2022)    |
| <b>Total risk (RQ<sub>mixture</sub>)</b> | 1.73             | 4.21 | 0.73       | 1.1  | 1.83 | 2.07 | 0.07      | 0.61 | 0.03                | 0.02 | 0.54 | 0.3  |                               |                           |
| <b>Total risk decrease (%)</b>           |                  |      | 58%        | 63%  | 57%  | 51%  | 96%       | 86%  | 98%                 | 99%  | 87%  | 93%  |                               |                           |

## **4.4 Conclusions**

The results of this chapter indicated that addition of NaY zeolites in the ozonation can be a suitable option to degrade pharmaceutical compounds in secondary effluents from MWWTPs, with low doses of catalyst and ozone concentration. The total mixture of PhACs was near completely removed (above 95%) with ozonation and combined with zeolite NaY-12 and the NaY-60 within the first minutes of treatment, 9 and 12 min, respectively, in the effluent A. Moreover, in the catalytic ozonation of micropollutants for both NaY zeolites it was necessary 31 mg L<sup>-1</sup> of TO<sub>3</sub>D, almost 27% less than in the single ozonation. This represents an economic advantage of the combined process due to the high cost of ozone production, making its application more viable at large scale. The amount of Brønsted and Lewis acid sites in the NaY zeolites influenced the degradation of PhACs compound in the wastewater. The NaY-12 zeolite offered more amount of Lewis and Brønsted acid sites on the surface compared to NaY-60 zeolite. Hence, more Lewis active acid sites imply more aqueous ozone attracted to oxidation of PhACs to enhance the redox process involved in ozone adsorption/decomposition. Concerning the application of individual systems, single ozonation can lead 95% to the complete removal of the PhCs after 25 min (46.2 mg O<sub>3</sub> L<sup>-1</sup> consumed). In adsorption, only 30% and 44% removals were reached using NaY-12 and NaY-60 zeolites, respectively, after 60 minutes of contact time. Physical-chemical properties of pharmaceuticals influence in the efficiency of the process; positively charged pharmaceuticals seem to be better adsorbed into the NaY zeolites when treating WWTP effluents. Additionally, the RQ values for all pharmaceuticals after the application of the coupled system ozonation and NaY zeolites (only 10 min of reaction) were significantly diminished compared with the initial wastewater, considerably reducing the risk in the receiving environment. Even, the single ozonation system could eliminate the risk associated with PhACs. These results provided a new insight on the catalytic mechanisms in NaY zeolites-catalyzed ozonation and can set the ground for further applications of treating real environmental matrices on a large scale.

# **Chapter 5. Evaluation of an ozone membrane contactor to enhance gas/liquid mass transfer and its application in the removal of pharmaceuticals in real wastewater**

## **5.1 Introduction**

Water ozonation processes have traditionally been applied injecting the O<sub>3</sub> gas stream into the liquid phase by sparging gas bubbles via gas diffusers or venturi injectors (Gottschalk et al., 2010). However, some drawbacks hinder the use of these conventional injection methods, such as low gas-liquid mass transfer. In addition, to ensure a higher dissolution efficiency of O<sub>3</sub> gas in the aqueous phase, large contact tanks are required (Gao et al., 2005; Gottschalk et al., 2010). In recent years, membrane contactors for ozone diffusion/dispersion in water have emerged as promising methods to overcome these limiting factors (Kukuzaki et al., 2010; Schmitt et al., 2022). In gas-liquid membrane contactors, the porous membrane acts as a passive barrier between the gas and water phases, separating the two fluids and enabling continuous contact in a stable interfacial area (Pabby and Sastre, 2013). This configuration offers several advantages over conventional reactors. Major benefits include a high volumetric mass transfer efficiency, predictable flow patterns, easy scale-up by modular design, and small reactor footprints (Pines et al., 2005; Schmitt et al., 2022). Moreover, using membrane contactors may minimize operational costs from a reduction in the required ozone dosage (due to the multiple injection points) and a decrease in the requirements for off-gas disposal (John et al., 2022).

Some studies have investigated the effectivity of ozone membrane contactors in their application in water treatment for CECs abatement. For instance, Schmitt et al., (2023) tested a polytetrafluoroethylene (PTFE) hollow fiber membrane contactor in the ozonation of real-treated wastewater spiked with two PhACs and found high removal rates with short residence times ( $< 3$  s). Similarly, Merle et al., (2017) observed better performance in a PTFE membrane contactor in the presence of hydrogen peroxide for the elimination of CECs in groundwater and surface water compared to the conventional peroxone process. Stylianou et al., (2018) demonstrated the technical feasibility of a ceramic tubular membrane contactor for the treatment of four micropollutants in natural surface waters. Recently, Presumido et al., (2022) proposed a novel tubular borosilicate membrane contactor to enhance ozone gas-liquid mass transfer and the elimination of a mixture of CECs spiked in demineralized water in a continuous mode operation. The authors reported removals higher than 80% for 13 of the 19 CECs with an ozone dose of  $12 \text{ g m}^{-3}$  and residence time of 3.9 s. The authors also found that the volumetric mass transfer coefficient ( $K_{La}$ ) was enhanced by 1.5–2.0 times with an increase in gas and liquid flow rate.

This brief review of the state of the art demonstrates that efforts are still required to investigate the ozonation processes when using membrane contactors for water/wastewater treatment applications and specifically for eliminating CECs at environmentally relevant concentrations in real effluents. In view of the above, the overall goal of this work was to evaluate the performance of a stainless-steel membrane contactor for the intensification of ozone gas-water mass transfer and its application in the elimination of a broad group of PhACs at realistic concentration levels (ppb:  $\mu\text{g L}^{-1}$ ) under continuous flow conditions. In this novel configuration, the  $\text{O}_3$  gas stream is fed by the lumen side of the membrane and rapidly transferred to the liquid phase through multiple ozone dosing points along the membrane length. The tangential liquid inlet and outlet enable a helical motion of the liquid stream around the membrane shell-side providing a more homogeneous radial dispersion of the injected gas and contributing to the enhancement of mass transfer and oxidation of pollutants (Presumido et al., 2022). The present chapter was focused on three main aspects: (i) the occurrence of relevant pharmaceuticals in secondary-treated municipal wastewater, (ii) the effect of different operational parameters, including the  $\text{O}_3$  concentration in the gas phase ( $C_{\text{O}_3,g,in}$ ), liquid ( $Q_L$ ) and gas ( $Q_G$ ) flow rates on the volumetric mass transfer

coefficient ( $K_{La}$ ), and (iii) the abatement of 23 PhACs detected in the secondary-treated municipal wastewater as a function of specific ozone dose. This work thus attempts to contribute to a better understanding of ozone membrane contactors for wastewater treatment.

## **5.2 Experimental setup and procedure**

Figure 2.5 presents a schematic representation of the experimental setup used in all trials. The ozone-oxygen gas mixture was fed by the lumen side of the membrane, permeating through the pores structure, and delivered to the membrane shell side. Meanwhile, the liquid phase was pumped from a 5 L-jacketed glass vessel, connected to a thermostatic bath for temperature control, to the ARZ of the membrane contactor, where  $O_3$  gas-water contacting occurs. For the gas/liquid mass transfer trials, the membrane reactor outlet was connected to the upper inlet of a column (1.5 dm<sup>3</sup>, maximum fluid column height of 370 mm and  $\varnothing_{inner} = 73$  mm) to separate the gas from the liquid phase, and water samples were collected in the bottom outlet of the column.

For PhACs removal trials, the outlet stream of the membrane contactor was connected to the inlet of the column located at the bottom, where water samples were collected at the upper outlet of the column. Samples were collected at pre-determined time intervals once steady-state conditions were reached. The residual concentration of  $O_3$  in the collected samples was removed immediately by placing the samples in a water bath at 80 °C. The off-gas was collected from the top of the column, passed through the dehumidifier, and directed to the  $O_3$  analyzer. Finally, the residual gas was vented through the catalytic  $O_3$  destruction unit and sequentially to washing bottles containing a 2% KI solution before going into exhaustion. After each experimental run, the membrane contactor was cleaned by pumping demineralized water through ARZ. The experimental conditions for all tests are presented in Table 5.1.

**Table 5.1** Experimental conditions employed in the ozone mass transfer tests and in PhACs removal experiments using secondary-treated wastewater.

| Ozone mass transfer tests (pH=2.2, T=20°C)  |  |   |  |   |   |   |   |   |
|---|--|---|--|---|---|---|---|---|
| Parameter                                   | $Q_G$<br>(Ndm <sup>3</sup> min <sup>-1</sup> ) | $C_{O_3,g,in}$<br>(g Nm <sup>-3</sup> ) | $Q_L$<br>(dm <sup>3</sup> h <sup>-1</sup> )    | $\tau$<br>(s)                           | $C_{O_3^*,l}^a$<br>(g m <sup>-3</sup> )   | $C_{O_3,l,out}^a$<br>(g m <sup>-3</sup> ) | $K_{La,20^\circ C}$ (min <sup>-1</sup> ) <sup>a</sup> |   |
| $Q_G$                                       | 0.30   | 80                                      | 70   | 8.2                                     | 23.5 ± 0.1                                | 4.7 ± 0.06                                | 1.7 ± 0.1   |   |
|   | 0.50   |   |  | 8.0                                     |   | 8.3 ± 0.2                                 | 3.4 ± 0.2   |   |
|   | 0.75   |   |  | 7.5                                     |   | 11.0 ± 0.1                                | 5.3 ± 0.1   |   |
|   | 0.85   |   |  | 7.4                                     |   | 12.1 ± 0.2                                | 6.1 ± 0.2   |   |
| $C_{O_3,g,in}$                              | 0.75   | 40                                      | 70   | 7.5                                     | 23.5 ± 0.1                                | 9.3 ± 0.03                                | 5.2 ± 0.2   |   |
|   |  | 60                                      |  |   |   | 16.4 ± 0.02                               | 7.6 ± 0.1   | 5.1 ± 0.3   |
|   |  | 80                                      |  |   |   | 23.5 ± 0.1                                | 11.0 ± 0.1  | 5.3 ± 0.1   |
| $Q_L$                                       | 0.75   | 80                                      | 30   | 17.5                                    | 23.5 ± 0.1                                | 14.0 ± 0.1                                | 3.2 ± 0.3   |   |
|   |  |   | 50   | 10.5                                    |   | 12.6 ± 0.1                                | 4.6 ± 0.06  |   |
|   |  |   | 70   | 7.5                                     |   | 11.0 ± 0.1                                | 5.3 ± 0.1   |   |
|   |  |   | 90   | 5.8                                     |   | 9.21 ± 0.08                               | 5.3 ± 0.4   |   |
|   |  |   | 100  | 5.3                                     |   | 8.47 ± 0.09                               | 5.5 ± 0.4   |   |
| PhACs removal tests (pH= ~7.4, T= ~20-22°C) |  |   |  |   |   |   |   |   |
| Test number                                 | $Q_L$<br>(dm <sup>3</sup> h <sup>-1</sup> )    | $\tau$<br>(s)                           | $Q_G$<br>(Ndm <sup>3</sup> min <sup>-1</sup> ) | $C_{O_3,g,in}$<br>(g Nm <sup>-3</sup> ) | AO <sub>3</sub> D<br>(g m <sup>-3</sup> ) | TO <sub>3</sub> D<br>(g m <sup>-3</sup> ) | CO <sub>3</sub> D<br>(g m <sup>-3</sup> )             | Specific O <sub>3</sub> dose<br>(g O <sub>3</sub> g DOC <sup>-1</sup> ) |
| 1   |  |   |  | 20                                      | 9   | 6.3                                       | 6.3   | 0.39  |
| 2   | 100  | 60                                      | 0.75   | 27                                      | 12  | 8.6                                       | 8.6   | 0.53  |
| 3   |  |   |  | 40                                      | 18  | 11.0                                      | 10.6  | 0.69  |
| 4   |  |   | 0.25   | 80                                      |   | 10.4                                      | 10.4  | 0.65  |
| 5   | 100  | 60                                      | 0.15   | 134                                     | 12  | 12.0                                      | 11.6  | 0.73  |

$a \pm$  standard error.

### 5.3 Estimation of ozone mass transfer in the membrane contactor

Ozone mass transfer experiments were conducted using demineralized water at acidic conditions (pH = 2.2) to avoid O<sub>3</sub> decomposition reactions. Initially, the O<sub>3</sub> gas stream was fed by the lumen side of the membrane, with the shut-off valve fully open, filling the inner space with gas. Afterward, the water was pumped into the annular zone, and the shut-off valve was immediately closed, enabling the permeation of the gas into the liquid side. The

concentration of ozone in the off-gas and in the liquid samples collected at membrane reactor outlet were measured over time until achieve steady-state conditions. All experiments were conducted at a constant temperature of 20°C. The effect of various operating parameters in the volumetric mass transfer coefficient, i.e., ozone concentration in the inlet gas stream ( $C_{O_3,g,in} = 40\text{-}80 \text{ g Nm}^{-3}$ ), liquid flow rate ( $Q_L = 30\text{-}100 \text{ dm}^3 \text{ h}^{-1}$ ), and gas flow rate ( $Q_G = 0.3\text{-}0.85 \text{ Ndm}^3 \text{ min}^{-1}$ ) was investigated under continuous mode operation. The volumetric mass transfer coefficient ( $K_La$ ) ( $\text{min}^{-1}$ ) has been estimated from the mass balance of ozone in the liquid phase, considering plug flow conditions.

Under steady-state conditions, considering  $C_{O_3,l,t} = 0$  at  $t = 0$  and  $C_{O_3,l,t} = C_{O_3,l,out}$  at  $t = \tau$ , the integration results in Eq. (5.1)

$$K_La = -\frac{1}{\tau} \times \ln \left( 1 - \frac{C_{O_3,l,out}}{C_{O_3^*,l}} \right) \quad (5.1)$$

where  $C_{O_3,l,out}$  ( $\text{mg dm}^{-3}$ ) is the dissolved ozone concentration in the outlet liquid stream at steady-state conditions, and  $\tau$  is the liquid residence time, calculated by Eq. (5.2).

$$\tau_L = (1 - \varepsilon_G) \times \frac{V_R}{Q_L} \quad (5.2)$$

where  $V_R$  ( $\text{dm}^3$ ) is the annular zone volume of the membrane reactor, and  $\varepsilon_G$  is the gas holdup fraction (see values in Fig. A3 in Annexes).

Based on gas hold-up measurements, the specific interfacial area,  $a$ , was determined by Eq. (5.3), taking into account the Sauter mean diameter ( $d_{32}$ ). These mean diameters were determined from measurements of all bubble sizes of the liquid–gas mixture by photographic method and processing through Eq. (5.4).

$$a = 6 \frac{\varepsilon_G}{d_{32}} \quad (5.3)$$

$$d_{32} = \frac{\sum_{i=1}^n n_i \times d_{eq}^3}{\sum_{i=1}^n n_i \times d_{eq}^2} \quad (5.4)$$

where  $n_i$  is the number of bubbles of diameter  $d_{eq}$  (m). More details about the experimental procedure are provided in TA.1 Annexes.

The overall mass transfer resistance,  $1/K_L$ , was also investigated for the hydrophilic membrane contactor, described as three resistances in series according to Eq. (5.5) (Kukuzaki et al., 2010).

$$\frac{1}{K_L} = \frac{1}{k_G H} + \frac{1}{k_M} + \frac{1}{k_L} \quad (5.5)$$

where  $k_G$ ,  $k_M$ , and  $k_L$  are the individual mass transfer coefficients for the gas phase, the membrane, and the liquid phase, respectively;  $\frac{1}{k_G H}$ ,  $\frac{1}{k_M}$  and  $\frac{1}{k_L}$  are the mass transfer resistances in the gas boundary layer, membrane matrix, and liquid boundary layer, respectively;  $H$  represents the adimensional Henry's law constant. When using a membrane contactor for gas-liquid absorption, the mass transfer resistance is controlled by the liquid side (Iversen et al., 1997; Johnson and Davis, 1996). Hence, the resistance to mass transfer in the gas phase can be neglected (i.e.,  $1/k_G H \approx 0$ ), as the diffusivity of ozone in gas is much larger than in the water phase ( $10^4$  times than liquid phase) (Johnson and Davis, 1996). Thus, Eq. (5.5) may be rewritten as:

$$\frac{1}{K_L} = \frac{1}{k_M} + \frac{1}{k_L} \quad (5.6)$$

For totally gas-filled membrane pores, the mass transfer coefficient depends on the  $O_3$  diffusion coefficient, and on the geometrical characteristics of the membrane, *i.e.*, thickness, pore size, porosity, and tortuosity, according to Eq. (5.7) (Mavroudi et al., 2006):

$$k_M = \frac{D_M \times \varepsilon_m}{\tau_m \times l_m} \quad (5.7)$$

where  $D_M$  ( $m^2 s^{-1}$ ) is the effective diffusion coefficient of ozone in the membrane,  $\varepsilon_m$  is the membrane porosity (21%),  $\tau_m$  is the tortuosity factor of the membrane, and  $l_m$  is the membrane thickness ( $2.0 \times 10^{-3}$  m). The  $\tau$  was estimated by the porosity-tortuosity relationship defined by (Iversen et al., 1997).



$$\tau_m = \frac{(2 - \varepsilon_m)^2}{\varepsilon_m} \quad (5.8)$$

Diffusion in macropores occurs mainly by the combined effects of bulk molecular diffusion (as in the free fluid) and Knudsen flow. Therefore,  $D_M$  can therefore be expressed as Eq. (5.9).

$$D_M = \frac{1}{\frac{1}{D_{O_3}} + \frac{1}{D_K}} = \frac{1}{\frac{1}{D_{O_3}} + \frac{1}{\frac{d_{pore}}{3} \times \sqrt{\frac{8RT}{\pi M}}}} \quad (5.9)$$

where  $D_K$  is the Knudsen diffusion coefficient, defined by  $D_K = \frac{d_{pore}}{3} \times \sqrt{\frac{8RT}{\pi M}}$  ( $\text{m}^2 \text{s}^{-1}$ ),  $D_{O_3}$  is the diffusion coefficient of ozone in the gas phase ( $2 \times 10^{-5} \text{ m}^2 \text{ s}^{-1}$  at  $20^\circ \text{C}$  (Bamperng et al., 2010)),  $T$  is the temperature ( $293.15^\circ \text{K}$ ),  $M$  is the molar mass of ozone ( $47.998 \text{ g mol}^{-1}$ ),  $R$  is the ideal gas constant ( $8.3145 \text{ J K}^{-1} \text{ mol}^{-1}$ ), and  $d_{pore}$  is the mean pore diameter ( $1.0 \times 10^{-6} \text{ m}$ ).

## 5.4 Results and discussion

The influence of three parameters on the volumetric ozone mass transfer coefficient, namely the flow rate of the inlet gas and liquid streams, and ozone concentration in the inlet gas stream, was investigated to gain a better understanding of the gas/liquid mixing.

### 5.4.1 Effect of inlet gas stream flow rate

The ozone mass transfer coefficient was investigated for inlet gas stream flow rates ranging from  $0.3$  to  $0.85 \text{ Ndm}^3 \text{ min}^{-1}$ , while ozone concentration and  $Q_L$  were kept at  $80 \text{ g Nm}^{-3}$  and  $70 \text{ dm}^3 \text{ h}^{-1}$ , respectively. As can be seen from Figure 5.1,  $K_L a$  increased 3.6 times as the input gas flow rate increased from  $0.3$  to  $0.85 \text{ Ndm}^3 \text{ min}^{-1}$ , indicating a considerable influence of gas flow rate in ozone mass transport. This behavior may be attributed to the greater mixing induced by a higher number of bubbles dispersed in the liquid as the inlet gas flow rate increases.

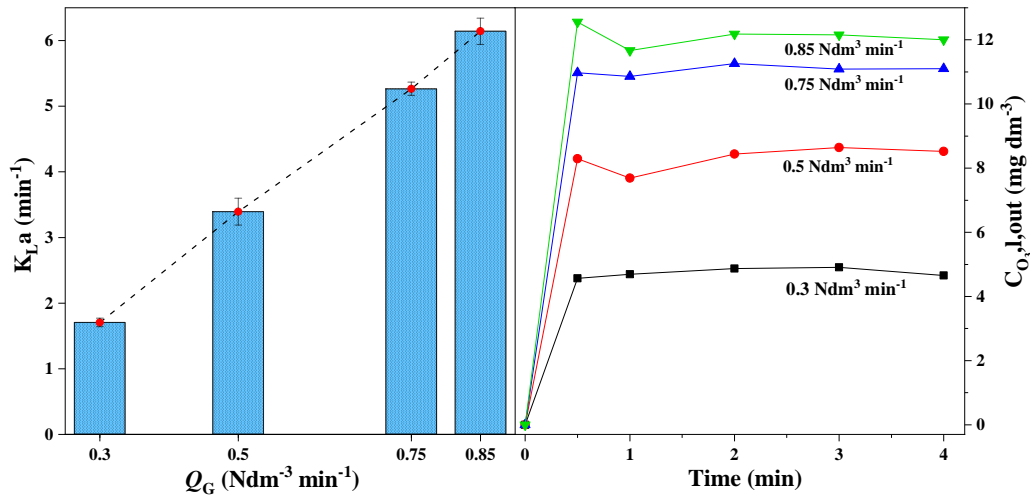


**Figure 5.1** Effect of the gas flow rate

As a result, a higher fraction of gas is inside the annular zone, subsequently boosting the liquid velocity in the gas boundary layer (lower liquid residence time inside the reactor). This, in turn, enables a higher driving force for ozone dissolution. In addition, the same principles explain an almost linear correlation between the increment in the ozone concentration in the liquid phase at the reactor outlet, at steady state conditions, and the inlet gas flow rate. These findings agree with previous studies regarding the positive influence of gas flow rate on the  $K_{La}$  using ozone membrane contactors (Presumido et al., 2022; Wang et al., 2021). Nevertheless, opposite trends were also observed by other authors (Bamperng et al., 2010; Berry et al., 2017).

#### 5.4.2 Effect of the ozone concentration in the inlet gas stream

Figure 5.2 shows a negligible impact of  $C_{O_3,g,in}$  in the  $K_{La}$  values, considering values ranging between 40 to 80  $\text{g Nm}^{-3}$ . On the other hand, dissolved ozone concentration at the reactor outlet under steady-state conditions increased almost proportionally with  $C_{O_3,g,in}$ , since more  $O_3$  molecules are available in the gas phase (higher partial pressure). As a consequence, the driving force of the mass transfer is enhanced, leading to larger values of  $C_{O_3,l,out}$ , in agreement with Henry's law (Sotelo et al., 1989). This trend was also observed for previous authors using membrane contactors (Berry et al., 2017; Kukuzaki et al., 2010; Sabelfeld and Geißen, 2019).

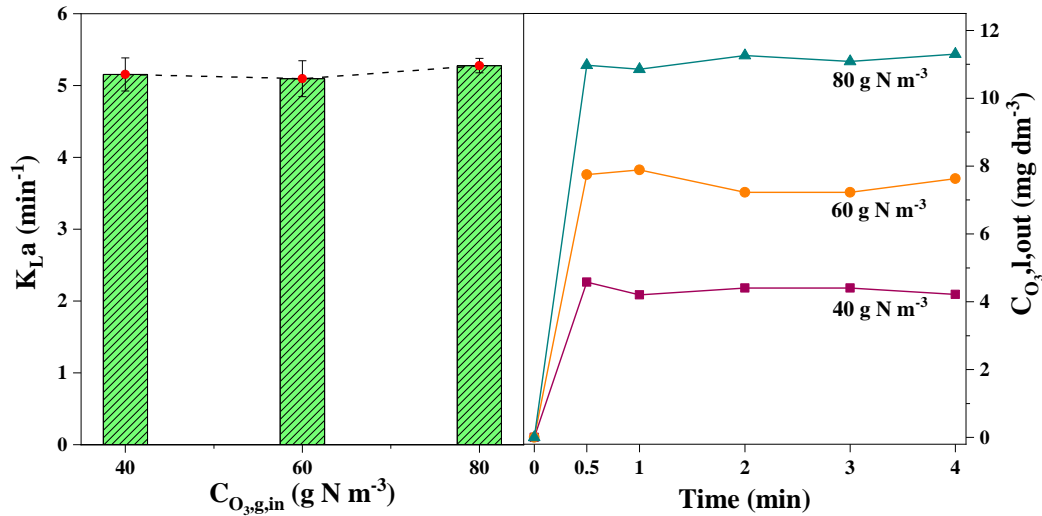
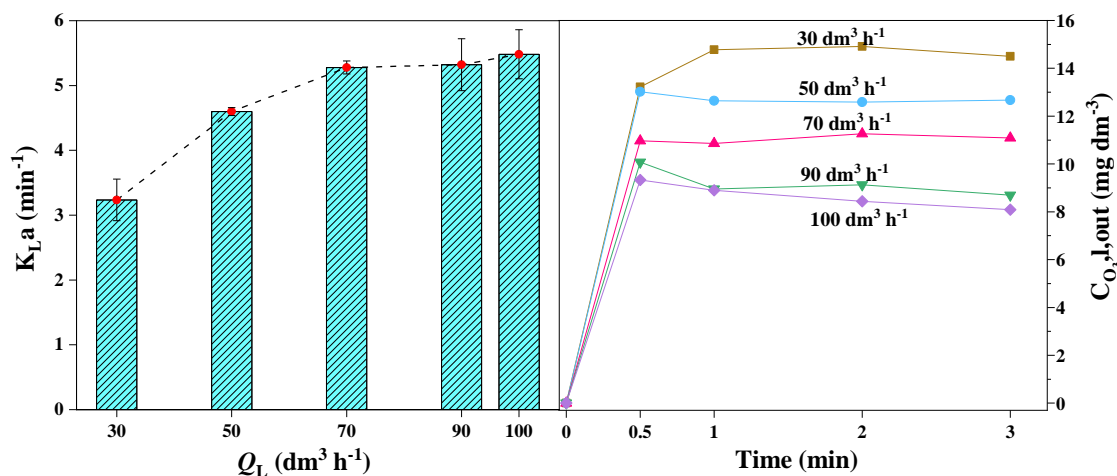


Figure 5.2 Effect of the ozone gas concentration in the inlet stream.

### 5.4.3 Effect of liquid flow rate

The gas-liquid mass transfer coefficient was investigated for liquid flow rates varying from 30 to 100  $dm^3 h^{-1}$  corresponding to Reynolds numbers of 181 to 604, respectively. As illustrated in Figure 5.3,  $K_{L,a}$  increased 1.6 times with the liquid flow rate from 30 to 70  $dm^3 h^{-1}$ , and after that, remained almost constant. This enhancement is attributed to higher Reynolds numbers, enabling smaller gas bubbles or thinner liquid films, reducing the boundary layer resistance, and boosting the mass transfer. Additionally, the inlet and outlet pipes located perpendicularly to the fluid flow direction and tangentially to the shell, in the horizontal plane and at the top on opposite sides, induce a helical motion, i.e. a swirl, of the water around the membrane shell-side, when a minimum value of liquid velocity is provided, according to the dimensions of the reactor (Moreira et al., 2019). This leads to a longer effective flow path, and enhances the shear rate on the membrane surface, dragging the gas bubbles from the membrane surface to the bulk (Presumido et al., 2022).



**Figure 5.3** Effect of the liquid flow rate on  $K_{La}$  values.

Previous studies have reported similar trends, indicating that changes in the liquid flow rate had the most significant effect on the volumetric mass transfer coefficient of ozone in water (Berry et al., 2017; Pines et al., 2005; Zoumpouli et al., 2018). However, higher liquid velocities shorten liquid residence time and mainly affect the dissolved ozone concentration in the reactor outlet. For instance,  $C_{O_3,l,out}$  was found to decrease from 14.0 to 8.5 mg L<sup>-1</sup> when  $Q_L$  increased from 30 to 100 dm<sup>3</sup> h<sup>-1</sup>. Selecting the optimal liquid velocity that ensures a desired level of dissolved O<sub>3</sub> concentration to get an adequate kinetic reaction is a key point. Moreover, the overall mass transfer coefficient,  $K_L$ , was calculated from experimental values of  $KLa$  and the gas-water interfacial area ( $a$ ). It was found that the tubular stainless membrane steel contactor provided an interfacial area in the range of 2054-2841 m<sup>-1</sup>, with a homogenous distribution of ozone gas bubbles with an average size of 0.25 mm (See Figure 5.4). Therefore,  $K_L$  values were estimated in the range of 1.9 and 4.5×10<sup>-5</sup> m s<sup>-1</sup> for  $Q_L$  between 30 to 100 dm<sup>3</sup> h<sup>-1</sup>, respectively.

The investigated gas-liquid membrane contactor showed  $K_{La}$  values in the range of 1.7-6.1 min<sup>-1</sup>, which are higher than those reported for the conventional bubble columns ( $K_{La} \sim 0.3$ -1.6 min<sup>-1</sup>) (Roustan et al., 1996), and slightly lower than venturi injection systems ( $K_{La} \sim 3.6$ -12.6 min<sup>-1</sup>) (Roustan, 2003). Nonetheless, in terms of energy consumption, venturi injectors require a higher specific power consumption compared to membrane contactors (Gottschalk et al., 2010; My Hanh Le et al., 2022).

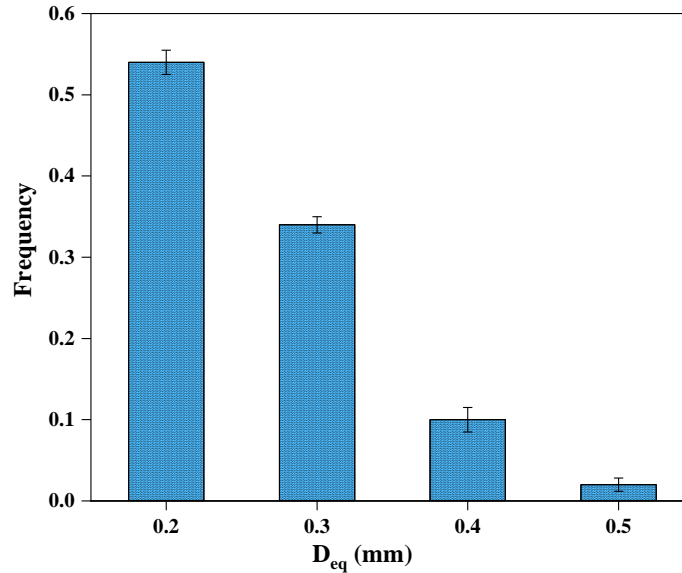


**Figure 5.4** Bubble size distribution in tubular porous stainless-steel membrane contactor.

#### 5.4.4 Estimation of membrane transfer coefficient and mass transfer resistances

Mass transfer is not only dominated by the resistance of the liquid boundary film but also by the membrane itself. The mass transfer coefficient in the membrane,  $k_M$ , was determined by using the so-called Wilson plot method (Wilson, 1915), which involves plotting the experimental data of  $1/K_L$  against  $1/Q_L$ .  $1/k_M$  was obtained by the interception of the straight line with the y-axis (where  $1/Q_L = 0$ , implying  $Q_L \rightarrow \infty$  and thus  $1/k_L \approx 0$ ) of the Wilson plot in Figure 5.5. Under the applied experimental conditions, the  $1/k_M$  was found to be  $(9.74 \pm 0.05) \times 10^3 \text{ s m}^{-1}$ , which corresponds to  $k_M$  value of  $(1.03 \pm 0.05) \times 10^{-4} \text{ m s}^{-1}$ .

The membrane mass transfer coefficient for a liquid-filled pores membrane, can be calculated from Eq. (5.7), considering the structural properties of the stainless-steel membrane. The theoretical value obtained was  $k_M = 2.19 \times 10^{-5} \text{ m s}^{-1}$ , which is 4.7 times higher than the experimental value ( $k_M = 1.03 \pm 0.05 \times 10^{-4} \text{ m s}^{-1}$ ). The possible reason for the large difference between the two values may be attributed to the fact that the assumptions in the Eq. (5.7) are based on cylindrical membrane pores, a constant tortuosity, and lognormal distribution of membrane pore size (Kreulen et al., 1993; Lu et al., 2008). These assumptions probably resulted in an overestimation of the resistance to mass transfer across the membrane. Khaisri et al., (2010) observed similar results in their study on  $\text{CO}_2$  absorption with a PTFE hollow

fiber membrane contactor. The authors found that the membrane mass transfer resistance calculated from the Wilson plot method produced higher accuracy than the theoretical method.

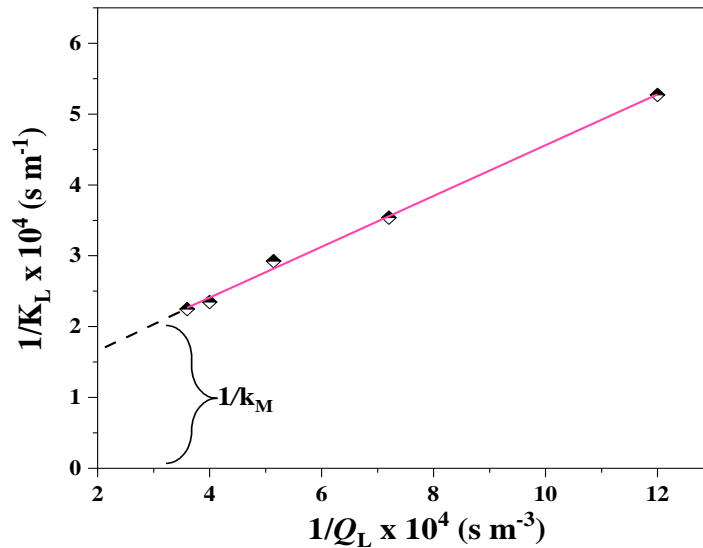


**Figure 5.5** Graphical scheme for calculating the mass transfer coefficient in the membrane by Wilson's plot method.

The analysis of the individual mass-transfer resistances in the liquid phase was calculated by substituting the experimental value of  $K_L$  and  $k_M$  obtained from the Wilson plot method in Eq. (5.6). Figure 5.6a shows the results of individual mass transfer resistances for ozone dissolution at different liquid flow rates. It can be noticed that the resistance to diffusion through the liquid phase boundary layer ( $1/k_L$ ) is the main resistance to ozone transfer for low liquid flow rates ( $Q_L = 30 \text{ dm}^3 \text{ h}^{-1}$ ), contributing to 82% of the total mass transfer resistance (Figure 5.6b), while 18% comes from the membrane. However, when increasing  $Q_L$  to  $100 \text{ dm}^3 \text{ h}^{-1}$ , the liquid-phase resistance becomes almost comparable with membrane resistance and contributes to 57% and 43% of the overall mass transfer resistance, respectively. Although a higher liquid flow rate can enhance gas transport in the liquid phase by reducing resistance in the liquid boundary layer, it may also intensify the membrane wetting to hinder gas transport in the membrane (Khaisri et al., 2009).

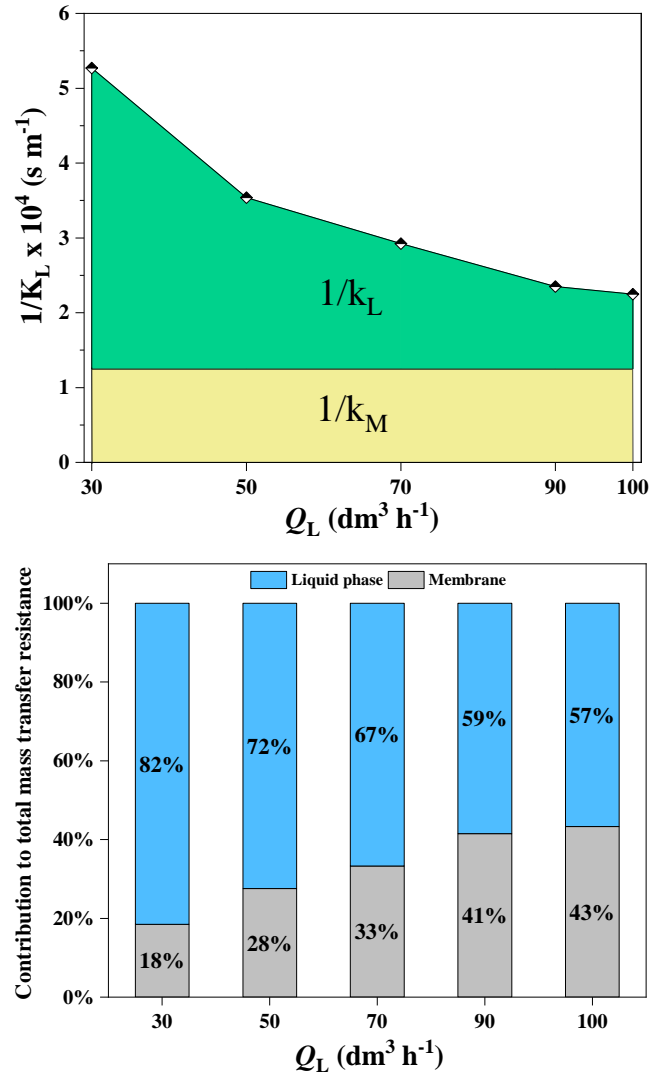


**Figure 5.6** (a) Analysis of mass-transfer resistances for ozone absorption in water, (b) contribution to total mass transfer resistance (%) in the liquid phase boundary film and in the membrane as a function of liquid flow rate.

The mass transfer resistance is also influenced by the material and properties of the membrane (porosity, pore size, and hydrophobicity). Membranes with lower porosity, lower pore size, and a low hydrophobicity exhibit higher resistance to ozone mass transfer (Li et al., 2020; Zhang et al., 2017). The investigated membrane is hydrophilic; thus, the water could more easily penetrate inside the pores and significantly increase the membrane resistance owing to the diffusion of ozone molecule in water is much slower than in gas (Johnson and Davis, 1996). However, the addition of a hydrophobic layer to the membrane shell-side can be a solution to overcome this limitation (Stylianou et al., 2015).

For similar conditions, the stainless-steel membrane (used in this study) presents a membrane resistance 1.4-fold higher than the borosilicate membrane tested by Presumido et al., (2022). These results may be attributed to the fact that the porosity and mean pore size of the borosilicate membrane used by authors were about 2.0 and 3.8 times greater, respectively, when compared to the stainless-steel membrane investigated in this study. Therefore, as the membrane porosity and pore size increase, higher amounts of ozone gas is able to diffuse through the membrane, decreasing the resistance on the membrane side. Nevertheless, higher pore size can also increase the risk of wetting, reducing the mass transfer (Bakeri et al., 2012). Although membrane resistance obtained in this study represented a disadvantage compared to the borosilicate membrane contactor, stainless steel material could be a better alternative regarding their thermal and mechanical stabilities to be implemented at full-scale (Song et al., 2011).

#### 5.4.5 Comparison with other gas-liquid contactor systems

A comparison of the performance of the membrane contactor with conventional gas-liquid systems is crucial to assess the degree of process intensification that can be achieved. In order to obtain a more accurate comparison of the membrane contactor performance with other gas-liquid contactors, the ASCE standards method for measuring oxygen mass transfer was used (ASCE, 2007). In this sense, two parameters were considered: standard oxygen transfer rate (SOTR, kg h<sup>-1</sup>) and standard oxygen transfer efficiency (SOTE, %). The SOTR, is defined as the amount of mass gas being dissolved per unit of time and SOTE is the ratio of the amount of gas transferred to the liquid phase to the amount of gas supplied to the system. The SOTR and SOTE were calculated by Eq. (5.10) and Eq. (5.11), respectively, at standard conditions.

$$\text{SOTR} = K_L a_{O_2} \times C_{O_2^*,l} \times V_R \quad (5.10)$$

$$\text{SOTE} = \frac{K_L a_{O_2} \times C_{O_2^*,l} \times V_R}{W_{O_2}} \quad (5.11)$$

where  $K_L a_{O_2}$  is the oxygen volumetric mass transfer coefficient (min<sup>-1</sup>),  $C_{O_2^*,l}$  is the equilibrium dissolved oxygen concentration (9.2 mg L<sup>-1</sup>),  $V_R$  is the annular zone volume of



the membrane reactor ( $\text{m}^3$ ), and  $W_{\text{O}_2}$  is the mass flow rate of  $\text{O}_2$  in the air stream ( $\text{kg O}_2 \text{ h}^{-1}$ ).  $W_{\text{O}_2}$  was calculated by assuming the air behaves as an ideal gas, containing 23 wt.% of  $\text{O}_2$  at standard conditions.

The  $K_{\text{L}}a_{\text{O}_2}$  values were estimated from the ozone mass transfer coefficients following the surface renewal theory (Beltrán et al., 1998), as given by the relation in Eq. (5.12).

$$\frac{K_{\text{L}}a_{\text{O}_3}}{K_{\text{L}}a_{\text{O}_2}} = \sqrt{\frac{D_{\text{O}_3}}{D_{\text{O}_2}}} = 0.9 \quad (5.12)$$

where  $D_{\text{O}_3}$  ( $1.76 \times 10^{-9} \text{ m}^2 \text{ s}^{-1}$ ) (Johnson and Davis, 1996) and  $D_{\text{O}_2}$  ( $2.17 \times 10^{-9} \text{ m}^2 \text{ s}^{-1}$ ) (Wilke and Chang, 1955) are the diffusion coefficients of  $\text{O}_3$  and  $\text{O}_2$  gases in water at  $20^\circ\text{C}$ , respectively.

The SOTR and SOTE values are presented in Table 5.2. It can be seen that the SOTR and SOTE values for traditional injection systems, such as fine bubble diffusers (DeMoyer et al., 2001; Gillot et al., 2005) and venturi injectors (Dayıoğlu, 2022; Therrien et al., 2019) were much higher compared to the membrane contactor. It is important to note that these parameters are strongly influenced by the reactor volume. Hence, the utilization of equipment with greater volumes results in higher values of SOTR and SOTE. For a better comparison, two additional parameters were included: the volumetric SOTR (VSOTR,  $\text{kg h}^{-1} \text{ m}^{-3}$ ), which was determined by dividing SOTR by the reactor volume, and the second term, the specific SOTE (SSOTE,  $\% \text{ m}^{-1}$ ), determined by dividing the SOTE by the height of the fluid or water depth ( $h$ , m).

From comparable data in terms of VSOTR, the membrane contactor transferred a higher amount of  $\text{O}_2$  mass into the water per unit of volume compared to bubble diffusers and venturi injectors. Similarly, regarding the SSOTE efficiency parameter, the membrane contactor achieved an  $\text{O}_2$  mass dissolution per unit of reactor height one to two orders of magnitude greater compared to traditional contactors. This feature make it an appealing device for practical applications in reactions of gas-liquid mass transfer.

**Table 5.2** Comparison of the SOTR, VSOTR, SOTE, and SSOTE values of commonly used gas-liquid contactors devices and the membrane contactor investigated in this study.

| Type of contactor    | Volume (m <sup>3</sup> ) | Height (m) | SOTR (kg h <sup>-1</sup> )   | SOTE (%) | VSOTR (kg h <sup>-1</sup> m <sup>-3</sup> ) | SSOTE (% m <sup>-1</sup> ) | Reference               |
|----------------------|--------------------------|------------|------------------------------|----------|---|----------------------------|-------------------------|
| Fine bubble diffuser | 108-757                  | 2.2-5.9    | 3.3-109                      | 8.1- 33  | 0.03-0.14                                   | 3.7-5.6                    | (Gillot et al., 2005)   |
|                      | 125-461                  | 3.4 - 9.6  | 0.28-0.29                    | 12 - 39  | 0.002-0.0006                                | 3.5 - 4.1                  | (DeMoyer et al., 2001)  |
| Venturi injector     | -                        | 0.4        | 0.012-0.032                  | 0.1-12   | -   | 0.25-30                    | (Therrien et al., 2019) |
|                      | 3.9                      | 0.75       | 0.176                        | 6.3      | 0.045                                       | 8.4                        | (Dayioğlu, 2022)        |
| Membrane contactor   | 1.66 × 10 <sup>-4</sup>  | 0.2        | 3.3 – 5.6 × 10 <sup>-4</sup> | 3-5%     | 2.0-3.4                                     | 15-25                      | This work               |

From comparable data in terms of VSOTR, the membrane contactor transferred a higher amount of O<sub>2</sub> mass into the water per unit of volume compared to bubble diffusers and venturi injectors. Similarly, regarding the SSOTE efficiency parameter, the membrane contactor achieved an O<sub>2</sub> mass dissolution per unit of reactor height 4 to 6 orders of magnitude higher than those in traditional contactors. This feature makes it an attractive device for practical applications in gas-liquid mass transfer reactions.

On the other hand, although the ASCE method (ASCE, 2007) was initially introduced to describe the oxygen dissolution into water, in this study, both parameters were also extended for the O<sub>3</sub> transfer efficiency (TE, %), as given in Eq. (5.13). For this case, the mass flow rate of O<sub>3</sub> ( $W_{O_3}$ ) was determined from the inlet  $Q_G$  and  $C_{O_3,g,in}$ . The TE is an important parameter for setting optimal operation conditions in ozone-based applications (Wang et al., 2023).

$$TE (\%) = \frac{K_L a \times C_{O_3^*,l} \times V_R}{W_{O_3}} \quad (5.13)$$

Figure 5.7 shows the transfer efficiency (TE) for  $O_3$  at different  $Q_L$  and  $Q_G$  calculated based on ASCE standard method. It can be observed that higher  $Q_L$  generated higher transfer efficiency values at a fixed  $Q_G$ . This characteristic becomes particularly advantageous for large-scale processes in which higher volumes of wastewater need to be treated, such as those produced by municipal WWTPs. On the other hand, for a fixed  $Q_L$ , the increase of  $Q_G$  developed an almost constant  $O_3$  transfer efficiency. This behavior was probably attributed that the variation of  $Q_G$  was small (from 0.50 to 0.85  $Ndm^3 \text{ min}^{-1}$ ) and thus, the efficiency loss remained almost constant for this range of  $Q_G$ . It is expected that with higher  $Q_G$  (e.g., 0.85 to 2  $Ndm^3 \text{ min}^{-1}$ ) efficacy will decrease, mainly attributed to the shorter contact time between gas–liquid phases.

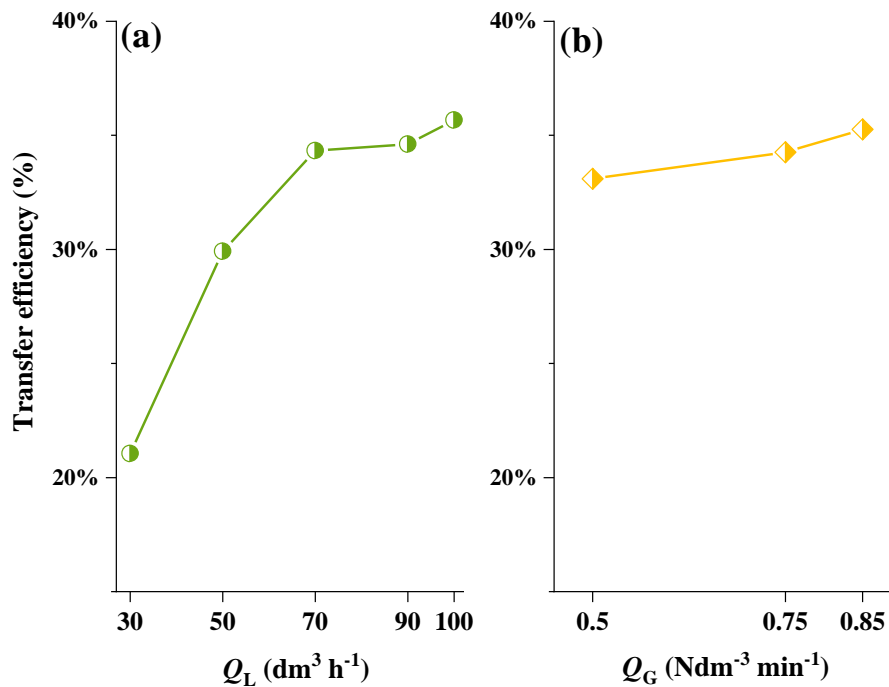


**Figure 5.7** Transfer efficiency (%) as a function of (a) liquid flow rate and (b) gas flow rate.

According to the experimental conditions that used demineralized water with no chemical reaction, the maximum TE of 35% was attained. In this way, considering the  $O_3$  doses required for PhACs abatement in the secondary-treated wastewater, it was selected a  $Q_G$  of 0.75  $Ndm^3 \text{ min}^{-1}$  (second value with highest TE) and a  $Q_L$  of 100  $dm^3 \text{ h}^{-1}$ .

### 5.4.6 Occurrence of pharmaceuticals

A total of 33 pharmaceuticals were selected for this study based on several criteria, including (i) high consumption rate, (ii) frequency detected in municipal WWTPs, and (iii) their potential risk to the environment (de Jesus Gaffney et al., 2017). The main detected pharmaceuticals and their concentrations are presented in Table 5.3. Within the pharmaceuticals class, 23 compounds were detected above the limit of quantification (LOQ), belonging to 11 different therapeutic classes: 2 anti-inflammatories, 6 antibiotics, 3 anticonvulsants, 3 antihypertensives, 1 anthelmintic drug, 2 anti-ulcer agents, 1 iodized contrast media, 1 lipid regulator, 1  $\beta$ -blocker, 2 anxiolytics, and 2 antidepressants.

**Table 5.3** Initial concentration of pharmaceuticals detected in the WWTP secondary effluent

| Therapeutic group      | Compound                       | Concentration ( $\mu\text{g L}^{-1}$ ) |
|------------------------|--------------------------------|--|
| Anti-inflammatory      | Diclofenac                     | 1.52                                   |
| Antibiotics            | Ciprofloxacin                  | 0.39                                   |
|                        | Clarithromycin                 | 0.13                                   |
|                        | Trimethoprim                   | 0.04                                   |
|                        | Sulfamethoxazole               | 0.10                                   |
|                        | Clindamycin                    | 0.03                                   |
|                        | Norfloxacin                    | 0.09                                   |
| Anticonvulsants        | Carbamazepine                  | 0.51                                   |
|                        | Gabapentin                     | 0.68                                   |
|                        | Primidone                      | 0.14                                   |
| Anti-hypertensive      | Irbesartan                     | 0.75                                   |
|                        | Losartan                       | 0.33                                   |
|                        | Valsartan                      | 0.02                                   |
| Anthelmintic           | Levamisole                     | 0.01                                   |
| Anti-ulcer agents      | Pantoprazole                   | 0.01                                   |
|                        | 4-hidroxy omeprazole sulfide   | 0.08                                   |
| Iodized contrast media | Iopromide                      | 1.04                                   |
| Lipid regulator        | Atorvastatin                   | 0.18                                   |
| Beta-blocker           | Metoprolol                     | 0.02                                   |
| Anxiolytic             | Lorazepam                      | 0.11                                   |
|                        | Alprazolam                     | 0.01                                   |
| Antidepressants        | Venlafaxine                    | 0.44                                   |
|                        | <i>O</i> -desmethylvenlafaxine | 0.68                                   |
|                        | Total load                     | 7.31                                   |

The concentration levels ranged from 0.01 to 1.52  $\mu\text{g L}^{-1}$  (1522  $\text{ng L}^{-1}$ ), whereas the sum of the pharmaceutical mixture reached a total of 7.31  $\mu\text{g L}^{-1}$ . Among the identified PhACs, the highest average concentrations were found for the non-steroidal anti-inflammatory drug (NSAID) diclofenac (1.52  $\mu\text{g L}^{-1}$ ), the iodized contrast media iopromide (1.04  $\mu\text{g L}^{-1}$ ), followed by the antihypertensive irbesartan (0.75  $\mu\text{g L}^{-1}$ ), whereas the lowest concentrations values were detected for the anthelmintic levamisole and the anti-ulcer agent pantoprazole (0.01  $\mu\text{g L}^{-1}$ ). The level found of diclofenac is correlated to its high consumption in Portugal, presenting the highest share of the over-the-counter drugs market (without no prescription), 18.4% in 2018 (Infarmed, 2018). In relation to antibiotics, fluoroquinolone ciprofloxacin was the antibiotic with the highest concentration detected (0.39  $\mu\text{g L}^{-1}$ ), followed by the macrolide clarithromycin (0.13  $\mu\text{g L}^{-1}$ ). The results obtained in this study are consistent with previous findings reported in European WWTP secondary effluents (de Jesus Gaffney et al., 2017; Lopez et al., 2022; Sá et al., 2022). For instance, de Jesus Gaffney et al., (2017) found diclofenac concentrations ranging between 0.05 and 4.2  $\mu\text{g L}^{-1}$  in Portuguese WWTP secondary effluents. Likewise, the authors detected ciprofloxacin at an average concentration of 0.35  $\mu\text{g L}^{-1}$ .

#### **5.4.7 PhACs removal using the ozone membrane contactor**

The efficiency of the ozonation membrane contactor, operated in continuous mode, in degrading the 23 PhACs detected in the secondary-treated municipal wastewater was assessed under several specific ozone doses (0.39, 0.53, and 0.69  $\text{g O}_3 \text{ g DOC}^{-1}$ ). As can be seen in Figure 5.8, increasing the ozone doses led to an increase in the extent of abatement of PhACs. At the lowest ozone dose of 0.39  $\text{g O}_3 \text{ DOC}^{-1}$ , only 3 out of the 23 compounds (atorvastatin, clindamycin, and diclofenac) were degraded by over 80%. The low removal may be attributed to the rapid consumption of ozone by the dissolved effluent organic matter (dEfOM) (HOIGNÉ and Bader, 1994). In fact, ozone was completely consumed within 20 s (system residence time), indicating that the ozone dose applied is below the Immediate Ozone Demand (IOD). For the intermediate ozone dose, 0.53  $\text{g O}_3 \text{ g DOC}^{-1}$ , 9 compounds (ciprofloxacin, sulfamethoxazole, diclofenac, trimethoprim, clindamycin, atorvastatin, carbamazepine, O-desmethylvenlafaxine - venlafaxine metabolite and 4-hydroxy-omeprazole sulfide - omeprazole metabolite) were eliminated over 80%. These compounds

contain electron-rich moieties such as phenols, anilines, olefins, or amines, which have a high affinity for the direct reaction with ozone (Table A2 presents the ozone- reactive moieties of each compound).

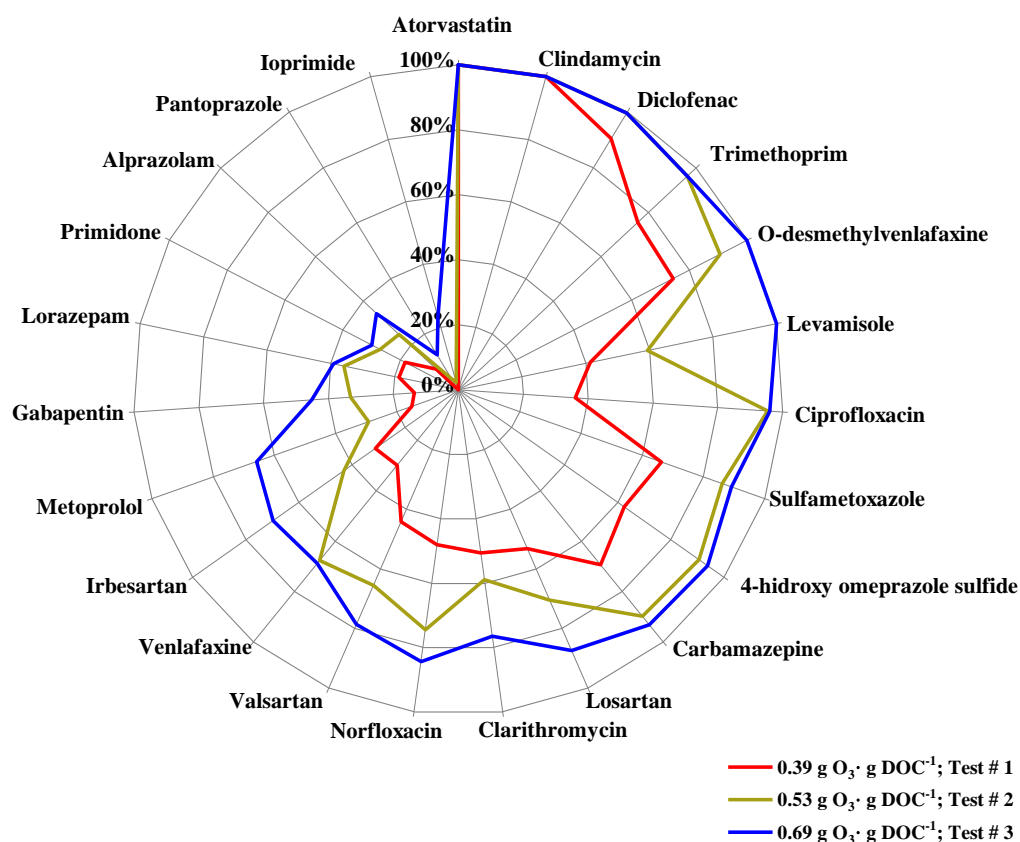


**Figure 5.8** Removal efficiency for the 23 pharmaceuticals detected in a secondary-treated wastewater, using the membrane reactor coupled with a column, operated in continuous mode ( $\tau = 60$  s) as a function of specific ozone doses 0.39, 0.53, and 0.69 g O<sub>3</sub> g DOC<sup>-1</sup> (the specific O<sub>3</sub> dose was corrected for nitrite consumption).

As shown in Figure 5.9, the PhACs abatement was strongly correlated with reported second-order rate constants with O<sub>3</sub> ( $k_{O_3}$ ). Compounds that typically exhibit  $k_{O_3} \geq 10^4$  M<sup>-1</sup> s<sup>-1</sup> at circumneutral pH present removal efficiencies higher than 80% even for low ozone transferred doses (>0.21 to 1.24 g O<sub>3</sub> g DOC<sup>-1</sup>) (Lee and von Gunten, 2012; Zimmermann et al., 2011). This trend was similar to that observed in Figure 5.9, in which compounds with higher  $k_{O_3}$  were more quickly eliminated from the wastewater during ozonation.

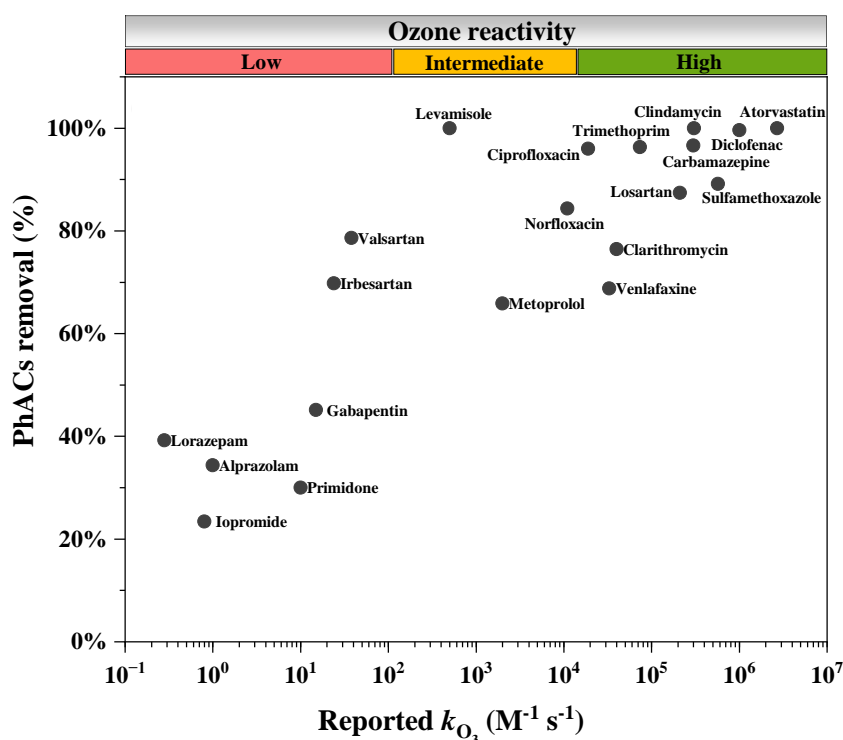


**Figure 5.9** Removal of pharmaceuticals at  $0.69 \text{ g O}_3 \text{ g DOC}^{-1}$  as a function of (a) ozone kinetic rate constants (pantoprazole and O-desmethylvenlafaxine were not included due to  $k_{O_3}$  values are not available).

For the highest specific ozone dose of  $0.69 \text{ g O}_3 \text{ g DOC}^{-1}$ , 17 out of the 23 PhACs reached removals of more than  $\geq 60\%$ , of which 12 compounds were abated higher than 80%. Moderately ozone-resistant compounds with  $k_{O_3}$  between  $10^2$  and  $10^4 \text{ M}^{-1} \text{ s}^{-1}$ , e.g., metoprolol, underwent an increase in elimination level by around 66% or in the case of levamisole which was removed to values lower than the limit of quantification. In contrast, compounds with low reaction rate with  $O_3$  ( $k_{O_3} < 10^2 \text{ M}^{-1} \text{ s}^{-1}$ ), such as alprazolam, gabapentin, lorazepam, and primidone, reached low removals (around 30-45%), with particularly low elimination levels for pantoprazole (13%) and iopromide (24%). The low removal of these compounds is attributed to the presence of carboxylic acid groups (gabapentin), halogen substituents (iopromide, alprazolam), or amides (primidone) that, due to their electron-withdrawing nature, are practically unreactive towards ozone oxidation (Nakada et al., 2007). The free radical  $HO^\bullet$ , generated from  $O_3$  natural decomposition plays an important role in

their abatement during ozonation (Elovitz and Von Gunten, 1999). For ozone-resistant compounds  $k_{O_3} < 10^2 \text{ M}^{-1} \text{ s}^{-1}$ , the main oxidation pathway is the radical-type chain mechanism through  $\text{HO}^\bullet$  radicals. In contrast, compounds with  $k_{O_3}$  between  $10^2$  and  $10^4 \text{ M}^{-1} \text{ s}^{-1}$ , both radical and ozone molecular mechanisms occur simultaneously with the same order of magnitude (Lee and Von Gunten, 2016). As depicted in Figure 5.10, the elimination efficiency of ozone-resistant compounds (highlighted region in light blue) was also well correlated with their  $k_{\text{HO}^\bullet}$  values. Considering that  $\text{HO}^\bullet$  kinetic rate for all compounds is quite similar, between  $1.2 \times 10^9 < k_{\text{HO}^\bullet} < 10^{10} \text{ M}^{-1} \text{ s}^{-1}$ , the abatement efficiency of these compounds was controlled by the magnitude of their  $k_{\text{HO}^\bullet}$  values. For instance, iopromide with lower  $\text{HO}^\bullet$  reactivity  $k_{\text{HO}^\bullet} < 1 \times 10^9 \text{ M}^{-1} \text{ s}^{-1}$ , reached the lowest percentage removal compared with hypertensive compounds such as valsartan and losartan ( $k_{\text{HO}^\bullet} > 5 \times 10^{10} \text{ M}^{-1} \text{ s}^{-1}$ ).

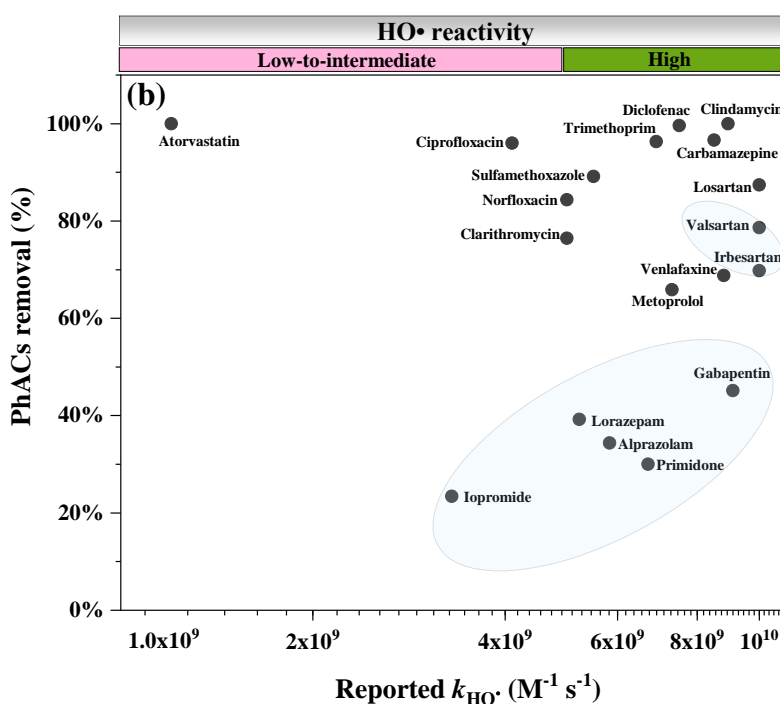


**Figure 5.10** Removal of pharmaceuticals at  $0.69 \text{ g O}_3 \text{ g DOC}^{-1}$  as a function of reported  $\text{HO}^\bullet$  radical kinetic constants. Highlighted region (light blue) represents ozone-resistant compounds ( $k_{O_3} < 10^2 \text{ M}^{-1} \text{ s}^{-1}$ ).

The wastewater matrix components, such as dEOM and alkalinity (bicarbonates/carbonates,  $\text{HCO}_3^-/\text{CO}_3^{2-}$ ), can considerably interfere with the oxidation capacity of radical-based



oxidation reactions, due to its scavenging effect over hydroxyl radicals (Asghar et al., 2022; Lado Ribeiro et al., 2019). Given the significantly high concentration of both constituents in the effluent (e.g., mg L<sup>-1</sup> of DOC and carbonate), most of the HO<sup>•</sup> radicals are consumed by the scavengers, decreasing the PhACs removal capacity by the indirect pathway. Mathon et al., (2021) found for a mixture of 47 CECs present in secondary treated wastewater that, the distribution of HO<sup>•</sup> consumption was 60% by the sum of all micropollutants, 11% by bicarbonates, 0.02% by nitrites and bromides, leaving 29% consumed by dEtOM and other chemical species.

Other studies have investigated higher specific ozone doses for the abatement of less reactive compounds with ozone in wastewater (Guillossou et al., 2020; Lee and Von Gunten, 2016; Margot et al., 2013). For instance, Margot et al., (2013) found that even the most ozone-resistant micropollutants were highly removed at an ozone dose of 2.6 g O<sub>3</sub> g<sup>-1</sup> DOC, with an average elimination of 80%. However, authors reported that higher ozone doses imply elevated costs, and the generation of toxic by-products is more feasible.

The results presented herein showed similar PhACs abatements using ozone membrane contactors for comparable ozone doses (0.14 to 0.7 g O<sub>3</sub> g<sup>-1</sup> DOC) and residence times (2.8-3.9 s) (Presumido et al., 2023; Schmitt et al., 2023). Presumido et al., (2023) found removals higher than 80% for up to 13 of the 19 CECs spiked in urban wastewater with an ozone dose of 18 g m<sup>-3</sup> and residence time of 3.9 s using a borosilicate tubular membrane. On the other hand, comparing to conventional processes, the PhACs removal rates achieved in this study were obtained at a very short residence time of 60 s instead of between 10 and 30 min as reported in a traditional process at full WWTP scale (Hollender et al., 2009; Kharel et al., 2020).

Figure 5.11 shows the PhACs removal applying the same ozone dose (12 g O<sub>3</sub> m<sup>-3</sup>) while varying  $C_{O_3,g,in}$  (27, 80, and 134 g Nm<sup>-3</sup>) and  $Q_G$  (0.15, 0.25 and 0.75 Ndm<sup>3</sup> min<sup>-1</sup>). It can be observed that for the highest ozone concentration ( $C_{O_3,g,in} = 134$  g Nm<sup>-3</sup>,  $Q_G = 0.15$  g Nm<sup>-3</sup>), 11 out of the 23 compounds reached removals higher than 96% or below the LOQ. This behavior can be explained according to the mass-transfer theory, in which increasing the ozone-gas input concentration enhances the driving force for O<sub>3</sub> mass transfer from the gaseous to the liquid phase (Wang et al., 2019). This, in turn, provides a higher dissolved O<sub>3</sub> concentration enhancing the PhACs removal. Moreover, O<sub>3</sub> transfer yield  $\eta(O_3)$  achieved

values near 97% for a  $C_{O_3,g,in}$  of  $134 \text{ g Nm}^{-3}$ , against 70% and 87% for the tests with  $C_{O_3,g,in}$  values of  $27 \text{ g Nm}^{-3}$  and  $80 \text{ g Nm}^{-3}$ , respectively.

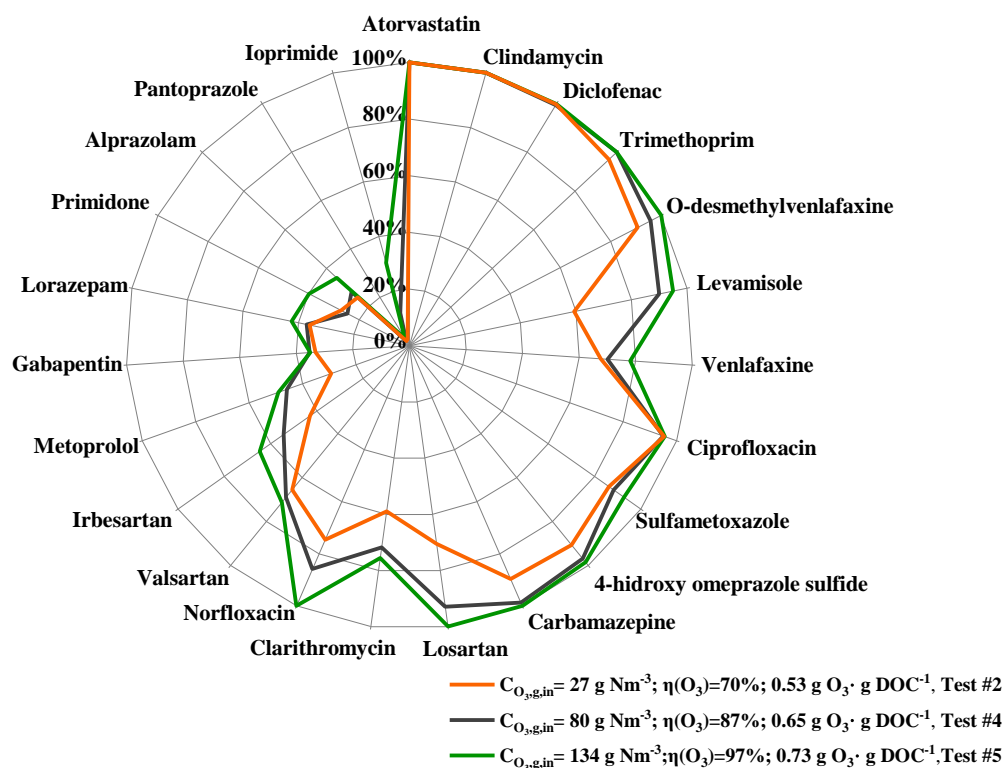


**Figure 5.11** Removal efficiency for the 23 pharmaceuticals detected in a secondary-treated wastewater, using the membrane reactor coupled with a column, operated in continuous mode ( $\tau = 60 \text{ s}$ ) as a function of  $O_3$  concentration in the inlet gas stream and same  $AO_3D$  applied ( $12 \text{ mg O}_3 \text{ L}^{-1}$ ).

These findings demonstrate a favorable characteristic when using the same ozone dose applied to the treatment, as reducing the gas flow rate and simultaneously increasing the  $O_3$  gas concentration can lead to lower operational costs during ozonation (Al-Abduly et al., 2014).

#### 5.4.8 Effect of the ozonation process on the global parameters

The removal of DOC, specific UV absorbance at 254 nm ( $UVA_{254}$ ), and turbidity after ozonation were also investigated as possible control parameters. Figure 5.12 shows the

removal of mentioned parameters as a function of both specific ozone doses and ozone concentration in the inlet gas stream.

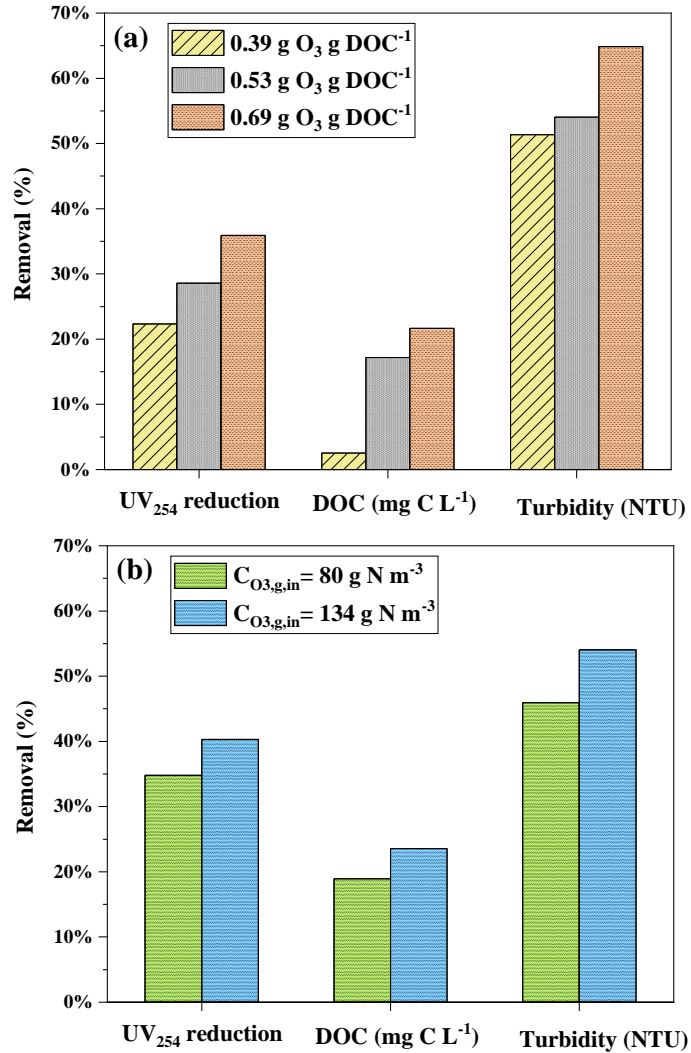


**Figure 5.12** UV<sub>254</sub>, DOC, and turbidity removal percentages after ozonation as a function of (a) specific ozone dose applied (0.39, 0.53, and 0.69 g O<sub>3</sub> g DOC<sup>-1</sup>) and (b) ozone concentration in the inlet gas stream (80 and 134 mg Ndm<sup>-3</sup>). For more details on the experimental conditions of each test, see Table 5.1.

As can be seen in Figure 5.12a, an improvement in DOC removal was attained when increasing the O<sub>3</sub> doses. Specifically, when applying an ozone dose of 0.39 g O<sub>3</sub> gDOC<sup>-1</sup>, DOC removal rate was found to be only 3%, whereas an ozone dose of 0.69 g O<sub>3</sub> g DOC<sup>-1</sup>

led to a removal of up to 22%. The highest DOC removal (27%) was achieved for the highest  $C_{O_3,g,in}$  (134 g Nm<sup>-3</sup>) (Figure 5.12b). These results confirm the inefficiency of ozone in terms of organic matter mineralization, with a very low DOC decrease even for the higher specific ozone dose (Marce et al., 2016; Rosal et al., 2008; Schmitt et al., 2023). Many authors attributed the low mineralization yield to the formation of recalcitrant organic intermediates that result from the oxidation of NOM initially present in wastewater (Hübner et al., 2015; Iakovides et al., 2019). However, although ozonation does not completely mineralize intermediate products, it can transform them into more biodegradable compounds, which are generally well removed during biological or physical post-treatments (*e.g.*, combined with activated carbon adsorption) (Margot et al., 2013; Völker et al., 2019).

The UVA<sub>254</sub> is a commonly used surrogate parameter to monitor water quality that contains aromatic rings or unsaturated carbon bonds. Therefore, a reduction of the UVA<sub>254</sub> indicates the decomposition of the organic compounds into lower molecular weight organics as well as a change in the aromatic nature of the contaminants (Chys et al., 2017; Mecha et al., 2016). A low reduction in UV<sub>254</sub> absorbance (22%) was reached with a specific ozone dose of 0.39 g O<sub>3</sub> g DOC<sup>-1</sup>, while a higher decrease (36%) was obtained for an ozone dose of 0.69 g O<sub>3</sub> g DOC<sup>-1</sup>. Similar behavior was observed when the highest  $C_{O_3,g,in}$  was applied, reaching a reduction of 40% in UV<sub>254</sub> absorbance.

Finally, a reduction in the turbidity of the treated effluent was observed, achieving efficiency values of 51% and 65% with the increase of the specific ozone dosage from 0.39 to 0.69 g O<sub>3</sub> g DOC<sup>-1</sup>, respectively. Marce et al., (2016) observed that ozone destroys the solid particles of organic matter, especially from the first moments of the reaction, when low ozone doses are transferred, which could explain the rapid decrease in turbidity.

#### 5.4.9 Mass transfer by chemical reaction in the liquid phase

Two important dimensionless parameters to take into consideration in gas-liquid mass transfer in the presence of a reaction are the Hatta number ( $Ha$ ) and enhancement factor ( $E$ ). The  $Ha$  number provides information about the kinetic regimes in a gas-liquid reaction and allows to identify where the chemical reactions take place (Beltrán and Rey, 2018).

For a second-order irreversible reactions, the  $Ha$  number can be defined by Eq. (5.14) (Whitman, 1962).

$$Ha = \frac{\sqrt{k_{O_3} \times D_{O_3} \times C_{P,0}}}{k_L} \quad (5.14)$$

where  $k_{O_3}$  is the rate constant of the direct reaction between ozone and the compound ( $M^{-1} s^{-1}$ ),  $D_{O_3}$  is the diffusivity of ozone in water ( $1.76 \times 10^{-9} m^2 s^{-1}$ ) (Johnson and Davis, 1996),  $C_{P,0}$  is the initial concentration of PhACs (M), and  $k_L$  is the ozone mass transfer coefficient for the liquid phase. The value of the mass transfer coefficient,  $k_L = 4.45 \times 10^{-5} m s^{-1}$ , was calculated considering the  $K_L a$  value obtained for the experimental conditions used in the PhACs ozonation.

The  $Ha$  numbers were only calculated for 11 of the 23 PhACs, i.e., those that were eliminated over 80% with ozonation (for  $0.69 g O_3 g DOC^{-1}$ ), as well as for the initial concentration of dEfOM (i.e., DOC) present in the effluent sample. Under experimental conditions applied in this study,  $Ha$  values (Table 5.4) were found to be in the range of 0.0002 and 0.17.

**Table 5.4** Dimensionless Hatta number values for the target compounds

| Compound               | $C_0$ (M)              | Hatta Number ( $Ha$ ) |
|------------------------|------------------------|-----------------------|
| Diclofenac             | $5.14 \times 10^{-9}$  | 0.07                  |
| Ciprofloxacin          | $1.17 \times 10^{-9}$  | 0.004                 |
| Trimethoprim           | $1.21 \times 10^{-10}$ | 0.003                 |
| Sulfamethoxazole       | $4.07 \times 10^{-10}$ | 0.014                 |
| Clindamycin            | $7.46 \times 10^{-10}$ | 0.004                 |
| Norfloxacin            | $2.82 \times 10^{-10}$ | 0.002                 |
| Carbamazepine          | $2.14 \times 10^{-9}$  | 0.02                  |
| Losartan               | $7.84 \times 10^{-10}$ | 0.01                  |
| Levamisole             | $4.34 \times 10^{-10}$ | 0.0002                |
| Atorvastatin           | $3.16 \times 10^{-10}$ | 0.10                  |
| O-desmethylvenlafaxine | $3.01 \times 10^{-10}$ | 0.003                 |

According to gas-liquid reaction kinetic theory (Charpentier, 1981),  $Ha < 0.3$  indicates the development of a slow kinetic regime, and most of the reaction occurs in the liquid bulk, i.e., beyond the film. This means that the ozone consumption rate by the PhACs is much slower than the ozone mass transfer from the gas to the liquid phase. Reactors with a large specific interfacial area and high liquid retention time are proper for promoting this type of reaction

(Charpentier, 1981). In this study, the membrane contactor provided a large interfacial area, however, the liquid retention time was very short (5.3 s). By increasing the residence time of the aqueous phase in the reactor, would probably have enhanced the interaction between the dissolved ozone and PhACs in the liquid bulk, and thus improving the CECs removal.

Finally, it should be highlighted due to the complexity of the wastewater matrix, other organic/inorganic species present in the sample were not considered in the calculation of Ha numbers. Hence, it is possible that these components may also have contributed to an enhancement in the transfer efficiency, as observed in Figure 5.11.

## 5.5 Conclusions

The findings of this study demonstrated that a tubular porous stainless steel ozone membrane contactor was successfully proven to enhance ozone-liquid mass transfer. The liquid and gas flow rates positively influenced the ozone mass transfer, probably due to an increase in the Reynold number and to the greater mixing induced by the gas stream. Although the resistance to mass transfer in the liquid boundary layer was demonstrated to be dominant for low liquid flow rates, it became almost comparable with membrane resistance for the highest liquid flow rate tested. The volumetric mass transfer coefficient  $K_{LA}$  values found in this study ( $1.7\text{-}5.5\text{ min}^{-1}$ ) proved to be three times higher than the conventional bubble columns but are in the same  $K_{LA}$  range as the venturi injection systems. A comparison associated with the oxygen transfer into water, the volumetric SOTR and the specific SOTE showed that the membrane contactor transferred  $O_2$  mass into the water between 4 and 6 orders of magnitude higher per each unit of volume height than those in traditional contactors. The significant mass transfer intensification in the membrane contactor makes it an attractive device for practical applications in gas-liquid mass transfer reactions.

The investigated ozone membrane contactor was also applied to eliminate 23 PhACs detected in the secondary-treated wastewater. Under continuous mode operation and residence time of 60 s, 12 out of the 23 PhACs achieved removals higher than 80% for the highest specific ozone dose of  $0.69\text{ g } O_3\text{ g}^{-1}\text{ DOC}$ . The micropollutant elimination was strongly correlated with  $k_{O_3}$  and  $k_{HO\cdot}$  values resulting in a characteristic elimination pattern for each compound group. Compounds containing carboxylic acid groups, halogen substituents, or amides were

highly resistant to ozonation. Regarding global physicochemical parameters, no significant mineralization was observed at the end of the treatment time at all experimental conditions examined. However, it is recommended that post-treatment methods such as biological filtration or activated carbon adsorption can be employed after ozonation to address the main limitations of this process. Future studies are needed to establish the mechanical properties changes in the membrane contactor after ozonation, energy consumption, and life cycle assessment associated with this ozonation membrane contactor system.

## Chapter 6. Conclusions and recommendations

The following conclusions are organized according to the specific objectives initially set for this thesis and results obtained.

Regarding to **the evaluation of different O<sub>3</sub>-based AOPs** (O<sub>3</sub>/UVC, O<sub>3</sub>/H<sub>2</sub>O<sub>2</sub>, O<sub>3</sub>/PMS and catalytic ozonation using NaY zeolites, NaY-12 and N ) in terms of degradation of ibuprofen it could be concluded that:

- O<sub>3</sub>-based AOPs not only enhanced the removal and mineralization of IBU but also improved the transfer and consumption O<sub>3</sub> doses during the coupled systems compared to the single ozonation. Combined O<sub>3</sub> processes, rather than single processes are required to achieve larger mineralization abatements.
- The O<sub>3</sub>/UVC system reached the highest O<sub>3</sub> utilization efficiency, compared to the other O<sub>3</sub> intensified systems. This attributed that UVC irradiation, provides an additional energy that accelerates ozone rate decomposition.
- Increasing 4-fold the H<sub>2</sub>O<sub>2</sub> and PMS concentration did not improve, the same factor in the removal of IBU. Hence, the optimal molar ratio H<sub>2</sub>O<sub>2</sub>:O<sub>3</sub> and PMS:O<sub>3</sub> molar ratio was 0.5.
- By comparing the performance of two oxidants H<sub>2</sub>O<sub>2</sub> and PMS in presence of ozonation, the O<sub>3</sub>/PMS system presented two-fold enhancement in the degradation rate of IBU when compared to the O<sub>3</sub>/H<sub>2</sub>O<sub>2</sub> system.
- The addition of zeolite catalysts to ozonation indicated that the use of NaY zeolites promoted the reaction between ozone and led to a faster IBU depletion, achieving a 5-fold increase compared to single ozonation, this attributed to the Lewis and Brønsted acid sites of zeolites.
- By comparing the performance of two NaY zeolites, the O<sub>3</sub>/NaY-12 combination exhibited better effect synergic in the IBU and mineralization removal compared to O<sub>3</sub>/NaY-60 system. This result can be related to the NaY-12 zeolite showed a stronger surface acidity compared to NaY-60 zeolite.



- The electrical energy consumption, as calculated using the  $E_{EO}$  parameter, showed that  $O_3$ -based processes were more efficient to abate the ozone resistant micropollutant in compared to conventional ozonation.
- The  $O_3$ /PMS combination showed the highest synergistic effect and the less energy-intensive process for both IBU and mineralization reduction. However, the  $O_3$ /PMS reached the highest operational costs, attributed to the high cost of the reagent.
- Catalytic ozonation using NaY-60 zeolites showed greater benefits, being the most profitable process in operational costs for the degradation of IBU and the reduction of mineralization.
- Catalytic ozonation by NaY zeolites was selected as the most adequate  $O_3$ -based AOP.

In view of the results obtained **in the identification of the main degradation products** to the best ozone-based AOPs and evaluation of the extent of the treatment and biocompatibility it is concluded that:

- The results indicated that both zeolites tested in presence of ozonation led to the formation of the same by-products, in which three major IBU degradation products were identified, evidenced that the attack sites of IBU by oxidative species.
- The predicted toxicity results using  $\Delta\text{Log P}$  factor indicated that all transformation products of IBU showed negative  $\Delta\text{Log P}$  values, which suggest that catalytic ozonation using NaY zeolites was able to reduce the toxicity of the parent compound.
- The theoretical oxygen demand ( $\Delta\text{ThOD}$ ) indicated that these intermediates are molecules more oxidized than the initial compound, associated with changes in the functional groups of IBU.
- The analysis of the predicted primary aerobic microbial biotransformation pathways showed that TPs generated cannot be easily transformed via aerobic biodegradation. Although this result are based on rational predictions, the corresponding experimental measurements are necessary to validate these predictions. This result may be suggested that additional reaction time is required to enable  $HO^\bullet$  radicals to attack these molecules and lead to a greater ring-opening, resulting in the formation of short-chain aliphatic acids.

Concerning the study of the **application on the catalytic ozonation using NaY zeolites** in the removal of a mixture of pharmaceuticals and environmental risk the main conclusions are:

- The addition of NaY zeolites in the ozonation can be a suitable option to degrade pharmaceutical compounds in secondary effluents from MWWTPs, with low doses of catalyst and ozone concentration.
- The amount of Brønsted and Lewis acid sites in the NaY zeolites influenced the degradation of PhACs compound in the wastewater.
- The NaY-12 zeolite offered more amount of Lewis and Brønsted acid sites on the surface compared to NaY-60 zeolite.
- Physical-chemical properties of pharmaceuticals influenced in the efficiency of the process, positively charged pharmaceuticals seems to be better adsorbed into the NaY zeolites when treating WWTP effluents.
- The RQ values for all pharmaceuticals after the application of the coupled system ozonation and NaY zeolites were significantly diminished (only 10 min of reaction) compared with the initial wastewater, considerably reducing the risk in the receiving environment.

From the study on the **investigation on the intensification of the ozone-liquid mass transfer** using a tubular porous stainless-steel membrane the following points could be highlighted:

- Tubular porous stainless steel ozone membrane contactor was successfully proven to enhance ozone-liquid mass transfer.
- The liquid and gas flow rates positively influenced the ozone mass transfer, probably due to an increase in the Reynold number and to the greater mixing induced by the gas stream.
- The volumetric mass transfer coefficient  $K_{La}$  values found ( $1.7-5.5 \text{ min}^{-1}$ ) proved to be three times higher than the conventional bubble columns but are in the same  $K_{La}$  range as the venturi injection systems.
- A comparison associated with the oxygen transfer into water, the volumetric SOTR and the specific SOTE showed that the membrane contactor transferred  $O_2$  mass into

the water between 4 and 6 orders of magnitude higher per each unit of volume height than those in traditional contactors.

- The significant mass transfer intensification in the membrane contactor makes it an attractive device for practical applications in gas-liquid mass transfer reactions.

Concerning the study of the **evaluation on the performance of the tubular membrane ozonation contactor in the elimination of a mixture of pharmaceuticals** in municipal wastewater matrices under continuous flow conditions, the main conclusions are:

- Under continuous mode operation and residence time of 60 s, 12 out of the 23 PhACs achieved removals higher than 80% for the highest specific ozone dose of 0.69 g O<sub>3</sub> g<sup>-1</sup> DOC. The micropollutant elimination was strongly correlated with  $k_{O_3}$  and  $k_{HO\cdot}$  values resulting in a characteristic elimination pattern for each compound group.
- Regarding global physicochemical parameters, no significant mineralization was observed at the end of the treatment time at all experimental conditions examined. However, it is recommended that post-treatment methods such as biological filtration or activated carbon adsorption can be employed after ozonation to address the main limitations of this process.
- The low Hatta number proved that the rate of mass transfer was enhanced by the ozone membrane contactor.

## 6.1 Recommendations and future work

Based on the results obtained in this thesis, the following recommendations might be of interest for further investigation of O<sub>3</sub>-based AOPs:

- Future works should be including the quantification of the main radicals involved in the ozone-based AOPs, SO<sub>4</sub><sup>•-</sup> (O<sub>3</sub>/PMS) and HO<sup>•</sup> radicals, in order to understand the free-radical mechanisms and provide a better insight on their potential contributions of each O<sub>3</sub>-based AOPs.
- An evaluation of toxicity of the transformation products generated during ozonation should be evaluated in order to investigate their possible environmental impact.
- The reusability of the catalyst should be considered in continuous operation and using real wastewater.
- The comparison of ozone-based AOPs should be evaluated in terms of environmental terms, through life cycle assessment (LCA) to comprehensively assess the potential environmental impacts using different end points.
- The investigation of the wastewater characteristics, such as alkalinity and nutrients such as P, N, S should be considered due to might affect the formation and availability of hydroxyl radical for the degradation of PhACs. Hence, evaluate their effect on catalytic ozonation is required to continue moving towards the implementation of the catalytic ozonation for wastewater treatment.
- Furthermore, a comprehensive understanding of the adsorption mechanism for specific PhACs should be gained. Unfortunately, this understanding is not within the scope of the current PhD thesis.
- Future studies are needed to establish the mechanical properties changes in the membrane contactor after ozonation.

## References

- Aa van der, N.G.F.M., Van Vlaardingen, P.L.A., Van Leeuwen, L.C., Post, M., 2001. Assessment of potential risks of 11 pharmaceuticals for the environment: Using environmental information from public databases.
- Adityosulindro, S., Julcour, C., Riboul, D., Barthe, L., 2022. Degradation of ibuprofen by photo-based advanced oxidation processes: exploring methods of activation and related reaction routes. *International Journal of Environmental Science and Technology* 19, 3247–3260. <https://doi.org/10.1007/s13762-021-03372-5>
- AEMPS, 2018. Consumption of antihypertensive drugs in Spain [WWW Document]. URL <https://www.aemps.gob.es/medicamentos-de-uso-humano/observatorio-de-uso-de-medicamentos/informes/>
- Al-Abduly, A., Christensen, P., Harvey, A., Zahng, K., 2014. Characterization and optimization of an oscillatory baffled reactor (OBR) for ozone-water mass transfer. *Chemical Engineering and Processing - Process Intensification* 84, 82–89. <https://doi.org/10.1016/j.cep.2014.03.015>
- Alejandro, S., Valdés, H., Zaror, Claudio.A., 2011. Natural Zeolite Reactivity Towards Ozone: The Role of Acid Surface Sites. *Journal of Advanced Oxidation Technologies* 14. <https://doi.org/10.1515/jaots-2011-0201>
- Alejandro-Martín, S., Valdés, H., Manero, M.H., Zaror, C.A., 2018. Catalytic ozonation of toluene using chilean natural zeolite: The key role of brønsted and lewis acid sites. *Catalysts* 8, 211. <https://doi.org/10.3390/catal8050211>
- Almeida, V.M., Orge, C.A., Pereira, M.F.R., Soares, O.S.G.P., 2022. O<sub>3</sub> based advanced oxidation for ibuprofen degradation. *Chin J Chem Eng* 42, 277–284. <https://doi.org/10.1016/j.cjche.2021.04.032>
- APHA, A.-W., 1998. Standard methods for the examination of water, 21st ed, Sewage and Industrial Waste. American Public Health Association. Amer Public Health Assn.
- ASCE, 2007. Measurement of oxygen transfer in clean water. American Society of Civil Engineers, Reston, USA.
- Asghar, A., Lutze, H. V., Tuerk, J., Schmidt, T.C., 2022. Influence of water matrix on the degradation of organic micropollutants by ozone based processes: A review on oxidant scavenging mechanism. *J Hazard Mater* 429, 128189. <https://doi.org/10.1016/J.JHAZMAT.2021.128189>

- aus der Beek, T., Weber, F.-A., Bergmann, A., Hickmann, S., Ebert, I., Hein, A., Küster, A., 2016. Pharmaceuticals in the environment-Global occurrences and perspectives. *Environ Toxicol Chem* 35, 823–835. <https://doi.org/10.1002/etc.3339>
- Bader, H., Hoigné, J., 1981. Determination of ozone in water by the indigo method. *Water Res* 15, 449–456. [https://doi.org/10.1016/0043-1354\(81\)90054-3](https://doi.org/10.1016/0043-1354(81)90054-3)
- Bakeri, G., Matsuura, T., Ismail, A.F., Rana, D., 2012. A novel surface modified polyetherimide hollow fiber membrane for gas–liquid contacting processes. *Sep Purif Technol* 89, 160–170. <https://doi.org/10.1016/J.SEPPUR.2012.01.022>
- Bamperng, S., Suwannachart, T., Atchariyawut, S., Jiraratananon, R., 2010. Ozonation of dye wastewater by membrane contactor using PVDF and PTFE membranes. *Sep Purif Technol* 72, 186–193. <https://doi.org/10.1016/j.seppur.2010.02.006>
- Beltran, F., 2003. *Ozone Reaction Kinetics for Water and Wastewater Systems*, Ozone Reaction Kinetics for Water and Wastewater Systems. Lewis Publishers. <https://doi.org/10.1201/9780203509173>
- Beltrán, F.J., Fernández, L.A., Álvarez, P., Rodríguez, E., 1998. Comparison Of Ozonation Kinetic Data From Film and Danckwerts Theories. *Ozone Sci Eng* 20, 403–420. <https://doi.org/10.1080/10874506.01919512.1998>
- Beltrán, F.J. (Fernando J., 2004. *Ozone reaction kinetics for water and wastewater systems*. Lewis Publishers.
- Beltrán, F.J., Rey, A., 2018. Free Radical and Direct Ozone Reaction Competition to Remove Priority and Pharmaceutical Water Contaminants with Single and Hydrogen Peroxide Ozonation Systems. *Ozone Sci Eng* 40, 251–265. <https://doi.org/10.1080/01919512.2018.1431521>
- Benner, J., Salhi, E., Ternes, T., von Gunten, U., 2008. Ozonation of reverse osmosis concentrate: Kinetics and efficiency of beta blocker oxidation. *Water Res* 42, 3003–3012. <https://doi.org/10.1016/j.watres.2008.04.002>
- Berry, M.J., Taylor, C.M., King, W., Chew, Y.M.J., Wenk, J., 2017. Modelling of ozone mass-transfer through non-porous membranes for water treatment. *Water (Switzerland)* 9. <https://doi.org/10.3390/w9070452>
- Bieber, S., Rauch-Williams, T., Drewes, J.E., 2016. An Assessment of International Management Strategies for CECs in Water. *ACS Symposium Series* 1241, 11–22. <https://doi.org/10.1021/BK-2016-1241.CH002>

- Bijlsma, L., Pitarch, E., Fonseca, E., Ibáñez, M., Botero, A.M., Claros, J., Pastor, L., Hernández, F., 2021. Investigation of pharmaceuticals in a conventional wastewater treatment plant: Removal efficiency, seasonal variation and impact of a nearby hospital. *J Environ Chem Eng* 9, 105548. <https://doi.org/10.1016/j.jece.2021.105548>
- Boix, C., Ibáñez, M., Sancho, J. V., Parsons, J.R., Voogt, P. de, Hernández, F., 2016. Biotransformation of pharmaceuticals in surface water and during waste water treatment: Identification and occurrence of transformation products. *J Hazard Mater* 302, 175–187. <https://doi.org/10.1016/j.jhazmat.2015.09.053>
- Bolton, J.R., Bircher, K.G., Tumas, W., Tolman, C.A., 2001. Figures-of-merit for the technical development and application of advanced oxidation technologies for both electric- and solar-driven systems (IUPAC Technical Report). *Pure and Applied Chemistry* 73, 627–637. <https://doi.org/10.1351/pac200173040627>
- Botero-Coy, A.M., Martínez-Pachón, D., Boix, C., Rincón, R.J., Castillo, N., Arias-Marín, L.P., Manrique-Losada, L., Torres-Palma, R., Moncayo-Lasso, A., Hernández, F., 2018. ‘An investigation into the occurrence and removal of pharmaceuticals in Colombian wastewater.’ *Science of The Total Environment* 642, 842–853. <https://doi.org/10.1016/j.scitotenv.2018.06.088>
- Bourgin, M., Beck, B., Boehler, M., Borowska, E., Fleiner, J., Salhi, E., Teichler, R., von Gunten, U., Siegrist, H., McArdell, C.S., 2018. Evaluation of a full-scale wastewater treatment plant upgraded with ozonation and biological post-treatments: Abatement of micropollutants, formation of transformation products and oxidation by-products. *Water Res* 129, 486–498. <https://doi.org/10.1016/j.watres.2017.10.036>
- Boyd, G.R., Reemtsma, H., Grimm, D.A., Mitra, S., 2003. Pharmaceuticals and personal care products (PPCPs) in surface and treated waters of Louisiana, USA and Ontario, Canada. *Science of The Total Environment* 311, 135–149. [https://doi.org/10.1016/S0048-9697\(03\)00138-4](https://doi.org/10.1016/S0048-9697(03)00138-4)
- Brillas, E., 2022. A critical review on ibuprofen removal from synthetic waters, natural waters, and real wastewaters by advanced oxidation processes. *Chemosphere* 286, 131849. <https://doi.org/10.1016/j.chemosphere.2021.131849>
- Carvalho, R.N., Ceriani, L., Ippolito, A., 2015. Development of the first Watch List under the Environmental Quality Standards Directive water policy. Ispra, Italy. <https://doi.org/10.2788/101376>
- Castro, J., Paz, S., Mena, N., Urresta, J., Machuca-Martinez, F., 2019. Evaluation of heterogeneous catalytic ozonation process for diclofenac degradation in solutions

- synthetically prepared. *Environmental Science and Pollution Research* 26, 4488–4497. <https://doi.org/10.1007/s11356-018-2582-1>
- Charpentier, J.C., 1981. Mass-Transfer Rates in Gas-Liquid Absorbers and Reactors. *Advances in Chemical Engineering* 11, 1–133. [https://doi.org/10.1016/S0065-2377\(08\)60025-3](https://doi.org/10.1016/S0065-2377(08)60025-3)
- Chen, N.Y., 1976. Hydrophobic properties of zeolites. *Journal of Physical Chemistry* 80, 60–64. <https://doi.org/10.1021/j100542a013>
- Chen, Y., Xi, X., Yu, G., Cao, Q., Wang, B., Vince, F., Hong, Y., 2015. Pharmaceutical compounds in aquatic environment in China: locally screening and environmental risk assessment. *Front Environ Sci Eng* 9, 394–401. <https://doi.org/10.1007/s11783-014-0653-1>
- Chopra, S., Kumar, D., 2020. Ibuprofen as an emerging organic contaminant in environment, distribution and remediation. *Heliyon* 6, e04087. <https://doi.org/10.1016/j.heliyon.2020.e04087>
- Chys, M., Audenaert, W.T.M., Deniere, E., Mortier, S.T.F.C., Van Langenhove, H., Nopens, I., Demeestere, K., Van Hulle, S.W.H., 2017. Surrogate-Based Correlation Models in View of Real-Time Control of Ozonation of Secondary Treated Municipal Wastewater - Model Development and Dynamic Validation. *Environ Sci Technol* 51, 14233–14243. <https://doi.org/10.1021/acs.est.7b04905>
- Chys, M., Audenaert, W.T.M., Vangrinsven, J., Bauwens, M., Mortier, S.T.F.C., Van Langenhove, H., Nopens, I., Demeestere, K., Van Hulle, S.W.H., 2018. Dynamic validation of online applied and surrogate-based models for tertiary ozonation on pilot-scale. *Chemosphere* 196, 494–501. <https://doi.org/10.1016/j.chemosphere.2017.12.168>
- Commission, E., 2003. Technical guidance document on risk assessment in support of Commission Directive 93/67/ EEC on risk assessment for new notified substances and Commission Regulation (EC) No. 1488/94 on risk assessment for existing substances. Part II. Technical Guidance Document on Risk Assessment Part II 337.
- Costa, E.P., Roccamante, M., Plaza-Bolaños, P., Oller, I., Agüera, A., Amorim, C.C., Malato, S., 2021. Aluminized surface to improve solar light absorption in open reactors: Application for micropollutants removal in effluents from municipal wastewater treatment plants. *Science of the Total Environment* 755, 142624. <https://doi.org/10.1016/j.scitotenv.2020.142624>



- Cruz-Alcalde, A., Esplugas, S., Sans, C., 2020. Continuous versus single H<sub>2</sub>O<sub>2</sub> addition in peroxone process: Performance improvement and modelling in wastewater effluents. *J Hazard Mater* 387, 121993. <https://doi.org/10.1016/j.jhazmat.2019.121993>
- Cuerda-Correa, E.M., Alexandre-Franco, M.F., Fernández-González, C., 2020. Advanced oxidation processes for the removal of antibiotics from water. An overview. *Water (Switzerland)*. <https://doi.org/10.3390/w12010102>
- Cuerda-Correa, E.M., Domínguez, J.R., Muñoz-Peña, M.J., González, T., 2016. Degradation of Parabens in Different Aqueous Matrices by Several O<sub>3</sub>-Derived Advanced Oxidation Processes. *Ind Eng Chem Res* 55, 5161–5172. <https://doi.org/10.1021/acs.iecr.6b00740>
- da Silva, J.C.C., Teodoro, J.A.R., Afonso, R.J. de C.F., Aquino, S.F., Augusti, R., 2014. Photolysis and photocatalysis of ibuprofen in aqueous medium: characterization of by-products via liquid chromatography coupled to high-resolution mass spectrometry and assessment of their toxicities against *Artemia Salina*. *Journal of Mass Spectrometry* 49, 145–153. <https://doi.org/10.1002/jms.3320>
- Dayioğlu, M.A., 2022. Experimental study on design and operational performance of solar-powered venturi aeration system developed for aquaculture – A semi-floating prototype. *Aquac Eng* 98, 102255. <https://doi.org/10.1016/J.AQUAENG.2022.102255>
- de Jesus Gaffney, V., Almeida, C.M.M., Rodrigues, A., Ferreira, E., Benoiel, M.J., Cardoso, V.V., 2015. Occurrence of pharmaceuticals in a water supply system and related human health risk assessment. *Water Res* 72, 199–208. <https://doi.org/10.1016/j.watres.2014.10.027>
- de Jesus Gaffney, V., Cardoso, V.V., Cardoso, E., Teixeira, A.P., Martins, J., Benoiel, M.J., Almeida, C.M.M., 2017. Occurrence and behaviour of pharmaceutical compounds in a Portuguese wastewater treatment plant: Removal efficiency through conventional treatment processes. *Environmental Science and Pollution Research* 24, 14717–14734. <https://doi.org/10.1007/s11356-017-9012-7>
- de Sousa, D.N.R., Insa, S., Mozeto, A.A., Petrovic, M., Chaves, T.F., Fadini, P.S., 2018. Equilibrium and kinetic studies of the adsorption of antibiotics from aqueous solutions onto powdered zeolites. *Chemosphere* 205, 137–146. <https://doi.org/10.1016/j.chemosphere.2018.04.085>
- DeMoyer, C.D., Gulliver, J.S., Wilhelms, S.C., 2001. Comparison of Submerged Aerator Effectiveness. *Lake Reserv Manag* 17, 139–152. <https://doi.org/10.1080/07438140109353982>

- Deniere, E., Van Hulle, S., Van Langenhove, H., Demeestere, K., 2018. Advanced oxidation of pharmaceuticals by the ozone-activated peroxydisulfate process: the role of different oxidative species. *J Hazard Mater* 360, 204–213. <https://doi.org/10.1016/J.JHAZMAT.2018.07.071>
- Dodd, M.C., Buffle, M.O., Von Gunten, U., 2006. Oxidation of antibacterial molecules by aqueous ozone: Moiety-specific reaction kinetics and application to ozone-based wastewater treatment. *Environ Sci Technol* 40, 1969–1977. <https://doi.org/10.1021/es051369x>
- Dong, Y., Yang, H., He, K., Wu, X., Zhang, A., 2008. Catalytic activity and stability of Y zeolite for phenol degradation in the presence of ozone. *Appl Catal B* 82, 163–168. <https://doi.org/10.1016/j.apcatb.2008.01.023>
- du Plessis, A., 2019. Current and Future Water Scarcity and Stress. *Springer Water* 13–25. [https://doi.org/10.1007/978-3-030-03186-2\\_2/COVER](https://doi.org/10.1007/978-3-030-03186-2_2/COVER)
- Eberle, S., Börnick, H., Stolte, S., 2022. Granular Natural Zeolites: Cost-Effective Adsorbents for the Removal of Ammonium from Drinking Water. *Water (Basel)* 14, 939. <https://doi.org/10.3390/w14060939>
- Elovitz, M.S., Von Gunten, U., 1999. Hydroxyl radical/ozone ratios during ozonation processes. I. The R(ct) concept. *Ozone Sci Eng* 21, 239–260. <https://doi.org/10.1080/01919519908547239>
- Emeis, C.A., 1993. Determination of integrated molar extinction coefficients for infrared absorption bands of pyridine adsorbed on solid acid catalysts. *J Catal* 141, 347–354. <https://doi.org/10.1006/jcat.1993.1145>
- EU, 2002. Directive 2000/60/EC of the European Parliament and of the Council establishing a framework for Community action in the field of water policy — European Environment Agency [WWW Document]. URL <https://www.eea.europa.eu/policy-documents/directive-2000-60-ec-of> (accessed 7.26.23).
- European Commission, 2021. Analytical quality control and method validation procedures for pesticide residues analysis in food and feed SANTE 11312/2021, in: Document N° SANTE 11945/2015. pp. 1–57.
- European Parliament, 2018. Commission Implementing Decision (EU) 2018/840 of 5 June 2018 establishing a watch list of substances for Union-wide monitoring in the field of water policy pursuant to Directive 2008/105/EC of the European Parliament and of the Council and repealing Comm. Off. J. Eur. Union L 141, 9–12.

- Fent, K., Weston, A., Caminada, D., 2006. Ecotoxicology of human pharmaceuticals. *Aquatic Toxicology* 76, 122–159. <https://doi.org/10.1016/j.aquatox.2005.09.009>
- Fernandes, E., Contreras, S., Medina, F., Martins, R.C., Gomes, J., 2020. N-doped titanium dioxide for mixture of parabens degradation based on ozone action and toxicity evaluation: Precursor of nitrogen and titanium effect. *Process Safety and Environmental Protection* 138, 80–89. <https://doi.org/10.1016/j.psep.2020.03.006>
- Figuière, R., Waara, S., Ahrens, L., Golovko, O., 2022. Risk-based screening for prioritisation of organic micropollutants in Swedish freshwater. *J Hazard Mater* 429, 128302. <https://doi.org/10.1016/j.jhazmat.2022.128302>
- Fu, M., He, M., Heijman, B., van der Hoek, J.P., 2021. Ozone-based regeneration of granular zeolites loaded with acetaminophen. *Sep Purif Technol* 256, 117616. <https://doi.org/10.1016/j.seppur.2020.117616>
- Gao, M.T., Hirata, M., Takanashi, H., Hano, T., 2005. Ozone mass transfer in a new gas-liquid contactor-Karman contactor. *Sep Purif Technol* 42, 145–149. <https://doi.org/10.1016/j.seppur.2004.07.004>
- Garoma, T., Gurol, M.D., 2004. Degradation of tert-butyl alcohol in dilute aqueous solution by an O<sub>3</sub>/UV process. *Environ Sci Technol* 38, 5246–5252. <https://doi.org/10.1021/es0353210>
- Gillot, S., Capela-Marsal, S., Roustan, M., Héduit, A., 2005. Predicting oxygen transfer of fine bubble diffused aeration systems—model issued from dimensional analysis. *Water Res* 39, 1379–1387. <https://doi.org/10.1016/J.WATRES.2005.01.008>
- Godoy, A.A., Kummrow, F., Pamplin, P.A.Z., 2015. Ecotoxicological evaluation of propranolol hydrochloride and losartan potassium to *Lemna minor* L. (1753) individually and in binary mixtures. *Ecotoxicology* 24, 1112–1123. <https://doi.org/10.1007/S10646-015-1455-3>
- Gomes, J.F., Costa, R., Quinta-Ferreira, R.M., Martins, R.C., 2017. Application of ozonation for pharmaceuticals and personal care products removal from water. *Science of the Total Environment* 586, 265–283. <https://doi.org/10.1016/j.scitotenv.2017.01.216>
- Gosling, S.N., Arnell, N.W., 2016. A global assessment of the impact of climate change on water scarcity. *Clim Change* 134, 371–385. <https://doi.org/10.1007/S10584-013-0853-X/FIGURES/4>
- Gottschalk, C., Libra, J.A., Saupe, A., 2010. *Ozonation of Water and Waste Water: A Practical Guide to Understanding Ozone and its Applications: Second Edition*,

Ozonation of Water and Waste Water: A Practical Guide to Understanding Ozone and its Applications: Second Edition. Wiley-VCH. <https://doi.org/10.1002/9783527628926>

Guillossou, R., Le Roux, J., Brosillon, S., Mailler, R., Vulliet, E., Morlay, C., Nauleau, F., Rocher, V., Gaspéri, J., 2020. Benefits of ozonation before activated carbon adsorption for the removal of organic micropollutants from wastewater effluents. *Chemosphere* 245. <https://doi.org/10.1016/j.chemosphere.2019.125530>

Gulde, R., Clerc, B., Rutsch, M., Helbing, J., Salhi, E., McArdell, C.S., von Gunten, U., 2021a. Oxidation of 51 micropollutants during drinking water ozonation: Formation of transformation products and their fate during biological post-filtration. *Water Res* 207, 117812. <https://doi.org/10.1016/j.watres.2021.117812>

Gulde, R., Rutsch, M., Clerc, B., Schollée, J.E., von Gunten, U., McArdell, C.S., 2021b. Formation of transformation products during ozonation of secondary wastewater effluent and their fate in post-treatment: From laboratory- to full-scale. *Water Res* 200, 117200. <https://doi.org/10.1016/j.watres.2021.117200>

H. Jones, O.A., Voulvoulis, N., Lester, J.N., 2005. Human Pharmaceuticals in Wastewater Treatment Processes. *Crit Rev Environ Sci Technol* 35, 401–427. <https://doi.org/10.1080/10643380590956966>

Hart, E.J., Sehested, K., Holcman, J., 1983. Molar Absorptivities of Ultraviolet and Visible Bands of Ozone in Aqueous Solutions. *Anal Chem* 55, 46–49. <https://doi.org/10.1021/ac00252a015>

Hernández, F., Ibáñez, M., Botero-Coy, A.-M., Bade, R., Bustos-López, M.C., Rincón, J., Moncayo, A., Bijlsma, L., 2015. LC-QTOF MS screening of more than 1,000 licit and illicit drugs and their metabolites in wastewater and surface waters from the area of Bogotá, Colombia. *Anal Bioanal Chem* 407, 6405–6416. <https://doi.org/10.1007/s00216-015-8796-x>

HOIGNÉ, J., Bader, H., 1994. Characterization of Water Quality Criteria for Ozonation Processes. Part II: Lifetime of Added Ozone. *Ozone Sci Eng* 16, 121–134. <https://doi.org/10.1080/01919519408552417>

Hollender, J., Zimmermann, S.G., Koepke, S., Krauss, M., Mcardell, C.S., Ort, C., Singer, H., Von Gunten, U., Siegrist, H., 2009. Elimination of organic micropollutants in a municipal wastewater treatment plant upgraded with a full-scale post-ozonation followed by sand filtration. *Environ Sci Technol* 43, 7862–7869. <https://doi.org/10.1021/es9014629>

- How, Z.T., Fang, Z., Chelme-Ayala, P., Ganiyu, S.O., Zhang, X., Xu, B., Chen, C., Gamal El-Din, M., 2023. Ozone-activated peroxymonosulfate (O<sub>3</sub>/PMS) process for the removal of model naphthenic acids compounds: Kinetics, reactivity, and contribution of oxidative species. *J Environ Chem Eng* 11, 109935. <https://doi.org/10.1016/j.jece.2023.109935>
- Huber, M.M., Canonica, S., Park, G.Y., Von Gunten, U., 2003. Oxidation of pharmaceuticals during ozonation and advanced oxidation processes. *Environ Sci Technol* 37, 1016–1024. <https://doi.org/10.1021/es025896h>
- Hübner, U., von Gunten, U., Jekel, M., 2015. Evaluation of the persistence of transformation products from ozonation of trace organic compounds - A critical review. *Water Res.* <https://doi.org/10.1016/j.watres.2014.09.051>
- Iakovides, I.C., Michael-Kordatou, I., Moreira, N.F.F., Ribeiro, A.R., Fernandes, T., Pereira, M.F.R., Nunes, O.C., Manaia, C.M., Silva, A.M.T., Fatta-Kassinos, D., 2019. Continuous ozonation of urban wastewater: Removal of antibiotics, antibiotic-resistant *Escherichia coli* and antibiotic resistance genes and phytotoxicity. *Water Res* 159, 333–347. <https://doi.org/10.1016/j.watres.2019.05.025>
- Ikhtlaq, A., Brown, D.R., Kasprzyk-Hordern, B., 2012. Mechanisms of catalytic ozonation on alumina and zeolites in water: Formation of hydroxyl radicals. *Appl Catal B* 123–124, 94–106. <https://doi.org/10.1016/j.apcatb.2012.04.015>
- Ikhtlaq, A., Waheed, S., Joya, K.S., Kazmi, M., 2018. Catalytic ozonation of paracetamol on zeolite A: Non-radical mechanism. *Catal Commun* 112, 15–20. <https://doi.org/10.1016/j.catcom.2018.01.010>
- Infarmed, 2018. Estatística Do Medicamento e Produtos de Saude [WWW Document]. URL <https://www.infarmed.pt/web/infarmed/entidades/medicamentos-uso-humano/monitorizacao-mercado/estatistica-anual/relatorios-anuais>
- Iversen, S.B., Bhatia, V.K., Dam-Johansen, K., Jonsson, G., 1997. Characterization of microporous membranes for use in membrane contactors. *J Memb Sci* 130, 205–217. [https://doi.org/10.1016/S0376-7388\(97\)00026-4](https://doi.org/10.1016/S0376-7388(97)00026-4)
- Javier Rivas, F., Sagasti, J., Encinas, A., Gimeno, O., 2011. Contaminants abatement by ozone in secondary effluents. Evaluation of second-order rate constants. *Journal of Chemical Technology and Biotechnology* 86, 1058–1066. <https://doi.org/10.1002/jctb.2609>
- Jelic, A., Gros, M., Ginebreda, A., Cespedes-Sánchez, R., Ventura, F., Petrovic, M., Barcelo, D., 2011. Occurrence, partition and removal of pharmaceuticals in sewage water and

- sludge during wastewater treatment. *Water Res* 45, 1165–1176. <https://doi.org/10.1016/j.watres.2010.11.010>
- Jiang, N., Shang, R., Heijman, S.G.J., Rietveld, L.C., 2018. High-silica zeolites for adsorption of organic micro-pollutants in water treatment: A review. *Water Res.* <https://doi.org/10.1016/j.watres.2018.07.017>
- Jing, C., Yibo, W., Yaxue, Z., Wenjuan, Z., Rui, Z., Zhe, W., Shaopo, W., 2023. Oxidation of ibuprofen in water by UV/O<sub>3</sub> process: Removal, byproducts, and degradation pathways. *Journal of Water Process Engineering* 53, 103721. <https://doi.org/10.1016/j.jwpe.2023.103721>
- Jjemba, P.K., 2006. Excretion and ecotoxicity of pharmaceutical and personal care products in the environment. *Ecotoxicol Environ Saf* 63, 113–130. <https://doi.org/10.1016/J.ECOENV.2004.11.011>
- John, A., Brookes, A., Carra, I., Jefferson, B., Jarvis, P., 2022. Microbubbles and their application to ozonation in water treatment: A critical review exploring their benefit and future application. *Crit Rev Environ Sci Technol.* <https://doi.org/10.1080/10643389.2020.1860406>
- Johnson, P.N., Davis, R.A., 1996. Diffusivity of ozone in water. *J Chem Eng Data* 41, 1485–1487. <https://doi.org/10.1021/je9602125>
- Junaid, M., Zainab, S.M., Xu, N., Sadaf, M., Malik, R.N., Wang, J., 2022. Antibiotics and antibiotic resistant genes in urban aquifers. *Curr Opin Environ Sci Health* 26, 100324. <https://doi.org/10.1016/j.coesh.2021.100324>
- Jurowski, K., Krzeczowska, M.K., Jurowska, A., 2015. Approaches To Determining the Oxidation State of Nitrogen and Carbon Atoms in Organic Compounds for High School Students. *J Chem Educ* 92, 1645–1652. <https://doi.org/10.1021/ed500645v>
- Kasprzyk-Hordern, B., Ziólek, M., Nawrocki, J., 2003. Catalytic ozonation and methods of enhancing molecular ozone reactions in water treatment. *Appl Catal B.* [https://doi.org/10.1016/S0926-3373\(03\)00326-6](https://doi.org/10.1016/S0926-3373(03)00326-6)
- Keller, V.D.J., Williams, R.J., Lofthouse, C., Johnson, A.C., 2014. Worldwide estimation of river concentrations of any chemical originating from sewage-treatment plants using dilution factors. *Environ Toxicol Chem* 33, 447–452. <https://doi.org/10.1002/ETC.2441>
- Kern, D.I., Schwaickhardt, R. de O., Mohr, G., Lobo, E.A., Kist, L.T., Machado, Ê.L., 2013. Toxicity and genotoxicity of hospital laundry wastewaters treated with photocatalytic

ozonation. *Science of the Total Environment* 443, 566–572.  
<https://doi.org/10.1016/j.scitotenv.2012.11.023>

Khaisri, S., DeMontigny, D., Tontiwachwuthikul, P., Jiraratananon, R., 2010. A mathematical model for gas absorption membrane contactors that studies the effect of partially wetted membranes. *J Memb Sci* 347, 228–239.  
<https://doi.org/10.1016/j.memsci.2009.10.028>

Khaisri, S., DeMontigny, D., Tontiwachwuthikul, P., Jiraratananon, R., 2009. Comparing membrane resistance and absorption performance of three different membranes in a gas absorption membrane contactor. *Sep Purif Technol* 65, 290–297.  
<https://doi.org/10.1016/j.seppur.2008.10.035>

Khan, A.H., Khan, N.A., Ahmed, S., Dhingra, A., Singh, C.P., Khan, S.U., Mohammadi, A.A., Changani, F., Yousefi, M., Alam, S., Vambol, S., Vambol, V., Khursheed, A., Ali, I., 2020. Application of advanced oxidation processes followed by different treatment technologies for hospital wastewater treatment. *J Clean Prod* 269, 122411.  
<https://doi.org/10.1016/j.jclepro.2020.122411>

Kharel, S., Stapf, M., Miehe, U., Ekblad, M., Cimbritz, M., Falås, P., Nilsson, J., Sehlén, R., Bester, K., 2020. Ozone dose dependent formation and removal of ozonation products of pharmaceuticals in pilot and full-scale municipal wastewater treatment plants. *Science of the Total Environment* 731. <https://doi.org/10.1016/j.scitotenv.2020.139064>

Kock, A., Glanville, H.C., Law, A.C., Stanton, T., Carter, L.J., Taylor, J.C., 2023. Emerging challenges of the impacts of pharmaceuticals on aquatic ecosystems: A diatom perspective. *Science of The Total Environment* 878, 162939.  
<https://doi.org/10.1016/j.scitotenv.2023.162939>

Koubaissy, B., Joly, G., Batonneau-Gener, I., Magnoux, P., 2011. Adsorptive Removal of Aromatic Compounds Present in Wastewater by Using Dealuminated Faujasite Zeolite. *Ind Eng Chem Res* 50, 5705–5713. <https://doi.org/10.1021/ie100420q>

Kreulen, H., Smolders, C.A., Versteeg, G.F., Van Swaaij, W.P.M., 1993. Determination of mass transfer rates in wetted and non-wetted microporous membranes. *Chem Eng Sci* 48, 2093–2102. [https://doi.org/10.1016/0009-2509\(93\)80084-4](https://doi.org/10.1016/0009-2509(93)80084-4)

Kukuzaki, M., Fujimoto, K., Kai, S., Ohe, K., Oshima, T., Baba, Y., 2010. Ozone mass transfer in an ozone-water contacting process with Shirasu porous glass (SPG) membranes-A comparative study of hydrophilic and hydrophobic membranes. *Sep Purif Technol* 72, 347–356. <https://doi.org/10.1016/j.seppur.2010.03.004>

- Lado Ribeiro, A.R., Moreira, N.F.F., Li Puma, G., Silva, A.M.T., 2019. Impact of water matrix on the removal of micropollutants by advanced oxidation technologies. *Chemical Engineering Journal* 363, 155–173. <https://doi.org/10.1016/j.cej.2019.01.080>
- Lange, F., Cornelissen, S., Kubac, D., Sein, M.M., von Sonntag, J., Hannich, C.B., Golloch, A., Heipieper, H.J., Möder, M., von Sonntag, C., 2006. Degradation of macrolide antibiotics by ozone: A mechanistic case study with clarithromycin. *Chemosphere* 65, 17–23. <https://doi.org/10.1016/j.chemosphere.2006.03.014>
- Lee, Woongbae, Choi, S., Kim, H., Lee, Woorim, Lee, M., Son, H., Lee, C., Cho, M., Lee, Y., 2023. Efficiency of ozonation and O<sub>3</sub>/H<sub>2</sub>O<sub>2</sub> as enhanced wastewater treatment processes for micropollutant abatement and disinfection with minimized byproduct formation. *J Hazard Mater* 454, 131436. <https://doi.org/10.1016/J.JHAZMAT.2023.131436>
- Lee, Y., Gerrity, D., Lee, M., Bogeat, A.E., Salhi, E., Gamage, S., Trenholm, R.A., Wert, E.C., Snyder, S.A., Von Gunten, U., 2013. Prediction of micropollutant elimination during ozonation of municipal wastewater effluents: Use of kinetic and water specific information. *Environ Sci Technol* 47, 5872–5881. <https://doi.org/10.1021/es400781r>
- Lee, Y., Kovalova, L., McArdell, C.S., von Gunten, U., 2014. Prediction of micropollutant elimination during ozonation of a hospital wastewater effluent. *Water Res* 64, 134–148. <https://doi.org/10.1016/j.watres.2014.06.027>
- Lee, Y., Von Gunten, U., 2016. Advances in predicting organic contaminant abatement during ozonation of municipal wastewater effluent: Reaction kinetics, transformation products, and changes of biological effects. *Environ Sci (Camb)*. <https://doi.org/10.1039/c6ew00025h>
- Lee, Y., von Gunten, U., 2012. Quantitative structure-activity relationships (QSARs) for the transformation of organic micropollutants during oxidative water treatment. *Water Res*. <https://doi.org/10.1016/j.watres.2012.06.006>
- Lester, Y., Mamane, H., Zucker, I., Avisar, D., 2013. Treating wastewater from a pharmaceutical formulation facility by biological process and ozone. *Water Res* 47, 4349–4356. <https://doi.org/10.1016/J.WATRES.2013.04.059>
- Li, C., Lu, J., Liu, J., Zhang, G., Tong, Y., Ma, N., 2016. Exploring the correlations between antibiotics and antibiotic resistance genes in the wastewater treatment plants of hospitals in Xinjiang, China. *Environmental Science and Pollution Research* 23, 15111–15121. <https://doi.org/10.1007/s11356-016-6688-z>



- Li, K., Zhang, Y., Xu, L., Liu, L., Wang, Z., Hou, D., Wang, Y., Wang, J., 2020. Mass transfer and interfacial reaction mechanisms in a novel electro-catalytic membrane contactor for wastewater treatment by O<sub>3</sub>. *Appl Catal B* 264. <https://doi.org/10.1016/j.apcatb.2019.118512>
- Liu, X., Fang, L., Zhou, Y., Zhang, T., Shao, Y., 2013. Comparison of UV/PDS and UV/H<sub>2</sub>O<sub>2</sub> processes for the degradation of atenolol in water. *Journal of Environmental Sciences* 25, 1519–1528. [https://doi.org/10.1016/S1001-0742\(12\)60289-7](https://doi.org/10.1016/S1001-0742(12)60289-7)
- Liu, X., Li, H., Fang, Y., Yang, Z., 2021. Heterogeneous catalytic ozonation of sulfamethazine in aqueous solution using maghemite-supported manganese oxides. *Sep Purif Technol* 274, 118945. <https://doi.org/10.1016/j.seppur.2021.118945>
- Loos, R., Marinov Dimitar, Sanseverino, Isabella., Napierska, D., Lettieri, T., 2018. Review of the 1st Watch List under the Water Framework Directive and recommendations for the 2nd Watch List. Publication Office of the European Union 265.
- Lopez, F.J., Pitarch, E., Botero-Coy, A.M., Fabregat-Safont, D., Ibáñez, M., Marin, J.M., Peruga, A., Ontañón, N., Martínez-Morcillo, S., Olalla, A., Valcárcel, Y., Varó, I., Hernández, F., 2022. Removal efficiency for emerging contaminants in a WWTP from Madrid (Spain) after secondary and tertiary treatment and environmental impact on the Manzanares River. *Science of the Total Environment* 812, 152567. <https://doi.org/10.1016/j.scitotenv.2021.152567>
- Lu, J.G., Zheng, Y.F., Cheng, M.D., 2008. Wetting mechanism in mass transfer process of hydrophobic membrane gas absorption. *J Memb Sci* 308, 180–190. <https://doi.org/10.1016/J.MEMSCI.2007.09.051>
- Lutze, H. V., Bircher, S., Rapp, I., Kerlin, N., Bakkour, R., Geisler, M., Von Sonntag, C., Schmidt, T.C., 2015. Degradation of chlorotriazine pesticides by sulfate radicals and the influence of organic matter. *Environ Sci Technol* 49, 1673–1680. <https://doi.org/10.1021/es503496u>
- Ma, S., Zuo, X., Xiong, J., Ma, C., Chen, Z., 2020. Sulfamethoxazole removal enhancement from water in high-silica ZSM-5/ozonation synchronous system with low ozone consumption. *Journal of Water Process Engineering* 33. <https://doi.org/10.1016/J.JWPE.2019.101083>
- MADS, 2015. Resolución 631 de 2015 - Ministerio de Ambiente y Desarrollo Sostenible [WWW Document]. URL <https://www.minambiente.gov.co/documento-normativa/resolucion-631-de-2015/> (accessed 7.26.23).

- Marce, M., Domenjoud, B., Esplugas, S., Baig, S., 2016. Ozonation treatment of urban primary and biotreated wastewaters: Impacts and modeling. *Chemical Engineering Journal* 283, 768–777. <https://doi.org/10.1016/J.CEJ.2015.07.073>
- Margot, J., Kienle, C., Magnet, A., Weil, M., Rossi, L., de Alencastro, L.F., Abegglen, C., Thonney, D., Chèvre, N., Schärer, M., Barry, D.A., 2013. Treatment of micropollutants in municipal wastewater: Ozone or powdered activated carbon? *Science of the Total Environment* 461–462, 480–498. <https://doi.org/10.1016/j.scitotenv.2013.05.034>
- Martins, R.C., Cardoso, M., Dantas, R.F., Sans, C., Esplugas, S., Quinta-Ferreira, R.M., 2015. Catalytic studies for the abatement of emerging contaminants by ozonation. *Journal of Chemical Technology and Biotechnology* 90, 1611–1618. <https://doi.org/10.1002/jctb.4711>
- Mathon, B., Coquery, M., Liu, Z., Penru, Y., Guillon, A., Esperanza, M., Miège, C., Choubert, J.M., 2021. Ozonation of 47 organic micropollutants in secondary treated municipal effluents: Direct and indirect kinetic reaction rates and modelling. *Chemosphere* 262. <https://doi.org/10.1016/j.chemosphere.2020.127969>
- Matzek, L.W., Carter, K.E., 2016. Activated persulfate for organic chemical degradation: A review. *Chemosphere* 151, 178–188. <https://doi.org/10.1016/j.chemosphere.2016.02.055>
- Mavroudi, M., Kaldis, S.P., Sakellaropoulos, G.P., 2006. A study of mass transfer resistance in membrane gas-liquid contacting processes. *J Memb Sci* 272, 103–115. <https://doi.org/10.1016/j.memsci.2005.07.025>
- McCusker, L.B., Olson, D.H., Baerlocher, C., 2007. *Atlas of Zeolite Framework Types*, Atlas of Zeolite Framework Types. Elsevier. <https://doi.org/10.1016/B978-0-444-53064-6.X5186-X>
- Mecha, A.C., Onyango, M.S., Ochieng, A., Momba, M.N.B., 2016. Impact of ozonation in removing organic micro-pollutants in primary and secondary municipal wastewater: Effect of process parameters. *Water Science and Technology* 74, 756–765. <https://doi.org/10.2166/wst.2016.276>
- Melnikov, F., Kostal, J., Voutchkova-Kostal, A., Zimmerman, J.B., T. Anastas, P., 2016. Assessment of predictive models for estimating the acute aquatic toxicity of organic chemicals. *Green Chemistry* 18, 4432–4445. <https://doi.org/10.1039/C6GC00720A>
- Méndez-Arriaga, F., Esplugas, S., Giménez, J., 2010. Degradation of the emerging contaminant ibuprofen in water by photo-Fenton. *Water Res* 44, 589–595. <https://doi.org/10.1016/j.watres.2009.07.009>

- Mendoza, A., Aceña, J., Pérez, S., López de Alda, M., Barceló, D., Gil, A., Valcárcel, Y., 2015. Pharmaceuticals and iodinated contrast media in a hospital wastewater: A case study to analyse their presence and characterise their environmental risk and hazard. *Environ Res* 140, 225–241. <https://doi.org/10.1016/j.envres.2015.04.003>
- Merle, T., Pronk, W., Von Gunten, U., 2017. MEMBRO3X, a novel combination of a membrane contactor with advanced oxidation (O<sub>3</sub>/H<sub>2</sub>O<sub>2</sub>) for simultaneous micropollutant abatement and bromate minimization. *Environ Sci Technol Lett* 4, 180–185. <https://doi.org/10.1021/acs.estlett.7b00061>
- Mezyk, S.P., Neubauer, T.J., Cooper, W.J., Peller, J.R., 2007. Free-radical-induced oxidative and reductive degradation of sulfa drugs in water: Absolute kinetics and efficiencies of hydroxyl radical and hydrated electron reactions. *Journal of Physical Chemistry A* 111, 9019–9024. <https://doi.org/10.1021/jp073990k>
- Michael, I., Achilleos, A., Lambropoulou, D., Torrens, V.O., Pérez, S., Petrović, M., Barceló, D., Fatta-Kassinos, D., 2014. Proposed transformation pathway and evolution profile of diclofenac and ibuprofen transformation products during (sono)photocatalysis. *Appl Catal B* 147, 1015–1027. <https://doi.org/10.1016/j.apcatb.2013.10.035>
- Miklos, D.B., Remy, C., Jekel, M., Linden, K.G., Drewes, J.E., Hübner, U., 2018. Evaluation of advanced oxidation processes for water and wastewater treatment – A critical review. *Water Res.* <https://doi.org/10.1016/j.watres.2018.03.042>
- Miller, T.H., Bury, N.R., Owen, S.F., MacRae, J.I., Barron, L.P., 2018. A review of the pharmaceutical exposome in aquatic fauna. *Environmental Pollution* 239, 129–146. <https://doi.org/10.1016/j.envpol.2018.04.012>
- Moreira, F.C., Bocos, E., Faria, A.G.F., Pereira, J.B.L., Fonte, C.P., Santos, R.J., Lopes, J.C.B., Dias, M.M., Sanromán, M.A., Pazos, M., Boaventura, R.A.R., Vilar, V.J.P., 2019. Selecting the best piping arrangement for scaling-up an annular channel reactor: An experimental and computational fluid dynamics study. *Science of The Total Environment* 667, 821–832. <https://doi.org/10.1016/J.SCITOTENV.2019.02.260>
- Mustafa, M., Wang, H., Lindberg, R.H., Fick, J., Wang, Y., Tysklind, M., 2021. Identification of resistant pharmaceuticals in ozonation using QSAR modeling and their fate in electro-peroxone process. *Front Environ Sci Eng* 15, 1–14. <https://doi.org/10.1007/S11783-021-1394-6/METRICS>
- My Hanh Le, T., Nuisin, R., Mongkolnavin, R., Painmanakul, P., Sairiam, S., 2022. Enhancing dye wastewater treatment efficiency in ozonation membrane contactors by chloro- and fluoro-organosilanes' functionality on hydrophobic PVDF membrane

- modification. *Sep Purif Technol* 288, 120711.  
<https://doi.org/10.1016/j.seppur.2022.120711>
- Naima, A., Ammar, F., Abdelkader, O., Rachid, C., Lynda, H., Syafiuddin, A., Boopathy, R., 2022. Development of a novel and efficient biochar produced from pepper stem for effective ibuprofen removal. *Bioresour Technol* 347, 126685.  
<https://doi.org/10.1016/j.biortech.2022.126685>
- Nakada, N., Shinohara, H., Murata, A., Kiri, K., Managaki, S., Sato, N., Takada, H., 2007. Removal of selected pharmaceuticals and personal care products (PPCPs) and endocrine-disrupting chemicals (EDCs) during sand filtration and ozonation at a municipal sewage treatment plant. *Water Res* 41, 4373–4382.  
<https://doi.org/10.1016/j.watres.2007.06.038>
- Nannou, C.I., Kosma, C.I., Albanis, T.A., 2015. Occurrence of pharmaceuticals in surface waters: analytical method development and environmental risk assessment. *Water Res* 95, 1242–1262.  
<https://doi.org/10.1080/03067319.2015.1085520>  
<https://doi.org/10.1080/03067319.2015.1085520>
- Nawrocki, J., Kasprzyk-Hordern, B., 2010. The efficiency and mechanisms of catalytic ozonation. *Appl Catal B* 99, 27–42. <https://doi.org/10.1016/j.apcatb.2010.06.033>
- Neta, P., Dorfman, L.M., 1968. Pulse Radiolysis Studies. XIII. Rate Constants for the Reaction of Hydroxyl Radicals with Aromatic Compounds in Aqueous Solutions. pp. 222–230. <https://doi.org/10.1021/ba-1968-0081.ch015>
- NORMAN, 2022. List of NORMAN Suspect List Exchange [WWW Document]. URL <https://www.norman-network.com/nds/SLE/>
- OCDE, 2020. Environment at a Glance 2020. OECD. <https://doi.org/10.1787/4ea7d35f-en>
- Orias, F., Perrodin, Y., 2013. Characterisation of the ecotoxicity of hospital effluents: A review. *Science of The Total Environment* 454–455, 250–276.  
<https://doi.org/10.1016/j.scitotenv.2013.02.064>
- Pabby, A.K., Sastre, A.M., 2013. State-of-the-art review on hollow fibre contactor technology and membrane-based extraction processes. *J Memb Sci*.  
<https://doi.org/10.1016/j.memsci.2012.11.060>
- Parsons, S., 2015. Advanced Oxidation Processes for Water and Wastewater Treatment. *Water Intelligence Online* 4, 9781780403076–9781780403076.  
<https://doi.org/10.2166/9781780403076>

- Pines, D.S., Min, K.N., Ergas, S.J., Reckhow, D.A., 2005. Investigation of an ozone membrane contactor system. *Ozone Sci Eng* 27, 209–217. <https://doi.org/10.1080/01919510590945750>
- Pipolo, M., Gmurek, M., Corceiro, V., Costa, R., Emília Quinta-Ferreira, M., Ledakowicz, S., Quinta-Ferreira, R.M., Martins, R.C., 2017. Ozone-Based Technologies for Parabens Removal from Water: Toxicity Assessment. *Ozone Sci Eng* 39, 233–243. <https://doi.org/10.1080/01919512.2017.1301246>
- Prada-Vásquez, M.A., Estrada-Flórez, S.E., Serna-Galvis, E.A., Torres-Palma, R.A., 2021. Developments in the intensification of photo-Fenton and ozonation-based processes for the removal of contaminants of emerging concern in Ibero-American countries. *Science of The Total Environment* 765, 142699. <https://doi.org/10.1016/j.scitotenv.2020.142699>
- Presumido, P.H., Montes, R., Quintana, J.B., Rodil, R., Feliciano, M., Puma, G.L., Gomes, A.I., Vilar, V.J.P., 2022. Ozone membrane contactor to intensify gas/liquid mass transfer and contaminants of emerging concern oxidation. *J Environ Chem Eng* 10, 108671. <https://doi.org/10.1016/j.jece.2022.108671>
- Presumido, P.H., Ribeirinho-Soares, S., Montes, R., Quintana, J.B., Rodil, R., Ribeiro, M., Neuparth, T., Santos, M.M., Feliciano, M., Nunes, O.C., Gomes, A.I., Vilar, V.J.P., 2023. Ozone membrane contactor for tertiary treatment of urban wastewater: Chemical, microbial and toxicological assessment. *Science of The Total Environment* 164492. <https://doi.org/10.1016/J.SCITOTENV.2023.164492>
- QuintilesIMS and its affiliates, 2015. *Global Medicines Use in 2020. Outlook and Implications*,.
- Real, F.J., Javier Benitez, F., Acero, J.L., Sagasti, J.J.P., Casas, F., 2009. Kinetics of the chemical oxidation of the pharmaceuticals primidone, ketoprofen, and diatrizoate in ultrapure and natural waters. *Ind Eng Chem Res* 48, 3380–3388. <https://doi.org/10.1021/ie801762p>
- Reiprich, B., Weissenberger, T., Schwieger, W., Inayat, A., 2020. Layer-like FAU-type zeolites: A comparative view on different preparation routes. *Front Chem Sci Eng*. <https://doi.org/10.1007/s11705-019-1883-3>
- Ren, Y., Lin, L., Ma, J., Yang, J., Feng, J., Fan, Z., 2015. Sulfate radicals induced from peroxymonosulfate by magnetic ferrosin MF<sub>2</sub>O<sub>4</sub> (M=Co, Cu, Mn, and Zn) as heterogeneous catalysts in the water. *Appl Catal B* 165, 572–578. <https://doi.org/10.1016/j.apcatb.2014.10.051>

- Rivera-Utrilla, J., Sánchez-Polo, M., Ferro-García, M.Á., Prados-Joya, G., Ocampo-Pérez, R., 2013. Pharmaceuticals as emerging contaminants and their removal from water. A review. *Chemosphere* 93, 1268–1287. <https://doi.org/10.1016/J.CHEMOSPHERE.2013.07.059>
- Rizzo, L., Malato, S., Antakyali, D., Beretsou, V.G., Đolić, M.B., Gernjak, W., Heath, E., Ivancev-Tumbas, I., Karaolia, P., Lado Ribeiro, A.R., Mascolo, G., McArdell, C.S., Schaar, H., Silva, A.M.T., Fatta-Kassinos, D., 2019. Consolidated vs new advanced treatment methods for the removal of contaminants of emerging concern from urban wastewater. *Science of the Total Environment*. <https://doi.org/10.1016/j.scitotenv.2018.11.265>
- Rosal, R., Rodríguez, A., Perdigón-Melón, J.A., Mezcua, M., Hernando, M.D., Letón, P., García-Calvo, E., Agüera, A., Fernández-Alba, A.R., 2008. Removal of pharmaceuticals and kinetics of mineralization by O<sub>3</sub>/H<sub>2</sub>O<sub>2</sub> in a biotreated municipal wastewater. *Water Res* 42, 3719–3728. <https://doi.org/10.1016/j.watres.2008.06.008>
- Rosenfeldt, E.J., Linden, K.G., Canonica, S., von Gunten, U., 2006. Comparison of the efficiency of OH radical formation during ozonation and the advanced oxidation processes O<sub>3</sub>/H<sub>2</sub>O<sub>2</sub> and UV/H<sub>2</sub>O<sub>2</sub>. *Water Res* 40, 3695–3704. <https://doi.org/10.1016/j.watres.2006.09.008>
- Roustan, M., 2003. Transferts gaz-liquide dans les procédés de traitement des eaux et des effluents gazeux. *Génie des Procédés de l'Environnement*.
- Roustan, M., Wang, R.Y., Wolbert, D., 1996. Modeling hydrodynamics and mass transfer parameters in a continuous ozone bubble column. *Ozone Sci Eng* 18, 99–115. <https://doi.org/10.1080/01919519608547331>
- Sá, M.F.T., Castro, V., Gomes, A.I., Morais, D.F.S., Silva Braga, R.V.P.S., Saraiva, I., Souza-Chaves, B.M., Park, M., Fernández-Fernández, V., Rodil, R., Montes, R., Quintana, J.B., Vilar, V.J.P., 2022. Tracking pollutants in a municipal sewage network impairing the operation of a wastewater treatment plant. *Science of the Total Environment* 817, 152518. <https://doi.org/10.1016/j.scitotenv.2021.152518>
- Sabale, R., Venkatesh, B., Jose, M., 2022. Sustainable water resource management through conjunctive use of groundwater and surface water: a review. *Innovative Infrastructure Solutions* 2022 8:1 8, 1–12. <https://doi.org/10.1007/S41062-022-00992-9>
- Sabelfeld, M., Geißen, S.U., 2019. Effect of helical structure on ozone mass transfer in a hollow fiber membrane contactor. *J Memb Sci* 574, 222–234. <https://doi.org/10.1016/j.memsci.2018.10.056>

- Saeid, S., Tolvanen, P., Kumar, N., Eränen, K., Peltonen, J., Peurla, M., Mikkola, J.P., Franz, A., Salmi, T., 2018. Advanced oxidation process for the removal of ibuprofen from aqueous solution: A non-catalytic and catalytic ozonation study in a semi-batch reactor. *Appl Catal B* 230, 77–90. <https://doi.org/10.1016/j.apcatb.2018.02.021>
- Sandermann, H., 2003. Differential lipid affinity of xenobiotics and natural compounds. *FEBS Lett* 554, 165–168. [https://doi.org/10.1016/S0014-5793\(03\)01143-8](https://doi.org/10.1016/S0014-5793(03)01143-8)
- Schmitt, A., Mendret, J., Brosillon, S., 2022. Evaluation of an ozone diffusion process using a hollow fiber membrane contactor. *Chemical Engineering Research and Design* 177, 291–303. <https://doi.org/10.1016/J.CHERD.2021.11.002>
- Schmitt, A., Mendret, J., Cheikho, H., Brosillon, S., 2023. Ozone Diffusion through a Hollow Fiber Membrane Contactor for Pharmaceuticals Removal and Bromate Minimization. *Membranes (Basel)* 13. <https://doi.org/10.3390/membranes13020171>
- Serna-Galvis, E.A., Isaza-Pineda, L., Moncayo-Lasso, A., Hernández, F., Ibáñez, M., Torres-Palma, R.A., 2019. Comparative degradation of two highly consumed antihypertensives in water by sonochemical process. Determination of the reaction zone, primary degradation products and theoretical calculations on the oxidative process. *Ultrason Sonochem* 58, 104635. <https://doi.org/10.1016/j.ultsonch.2019.104635>
- Shiklomanov, I.A., 2009. Appraisal and Assessment of World Water Resources. <http://dx.doi.org/10.1080/02508060008686794> 25, 11–32. <https://doi.org/10.1080/02508060008686794>
- Sleeper, W., Henry, D., 2002. Durability Test Results of Construction and Process Materials Exposed to Liquid and Gas Phase Ozone. *Ozone Sci Eng* 24, 249–260. <https://doi.org/10.1080/01919510208901616>
- Soares, O.S.G.P., Freitas, C.M.A.S., Fonseca, A.M., Órfão, J.J.M., Pereira, M.F.R., Neves, I.C., 2016. Bromate reduction in water promoted by metal catalysts prepared over faujasite zeolite. *Chemical Engineering Journal* 291, 199–205. <https://doi.org/10.1016/j.cej.2016.01.093>
- Solís, R.R., Medina, S., Gimeno, O., Beltrán, F.J., 2019. Solar photolytic ozonation for the removal of recalcitrant herbicides in river water. *Sep Purif Technol* 212, 280–288. <https://doi.org/10.1016/j.seppur.2018.11.035>
- Song, R.B., Xiang, J.Y., Hou, D.P., 2011. Characteristics of Mechanical Properties and Microstructure for 316L Austenitic Stainless Steel. *Journal of Iron and Steel Research, International* 18, 53–59. [https://doi.org/10.1016/S1006-706X\(11\)60117-9](https://doi.org/10.1016/S1006-706X(11)60117-9)

- Sotelo, J.L., Beltrán, F.J., Benitez, F.J., Beltrán-Heredia, J., 1989. Henry's law constant for the ozone-water system. *Water Res* 23, 1239–1246. [https://doi.org/10.1016/0043-1354\(89\)90186-3](https://doi.org/10.1016/0043-1354(89)90186-3)
- Souza, F.S., Da Silva, V. V., Rosin, C.K., Hainzenreder, L., Arenzon, A., Pizzolato, T., Jank, L., Féris, L.A., 2018. Determination of pharmaceutical compounds in hospital wastewater and their elimination by advanced oxidation processes. *J Environ Sci Health A Tox Hazard Subst Environ Eng* 53, 213–221. <https://doi.org/10.1080/10934529.2017.1387013>
- Sposito, G., 1998. On Points of Zero Charge. *Environ Sci Technol* 32, 2815–2819. <https://doi.org/10.1021/es9802347>
- Staehelin, Johannes., Hoigne, Juerg., 1985. Decomposition of ozone in water in the presence of organic solutes acting as promoters and inhibitors of radical chain reactions. *Environ Sci Technol* 19, 1206–1213. <https://doi.org/10.1021/es00142a012>
- Staehelin, Johannes., Hoigne, Juerg., 1982. Decomposition of ozone in water: rate of initiation by hydroxide ions and hydrogen peroxide. *Environ Sci Technol* 16, 676–681. <https://doi.org/10.1021/es00104a009>
- Stylianou, S.K., Katsoyiannis, I.A., Mitrakas, M., Zouboulis, A.I., 2018. Application of a ceramic membrane contacting process for ozone and peroxone treatment of micropollutant contaminated surface water. *J Hazard Mater* 358, 129–135. <https://doi.org/10.1016/j.jhazmat.2018.06.060>
- Stylianou, S.K., Sklari, S.D., Zamboulis, D., Zaspalis, V.T., Zouboulis, A.I., 2015. Development of bubble-less ozonation and membrane filtration process for the treatment of contaminated water. *J Memb Sci* 492, 40–47. <https://doi.org/10.1016/j.memsci.2015.05.036>
- Su, L., Chen, X., Wang, H., Wang, Y., Lu, Z., 2022. Oxygen vacancies promoted heterogeneous catalytic ozonation of atrazine by defective 4A zeolite. *J Clean Prod* 336. <https://doi.org/10.1016/j.jclepro.2022.130376>
- Szabó, R.K., Megyeri, Cs., Illés, E., Gajda-Schranz, K., Mazellier, P., Dombi, A., 2011. Phototransformation of ibuprofen and ketoprofen in aqueous solutions. *Chemosphere* 84, 1658–1663. <https://doi.org/10.1016/j.chemosphere.2011.05.012>
- Tell, J., Caldwell, D.J., Häner, A., Hellstern, J., Hoeger, B., Journal, R., Mastrocco, F., Ryan, J.J., Snape, J., Straub, J.O., Vestel, J., 2019. Science-based Targets for Antibiotics in Receiving Waters from Pharmaceutical Manufacturing Operations. *Integr Environ Assess Manag* 15, 312–319. <https://doi.org/10.1002/ieam.4141>



- Therrien, J.D., Vanrolleghem, P.A., Dorea, C.C., 2019. Characterization of the performance of venturi-based aeration devices for use in wastewater treatment in low-resource settings. *Water SA* 45, 251–258. <https://doi.org/10.4314/WSA.V45I2.12>
- Valdés, H., Farfán, V.J., Manoli, J.A., Zaror, C.A., 2009. Catalytic ozone aqueous decomposition promoted by natural zeolite and volcanic sand. *J Hazard Mater* 165, 915–922. <https://doi.org/10.1016/j.jhazmat.2008.10.093>
- Valdés, H., Tardón, R.F., Zaror, C.A., 2012. Role of surface hydroxyl groups of acid-treated natural zeolite on the heterogeneous catalytic ozonation of methylene blue contaminated waters. *Chemical Engineering Journal* 211–212, 388–395. <https://doi.org/10.1016/j.cej.2012.09.069>
- Valdés, M.E., Huerta, B., Wunderlin, D.A., Bistoni, M.A., Barceló, D., Rodriguez-Mozaz, S., 2016. Bioaccumulation and bioconcentration of carbamazepine and other pharmaceuticals in fish under field and controlled laboratory experiments. Evidences of carbamazepine metabolization by fish. *Science of The Total Environment* 557–558, 58–67. <https://doi.org/10.1016/j.scitotenv.2016.03.045>
- Vasilachi, I.C., Asiminicesei, D.M., Fertu, D.I., Gavrilescu, M., 2021. Occurrence and Fate of Emerging Pollutants in Water Environment and Options for Their Removal. *Water* 2021, Vol. 13, Page 181 13, 181. <https://doi.org/10.3390/W13020181>
- Völker, J., Stapf, M., Miehe, U., Wagner, M., 2019. Systematic review of toxicity removal by advanced wastewater treatment technologies via ozonation and activated carbon. *Environ Sci Technol*. <https://doi.org/10.1021/acs.est.9b00570>
- von Sonntag, C., von Gunten, U., 2012. *Chemistry of Ozone in Water and Wastewater Treatment: From Basic Principles to Applications*, Chemistry of Ozone in Water and Wastewater Treatment: From Basic Principles to Applications. IWA Publishing. <https://doi.org/10.2166/9781780400839>
- Wang, B., Xiong, X., Shui, Y., Huang, Z., Tian, K., 2019. A systematic study of enhanced ozone mass transfer for ultrasonic-assisted PTFE hollow fiber membrane aeration process. *Chemical Engineering Journal* 357, 678–688. <https://doi.org/10.1016/j.cej.2018.09.188>
- Wang, B., Zhang, H., Meng, Q., Ren, H., Xiong, M., Gao, C., Wang, B., 2021. The enhancement of ozone-liquid mass transfer performance in a PTFE hollow fiber membrane contactor using ultrasound as a catalyzer. *RSC Adv* 11, 14017–14028. <https://doi.org/10.1039/d1ra00452b>

- Wang, H., Zhang, S., He, X., Yang, Y., Yang, X., Van Hulle, S.W.H., 2023. Comparison of macro and micro-pollutants abatement from biotreated landfill leachate by single ozonation, O<sub>3</sub>/H<sub>2</sub>O<sub>2</sub>, and catalytic ozonation processes. *Chemical Engineering Journal* 452, 139503. <https://doi.org/10.1016/j.cej.2022.139503>
- Wang, J., Chen, H., 2020. Catalytic ozonation for water and wastewater treatment: Recent advances and perspective. *Science of The Total Environment* 704, 135249. <https://doi.org/10.1016/J.SCITOTENV.2019.135249>
- Wang, J., Wang, S., 2018. Activation of persulfate (PS) and peroxymonosulfate (PMS) and application for the degradation of emerging contaminants. *Chemical Engineering Journal* 334, 1502–1517. <https://doi.org/10.1016/j.cej.2017.11.059>
- Wang, X.H., Yu, Y., Huang, T., Qin, W.C., Su, L.M., Zhao, Y.H., 2016. Comparison of Toxicities to *Vibrio fischeri* and Fish Based on Discrimination of Excess Toxicity from Baseline Level. *PLoS One* 11, e0150028. <https://doi.org/10.1371/journal.pone.0150028>
- Whitman, W.G., 1962. The two film theory of gas absorption. *Int J Heat Mass Transf* 5, 429–433. [https://doi.org/10.1016/0017-9310\(62\)90032-7](https://doi.org/10.1016/0017-9310(62)90032-7)
- WHO, 2021. WHO model list of essential medicines - 22nd list, 2021 [WWW Document]. URL <https://www.who.int/publications/i/item/WHO-MHP-HPS-EML-2021.02>
- Wilke, C.R., Chang, P., 1955. Correlation of diffusion coefficients in dilute solutions. *AIChE Journal* 1, 264–270. <https://doi.org/10.1002/AIC.690010222>
- Wilson, E.E., 1915. A basis for rational design of heat transfer apparatus. *Trans. ASME*, 37(47), pp.47-82. *The J Am Soc Mech Engrs* 53, 1689–1699.
- World Water Assessment Programme, 2018. The United Nations world water development report 2018: nature-based solutions for water. *UN Water Report* 154.
- Yang, Y., Jiang, J., Lu, X., Ma, J., Liu, Y., 2015. Production of Sulfate Radical and Hydroxyl Radical by Reaction of Ozone with Peroxymonosulfate: A Novel Advanced Oxidation Process. *Environ Sci Technol* 49, 73307339. <https://doi.org/10.1021/es506362e>
- Yao, W., Ur Rehman, S.W., Wang, H., Yang, H., Yu, G., Wang, Y., 2018. Pilot-scale evaluation of micropollutant abatements by conventional ozonation, UV/O<sub>3</sub>, and an electro-peroxone process. *Water Res* 138, 106–117. <https://doi.org/10.1016/j.watres.2018.03.044>

- You, W.D., Ye, P., Yang, B., Luo, X., Fang, J., Mai, Z.T., Sun, J.L., 2021. Degradation of 17 Benzodiazepines by the UV/H<sub>2</sub>O<sub>2</sub> Treatment. *Front Environ Sci* 9, 474. <https://doi.org/10.3389/FENVS.2021.764841/BIBTEX>
- Yu, G., Wang, Y., Cao, H., Zhao, H., Xie, Y., 2020. Reactive Oxygen Species and Catalytic Active Sites in Heterogeneous Catalytic Ozonation for Water Purification. *Environ Sci Technol* 54, 5931–5946. <https://doi.org/10.1021/acs.est.0c00575>
- Yu, X., Qin, W., Yuan, X., Sun, L., Pan, F., Xia, D., 2021. Synergistic mechanism and degradation kinetics for atenolol elimination via integrated UV/ozone/peroxymonosulfate process. *J Hazard Mater* 407, 124393. <https://doi.org/10.1016/j.jhazmat.2020.124393>
- Yuan, Z., Sui, M., Yuan, B., Li, P., Wang, J., Qin, J., Xu, G., 2017. Degradation of ibuprofen using ozone combined with peroxymonosulfate. *Environ Sci (Camb)* 3, 960–969. <https://doi.org/10.1039/c7ew00174f>
- Zhang, Y., Li, K., Wang, J., Hou, D., Liu, H., 2017. Ozone mass transfer behaviors on physical and chemical absorption for hollow fiber membrane contactors. *Water Sci Technol* 76, 1360–1369. <https://doi.org/10.2166/WST.2017.254>
- Zhou, S., Di Paolo, C., Wu, X., Shao, Y., Seiler, T.B., Hollert, H., 2019. Optimization of screening-level risk assessment and priority selection of emerging pollutants – The case of pharmaceuticals in European surface waters. *Environ Int* 128, 1–10. <https://doi.org/10.1016/j.envint.2019.04.034>
- Zimmermann, S.G., Wittenwiler, M., Hollender, J., Krauss, M., Ort, C., Siegrist, H., von Gunten, U., 2011. Kinetic assessment and modeling of an ozonation step for full-scale municipal wastewater treatment: Micropollutant oxidation, by-product formation and disinfection. *Water Res* 45, 605–617. <https://doi.org/10.1016/J.WATRES.2010.07.080>
- Zoumpouli, G.A., Baker, R., Taylor, C.M., Chippendale, M.J., Smithers, C., Ho, S.S.X., Mattia, D., Chew, Y.M.J., Wenk, J., 2018. A single tube contactor for testing membrane ozonation. *Water (Switzerland)* 10, 1416. <https://doi.org/10.3390/w10101416>

# Annexes

## List of supplementary texts

### T.A1-Determination of bubble size distribution mean bubble size and gas hold up

To assess the bubble size distribution and mean bubble size, an experiment was carried out under batch conditions using a pure oxygen stream at a flow rate of  $0.75 \text{ Ndm}^3 \text{ min}^{-1}$  and at liquid flow rate of  $70 \text{ L h}^{-1}$ . The acquisition of bubble images was obtained using a digital camera. The photographs were taken by illuminating the flow with uniform, diffused yellow light, from a distance of 30 cm from the reactor and at 3 different angles around it (top, middle and bottom). Fig. A2 shows the images taken of bubbles detected at various gas flow rates.

The digital photographs were processed and enhanced by using ImageJ software with the "Analyze Particles" tool. The algorithm converts the pixel count within a projected area on the plane ( $A_p$ ) for each counted bubble, in which can be calculated from the equivalent spherical diameter ( $D_{eq}$ ) given by Eq. (A1).

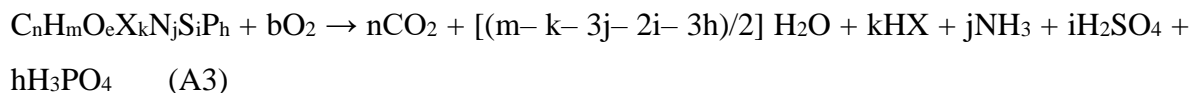
$$d_{eq} = 2 \sqrt{\frac{A_p}{\pi}} \quad (\text{A1})$$

The average size of the bubbles formed by the ozone membrane contactor was approximately  $0.20 \pm 0.02 \text{ mm}$ , corresponding to Sauter mean diameter ( $d_{32} = 0.26 \text{ mm}$ ). With the same digital images, the volume fraction of the gas phase ( Figure A.3) was calculated according to Eq. A2 and a value of 12% was obtained. The gas holdup method involves measuring the liquid heights without the presence of gas,  $h_0$  (cm), and the corresponding level,  $h$  (cm), when gas is continuously injected into the membrane for different gas flow rate conditions considered.

$$\varepsilon_G = \frac{h - h_0}{h} \quad (\text{A2})$$

## T.A2- Determination of the theoretical oxygen demand (ThOD)

The determination of theoretical oxygen demand (ThOD) for an organic substance (given by the formula  $C_nH_mO_eX_kN_jSiP_h$ ) assumes that organic nitrogen is transformed to ammonia and the stoichiometric oxidation of carbon, phosphorus, and sulfur on the molecule occurred according to the equation A3.



where X represents the sum of all halogens and b the moles of oxygen (which is calculated with equation A4) required to oxidize one mole of the organic substance.

$$b = n + [(m-k-3j-2i-3h)/4] - (e/2) + 2i + 2h \quad (A4)$$

Therefore, the ThOD (in mg  $O_2 L^{-1}$ ) for 1 mmol  $L^{-1}$  of the organic substance ( $C_nH_mO_eX_kN_jSiP_h$ ) is obtained as follows (equation A5):

$$ThOD = b * 32 \quad (A5)$$

$\Delta ThOD$  is calculated, as the difference between the ThOD for the degradation product and for the parent antihypertensive, according to equation A6.

$$\Delta ThOD = ThOD_{degradation\ product} - ThOD_{parent\ compound} \quad (A6)$$

## List of figures

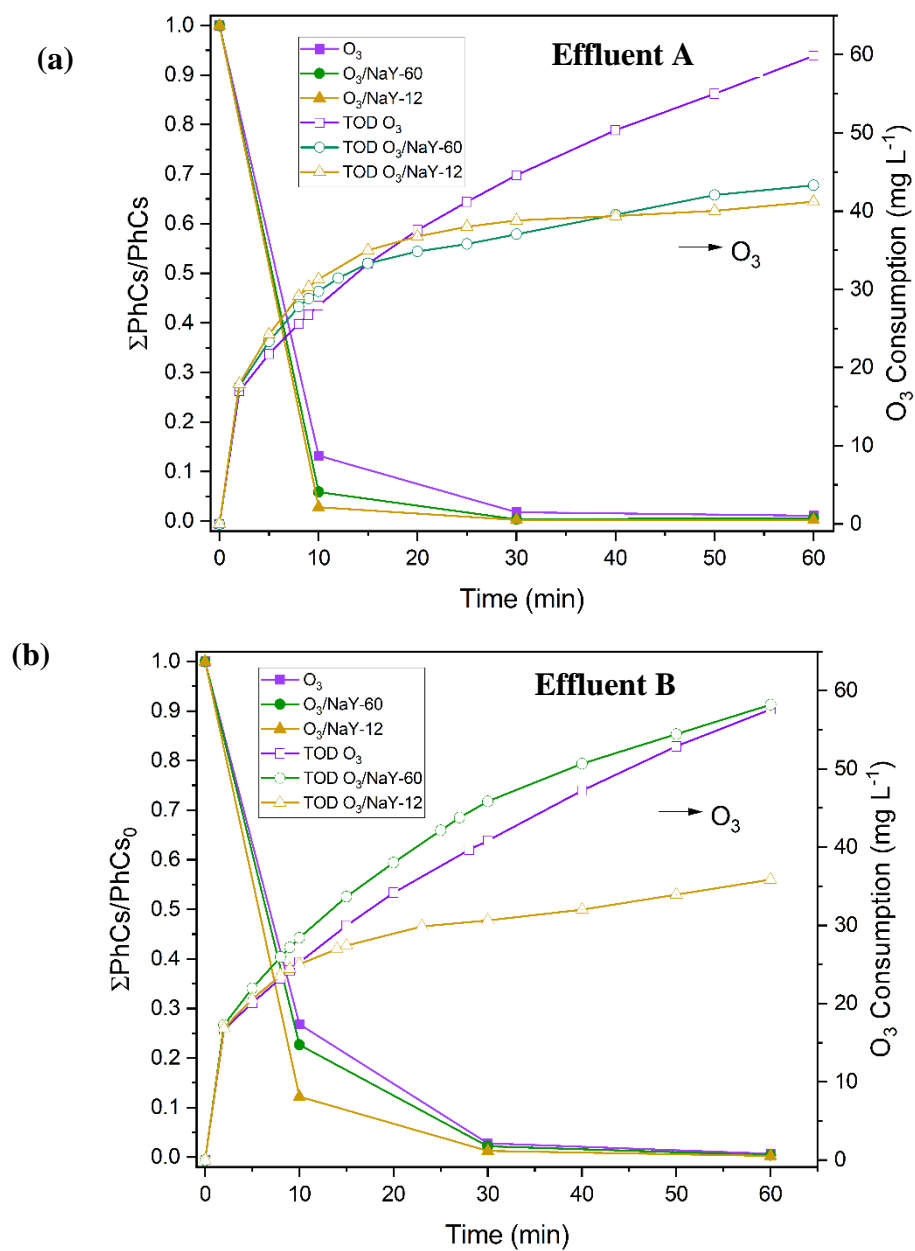


**Figure A.1** Removal of the mixture of PhACs during  $\text{O}_3$  and catalytic ozonation using NaY-12 and NaY-60 zeolite as a function of TOD, in a) Effluent A, and (b) Effluent B.

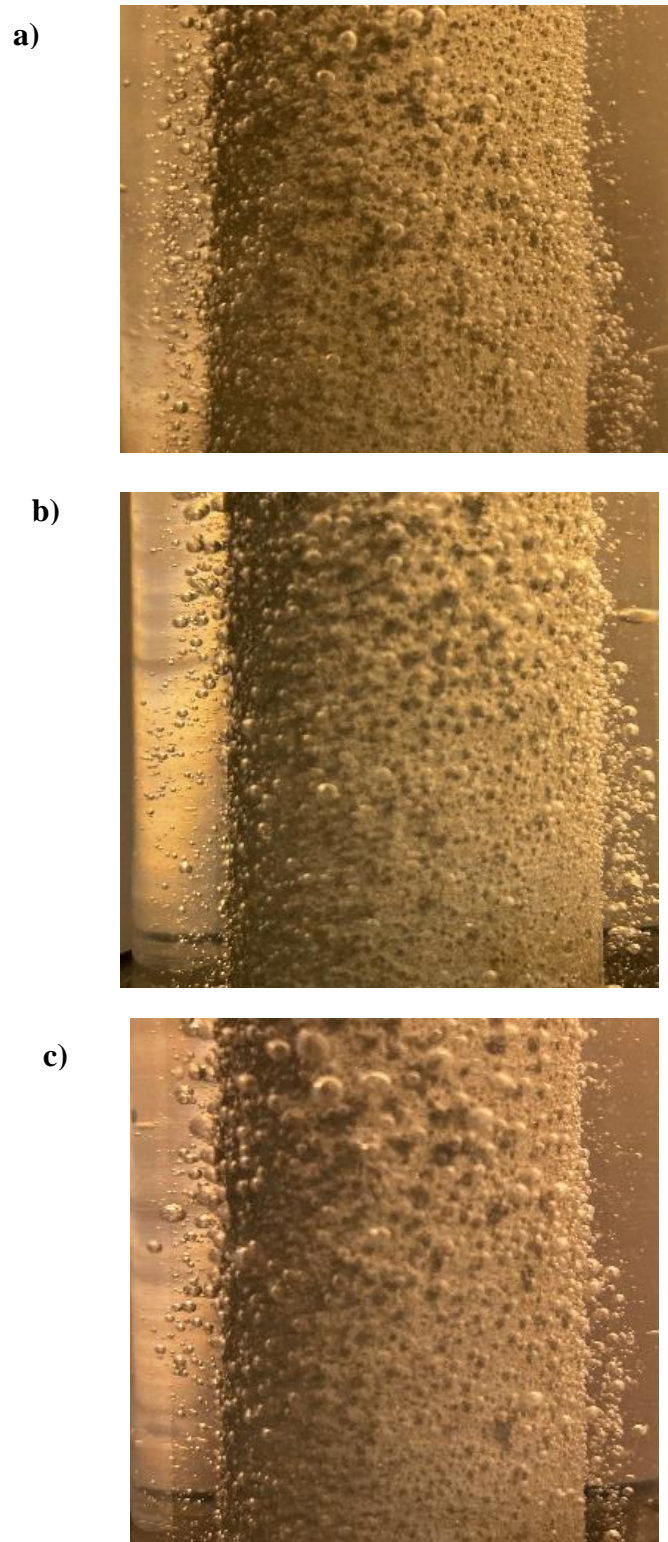


**Figure A.2** Examples of images of detected bubbles at various gas flow rates,  $Q_{\text{gas}}$ : a)  $0.3 \text{ Ndm}^3 \text{ min}^{-1}$ ; b)  $0.5 \text{ Ndm}^3 \text{ min}^{-1}$  and c)  $0.75 \text{ Ndm}^3 \text{ min}^{-1}$ .  $Q_{\text{liq}} = 70 \text{ L h}^{-1}$ .

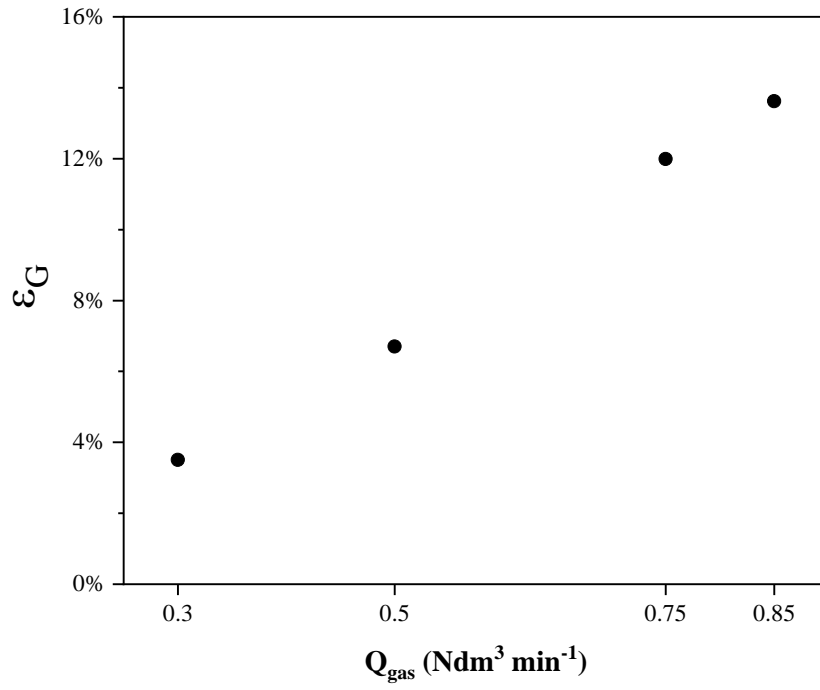


**Figure A.3.** Influence of the gas flow rate ( $Q_{\text{gas}}$ ) on the gas holdup  $\epsilon_G$  (%).  $Q_{\text{liq}} = 50 \text{ L h}^{-1}$



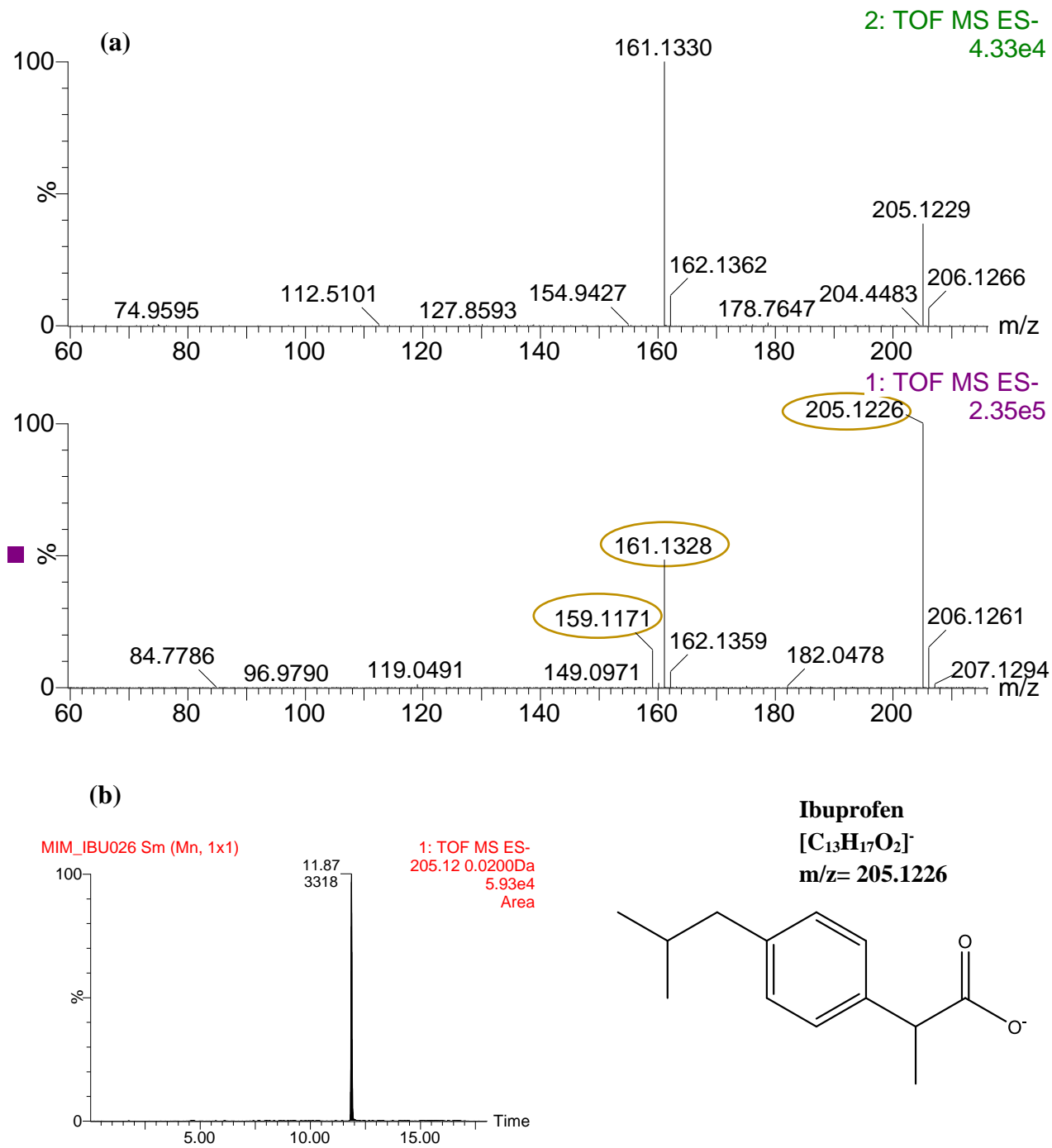
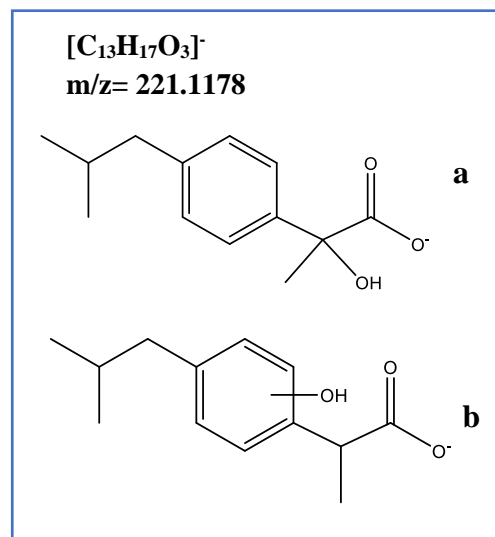
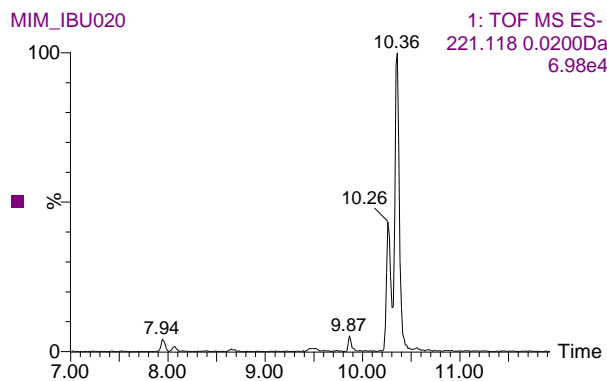
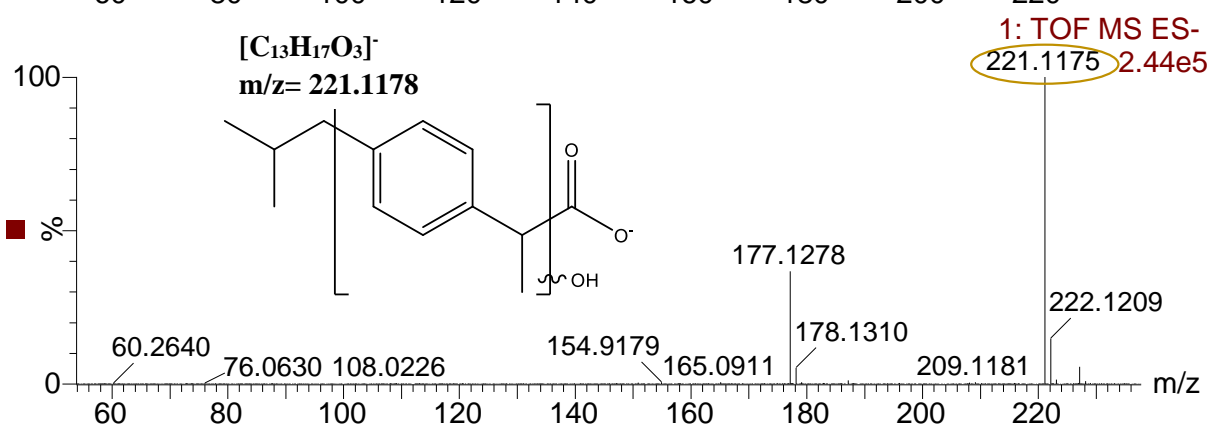
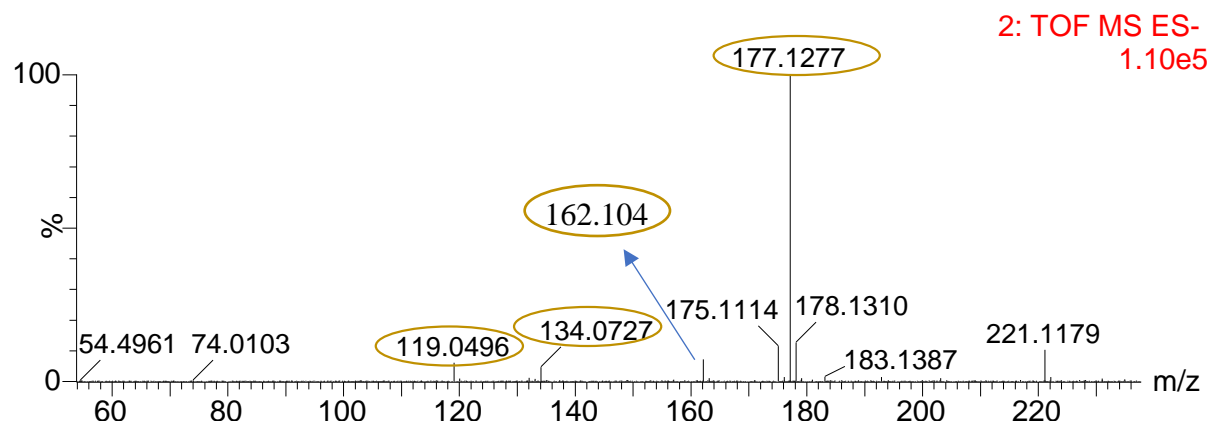


**Figure A.4** (a) MS/MS spectra and (b) chromatogram of ibuprofen (retention time 11.87 min)



Possible isomers of hydroxylation

**Figure A.5** MS/MS spectra, chromatogram of TP1,a,b (retention time 10.36 min) and possible hydroxylation sites

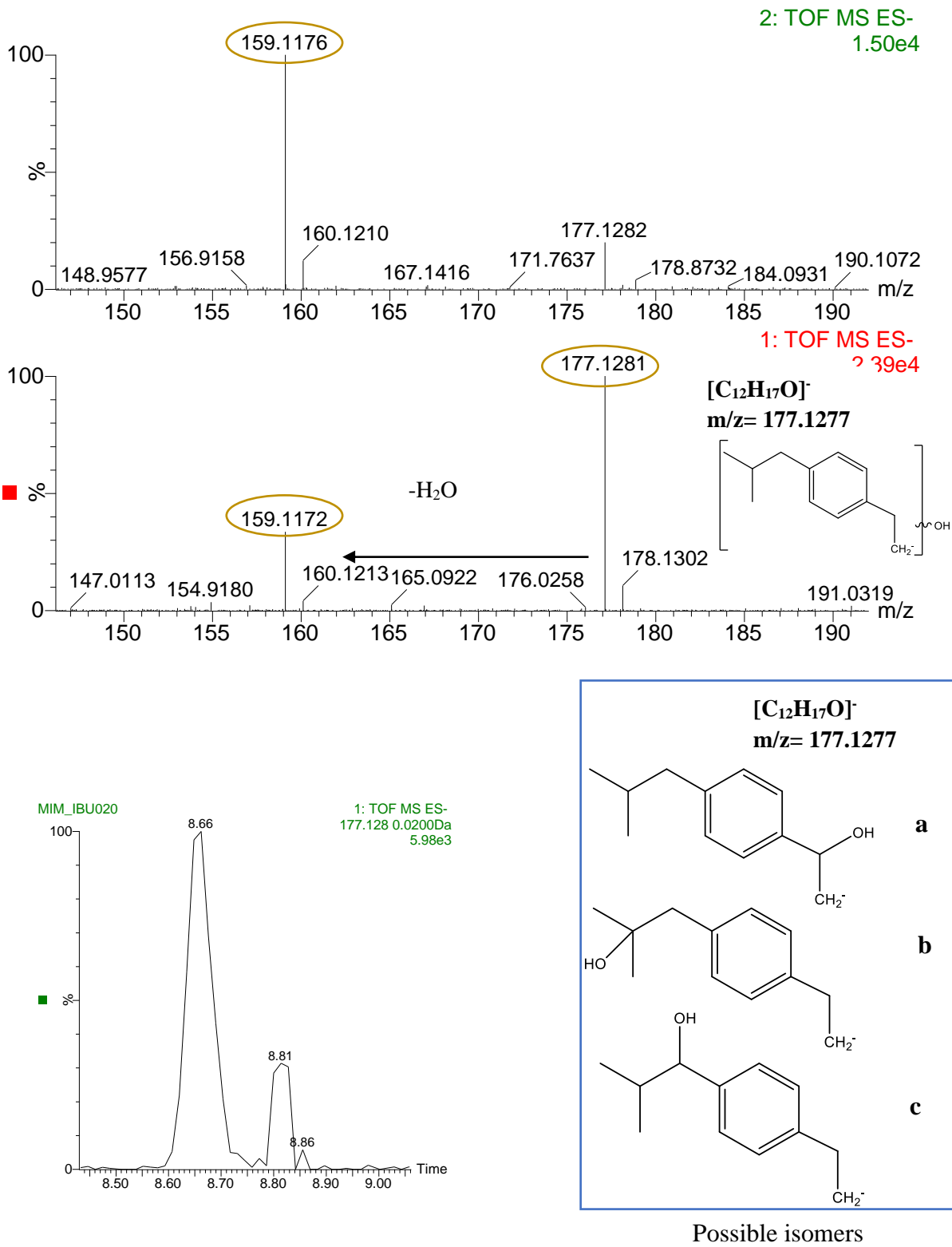
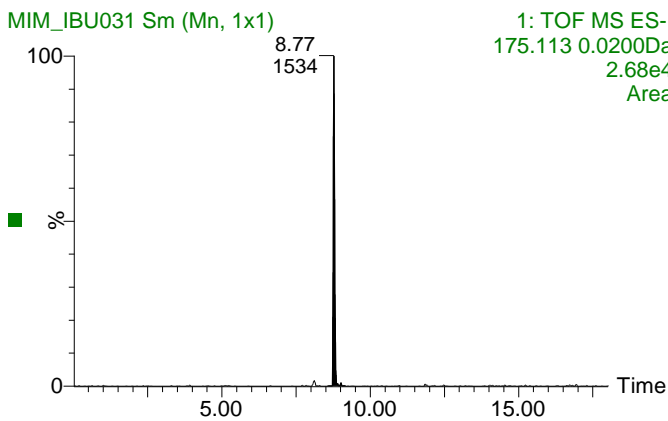
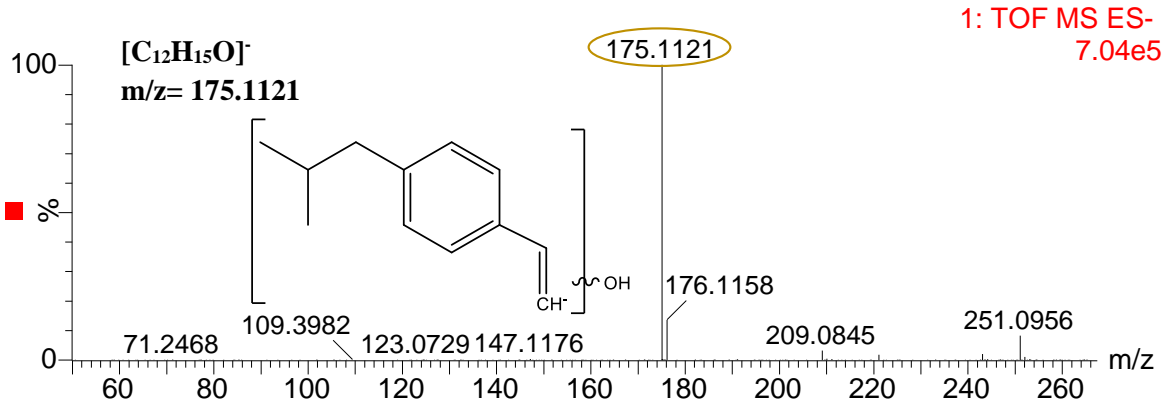
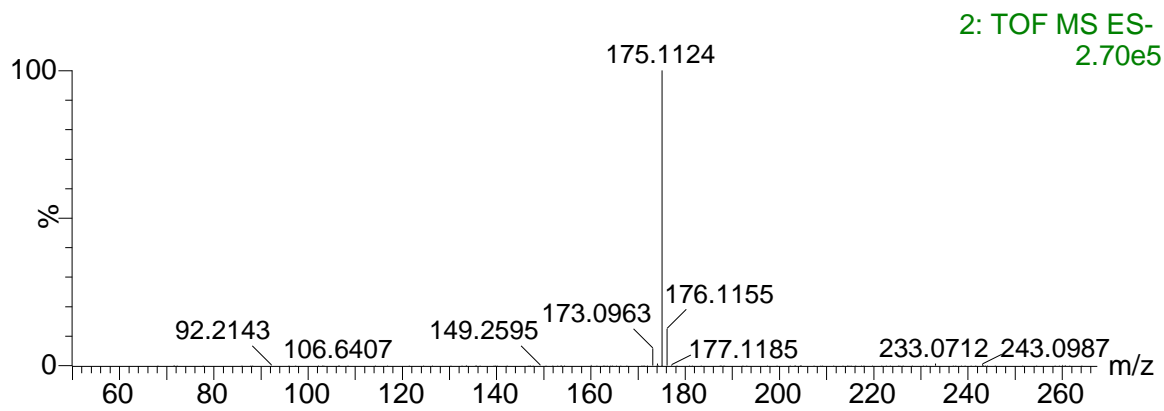
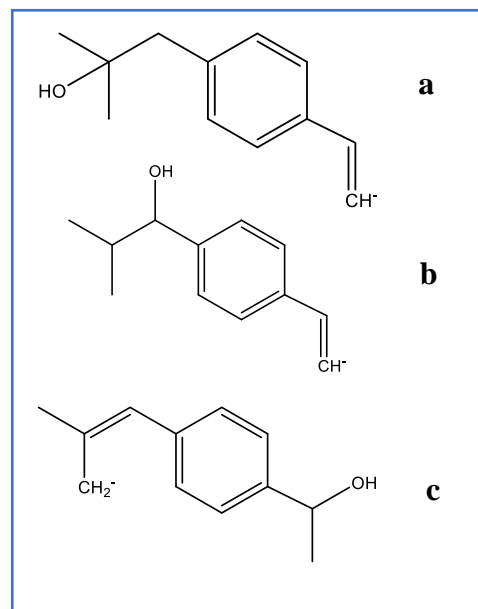


**Figure A.6** MS/MS spectra, chromatogram of TP2,a,b,c (retention time 8.66 min)



1: TOF MS ES-  
175.113 0.0200Da  
2.68e4  
Area



Possible isomers

**Figure A.7** (a) MS/MS spectra and (b) chromatogram of TP3a,b,c (retention time 8.77 min).

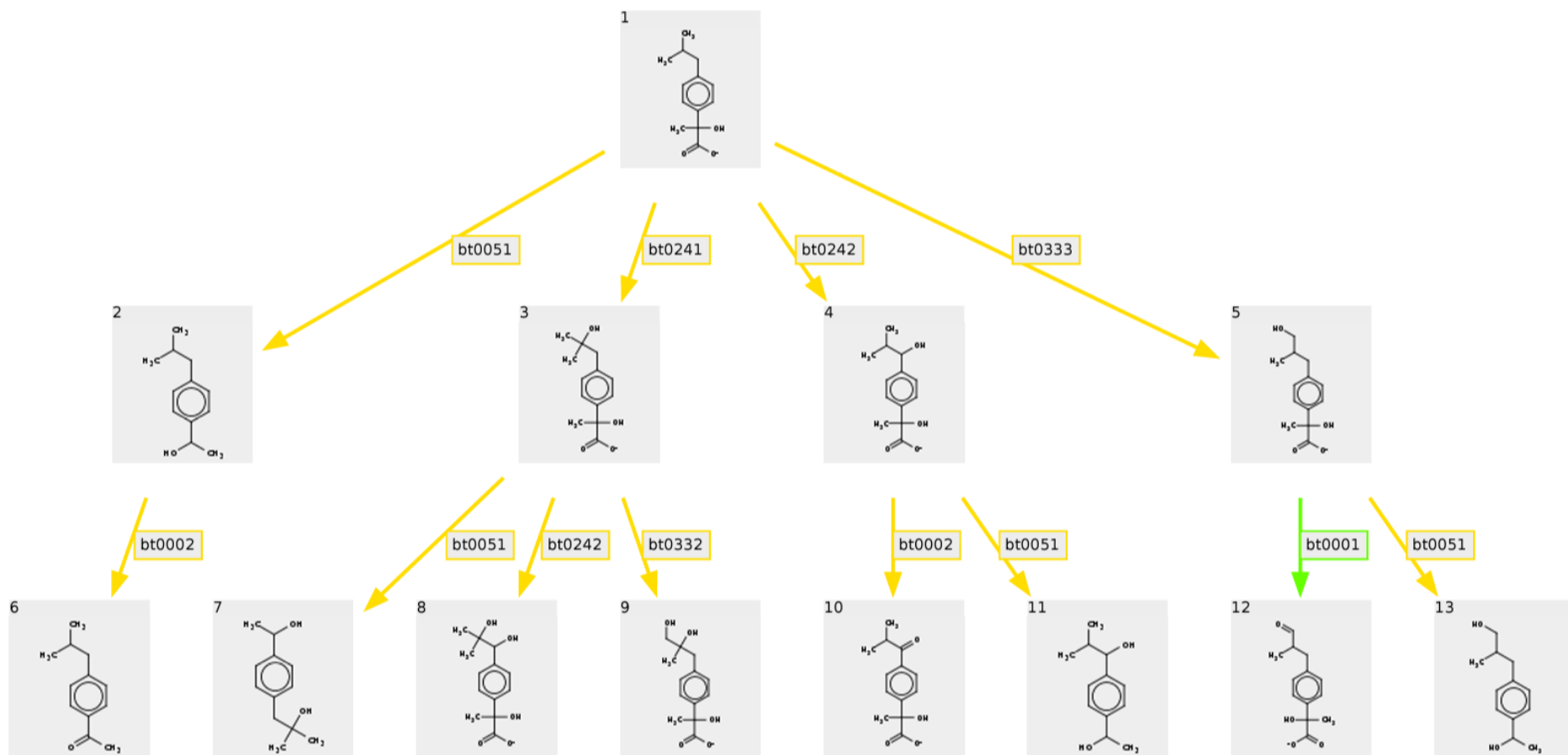


**Figure A.8** Possible primary biotransformation pathways of the TP1 product.

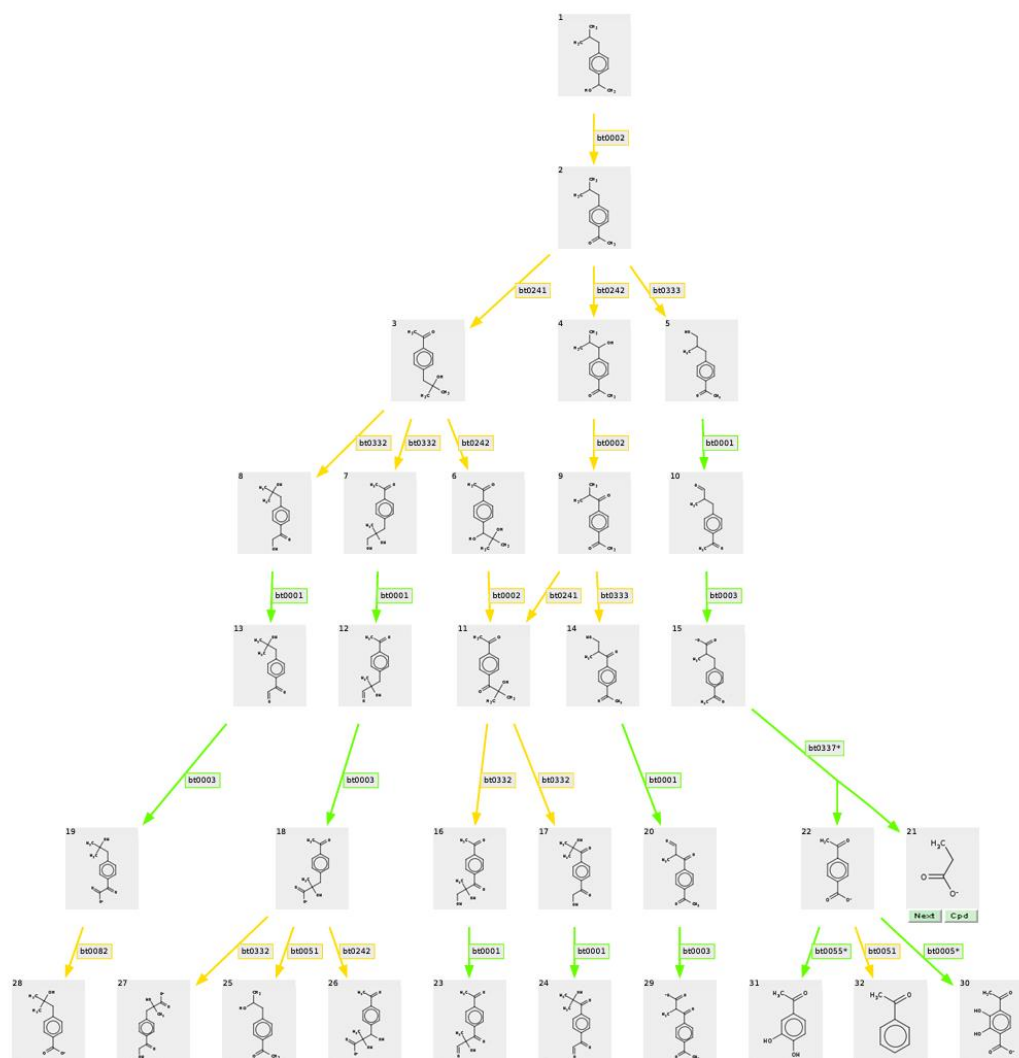


**Figure A.9** Possible primary biotransformation pathways of the TP2 product.

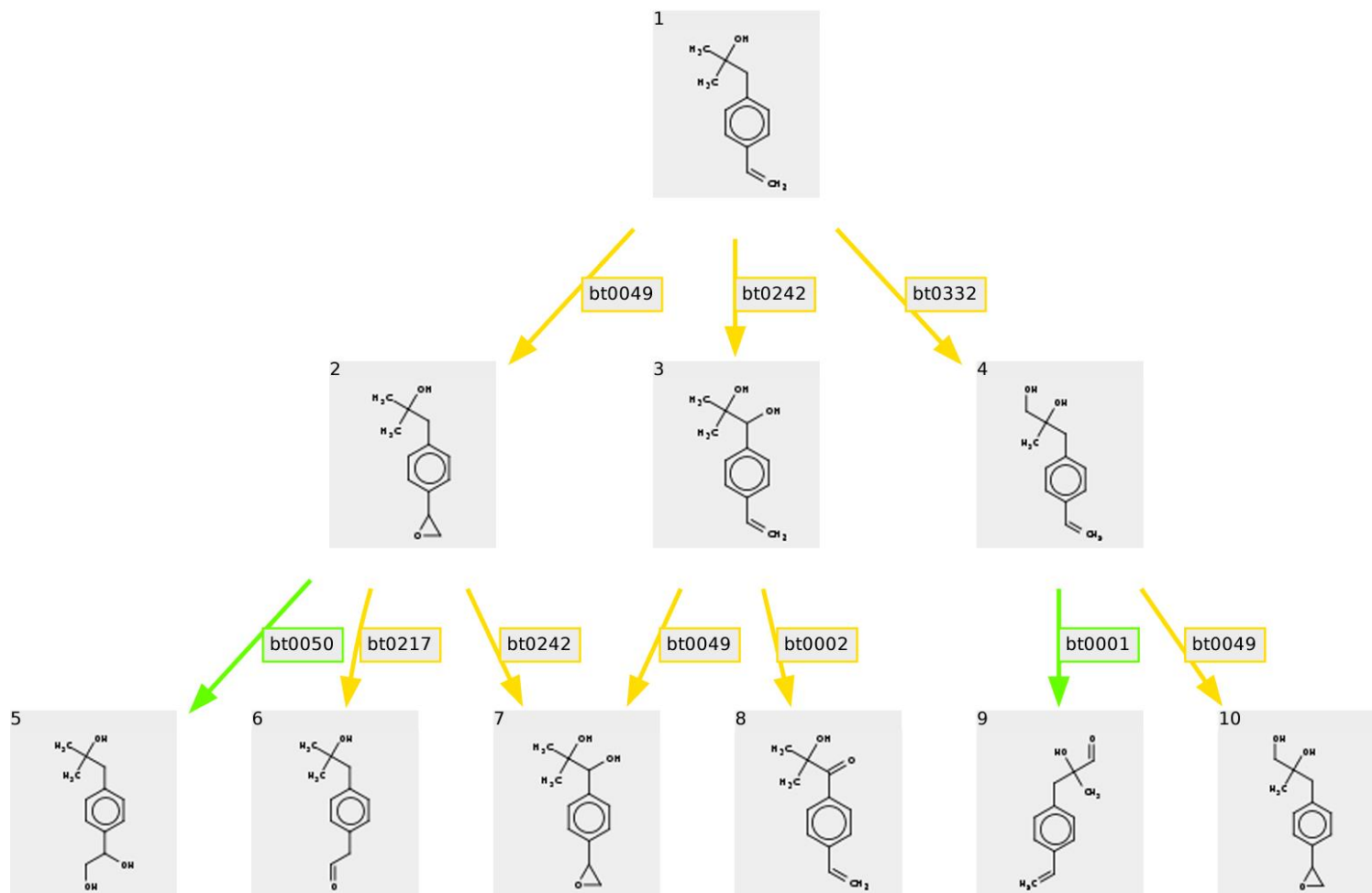


**Figure A.10** Possible primary biotransformation pathways of the TP3 product.

## List of tables

**Table A1.** Physico-chemical characteristics of selected pharmaceuticals. pKa acid dissociation constant, charge (the dominant form at the effluent pH (i.e.,=7.6))

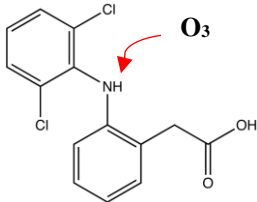
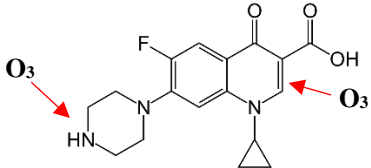
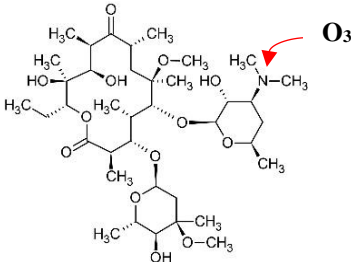
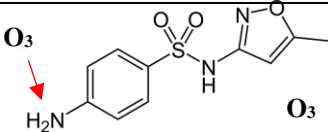
| Compound               | pKa <sup>a</sup> | Charge at pH 7.6 | Approx. Dimensions Length, width, and height (Å) <sup>b</sup> |
|------------------------|------------------|------------------|---|
| Diclofenac             | 4.2              | (-)              | 11.7 x 7.2 x 10   |
| Phenazone              | 1.4.             | (-)              | 11.8 x 7.8 x 5.0  |
| Tramadol               | 9.4              | (+)              | 10.7 x 12.7 x 7.0   |
| Ciprofloxacin          | 6.18, 8.76       | (+/-)            | 10.18 x 14.2 x 6.6  |
| Clarithromycin         | 8.99             | (+)              | 11.94 x 12 x 4.3  |
| Erythromycin           | 8.74             | (+)              | 9.9 x 18.19 x 15.14   |
| Trimethoprim           | 7.6              | 0                | 10.5 x 8.5 x 4.3  |
| Sulfamethoxazole       | 1.97,6.16        | (-)              | 11.4 x 6.2 x 4.1  |
| Clindamycin            | 7.8              | (+)              | 12.18 x 8.0 x 4.2   |
| Norfloxacin            | 6.34, 8.75       | (+/-)            | 14.6 x 9.8 x 6.7  |
| Metronidazole          | 2.38             | (+/-)            | 4.8 x 8.9 x 8.3   |
| Tetracycline           | 3.3, 9.25        | (+/-)            | 11.26 x 7.4 x 4.2   |
| Carbamazepine          | 13.94            | 0                | 8.5 x 11.3 x 7.0  |
| Gabapentin             | 3.68, 10.70      | (+/-)            | 7.4 x 5.1 x 4.3   |
| Primidone              | 12.3             | 0                | 8.6 x 7.6 x 10.18   |
| Irbesartan             | 4.08, 4.29       | (-)              | 8.1 x 11.8 x 4.2  |
| Losartan               | 5.50             | (-)              | 9.5 x 12 x 15.7   |
| Enalapril              | 3.0, 5.5         | (-)              | 11 x 8.0 x 4.2  |
| Valsartan              | 4.00, 4.61       | (-)              | 7.6 x 16.9 x 11.2   |
| Levamisole             | 8.0              | (+)              | 7.4 x 12.2 x 6.2  |
| Iopromide              | 11.4             | 0                | 13.15 x 7.7 x 4.2   |
| Atorvastatin           | 4.46             | (-)              | 14.7 x 9.1 x 4.2  |
| Metoprolol             | 9.6              | (+)              | 13.8 x 6.1 x 4.2  |
| Lorazepam              | 13               | 0                | 11.4 x 10.9 x 8.0   |
| Venlafaxine            | 10.09            | (+)              | 7.0 x 10.4 x 13.6   |
| O-Desmethylvenlafaxine | 10               | (+)              | 8.5 x 7.5 x 4.2   |

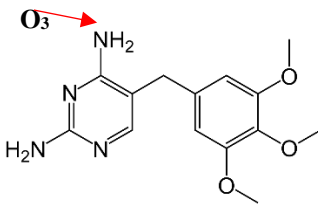
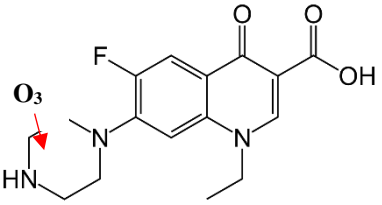
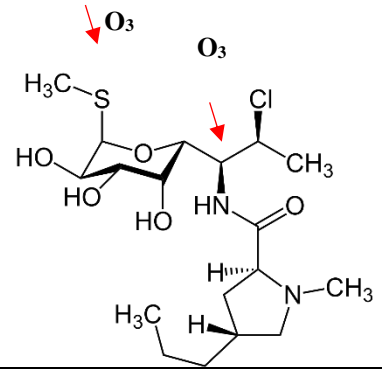
<sup>a</sup> pKa values were taken from: [www.chemicalize.org](http://www.chemicalize.org) and [www.chemspider.com](http://www.chemspider.com)

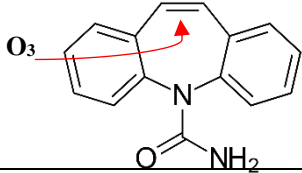
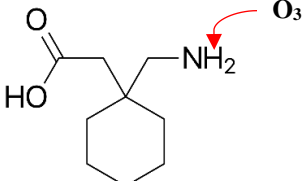
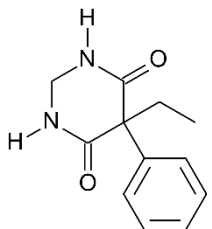
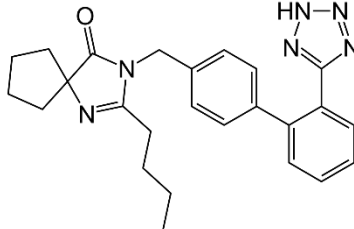
<sup>b</sup> Values estimated by Multiwfn software

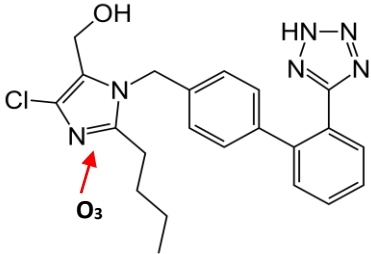
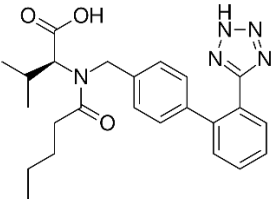
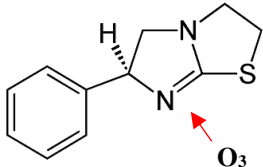
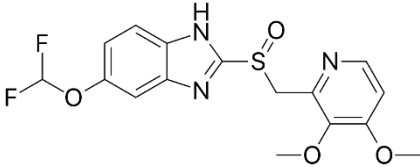


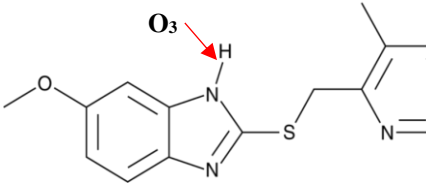
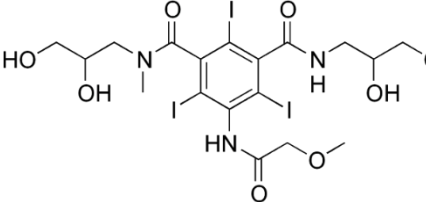
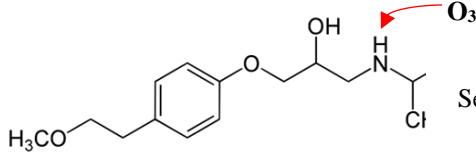
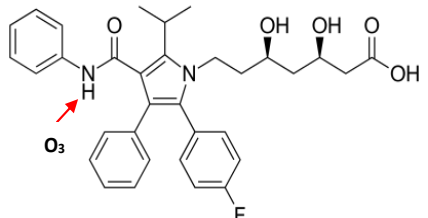
**Table A2.** Second-order kinetic constants reaction for emerging contaminants selected with ozone ( $k_{O_3}$ ) and hydroxyl radicals ( $k_{HO\cdot}$ ).

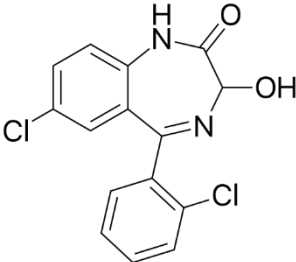
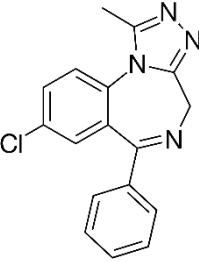
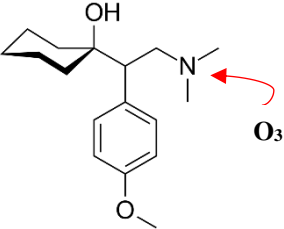
| Therapeutic group | Compound         | Molecular Structure  | Reactive moieties | Literature                             |  |  | Ozone Rea. | Group |
|-------------------|------------------|--|-------------------|--|--|--|------------|-------|
|                   |                  |  |                   | $k_{O_3}$<br>( $M^{-1} \cdot s^{-1}$ ) | $k_{HO\cdot}$<br>( $M^{-1} \cdot s^{-1}$ ) | Ref.                                   |            |       |
| Anti-inflammatory | Diclofenac       |    | Aniline           | $\sim 1 \times 10^6$                   | $7.5 \times 10^9$                          | (Huber et al., 2003)                   | High       | I     |
| Antibiotics       | Ciprofloxacin    |    | Secondary amine   | $1.9 \times 10^4$                      | $4.1 \times 10^9$                          | (Dodd et al., 2006)                    | High       | I     |
|                   | Clarithromycin   |   | Tertiary amine    | $4.0 \times 10^4$                      | $\sim 5 \times 10^9$                       | (Lange et al., 2006; Lee et al., 2014) | High       | I     |
|                   | Sulfamethoxazole |  | Aniline           | $5.7 \times 10^5$                      | $5.5 \times 10^9$                          | (Huber et al., 2003;)                  | High       |       |

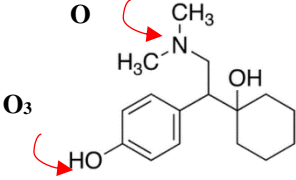
|              |   |                           |                    |                      |   |      |                     |   |   |
|--------------|---|---------------------------|--------------------|----------------------|---|------|---------------------|---|---|
|              |   |                           |                    |                      |   |      | Mezyk et al., 2007) |   | I |
| Trimethoprim |    | Aniline, anisole          | $7.4 \times 10^4$  | $6.9 \times 10^9$    | (Dodd et al., 2006)                           | High |                     | I |   |
| Norfloxacin  |   | Secondary amine           | $1.10 \times 10^4$ | $\sim 5 \times 10^9$ | (Javier Rivas et al., 2011; Lee et al., 2014) | High |                     | I |   |
| Clindamycin  |  | Tertiary amine, thioether | $3.05 \times 10^5$ | $8.94 \times 10^9$   | (Mathon et al., 2021)                         | High |                     | I |   |

|                 |               |   |               |                   |                   |                        |      |     |
|-----------------|---------------|---|---------------|-------------------|-------------------|------------------------|------|-----|
|                 | Carbamazepine |   | Olefin        | $3.0 \times 10^5$ | $8.5 \times 10^9$ | (Lee et al., 2014)     | High | I   |
| Anticonvulsants | Gabapentin    |   | primary amine | 15                | $9.1 \times 10^9$ | (Lee et al., 2014)     | Low  | III |
|                 | Primidone     |    | None          | <10               | $6.7 \times 10^9$ | (Real et al., 2009)    | Low  | III |
|                 | Irbesartan    |  | None          | 24                | $10^{10}$         | (Bourgin et al., 2018) | Low  | III |

|                   |              |  |           |                   |                |                        |              |     |
|-------------------|--------------|--|-----------|-------------------|----------------|------------------------|--------------|-----|
| Antihypertensive  | Losartan     |    | Imidazole | $2.1 \times 10^5$ | $1.0^{10}$     | (Bourgin et al., 2018) | High         | I   |
|                   | Valsartan    |     | None      | 38                | $\sim 10^{10}$ | (Lee et al., 2014)     | Low          | III |
| Anthelmintic drug | Levamisole   |   | Imidazole | $5.0 \times 10^2$ | n.a            | (Gulde et al., 2021b)  | Intermediate | II  |
| Anti-ulcer agent  | Pantoprazole |  | None      | n.a               | n.a            | -                      | Low          | -   |

|                        |                              |   |                  |                   |                   |                       |              |     |
|------------------------|------------------------------|---|------------------|-------------------|-------------------|-----------------------|--------------|-----|
|                        | 4-hydroxy-omeprazole sulfide |   | Secondary amine  | n.a               | n.a               | -                     | High         | -   |
| Iodized contrast media | Iopromide                    |   | None             | < 0.8             | $3.3 \times 10^9$ | (Huber et al., 2003)  | Low          | III |
| $\beta$ -Blocker       | Metoprolol                   |   | Secondary amine  | $2.0 \times 10^3$ | $7.3 \times 10^9$ | (Benner et al., 2008) | Intermediate | II  |
| Lipid regulator        | Atorvastatin                 |  | Pyrrole, aniline | $2.7 \times 10^6$ | $1.2 \times 10^9$ | (Lee et al., 2023)    | High         | I   |

|                  |             |  |                |                   |                    |  |      |     |
|------------------|-------------|--|----------------|-------------------|--------------------|--|------|-----|
| Anxiolytic       | Lorazepam   |  | None           | 0.28              | $5.23 \times 10^9$ | (Mustafa et al., 2021; You et al., 2021) | Low  | III |
| Anxiolytic       | Alprazolam  |   | None           | <1                | $5.83 \times 10^9$ | (Chys et al., 2018; You et al., 2021)    | Low  | III |
| Anti-depressants | Venlafaxine |  | Tertiary amine | $3.3 \times 10^4$ | $8.8 \times 10^9$  | (Lester et al., 2013)                    | High | III |

|                        |  |                        |     |     |   |      |   |
|------------------------|--|------------------------|-----|-----|---|------|---|
| O-desmethylvenlafaxine |  | Tertiary amine, phenol | n.a | n.a | - | High | - |
|------------------------|--|------------------------|-----|-----|---|------|---|

n.a. = not available in literature

### Categorization of PhACs removal according to their reaction rate constant with O<sub>3</sub> based on Bourgin et al., (2018).

Group I, Reaction rate  $k_{O_3} > 10^4 \text{ M}^{-1}\text{s}^{-1}$ , high reactivity with ozone

Group II, Reaction rate  $10^2 < k_{O_3} < 10^4 \text{ M}^{-1}\text{s}^{-1}$ , intermediate reactivity with ozone

Group III, Reaction rate  $k_{O_3} < 10^2 \text{ M}^{-1}\text{s}^{-1}$ , low or no reactivity with ozone